Zsolt Schléder

Deformation mechanisms of naturally deformed rocksalt

RWTH AACHEN UNIVERSITY

Deformation mechanisms of naturally deformed rocksalt

Von der Fakultät für Georessourcen und Materialtechnik
der Rheinisch -Westfälischen Technischen Hochschule Aachen

zur Erlangung des akademischen Grades eines
Doktors der Naturwissenschaften
genehmigte Dissertation

vorgelegt von M.Sc. Zsolt Schléder
aus Sárbogárd, Ungarn

Berichter: Univ.-Prof. Dr. János L. Urai
Prof. Dr. Christopher J. Spiers
Univ.-Prof. Dr. Peter A. Kukla

Tag der mündlichen Prüfung: 02 Juni 2006

Dedicated to
my parents
and
Windhoffer Gábor

Acknowledgements

I would like to sincerely thank the various people who, during the three years in which this work lasted, provided me with useful and helpful assistance.

János Urai is sincerely thanked for supervising of this thesis and for finding time in his rather busy schedule to provide me with an insightful introduction at the beginning of the project and a thorough review during the whole work. Without his care and consideration, this work would not have matured.

I would like to thank all the colleagues at Aachen for their dedication, interest and enthusiasm. To Sofie Nollet, Katerina Scholz, Oliver Schenk, Johannes Schoenherr and Marc Holland who were always ready for discussing any kinds of problems and for carefully reading and correcting many parts of this thesis. Thanks to all the HiWis at GED; Joyce Schmatz, Manuel Bumenthal, Ansgar Heimann and Frank Strozyk for the countless immediate help in sample preparation, photocopying and other monotonous tasks. GED secretary, Bettina Dulle, is heartily thanked for her patience and professionalism in explaining the official ways in German bureaucracy. Werner Kraus preparator provided me feedback and invaluable insights in rocksalt sample preparation, which is greatly acknowledged. Kai Jasper, Danilo Cifola and Heijn van Gent, who worked at the neighbor department or joined the GED group for some period, were always ready for a small chat and their presence made the GED atmosphere even more colourful.

Chris Hilgers demonstrated interest in this work early on, provided assistance throughout some important questions, and has been an enthusiastic supporter and partner. Wim Paar provided rocksalt samples from Hengelo and provided me with all the desired detail information during the work. Stanislaw Burliga is thanked for organizing a fieldwork in Poland, for the hospitality, and for the discussions on salt tectonics. Chris Talbot provided me the opportunity to join him in the 2005 field season in central Iran. His introduction into the salt tectonic processes in Iran and his guidance is kindly acknowledged. Abbas Bahroudi and his colleagues at GSI are heartily thanked for the hospitality while staying in Iran. The fieldwork in Neuhof salt mine would have not been possible without the help of Reiner Stax at K+S. Both the samples and the discussion on salt tectonics-related features of the mine are thanked. I would like to commend the interest, supervision and great job done by Manfred Thomé at the Jülich Forschungszentrum throughout the overall gamma-irradiation process.

Friends at Budapest, especially Bodó Péter and Windhoffer Gábor, are thanked for their – very likely unconscious – encouragement and support. Most important, thanks to Nóra, who put up with a string of lost weekends and odd working hours.

Abstract

This thesis presents an analysis of deformation and recrystallization processes in a variety of naturally deformed rocksalt. Tools used for the analysis involve simple microtectonic methods: transmitted and reflected light microscopy of gamma-irradiated thin sections and orientation measurements with EBSD. Case studies were chosen to represent different tectonic settings. Slightly deformed bedded Lower Triassic Röt rocksalt from Hengelo, The Netherlands; horizontal, though locally folded Z1 Zechstein salt from Neuhof-Ellers salt mine, Germany; highly strained Z4 Zechstein domal salt from Klodawa salt mine, Poland and highly deformed extrusive salt from Qum Kuh and Gramsar Hills (central Iran) were studied.

The Hengelo and Neuhof-Ellers samples show abundant primary structures such as fluid-inclusion-outlined chevron or hopper crystals. The microstructures suggest that the sedimentary environment was ephemeral salt-pan for the Hengelo samples and perennial salt lake for the Neuhof-Ellers samples. The main deformation mechanisms are dislocation processes and solution-precipitation in the Hengelo samples, while the samples from Neuhof-Ellers deform solely by solution-precipitation creep due to its very fine grain size (~1 mm). In both set of samples, widespread evidence for grain boundary migration recrystallization (GBM) is present. The GBM swept out the primary fluid inclusions and transferred them to grain boundary fluid.

The Klodawa samples show no primary microstructures, suggesting that it is completely recrystallized by process of GBM. The main deformation mechanism was dislocation creep as evidenced by the widespread presence of subgrains. Presence of static recrystallization related euhedral grains in some samples suggest that mine-wall convergence induced static recrystallization may alter the natural deformation-related microstructures.

The highly deformed extrusive salt samples from Iran contain thin shear zones. In the shear zones, the deformation mechanism is solution-precipitation creep. The preserved porphyroclasts are rich in subgrain, indicating climb controlled dislocation creep in the subsurface. Orientation measurements demonstrate that the grain size reduction involves subgrain rotation and perhaps nucleation during the upward transport of the salt.

Based on subgrain size piezometry the differential stress was less than 2 MPa for all the samples studied except that for the extrusive Iran samples, where the differential stress of ~3 MPa was calculated. This high stress value very likely represents the conditions during the upward transport of the salt.

Zusammenfassung

Die vorliegende Doktorarbeit präsentiert zahlreiche Untersuchungen zu Deformations- und Rekristallisationsprozessen natürlich deformierter Salzgesteine. Zur Analyse wurden die in der Halit-Mikrotektonik üblichen Methoden angewandt: Durchlicht- und Auflichtmikroskopie von Gamma-bestrahlten Salzdünnschliffen sowie Orientierungsmessungen mit EBSD.
Zur Untersuchung von unterschiedlichen tektonischen Szenarien wurden entsprechende Fallstudien gewählt: Schwach deformiertes geschichtetes Röt Steinsalz (Untere Trias) aus Hengelo (Niederlande), horizontal bis lokal gefaltetes Werra Zechsteinsalz (Z1) aus dem Neuhof-Ellers Salzbergwerk (Deutschland), hoch verformtes Aller (Z4) Steinsalz aus einem Salzstock Bergwerk in Klodawa (Polen) und hoch deformierte Salz-Extrusiva aus Qum Kuh and Gramsar Hills (Zentral-Iran).
Proben aus Hengelo und Neuhof enthalten eine Vielzahl von Primärstrukturen, wie zum Beispiel Fluideinschlüsse – in der Literatur als „chevron"- oder „hopper"-Kristalle bezeichnet. Mikrostrukturelle Beobachtungen deuten darauf hin, dass Proben aus Hengelo einem kurzzeitig vorhandenen (ephemeralen) Salz-Becken entstammen und Salzgesteine aus Neuhof sich in einem langlebigen Salzsee bildeten.
Die Hauptdeformationsmechanismen in den Hengelo-Proben sind Versetzungskriechen sowie Drucklösung. Das extrem feinkörnige Gefüge der Salzproben aus Neuhof deutet dagegen ausschließlich auf Drucklösungs-Prozesse hin. Gleichzeitig verweisen die Mikrostrukturen der Hengelo- und Neuhof-Proben auf Korngrenzmigrationsprozesse. Während der Korngrenzmigration (KGM) werden die im Salzkristall primär enthaltenen Fluideinschlüsse entlang von Korngrenzen freigesetzt.
Salzgesteine aus Klodawa weisen keine primären Mikrostrukturen (z.B. „hopper"-Kristalle) auf, was auf eine komplette Rekrisatllisation des Salzgefüges durch KGM hindeutet. Das weit verbreitete Auftreten von Subkörnern in den Klodawa-Proben lässt eindeutig auf Versetzungskriechen als vorwiegend aktiven Hauptdeformationsmechanismus schließen. Idiomorph gewachsene statisch rekristallisierte Körner in einigen der Proben aus Klodawa, weisen höchst wahrscheinlich auf Rekristallisationsprozesse hin, die durch Konvergenzbewegungen von Bergbauwänden in der Salzmine hervorgerufen wurden und dadurch die natürlich deformierten Mirkostukturen überprägen.
Hoch deformierte extrusive Salzgesteine aus Iran beinhalten gering-mächtige Scherzonen. Die Mikrostrukturen in diesen Proben sind im Wesentlichen durch Drucklösungsprozesse entstanden. In diesem Gefüge vorhandene Porphyroklasten weisen zahlreiche Subkörner auf, die vermutlich durch Versetzungsklettern im Kristallgitter der Salzkristalle noch vor dem Salzaustritt an die Erdoberfläche entstanden. Orientierungsmessungen (EBSD) zeigen, dass in diesen Proben Korngrößen-Reduktion durch Subkornrotationsrekristallisation und vermutlich durch Kristallneuwachstum während der Aufwärtsbewegung des Salzes stattfand.
Anhand von Paleo-Piezometriemessungen an Subkörnern ergibt sich eine Differenzialspannung von < 2 MPa für fast alle untersuchten Proben, ausgenommen den Salz-Extrusiva aus dem Iran. In diesen Proben wurde eine Differenzialspannung von ca. 3 MPa gemessen, welche sehr wahrscheinlich die Bedingungen im Diapirbereich eines Salzstockes widerspiegelt.

Table of contents

Chapter 1: Introduction, definition of problems and aims

1 Introduction

Properties of rocksalt are extensively discussed in the scientific and industrial literature. The fluid sealing capacity, its role in sedimentary basin evolution, drilling problems in exploration industry, the possibility of waste disposal in salt mines, saltmining; give the topic enormous economic importance and emphasize the need for the proper knowledge of the mechanical properties of halite rocks deforming in nature. In addition, salt is useful as an analogue for understanding the microstructural processes and texture development in silicate rocks (Drury and Urai, 1990).

Quantitative understanding of salt tectonics is only possible when complete mechanical models can be constructed and tested (Pollard and Fletcher, 2005), and these require accurate description of the mechanical properties of the materials involved. This poses a fascinating scientific challenge. Conditions of deformation can be deduced from deformation microstructures and mechanisms because they imply particular relations between stress, strain rate, strain, temperature and fluids. The stress-strain rate relationship for flow accommodated by various deformation mechansisms (e.g. crystal plastic, diffusion) is given by flaw laws. From laboratory experiments and theories of material deformation these relations can be obtained. These laws are necessary tools for interpreting and modelling a given structure but they are based on short-term, high stress laboratory tests thus they have their limitations when extrapolated to low stress, long-term natural conditions. The key for the extrapolation is the correspondence between deformation mechanisms in nature and experiment. Analysis of microstructures may offer a solution to that problem. If the deformation microstructure and mechanism can be identified in nature that correspond to that in experiment, then laboratory results can be more confidently extrapolated. Observations on microstructures of naturally deformed salt have to be interpreted carefully, as these are commonly superposition of microstructures developed at different time during the complex evolution.

2 Scope

In order to gain quantitative insight into salt tectonic processes and to model such processes either numerically or using physical analogue techniques appropriate data on the flow properties of rocksalt and the underlying deformation mechanisms are needed. This contribution examines the state-of-the-art in this field focusing on deformation, recrystallization and fluid transport properties of a variety of naturally deformed rocksalt. Tools used for the analysis involve simple microtectonic methods: transmitted and reflected light microscopy of gamma-irradiated thin sections and orientation measurements with EBSD. Since we lack of extensive studies on naturally deformed rocksalts, this work is therefore a description of microstructures in the light of our recent laboratory-tests-based knowledge on rocksalt deformation.

Where it was possible, based on combination of microstructures and geological history, possible microstructure evolution path for the studied locations is also given.

3 Background and previous work

Due to its cubic symmetry and usually large grain size, halite cannot be studied by the same techniques as used for most other minerals and studies of textures and microstructures are less advanced. Although the main types of textures and microstructures in halite are documented and the basic deformation mechanisms are understood, much remains to be learned about the deformation, recrystallization and texture development in halite in nature. One of the reasons for this is that very few studies have integrated the available techniques and microtectonic studies on halite are not as advanced as those on silicate and carbonate rocks (Vernon, 1976; Humphreys and Hatherly, 1996; Vernon, 2004; Passchier and Trouw, 2005).

3.1 Deposition of halite rocks

Evaporitic sequences are being deposited in some recent environments, though the amount of deposited salt is considerably smaller than that in the ancient deposits, implying that they are not necessarily good analogues when interpreting salt textures in ancient deposits (Warren, 2006). Although there is a controversy in the literature, it is generally agreed that there are two types of salt sequences; cyclic sequences with thin beds of impure halite deposited in ephemeral brines on shelves (e.g. most of the Zechstein) and thick beds of pure salt that probably formed in deep permanent brines in marine environment (e.g. some part of the Zechstein). The first type is comparatively well known the second has a less well known origin (Kendall and Harwood, 1996).

Modern ephemeral and desiccated salinas produce brine-pan sequences and are good analogues for microstructural evolution of many ancient, shallow-water deposits. A common sedimentary feature of salt in such an environment is the frequent rhythmic variation in grain size and in secondary mineral content such as anhydrite, polyhalite due to alteration in water depth (Shearman, 1970; Lowenstein and Hardie, 1985). The cycle invariably starts with intercalation of gypsum/anhydrite and polyhalite in the deep-water (depth of 1-2 m) stage, which is subsequently overlie with a fine-grained layer (grain size 1 mm), in turn which is overgrown with coarser crystals (5-20 mm). The anhydrite, polyhalite and fine-grained layer is usually thin (few mm thick), while the coarser grained layer makes up the rest of such a cycle. The thickness of a complete cycle ranges from a few cm to 20 cm. A characteristic microstructure for this type of salt is the presence of inclusion-rich grains truncated by fluid-inclusion-free, clear halite-filled cavities and dissolution surfaces (Lowenstein and Hardie, 1985).

Detailed studies on recent rocksalt also showed that as the deposited sequence is buried, after some 50 m all the pores are filled out with clear, fluid-inclusion-free halite (Casas and Lowenstein, 1989).

The syndepositional processes are not well known in deep water marine environment. Fine-grained halite laminites built up of sunken surface nucleated rafts (“rain from heaven”) are interpreted to have formed in such an environment (Warren, 2006). Other potentially characteristic microstructure in deep-water environment is based on studies of the Dead Sea, where it has been showed that dm large clear, idiomorphic halite grains grow at the bottom of the

sea (Warren pers. comm.). Similar coarse-grained, presumably primary halite can also be found in some parts of the Zechstein as well.

3.2 Deformation mechanisms and rheology of halite

In the last decades, numerous experimental studies have been conducted on the steady state and near steady state deformation behaviour of natural rocksalt at low temperature conditions (20-200 °C) relevant to salt tectonics. Several deformation mechanisms have been reported (Fig. 1). At room temperature and low effective pressure crystal plasticity is usually accompanied by microcracking and semi-brittle processes (Fig. 1) (Peach et al., 2001; Popp et al., 2001). Even at room temperature, dislocation creep processes accompanied by dynamic recrystallization become active in coarse-grained wet salt (Carter et al., 1993; Schenk and Urai, 2004). A characteristic microstructure for dislocation processes in halite is the presence of subgrains and slip bands (Senseny et al., 1992). Dynamic recrystallization is greatly enhanced by small amounts of water in the grain boundaries, although the detailed nanoscale structure of these boundaries is not well known (Rutter, 1976; Hickman and Evans, 1991; Renard and Ortoleva, 1997; Schutjens and Spiers, 1999; den Brok et al., 2002; Schenk et al., 2006).
The vast amount of experimental creep data shows that there is a significant factor of 100-1000 variation in creep strength for different types of natural salt rocks (e.g. Hunsche et al., 2003). Differences in chemistry, water content, second phases and deformation history is accounted for those variations. It has been experimentally demonstrated that samples containing K^+, Ca^{2+} and Mg^{2+} ions in solid solution have substantially different behaviour as predicted by theory (Heard and Ryerson, 1986). The solid solution hardening can be attributed to the interaction between the moving dislocation and the local elastic strain in the crystal lattice produced by substitution cations having different radii than that of Na^+.

In sufficiently fine-grained wet halite, solution-precipitation (Spiers et al., 1990) creep can become the dominant deformation mechanism. Solution-precipitation creep in halite is a well-documented process. (Dysthe et al., 2002; Ford et al., 2004; Ford and Wheeler, 2004; Gratier et al., 2003; Gratier et al., 2002; Gratier and Guiguet, 1986; Hickman and Evans, 1991; Renard et al., 2001; Schutjens, 1991; Spiers et al., 1990; Spiers and Schutjens, 1990; Wheeler, 1992).
The process has been studied as an important component of densification creep in backfills of waste repositories, and as an analogue for similar processes in silicates, which are much slower and more difficult to study. The experiments reveal a wide variety of rates and microstructures, depending on subtle differences in conditions. Especially important is the structure of the brine phase in the grain boundaries, which must be present to allow the rapid deformation observed. Under some conditions these brine-containing grain boundaries are stable but under certain conditions of orientation, stress and grain boundary curvature they are unstable; contact healing produces a solid-solid interface between fluid inclusions, and a many orders of magnitude drop in strain rate.

Various creep laws are available which adequately describe the observed behaviour (Fig. 2). Data on subgrain size and recrystallized grain size versus flow stress are also available for the dislocation creep regime with potential applications as paleostress and even in-situ stress indicators (Carter et al., 1993; Franssen, 1993). Combining the flow laws for the different

mechanisms behaviour leads to a multi-mechanism creep equation and deformation map for rocksalt (Spiers and Carter, 1998). The maps suggest that under natural conditions flow will occur either by climb-controlled creep (coarse grained domal salt) or pressure solution (salt glacier), or by both. The maps also imply that the effective viscosity of salt during natural flow falls in the range 10^{16}-10^{20} Pa·s.

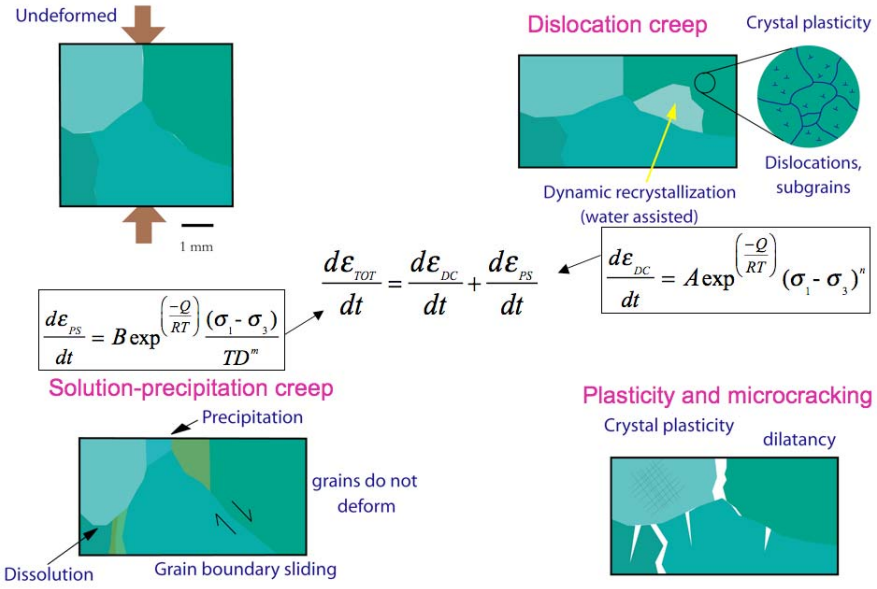

Fig. 1. Deformation mechanisms and corresponding constitutive laws for halite (Urai, 1993). Note that the plasticity and microcracking was observed very rarely in naturally deformed salts.

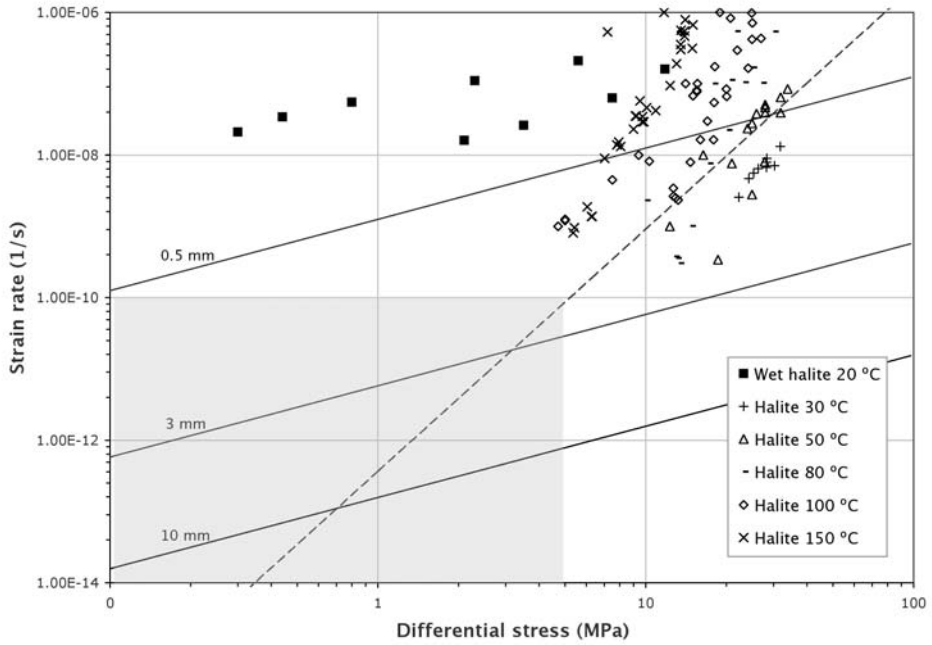

Fig. 2. Experimental data on the rheology of halite (Hansen and Mellegard, 1980; Hansen and Carter, 1984; Handin et al., 1986; Spiers et al., 1986; Senseny, 1988; Horseman and Handin, 1990; Horseman et al., 1992; Hunsche et al., 2003). The dashed line represents creep law for dislocation creep (T = 50 °C, Carter et al., 1993). The continuous lines represent extrapolation of experimental data from fine grained halite where solu-

tion-precipitation creep is dominant, to larger grain sizes, at T=50ºC, (Spiers et al., 1990). The grain size in natural rocksalt is usually larger than 0.5 mm. The grey shaded area represents the deformation conditions in nature for rocksalt.

3.3 Texture and microstructure development

In naturally deformed salt grain shapes usually show at least a weak anisotropy (Jackson, 1985). Grains are frequently elongated parallel to the foliation and grain aspect ratios can be up to 6 but are usually much lower, around 1.5. The shape of the grains is usually interpreted to not correspond to the finite strain ellipsoid of the salt due to recrystallization. Crystallographic preferred orientations (texture, CPO) are usually present in naturally and experimentally deformed salt.

Orientation measurements can be done in thin sections with a modified U-stage, after exposing the thin section to a thermal shock to generate cleavage cracks that are measured (Schwerdtner, 1968).

Alternatively, large volume samples can be measured using neutron diffraction (Scheffzük, 1998). This method is accurate but only allows determination of the bulk fabric without information of the individual grains.

One of the techniques which have made a large impact in recent years is EBSD that allows imaging the orientation of micrometer-sized local areas (Prior et al., 1999; Trimby et al., 2000b; Wheeler et al., 2001; Prior et al., 2002). This technique allows determination of full crystallographic orientation of individual grains and has widely been applied to experimentally deformed halite. Measurements on rocksalt deformed in dry/wet conditions showed that in the dry samples a strong CPO develops, together with a few degree of misorientations in between the subgrains (Trimby et al., 2000a; Trimby et al., 2000b). In the wet samples (water content > 10 ppm) the lack of strong CPO is explained by the continuous fluid-assisted grain boundary migration together with solution-precipitation creep, which prohibits the development of CPO.

According to Skrotzki (1994) in experimentally deformed salt the textures reflect the symmetry of the deformation, as expected. In salt domes textures often are present as a pronounced <110> fibre texture with the orientation of the fibre axis unrelated to the orientation of the foliation. The current interpretation is that the textures are formed by a flow field similar to that in an extrusion process, accompanied by dynamic recrystallization.

Etching of salt samples is an old technique, but still remains one of the basic elements of microstructural studies on rocksalt. It reveals the dislocation structures in the sample (grain and subgrain boundaries). Gamma-irradiation is a relatively new technique to decorate the microstructures in halite (Urai et al., 1987; Garcia Celma and Donker, 1996). The technique is based on the inhomogeneous distribution of colouring induced by irradiating the samples with high doses of gamma rays. Thin sections show a surprisingly rich detail of microstructure (grain, subgrain boundaries and zonation), which can be used to obtain information on the deformation, recrystallization and fluid transport processes in the samples. Gamma-irradiation decorated growth bands are common structures in salt samples (Urai et al., 1986; Urai et al., 1987). These bands are interpreted to reflect differences in chemistry of grain boundary fluids and show the former position of the grain boundaries and thus help to unravel how the grains have rotated during deformation.

3.4 Fluid transport processes

Permeability of domal halite is low. This has been shown by extensive studies of transport properties in the laboratory, by the performance of gas storage caverns and is demonstrated by halite being a seal for large hydrocarbon columns and fluid pressure cells.

After the deposition of halite-dominated sequence its syndepositional alteration and cementation continues as long as permeability exists. Study of Casas and Lowenstein (1989) on Quaternary halite deposition showed that the effective porosity and permeability decreases drastically in shallow subsurface. After about 50 m of burial the halite is nearly completely cemented and is without any visible porosity. At the depth of 100 m the halite is tight, entirely cemented and has no measurable permeability. This very low permeability is maintained during halokinesis, although there are some processes, which can lead to the increase in permeability.

Permeability of halite can increase by many orders of magnitude if deformation at low temperature and mean effective stress leads to microcracking and dilatancy (Popp et al., 2001). This effect is well documented in the walls of underground openings in salt but is thought to be much less important during deformation in nature. Conditions under which such processes might operate in the subsurface have been discussed by Fokker (1995) who considered the long term evolution of salt permeability after abandonment of solution mining caverns. He showed that when fluid pressures in the cavern approach lithostatic due to creep convergence the permeability of the salt increases and allows slow escape of the fluids. Similar high-pressure fluid pockets are quite common in salt, these are presumably also slowly moving upwards by similar processes.

A different process leading to increased permeability of salt was reported by Lewis and Holness (1996), who measured the equilibrium water-halite dihedral angles in grain boundary triple junctions. At low temperatures these were higher than 60°, such that the small amounts of brine present in the salt are distributed in micrometer-size isolated fluid inclusions, dramatically reducing the permeability. At temperatures above 100 °C and pressures of 70 MPa this value decreases below 60°, leading to a redistribution of the fluid into a thermodynamically stable network of connected, fluid filled channels at grain boundary triple junctions, dramatically increasing the permeability.

Another process which might lead to increase in premeability was proposed by Lux (2005) who found in experiments that hydrofracturing occurred when the fluid pressure significantly exceeded σ_3, while diffuse dilatancy occurred with dilated grain boundaries when the fluid pressure was only slightly larger than σ_3. Schoenherr et al., 2005, who analyzed halite microstructures from vicinity of oil fields of the Oman salt basin and found oil entrapped along cleavage planes and at grain boundaries in halite. They suggested that in the presence of high fluid pressure the effective stress was decreased in the salt so that diffuse dilatancy was reached. They added that the presence of oil as inclusions inside halite grains implies that fluid entrapment was subsequently followed by deformation and recrystallization.

3.5 Numerical modelling of evaporite deformation

3.5.1 Large scale (salt tectonics)

Building on geometric and kinematic reconstructions, study of the dynamics of salt structures and associated sediments has made rapid progress in the past two decades (Jackson, 1995). The rapidly developing area of research of salt tectonics modelling highlights the urgent need for realistic rheological data on sedimentary overburden rocks and for data for salt rheology in different tectonic settings. In recent years numerical models has started to produce quite realistic results; however much remains to be done until the full mechanical complexity of salt tectonic systems is properly modelled. Existing works commonly use Finite Element techniques (Last, 1988; van Keken et al., 1993; Podladchikov et al., 1993; Daudré and Cloetingh, 1994; Ismail-Zadeh et al., 2001; Kraus and Podladchikov, 2001; Schultz-Ela and Walsh, 2002; Gemmer et al., 2004), however the technique has its disadvantages which are the numerical problems with modelling localization of deformation, with poorly constrained initial conditions and controversy on the appropriate rheologies.

To date, almost all work has been in 2D, concentrating on forward modelling of systems at different scales and incorporating different levels of complexity – though still strongly simplified – in different parts of the models. Some models try to incorporate realistic two-component rheology of the salt, while others use simple, temperature independent rheology. Some other models focus on a detailed description of the stress field in applied studies of hydrocarbon reservoirs around salt structures but only consider small-scale deformations. In some models the rheology of the overburden is modelled as frictional-plastic with attempts to consider localized deformation, while some other models assume linear viscous overburden. Most models results in features, which are in some certain aspects comparable with the natural counterpart, however at this moment it is not entirely clear how the combination of simplifications at different stages of the modelling might interact.

3.5.2 Small scale (deformation mechanisms at the grain scale)

In the last two decades one of the most important developments in materials science is the availability of numerical models. Using these models our understanding moved from the qualitative description of natural processes towards the quantitative description. The ability to unravel the microstructural history of salt samples is an important control on our understanding of the larger scale history of a salt body. The Elle simulation platform allows the simulation of a range of simple and coupled grain scale processes (Jessell et al., 2001; Piazolo et al., 2001; Piazolo et al., 2002; Jessell et al., 2003), but application of this technique to halite is still in its infancy.

4 Aims of this thesis

As it has been outlined above, the extrapolation of the laboratory experiments to natural conditions relies heavily on the correspondence between microprocesses in laboratory and nature. Although the microstructures of the laboratory experiments are well known, no systematic study is available on microstructures in naturally deformed rocksalts. The aim of this

thesis is to provide an improved and extensive description of deformation and recrystallization related microstructures of rocksalts of different age and deformation history. Thus this thesis focuses on salts ranging from bedded, slightly deformed salt to the highly deformed salt extrusions.
The specific aims of this thesis were:

- Study slightly deformed rocksalt with the aim to document the primary microstructures. The lack of accurate understanding of microstructures produced by primary (synsedimetary) processes might lead to erroneous or invalid interpretations of microstructures in deformed rocksalt.
- Investigate rocksalt from the vicinity of potash mineral layers, with the aim to get a better insight into the behaviour of the rocksalt when other, weaker phase is present. Commonly the potash mineral undergoes metamorphosis, which results in release of structural water. The effect of the released fluid on rocksalt is also investigated.
- Systematically analyze samples from highly deformed salt layers from salt diapir. That gives insights into the deformation mechanisms involved during large-scale halokinetic movement.
- Study the spectacular, highly deformed extrusive salts. These salt glaciers – after heavy rains – advance downhill with a geologically extremely high strain rate. There is no extensive microstructural analysis available on these glaciers that would clearly demonstrate what is the main deformation mechanism in the salt glaciers.

5 Overview of this thesis

In this Chapter 1, the problems and aims of this thesis are described. In Chapter 2 the microstructural processes in slightly deformed, bedded Röt rocksalt from Hengelo (The Netherlands) are studied. The emphasis is laid on the differentiation between primary (synsedimentary) microstructures and the deformation-related microstructures.
In Chapter 3 highly deformed Zechstein bedded rocksalt is analyzed from the Neuhof salt mine (Germany) and based on the observed microstructures the deformation mechanisms and fluid transport properties are discussed.
Chapter 4 describes Zechstein (Z4) rocksalt samples from the Klodawa salt mine (Poland) with the aim to distinguish between natural-deformation-related microstructures from those produced by mine-wall convergence.
Chapter 5 and 6 deal with microstructures in Eocene-Miocene extrusive salts from central Iran. The deformation mechanism in halite shear zones (Chapter 5) and the process, which leads to grain size reduction, (Chapter 6) are discussed.
Chapter 7 attempts to summarize the deformation and recrystallization mechanisms in different tectonic settings and tries to define a consistent set of rheologies during the evolution of a salt structure.
Most of the chapters contain an Appendix part, which include some more field and microstructure photos related to the material discussed in that chapter.
All the chapters are presented as self-standing entities, which has been published, submitted or intended to be published as separate papers. As a consequence, repetition of some parts was unavoidable.

6 Parts of this thesis which have been published

6.1 Articles

Schléder, Z., Urai, J. L., Nollet, S., Hilgers, C., In Press. Deformation and recrystallization mechanisms and fluid flow properties of rocksalt as evidenced by microstructures – a case study on Zechstein (Z1) rocksalt from Neuhof salt mine (Germany). International Journal of Earth Sciences.

Schléder, Z., Burliga, S., Urai, J. L., In Press. Dynamic and static recrystallization-related microstructures in halite samples from the Kłodawa salt wall (central Poland) as revealed by gamma-irradiation. Neues Jahrbuch für Mineralogie und Petrologie.

Schléder, Z., Urai, J. L., 2007. Deformation and recrystallization mechanisms in mylonitic shear zones in naturally deformed extrusive Eocene-Oligocene rocksalt from Eyvanekey plateau and Garmsar hills (central Iran). Journal of Structural Geology 29/2, 241-255.

Schleder, Z., Urai, J. L., 2005. Microstructural evolution of deformation- modified primary Halite from Hengelo, the Netherlands. International Journal of Earth Sciences 94(5-6), 941-956.

6.2 Conference proceedings

Kukla, P., Holland, M., Mohr, M., Schleder, Z., Schoenherr, J., Urai, J., in press. Fortschritte bei der Integration von strukturellen, sedimentären und analogen Simulationstechniken in der Erdöl-Geologie. Erdöl, Erdgas und Kohle.

Hilgers, C., Pennock, G., Schleder, Z., Burliga, S., Urai, J. L. 2006. Microstructures of fibrous halite veins. TSK 11, Goettingen, Germany.

Hilgers, C., Schleder, Z., Urai, J. L. 2006. Microstructures in halite veins and their implication on the bulk permeability of rock. 7th Middle East Geosciences Conference and Exhibition, March 27 -29.

Urai, J., Schoenherr, J., Schleder, Z., 2006. Rheology of Ara salt based on creep tests (unpublished report prepared for Shell), Geologie-Endogene Dynamik, Aachen, Germany.

Schleder, Z., Schoenherr, J., Nollet, S., Urai, J. L., Hilgers, C., Kukla, P., Littke, R. 2006. Limits to the sealing capacity of Halite. General Assembly, European Geosciences Union, Vienna, Austria, 02-07 April 2006.

Schleder, Z., Urai, J. L. 2005. Deformation and Recrystallization Mechanisms in Mylonitic Zones in Naturally Deformed Extrusive Salts From Garmsar Hills and Qum Kuh (Central Iran). AGU Fall Meeting, San Francisco, CA, United States, 3-9.12.2005.

Schleder, Z., Urai, J. L. 2005. Deformation mechanisms and fluid flow properties of rocksalt. 4. Rundgespraech DFG-Schwerpunktprogramm, Geseke, Germany, 30.11-02.12.2005, 72-74.

Schleder, Z., Urai, J. L., Kirch, D., Talbot, C., Hunsche, U. 2005. Deformation mechanisms in naturally deformaed extrusive salt from Iran. 15th Conference on Deformation mechanisms, Rheology and Tectonics, ETH Zürich, Zürich, Switzerland, 2-4.05.2005, 186.

Kukla, P. A., Holland, M., Mohr, M., Schleder, Z., Schoenherr, J., Urai, J. L. 2005. Fortschritte bei der Integration von strukturellen, sedimentären und analogen Simulationstechniken in der Erdöl-Geologie. Frühjahrstagung des DGMK-Fachbereichs 'Aufsuchung und Gewinnung', Celle, Germany, 28.-29. 04.2005, DGMK-Tagungsbericht, 2005-1, 83-93.

Schleder, Z., Burliga, S., Urai, J. L. 2004. Highly deformed rock salt from the Klodawa salt wall (Central Poland): a microtectonics study. GeoLeipzig, Leipzig, Germany, 29.09.-01.10.2004, Schriftenreihe der Deutschen Geologischen Gesellschaft, Heft 34, 60.

Urai, J. L., Schleder, Z., Wouter, v. d. Z. 2004. Squeezing salts: Review of relevant salt rheologies, models of flow around borehole and a case study of salt flow around a casing. "Squeezing Salts" - an expensive problem, Utrecht, The Netherlands, 05.11.2004.

Schleder, Z., Urai, J. L. 2004. Microstructural study on slightly deformed Röt salt samples from Hengelo, the Netherlands. 10. Symposium Tektonik - Strukturgeologie - Kristallingeologie TSK, Aachen, Germany, 31.03.-02.04.2004, Terra Nostra, Schriften der Alfred-Wegener-Stiftung, 2004/1, 83.

Schleder, Z., Burliga, S., Urai, J. L. 2004. Microstructures of Halite from highly strained rocks in Klodawa salt wall, central Poland. EGU - 1st General Assembly, Nice, France, 25.-30.04.2004, Geophysical Reseach Abstracts, 238.

Schleder, Z., Urai, J. L. 2004. Recrystallization modified primary halite from the Middle Triassic Röt formation at Hengelo, the Netherlands. 3. Rundgespraech DFG-Schwerpunktprogramm, Geseke, Germany, 01.-03.12.2004, 72-74.

Schleder, Z., Urai, J., 2003. Estimation of the creep strength of Halite in core samples from the South Oman salt basin based on chemical analyses of impurity doping (unpublished report prepared for Shell), Geologie-Endogene Dynamik, Aachen, Germany.

Schleder, Z., Urai, J. L. 2003. Deformation and transport processes in halite. First results and outlook for further work. SPP 1135 Workshop: Temperaturentwicklung, KW-Systeme, Fluide und Salze, Hannover, Germany, 18.06.2003.

Schleder, Z., Urai, J. L. 2003. Microtectonic study on Halite samples from Central-European Basin. 2. Rundgespraech DFG-Schwerpunktprogramm, Bonn, Germany, 03.-05.12.2003.

Urai, J. L., Schleder, Z. 2002. Deformation and transport processes in halite: a microtectonics study - project overview. 1. Rundgespraech DFG-Schwerpunktprogramm, Schloss Eringerfeld, Geseke, Germany, 28.-29.11.2002.

References

Carter, N. L., Horseman, S. T., Russell, J. E., Handin, J., 1993. Rheology of rocksalt. Journal of Structural Geology 15(9-10), 1257-1271.

Casas, E., Lowenstein, T. K., 1989. Diagenesis od saline pan halite: comparison of petrographic features of modern, Quaternary and Permian halites. Journal of Sedimentary Petrology 59(5), 724-739.

Daudré, B., Cloetingh, S., 1994. Numerical modelling of salt diapirism: influence of the tectonic regime. Tectonophysics 240(59-79).

den Brok, B., Morel, J., Zahid, M. 2002. In situ experimental study of roughness development at a stressed solid/fluid interface. In: de Meer, S., Drury, M. R., de Bresser, H. & Pennock, G. M. (Eds.), Geological Society Special Publications 200. Geological Society of London: London, United Kingdom, United Kingdom, 73-83.

Drury, M. R., Urai, J. L., 1990. Deformation-related recrystallization processes. Tectonophysics 172, 235-253.

Dysthe, D., Renard, F., Porcheron, F., B., R., 2002. Water in mineral interfaces - molecular simulations of structure and diffusion. Geophysical Research Letters 29, 13208-13211.

Fokker, P. A. 1995. The behaviour of salt and salt caverns, TU Delft.

Ford, J. M., Ford, N. J., Wheeler, J., 2004. Simulation of grain boundary diffusion creep: analysis of some new numerical techniques. Proceedings of the Royal Society of London Series A 460, 2395-2413.

Ford, J. M., Wheeler, J., 2004. Modelling interface diffusion creep in two-phase materials. Acta Materialia 52, 2365-2376.

Franssen, R. C. M. W. 1993. Rheology of Synthetic Rocksalt with Emphasis on the Influence of Deformation History and Geometry on the Flow Behaviour, Rijksuniversiteit Utrecht.

Garcia Celma, A., Donker, H. (Editors), 1996. The Effect of Gamma Radiation in Salt, EUR-Report 16743EN.

Gemmer, L., Ings, S. J., Medvedev, S., Beaumont, C., 2004. Salt tectonics driven by differential sediment loading: Stability analysis and finite element experiments. Basin Research 16, 199-218.

Gratier, J. P., Favreau, P., Renard, F., 2003. Modelling fluid transfer along Californian faults when integrating pressure solution crack-sealing and compaction processes. Journal of Geophysical Research 108(B2), 2104.

Gratier, J. P., Favreau, P., Renard, F., Pili, E., 2002. Fluid pressure evolution during the earthquake cycle controlled by fluid flow and pressure solution crack sealing. Earth, Planets and Space 54, 1139-1146.

Gratier, J. P., Guiguet, R., 1986. Experimental pressure solution-deposition on quartz grains: the crucial effect of the nature of the fluid. Journal of Structural Geology 8(8), 845-855.

Handin, J., Russell, J. E., Carter, N. L. 1986. Experimental deformation of rocksalt. In: Hobbs, B. E. & Heard, H. C. (Eds.), Mineral and rock deformation: laboratory studies. AGU Geophysical Monograph 36. American Geophysical Union, 161-199.

Hansen, F. D., Carter, N. L. 1984. Creep of Avery Island rocksalt. Proceedings of the first Conference on mechanical Behavior of Salt, Clausthal-Zellerfeld, Germany, Trans. Tech. Publications, 53-69.

Hansen, F. D., Mellegard, K. D., 1980. Quasi-static strength and deformational characeristic of domal salt from Avery Island, Lousiana. ONWI-116, Report prepared by RE/SPEC Inc. for Office of Nuclear Waste Isolation.

Heard, H. C., Ryerson, F. J. 1986. Effect of cation impurities on steady-state flow of salt. In: Hobbs, B. E. & Heard, H. C. (Eds.), Mineral and rock deformation: laboratory studies. AGU Geophysical Monograph 36. American Geophysical Union, 99-115.

Hickman, S. H., Evans, B., 1991. Experimental pressure solution in halite; the effect of grain/interphase boundary structure. Journal of the Geological Society 148, 549-560.

Horseman, S. T., Handin, J. 1990. Triaxial compression tests on rocksalt at temperatures from 50 °C to 200 °C and strain rates from 10−4 to 10−9 1/s. In: Duba, A. G., Durham, W. B., Handin, J. W. & Wang, H. F. (Eds.), The brittle-ductile transition in rocks 56. American Geophysical Union, Washington, DC, United States, 103-110.

Horseman, S. T., Russell, J. E. H., J., Carter, N. L. 1992. Slow experimental deformation of Avery Island salt. Proceedings of the Seventh Internation Symposium on salt, Kyoto, Japan, April 6-9 1992, Elsevier, Amsterdam, 1, 67-74.

Humphreys, F. J., Hatherly, M. 1996. Recrystallization and related annealing phenomena. Pergamon, p 497

Hunsche, U., Schulze, O., Walter, F., Plischke, I., 2003. Projekt Gorleben. Thermomechanisches Verhalten von Salzgestein. 9G2138110000, BGR, Hannover.

Ismail-Zadeh, A. T., Talbot, C. J., Volozh, Y. A., 2001. Dynamic restoration of profiles across diapiric salt structures: numerical approach and its applications. Tectonophysics 337(1-2), 23-38.

Jackson, M. P. A., 1985. Natural strain in diapiric and glacial rock salt, with emphasis on Oakwood dome, East Texas, Bureau of Economic Geology, The University of Texas at Austin, Texas.

Jackson, M. P. A. 1995. Retrospective salt tectonics. In: Jackson, M. P. A., Roberts, D. G. & Snelson, S. (Eds.), Salt tectonics: a global perspective. AAPG Memoir 65, 77-108.

Jessell, M., Bons, P., Evans, L., Barr, T., Stuwe, K., 2001. Elle: the numerical simulation of metamorphic and deformation microstructures. Computers & Geosciences 27(1), 17-30.

Jessell, M. W., Kostenko, O., Jamtveit, B., 2003. The preservation potential of microstructures during static grain growth. Journal of metamorphic Geology 21, 481-491.

Kendall, A. C., Harwood, G. M. 1996. Marine evaporites: arid shorelines and basins. In: Reading, H. G. (Ed.), Sedimentary Environments: Processes, Facies and Stratigraphy. Blackwell, 281-324.

Kraus, B. J., Podladchikov, Y. Y., 2001. Forward and reverse modelling of the three-dimensional viscous Rayleigh-Taylor instability. Geophysical Research Letters 28(6), 1095-1098.

Last, N. C. 1988. Deformation of a sedimentary overburden on a slowly creeping substratum. In: Swoboda, G. S. (Ed.), Numerical Methods in Geomechanics, 577-585.

Lewis, S., Holness, M., 1996. Equilibrium halite-H2O dihedral angles: High rock-salt permeability in the shallow crust? Geology 24(5), 431-434.

Lowenstein, T. K., Hardie, L. A., 1985. Criteria for the recognition of salt-pan evaporites. Sedimentology 32, 627-644.

Lux, K.-H., 2005. Long-term behaviour of sealed liquid-filled salt cavities - A new approach for physical modelling and numerical simulation - Basics from theory and lab investigations. Erdöl Erdgas Kohle 121, 414-422.

Passchier, C. W., Trouw, R. A. J. 2005. Microtectonics. Springer, 366

Peach, C., Spiers, C. J., Trimby, P. W., 2001. Effect of confining pressure on dilatation, recrystallization, and flow of rock salt at 150 °C. Journal of Geophysical Research 106(13315-13328).

Piazolo, S., Bons, P. D., Jessel, M. W., Evans, B., Passchier, C. W. 2002. Dominance of microstructural processes and their effect on microstructural development: Insight from numerical modelling of dynamic recrystallization. In: Meer, S. d., Drury, M. R., Bresser, J. H. P. d. & Pennock, G. M. (Eds.), Deformation Mechanisms, Rheology and Tectonics: Current Status and Future Perspectives. Geological Society Special Publication 200.

Piazolo, S., Jessel, M. W., Bons, P. D., Evans, L., 2001. Animations of dynamic recrystallization with the numerical modelling system Elle. Journal of virtual explorer 4, 45-49.

Podladchikov, Y. Y., Talbot, C. J., Poliakov, A., 1993. Numerical models of complex diapirs. Tectonophysics 228, 189-198.

Pollard, D. D., Fletcher, R. C. 2005. Fundamentals of structural geology. Cambridge University Press, 520

Popp, T., Kern, H., Schulze, O., 2001. Evolution if dilatancy and permeability in rock salt during hydrostatic compaction and triaxial deformation. Journal of Geophysical Research 106(B3), 4061-4078.

Prior, D. J., Boyle, A. P., Brenker, F., Cheadle, M., Day, A., Lopez, G., Peruzzo, L., Potts, G. J., Reddy, S., Spiess, R., Timms, N. E., Trimby, P. W., Wheeler, J., Zetterstrom, L., 1999. The application of electron backscatter diffraction and orientation contrast imaging in the SEM to textural prolems in rocks. American Mineralogist 84, 1741-1759.

Prior, D. J., Wheeler, J., Peruzzo, L., Spiess, R., Storey, C., 2002. Some garnet microstructures: an illustration of the potential of orintation maps and misorientation analysis in microstructural studies. 2002 24, 999-1011.

Renard, F., Dysthe, D., Feder, J., Bjørlykke, K., Jamtveit, B., 2001. Enhanced pressure solution creep rates induced by clay particles: Experimental evidence in salt aggregates. Geophysical Research Letters 28, 1295-1298.

Renard, F., Ortoleva, P., 1997. Water films at grain-grain contacts: Debye-Huckel, osmotic model of stress, salinity, and mineralogy dependence. Geochimica et Cosmochimica Acta 61(10), 1963-1970.

Rutter, E. H., 1976. The kinetics of rock deformation by pressure solution. Philosophical Transactions of the Royal Society of London A 283, 203-219.

Scheffzük, C. M. 1998. Neutronographische texturanalysen und Mikrostrukturuntersuchungen natürlicher und triaxialer verformter halite. Unpublished PhD thesis.

Schenk, O., Urai, J., Piazolo, S., 2006. Structure of grain boundaries in wet, synthetic polycrystalline, statically recrystallizing halite – evidence from cryo-SEM observations. Geofluids 6(1), 93-104.

Schenk, O., Urai, J. L., 2004. Microstructural evolution and grain boundary structure during static recrystallization in synthetic polycrystals of Sodium Chloride containing saturated brine. Contributions to Mineralogy and Petrology 146(6), 671-682.

Schoenherr, J., Urai, J. L., Littke, R., Kukla, P., Newall, M., Al-Abry, N., Larroque, J.-M. 2005. Hydrocarbon-bearing Halite in the Ara Group (South Oman Salt Basin). General Assembly, European Geosciences Union, Vienna, 24-29 April 2005, 692.

Schultz-Ela, D. D., Walsh, P., 2002. Modeling of grabens extending above evaporites in Canyonlands National Park, Utah. Journal of Structural Geology 24(2), 247-275.

Schutjens, P. 1991. Intergranular pressure solution in halite aggregates and quartz sands: an experimental investigation. Unpublished Ph.D. thesis, Universiteit Utrecht.

Schutjens, P., Spiers, C. J., 1999. Intergranular pressure solution in NaCl: Grain-to-grain contact experiments under the optical microscope. Oil & Gas Science and Technology - Rev 54(6), 729-750.

Schwerdtner, W. M., 1968. Intragranular gliding in domal salt. Tectonophysics 5(5), 353-380.

Senseny, P. E. 1988. Creep properties of four salt rocks. Proceedings of the Second Conference on mechanical Behavior of Salt, Clausthal-Zellerfeld, Germany, Trans. Tech. Publications, 431-444.

Senseny, P. E., Hansen, F. D., Russell, J. E., Carter, N. L., Handin, J., 1992. Mechanical behaviour of rock salt: phenomenology and micromechanisms. Int. J. Rock Mech. Min. Sci & Geomech. Abstr. 29(4), 363-378.

Shearman, D. J., 1970. Recent halite rock, Baja California, Mexico. Transaction of Mining and Metallurgy 79B, 155-162.

Skrotzki, W. 1994. Mechanisms of texture develompent in rocks. In: Bunge, H. J., Siegesmund, S., Skrotzki, W. & Weber, K. (Eds.), Texture of Geological Materials. DGM Informationsgesellschaft, Oberursel, 167-186.

Spiers, C. J., Carter, N. L. 1998. Microphysics of rocksalt flow in nature. Fourth Conference on the Mechanical behaviour of Salt, The Pennsylvania State University, June 17 and June 18, 1996, Trans Tech Publication Series on Rock and Soil Mechanics, 22, 115-128.

Spiers, C. J., Schutjens, P. 1990. Densification of crystalline aggregates by fluid phase diffusional creep. In: Barber, D. J. & Meredith, P. D. (Eds.), Deformation processes in minerals, ceramics and rocks. Unwin Hyman, 334-353.

Spiers, C. J., Schutjens, P. M., Brzesowsky, R. H., Peach, C. J., Liezenberg, J. L., Zwart, H. J. 1990. Experimental determination of constitutive parameters governing creep of rocksalt by pressure solution. In: Knipe, R. J. & Rutter, E. H. (Eds.), Deformation mechanisms, rheology and tectonics. Geological Society of London Special Publications 54, 215-227.

Spiers, C. J., Urai, J. L., Lister, G. S., Boland, J. N., Zwart, H. J., 1986. The influence of fluid-rock interaction on the rheology of salt rock, Department of Structural and Applied Geology, Institute of Earth Sciences, Sate of University of Utrecht, The Netherlands.

Trimby, P. W., Drury, M. R., Spiers, C. J., 2000a. Misorientations across etched boundaries in deformed rocksalt: a study using electron backscatter diffraction. Journal of Structural Geology 22, 81-89.

Trimby, P. W., Drury, M. R., Spiers, C. J., 2000b. Recognising the crystallographic signature of recrystallisation processes in deformed rocks: a study of experimentally deformed rocksalt. Journal of Structural Geology 22, 1609-1620.

Urai, J. L., 1993. The creep of rock salt. Advances in EP Research, 4-5.

Urai, J. L., Spiers, C. J., Peach, C., Franssen, R. C. M. W., Liezenberg, J. L., 1987. Deformation mechanisms operating in naturally deformed halite rocks as deduced from microstructural investigations. Geologie en Mijnbouw 66, 165-176.

Urai, J. L., Spiers, C. J., Zwart, H. J., Lister, G. S., 1986. Weakening of rocksalt by water during long term creep. Nature 324, 554-557.

van Keken, P. E., Spiers, C. J., van den Berg, A. P., Muyzert, E. J., 1993. The effective viscosity of rocksalt: implementation of steady-state creep laws in numerical models of salt diapirism. Tectonophysics 225(4), 457-476.

Vernon, R. 2004. A Practical guide to rock microstructure. Cambridge University Press, Cambridge, 594

Vernon, R. H. 1976. Metamorphic processes: reactions and microstructure development. Allen & Unwin Ltd, London, 247

Warren, J. 2006. Evaporites: sediments, resources and hydrocarbons. Springer, 1036

Wheeler, J., 1992. The importance of pressure solution and Coble creep in the deformation of polymineralic rocks. Journal of Geophysical Research 97, 579-4586.

Wheeler, J., Prior, D. J., Jiang, Z., Spiess, R., Trimby, P. W., 2001. The petrological significance of misorientation between grains. Contributions to Mineralogy and Petrology 141, 109-124.

Chapter 2: Microstructural evolution of deformation–modified primary halite from the Middle Triassic Röt Formation at Hengelo, the Netherlands *

Zsolt Schléder, János L. Urai

Abstract

The microstructure of halite from the subhorizontal, bedded Main Röt Evaporite Member at Hengelo, the Netherlands (AKZO well 382, depth interval of 420-460 m), was studied by transmitted and reflected light microscopy of gamma-irradiation decorated samples. Primary microstructures compare favourably with those found in recent ephemeral salt pans. Large, blocky, fluid-inclusion-poor halite grains and elongated chevrons are interpreted to have formed in the saline lake stage, while void-filling clear halite is interpreted to have formed during the desiccation stage of the salt pan. In addition, in all layers the grains are rich in deformation-related substructures such as slip bands and subgrains indicating strains of a few percent. The study of gamma-irradiation decorated thin sections shows that the main recrystallization mechanism is grain boundary migration. Grain boundary migration removes primary fluid inclusions and produces clear, strain-free new grains. Differential stresses as determined by subgrain size piezometry were 0.45 – 0.97 MPa. The deformation of the salt layers is probably related to Cretaceous inversion in the area.

Keywords: Hengelo (the Netherlands) – Triassic bedded rock salt – Synsedimentary structures – Deformation microstructures – Recrystallization

1 Introduction

The microstructure of natural rock salt is a product of a complex series of depositional, diagenetic and deformation processes. Depending on the relative importance of these, a wide range of microstructures can be formed, starting from the typical primary structures in young, shallow halite to the strongly deformed and completely recrystallized tectonites in salt diapirs. Although both synsedimentary and deformation-related microstructural processes are documented (e.g. Shearman, 1970; Lowenstein and Hardie, 1985; Urai et al., 1987; Casas and Lowenstein, 1989), details are not well understood, making the interpretation of halite microstructures difficult.

One commonly observed microstructure consists of composite halite grains locally rich in fluid inclusions, but also containing irregular patches of clear halite free of fluid inclusions.

* Schléder, Z., Urai, J. L., 2005. Microstructural evolution of deformation-modified primary halite from the Middle Triassic Röt Formation at Hengelo, The Netherlands. International Journal of Earth Sciences 94, 941-955.

Not uncommonly, the transition from fluid-inclusion-rich material to clear halite is defined by a sharp curved surface within single halite grains. One possible explanation for this structure is a syndepositional solution-reprecipitation process in ephemeral or shallow brine system (shallow enough to become undersaturated with respect to halite when diluted by floodwater). In an ephemeral salt pan environment, a flooding stage (when floodwater arrives and partly dissolves the existing halite crust) is followed by an evaporation stage, in which the irregularly dissolved halite framework is covered by a new layer of fluid-inclusion-rich grains. Finally, when the saline lake shrinks and dries out, clear halite slowly crystallizes in the dissolution voids from the residual groundwater brine (Lowenstein and Hardie, 1985).
After burial, if the halite is deformed and recrystallized, a similar patchy core-and-mantle structure can form by grain boundary migration, where the migrating grain boundaries erase primary fluid inclusion bands. Thus the presence of patches of clear halite in fluid inclusion-rich grains can also be explained by a deformation-induced recrystallization process (Urai et al., 1987).

This problem, i.e. distinguishing between primary and secondary features in halite, has been recognized by several authors (Wardlaw and Schwerdtner, 1966; Hardie et al., 1983; Roedder, 1984) but these authors did not provide criteria for distinguishing between microstructures resulting from deformation and those resulting from recrystallization.
The aim of this paper is to present a detailed microstructural analysis of bedded salt from a core taken near Hengelo, the Netherlands (Fig. 1), in an attempt to separate primary and deformation-related microstructures, and to quantify the paleostress in the salt sequence using subgrain size piezometry.

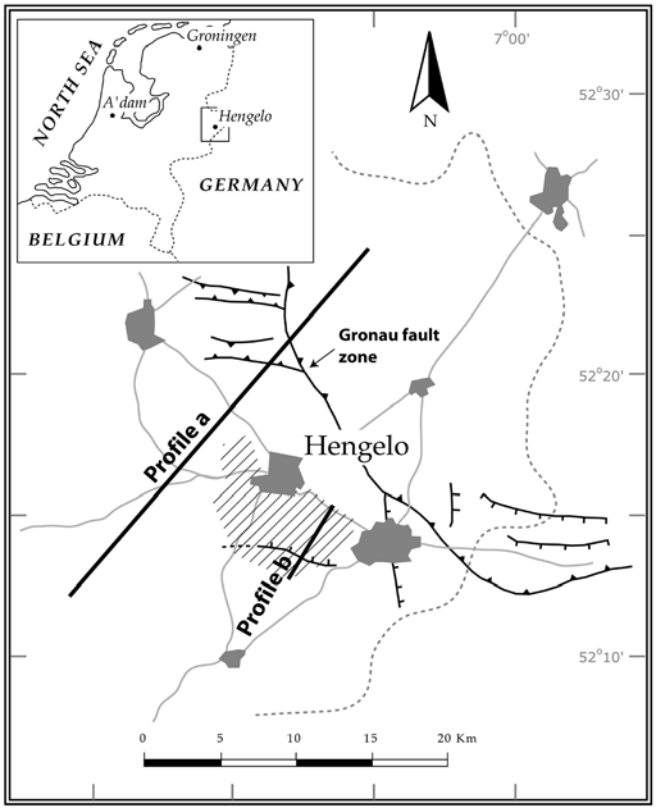

Fig. 1. Map of study area showing the Gronau fault zone (with Late Cretaceous movements) and approximate location of the normal fault in the study area (after Geluk and Duin, 1997; NITG, 1998; Doornenbal et al., 2002). The stippled polygon indicates the Twenthe-Rijn concession area.

2 Lithostratigraphy of the Röt strata and location of the study material

Samples described in this paper are from the Röt Formation in the Twenthe-Rijn concession area, where more than 400 wells have been drilled for solution mining since 1919. The Röt Formation (Early Anisian) comprises the strata between the Solling Formation and the Muschelkalk Formation (Geluk and Röhling, 1997) (Figs. 2 and 3). The Röt Formation is divided into two members. At the base lies the Main Röt Evaporite Member, which consists of four salt layers denoted by the Akzo Nobel company as salt A to D from bottom to top (Harsveldt, 1980; van Lange, 1994; Kovalevych et al., 2002). Salt layers A and C are the thickest (25 to 30 m), while layers B and D are only a few meters thick. The D salt layer is laterally discontinuous, developed as lenses in former topographic depressions. The salt layers are separated by 1 to 2 m thick shaly anhydritic mudstones and dolomitic claystones (Harsveldt, 1980; van Lange, 1994) (Fig. 3). Lateral variations in thickness of the Röt salt are interpreted as syndepositional, reflecting the relief of the underlying formation, and not due to salt tectonics (Harsveldt, 1980; van Lange, 1994). The depositional environment of the Main Röt Evaporite Member is interpreted as an enclosed sea with alternating periods of non-clastic (pure evaporite) deposition and increased sediment influx (RGD, 1993; van Lange, 1994; NITG, 1998). Above the Main Röt Evaporite Member lies the Upper Röt

Claystone Member, which is made up mainly of silty claystone with gypsum and anhydrite nodules (Fig. 3). The thickness of the Upper Röt Claystone Member is up to 200 m (van Lange, 1994; NITG, 1998).

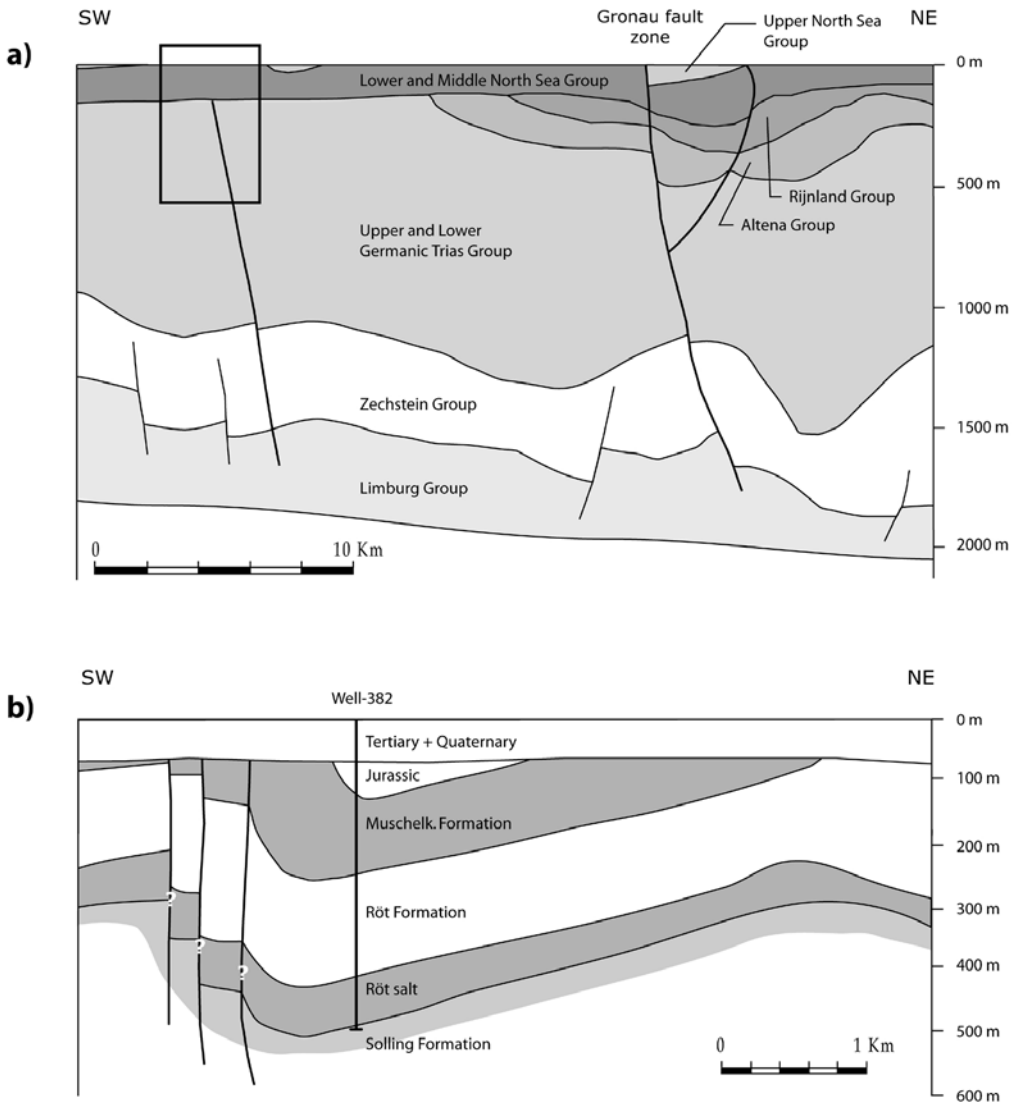

Fig. 2. a) A large-scale profile through the Twenthe-Rijn concession area. Note that displacement along faults can be traced from the Carboniferous basement (Limburg Group) up to the base of Tertiary. The approximate location of profile "b" is indicated by the rectangle. b) Profile through the Twenthe-Rijn concession area with the location of AKZO well 382 indicated. The profile is based on maps of Geluk and Duin (1997) and Doornenbal et al. (2002). For the position of the profiles see Fig. 1, and note that the positions are not identical.

The NW-SE trending Gronau fault zone, situated approximately 15 km NE of the study area, is the main structural element in the region (NITG, 1998, Figs. 1 and 2). Movement along the fault zone occurred since the Carboniferous and this zone has been reactivated in tectonic phases of Austurian and Saalian, Late Permian, Early-, and Late Kimmerian, Sub-Hercynian and Savian age (c.f. NITG, 1998 p. 112). At the local scale, within the Twenthe-Rijn concession area, a few NW-SE running faults with a maximum displacement of 50-100 m were reported (Harsveldt, 1980) (Fig. 2). Displacement along those faults can be traced up to the

base of Tertiary, although their structure within the salt layers is not clear (Geluk and Duin, 1997; Doornenbal et al., 2002b). The presence of these faults is probably related to Cretaceous inversion in the area (de Jager, 2003). The Tertiary is characterized by tectonic inactivity (de Jager, 2003).

In this paper we describe samples from AKZO well 382 in the Twenthe-Rijn concession area (Fig. 3). Samples were taken from the "A" salt layer (457.5 m), from the "C" salt layer (443.5 m and 430.9 m) and "D" salt layer (423.3 m). The diameter of the core was 10 cm; the length was between 10 cm and 15 cm. All photographs and illustrations presented in the paper are oriented with the top of the section toward the top of the page.

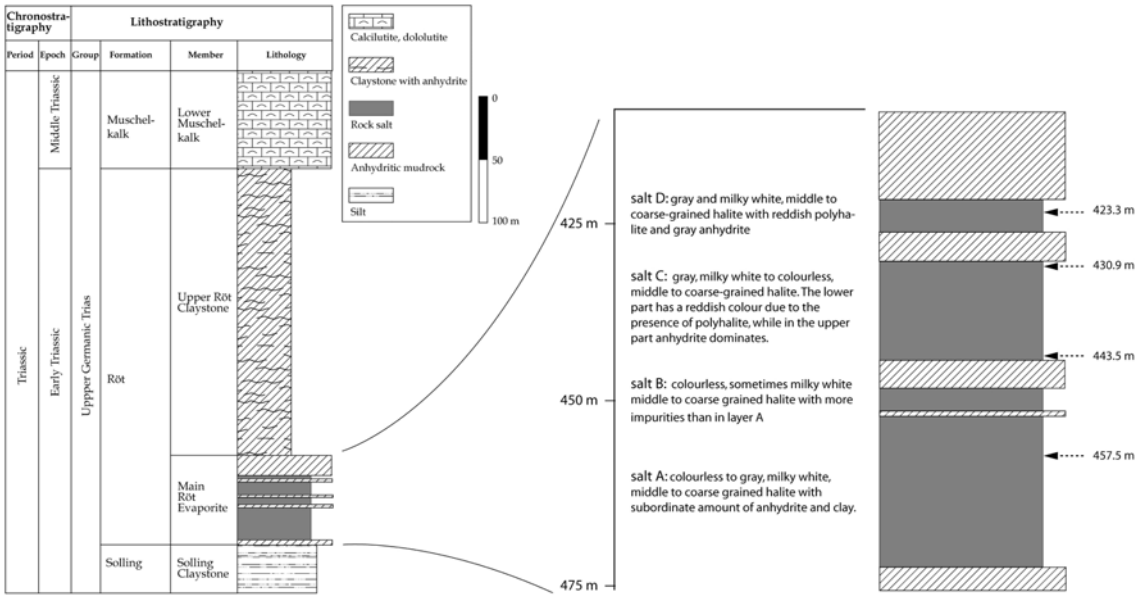

Fig. 3. Triassic lithostratigraphy of AKZO well 382 (after van Lange, 1994; Geluk and Duin, 1997). Arrows indicate the studied intervals.

3 Sample preparation and methods of study

We cut 2 x 5 x 8 cm slabs from the core, parallel to the core axis, using a diamond saw with a small amount of water (this prevents the development of microcracks in the halite, without causing significant dissolution artefacts perhaps due to the Joffé-effect, Joffé, 1928). Microstructures were decorated by gamma-irradiation in the Research Reactor of Forschungszentrum Jülich, using a technique similar to that described by Urai et al., 1985. Two sets of irradiations were carried out. One irradiation was done at a temperature of 35 °C with a dose rate between 1 kGy/h and 3 kGy/h to a total dose of about 1.5 MGy. The other set was done at a temperature of 100 °C with a dose rate between 4 kGy/h and 6 kGy/h to a total dose of about 4 MGy. Depending on the temperature of the gamma-irradiation the slabs became brown (35 °C) or blue coloured (100 °C). The colour intensity seen in the halite samples is heterogeneous, reflecting the heterogeneous distribution of solid solution impurities and other crystal defects in the halite grains (Przibram, 1954; van Opbroek and den Hartog, 1985; Urai et al., 1985; Garcia Celma and Donker, 1996). After irradiation the slabs were polished dry on grinding paper, etched with pure water for 2 seconds and quickly

dried with a tissue. This etching technique removes scratches and provides a micro-relief on the surface of the slabs improving the stability of mounting. The slabs were mounted on glass plates at room temperature using epoxy (Körapox 439), and were cut into thick sections of 4 mm using the wet cutting technique. The sections were then ground down to a thickness of 1 mm with grinding paper (dry) and finally etched using the method described by Urai et al., 1987. The thin sections were studied with reflected and transmitted, plane polarized light microscopy.

4 Petrography of the halite samples

Two types of halite occur in the samples: a milky, fluid-inclusion-rich halite that comprises up to 40 volume percent of the material, and a clear, fluid-inclusion-poor halite. The two types commonly occur together, with most halite grains having one or more milky cores surrounded by clear halite. Some of the grains have no apparent milky core, and consist entirely of clear halite. The milky core invariably has a banded structure: fluid-inclusion-rich bands alternate with fluid-inclusion-poor bands (Fig. 4). The fluid inclusion bands are about 200 to 400 µm thick and contain cubic (negative crystal form) fluid inclusions. The alternating fluid inclusion bands define chevrons, cubes and hoppers.

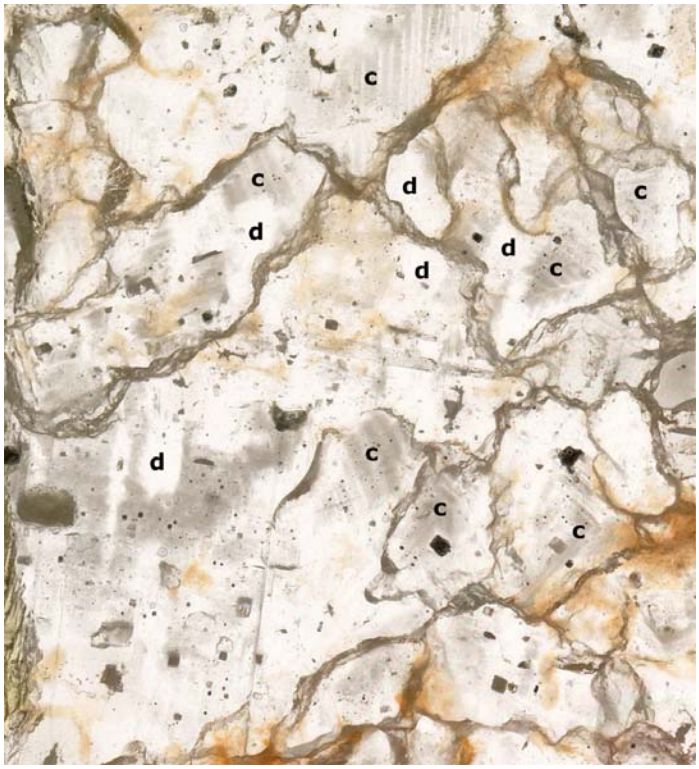

Fig. 4. Photomicrograph of an unirradiated sample (salt layer D, 423.3 m) showing primary fluid-inclusion-rich bands (c) and zones of clear halite (d). Clear halite commonly truncates fluid-inclusion-rich domains across sharp, curved, intracrystalline boundaries. Grain boundaries show up as dark curves in thin section. Secondary phases occurring at grain boundaries are anhydrite and polyhalite. Transmitted light image, image width is 2 cm.

Chevrons were found in the A, C and D (457.5 m, 443.5 m and 423.3 m) layers. The chevron halite grains are 0.5 cm to 2 cm long, vertically elongated grains, which are very often truncated or rimmed by clear halite (Fig. 5). Commonly, the clear rim comprises 50-70 volume percent of a chevron grain, rarely up to 90 percent. The transition from the milky, fluid-inclusion-rich core to the clear halite is defined by a sharp, curved surface (Fig. 5). In gamma-irradiated samples usually there is no difference in irradiation colour between the milky and clear halite within one grain (Fig. 6 and Appendix Fig. 2). In some cases the top of the chevrons is truncated by layers of anhydrite and polyhalite partings (Fig. 7).

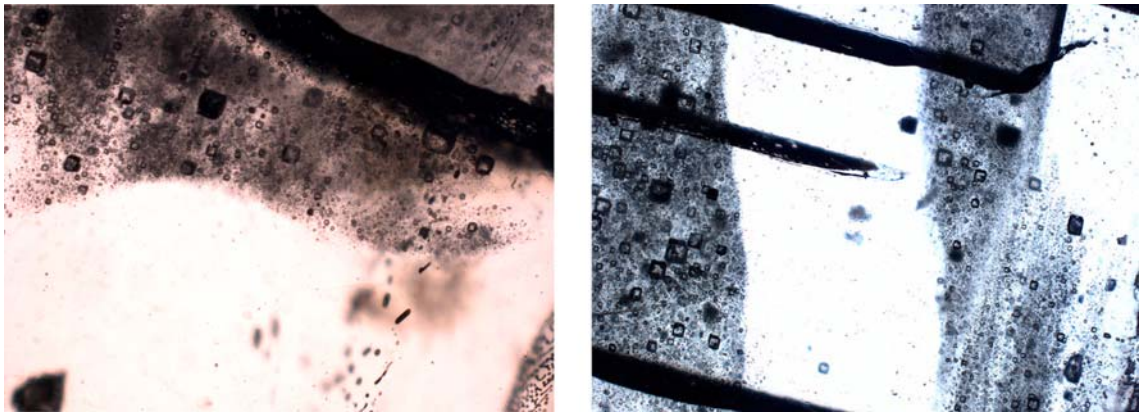

Fig. 5. Photomicrographs of halite from salt layer C (443.5 m) show sharp, commonly curved boundaries between milky, fluid-inclusion-rich and clear halite regions within a single grain. The black straight lines seen in the right hand side image are cleavage planes, introduced during sample preparation. Plane polarized, transmitted light images of unirradiated samples. Image width is 2.7 mm.

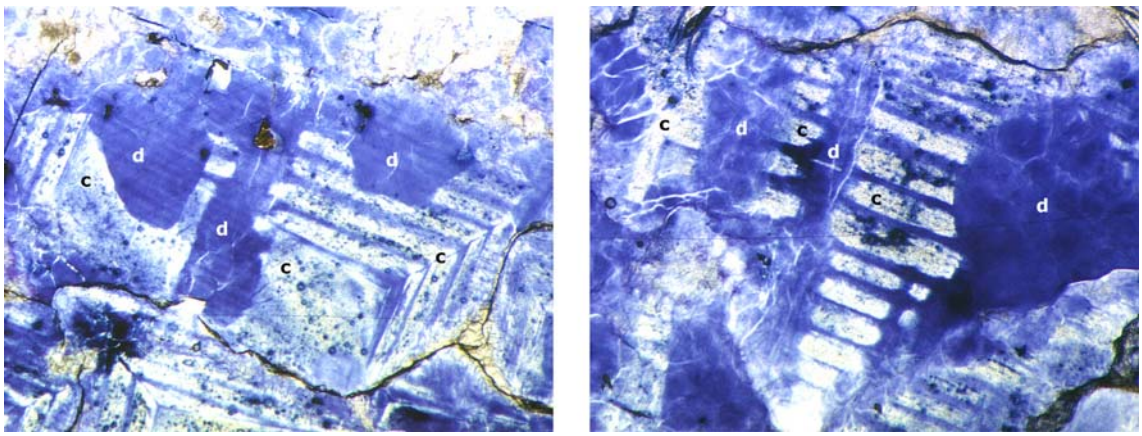

Fig. 6. Microstructure in halite from salt layer D (423.3 m). Fluid inclusion bands (c), truncated by clear halite (d). Note that individual fluid inclusion bands can be traced over the clear halite regions. This microstructure compares well with those produced by dissolution-reprecipitation processes in present-day salt pan halites (c.f. Shearman, 1970; Lowenstein and Hardie, 1985). Plane polarized, transmitted light images of samples irradiated at 100 °C. Image width is 7 mm.

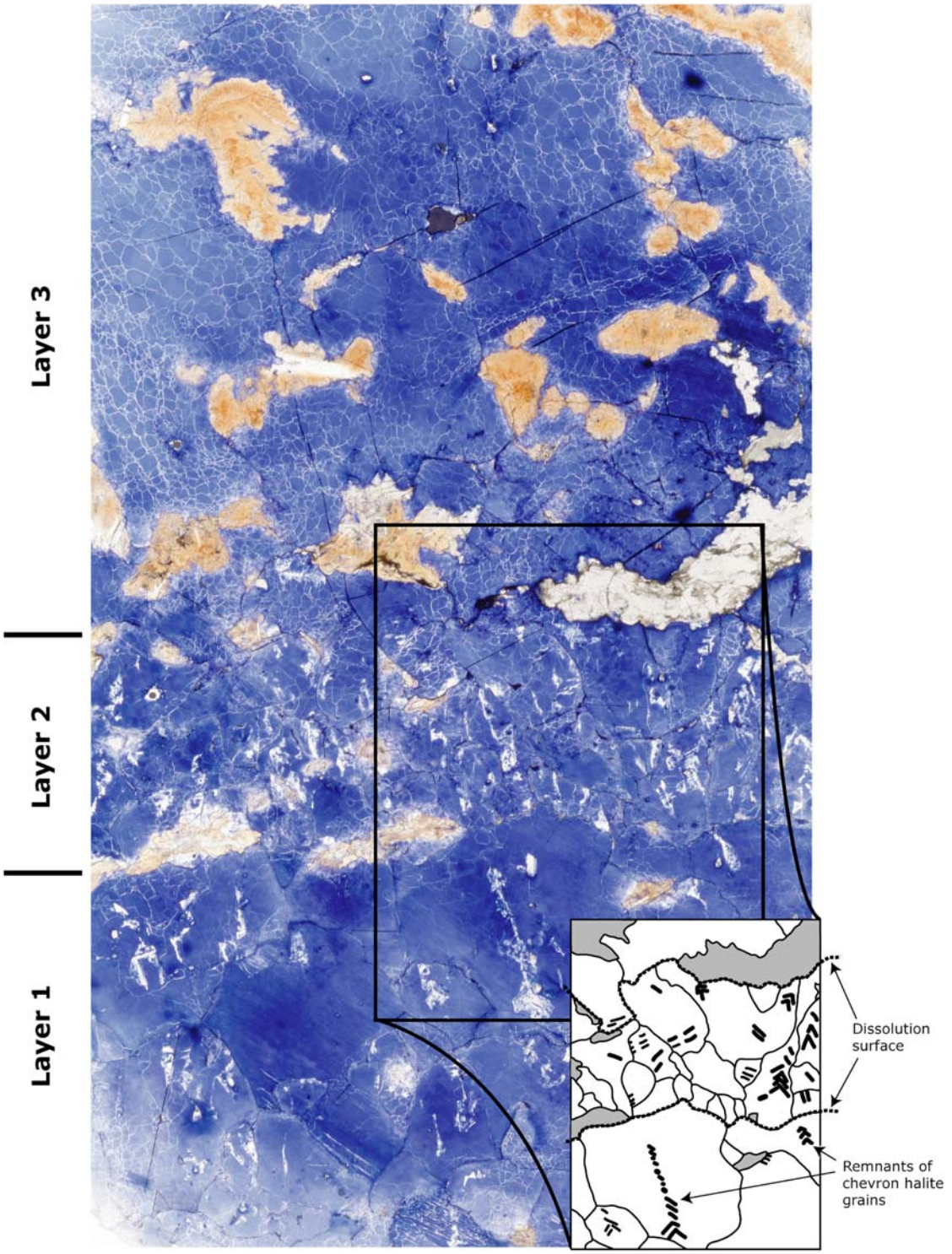

Fig. 7. Overview image of a thin section of gamma-irradiation decorated sample (irradiated at 100 °C) from salt layer C (443.5 m) photographed in transmitted light. White patches are chevron halite grains. Grain boundaries occur as dark, nearly black lines, the white polygons within grains are subgrain boundaries. Three different layers can be distinguished. Layer 1 (at the bottom) consists of chevron halite grains and is extensively truncated by dissolution pipes. The boundary between layers 1 and 2 is marked by anhydrite and polyhalite partings. The layer 2 is much alike as layer 1, and also characterized by the presence of chevrons and clear grains. The boundary between the layers 2 and 3 also characterized by the presence of anhydrite and polyhalite partings. At the top (layer 3) large, blocky halite grains occur. New, strain-free grains, or

migrated grain boundaries were rarely observed, suggesting that deformation-induced recrystallization did not alter the primary structures. Image width is 4.5 cm.

Cubes and hoppers outlined by fluid inclusion bands were found in the A, C and D (457.5 m, 443.5 m and 423.3 m) layer, although these occur less frequently than chevrons. The size of cube and hopper grains varies between 0.5 cm and 3 cm, however the larger grains (1.5 cm to 3 cm) very rarely contain well-developed fluid inclusion bands (Fig. 8).
Such large, blocky halite grains were found in the C layer (443.5 m and 430.9 m). In some cases, small (0.5 cm to 1.5 cm) grains are intercalated in these large, blocky grains. These hopper-shaped small grains are visible only by the different irradiation colouring (less intensively coloured, Fig. 8b).
Clear halite grains, rarely observed, occur as 0.3 cm to 1 cm crystals, locally as elongated grains and usually among chevrons, or rarely as smaller (0.1 cm to 0.6 cm) equiaxed grains (Fig. 9).
Anhydrite and polyhalite occur at grain boundaries of the halite grains, and commonly within grains either as inclusions or as small grains arranged into thin, curved bands. In many cases the anhydrite and polyhalite have a spherulitic appearance with the laths arranged radially around a central core (Fig. 8a).

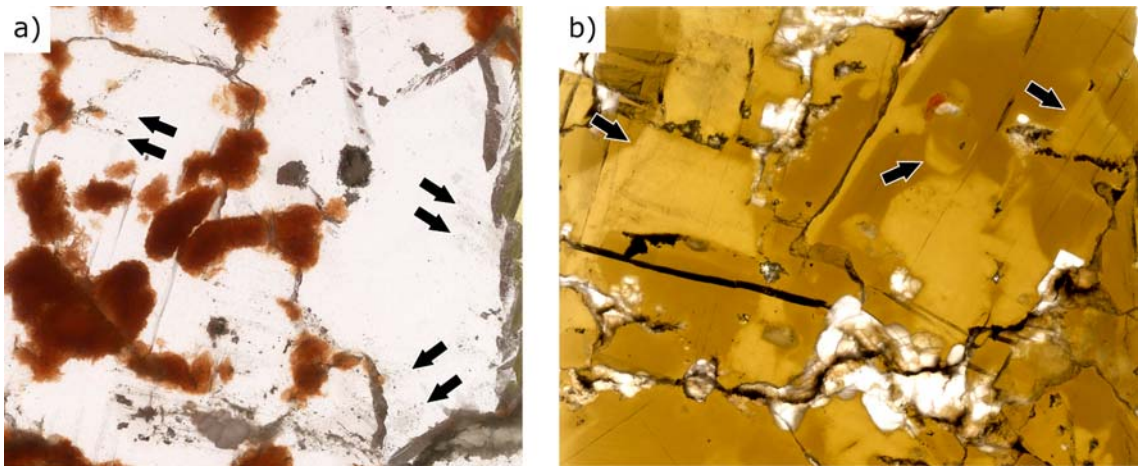

Fig. 8. Photomicrographs of large, blocky halite grains. Transmitted light images.
a) Large, blocky, clear halite grains with few fluid inclusion bands (see arrows). Dark lines are grain boundaries, the grey and red patches are anhydrite and polyhalite. Unirradiated sample from salt layer C (443.5 m). Image width is 3 cm.
b) Hopper crystals intercalated with the large, blocky grains (see arrows) as revealed by 35 °C gamma-irradiation. Note that the subgrain boundaries were not decorated by the 35 °C irradiation. Sample from salt layer C (430.9 m). Image width is 4.5 cm.

The majority of both clear and milky grains contain subgrains, as shown by etching and gamma-irradiation (decorated subgrain boundaries were observed only in slabs irradiated at 100 °C and high total dose). In most grains, subgrains occur as equiaxied polygons with triple junctions of about 120° and with an average size between 250 and 400 μm (Fig. 9). In some of the large grains (e.g. C sample, 430.9 m) the subgrains are arranged into wavy, crystallographically controlled bands (Fig. 10, and Appendix Fig. 1). Much less frequently, elongated subgrains are found in grain boundary regions. Subgrain-free grains and grain boundary regions were observed in all samples, comprising up to 5 to 10 % of halite volume. Subgrain-free grains are relatively small (usually <0.5 cm) and are equiaxed and fluid-inclusion-free (Figs. 9 and 11). Subgrain-free grain boundary regions are always narrow (<0.3 cm) and are less intensively coloured by 35 °C irradiation (Figs. 12 and 13). Gamma-irradiation decorated bands, believed to be slip lamellae, were observed in a number of cases in both subgrain-rich and subgrain-free grains (Fig. 14). The direction of the decorated glide planes slightly changes direction at some subgrain boundaries (Fig. 14).
Grain boundaries are usually serrated at the contact of subgrain-rich grains, and commonly smooth at the contact of subgrain-rich and subgrain-free grains (Fig. 15). Very rarely bulged grain boundaries between subgrain-rich and subgrain-free grains were observed (Fig. 12). Arrays of fluid inclusions are common on grain boundaries (Fig. 16).

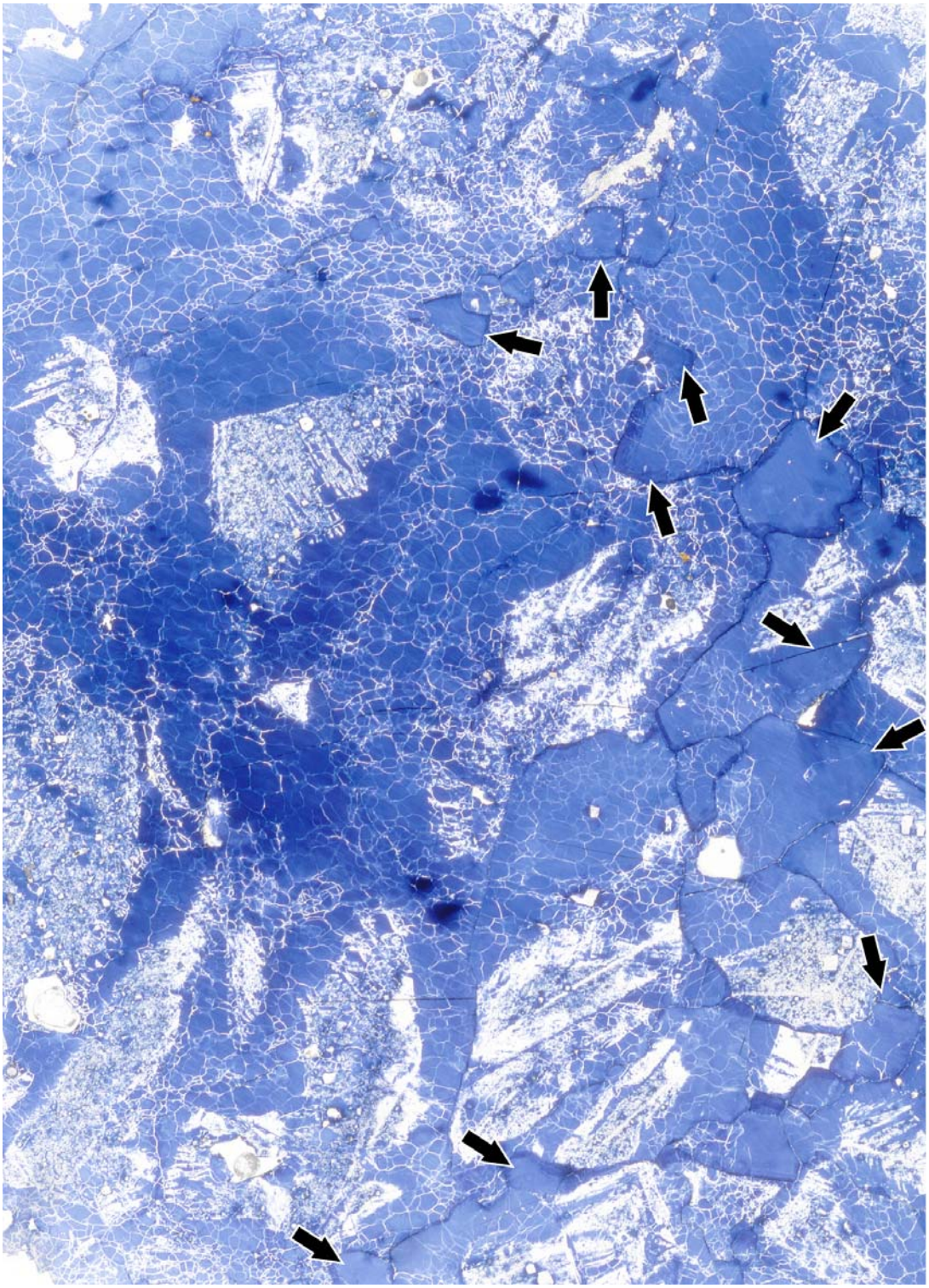

Fig. 9. Overview image of a thin section of sample gamma-irradiation decorated at 100 °C from salt layer A (457.5 m), photographed in transmitted light. Grain boundaries occur as dark curves; white patches are fluid-inclusion-outlined chevrons and hoppers; and white polygons are subgrains. A few new, recrystallized, strain-free grains or grain regions are visible (see arrows). Image width is 4 cm.

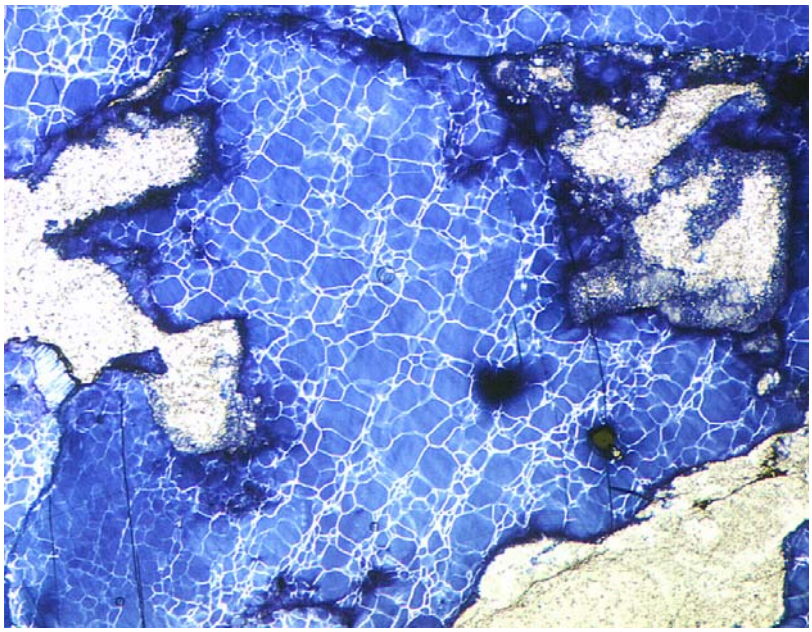

Fig. 10. Microstructure of gamma-irradiated (irradiated at 100 ºC) halite sample from salt layer C (430.9 m), photographed in plane polarized transmitted light. Subgrains are arranged into NE-SW trending, wavy, crystallographically controlled bands, perhaps suggesting cross-slip as one of deformation mechanisms. Image width is 17 mm.

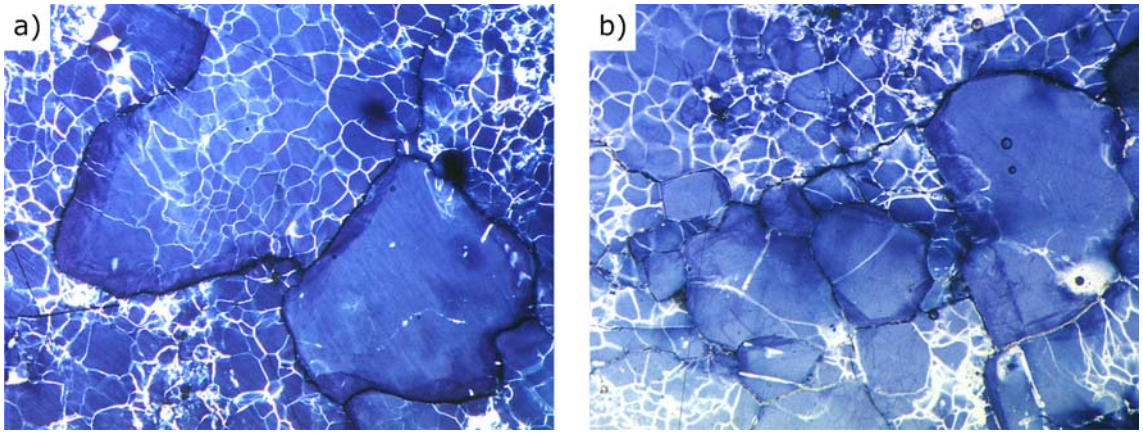

Fig. 11. Photomicrographs show the microstructures of sample from salt layer A (457.5 m). Plane polarized transmitted light images of sample gamma-irradiated at 100 ºC.
a) Migration of high-angle grain boundaries as recorded by elongated subgrains, and strain-free new material, which grows at the expense of old, heavily substructured grains. Image width is 11 mm.
b) Strain-free grains grew at the expense of deformed ones. The size of some of the new grains is comparable to that of subgrains. Image width is 7 mm.

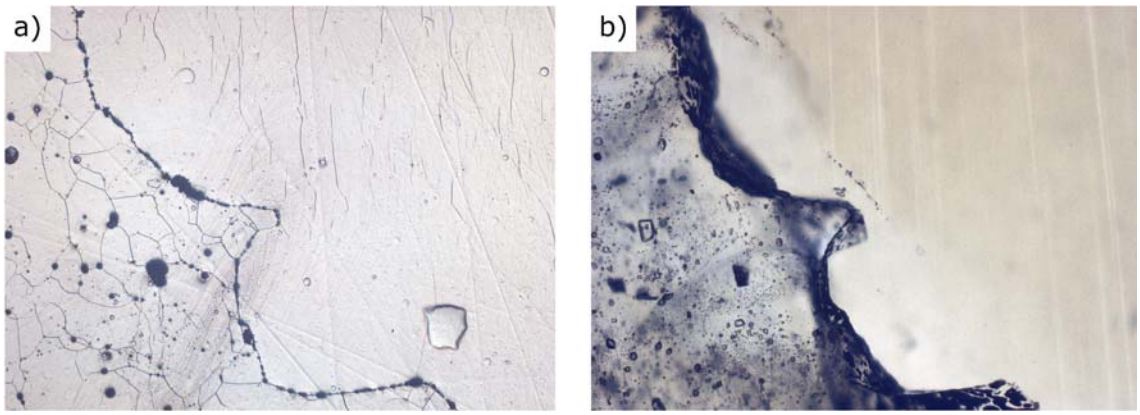

Fig. 12. Microstructures of gamma-irradiated sample from salt layer A (457.5 m). Image width is 2.7 mm.
a) Plane polarized, reflected light image of the polished and etched surface. The grain boundary (NW-SE trending line) is interpreted to have migrated to the SW, as the area to the NW of the boundary is virtually subgrain-free. The dark spots at the grain boundary and in the highly substructured grain are fluid inclusions that decrepitated during sample preparation. Note the bulged shape of the grain boundary.
b) Same area photographed in plane polarized transmitted light. The area interpreted as swept by grain boundary migration is less intensively coloured by 35 ºC gamma-irradiation. Note that the subgrain boundaries were not decorated by the irradiation. Also note that the area, which was swept by the migrating grain boundary, is fluid-inclusion-free.

Fig. 13. Photomicrograph of sample gamma-irradiated at 35 ºC from salt layer D (423.3 m). Minor grain boundary migration occurred in the grain in the middle of the image (see arrows), where the former (100) crystal face (grain boundary) migrated. The area swept by grain boundary migration is less colored. Grain boundaries occur as dark lines. Note that subgrain boundaries were not decorated with Na-precipitates by 35 ºC irradiation. Note also that the thickness of the thin section is approximately 2 mm, so grain boundaries not perpendicular to the plane of image appear thicker. Plane polarized transmitted light image, image width is 2.4 cm.

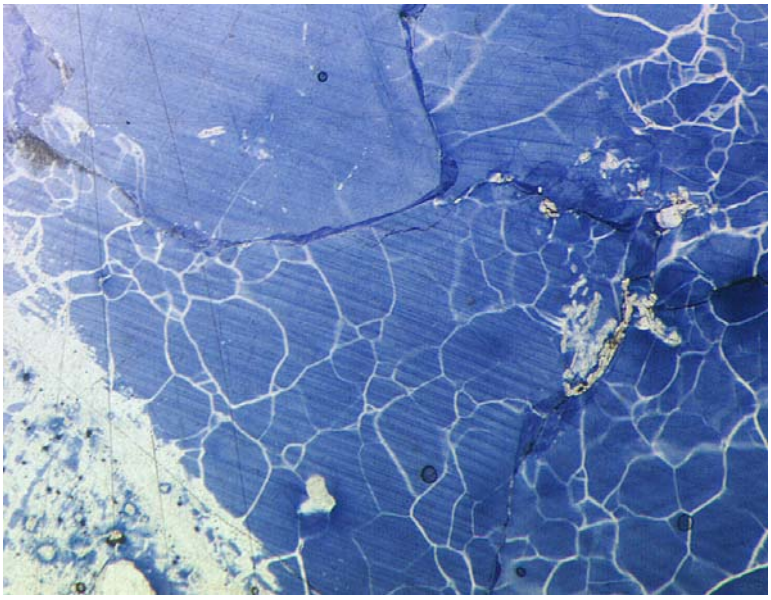

Fig. 14. Photomicrographs show microstructure of sample from salt layer A (457.5 m) gamma-irradiated at 100 °C. The milky, substructured, fluid-inclusion-rich grain at the bottom part is interpreted as old grain, which is replaced by a new, clear, strain-free grain (upper left corner). Note the presence of decorated planes, interpreted to be glide planes, in both the old and new grains. Also note how the decorated glide planes change direction at some subgrain boundaries due to the slight misorientation of the subgrains. Plane polarized transmitted light image, image width 6 mm.

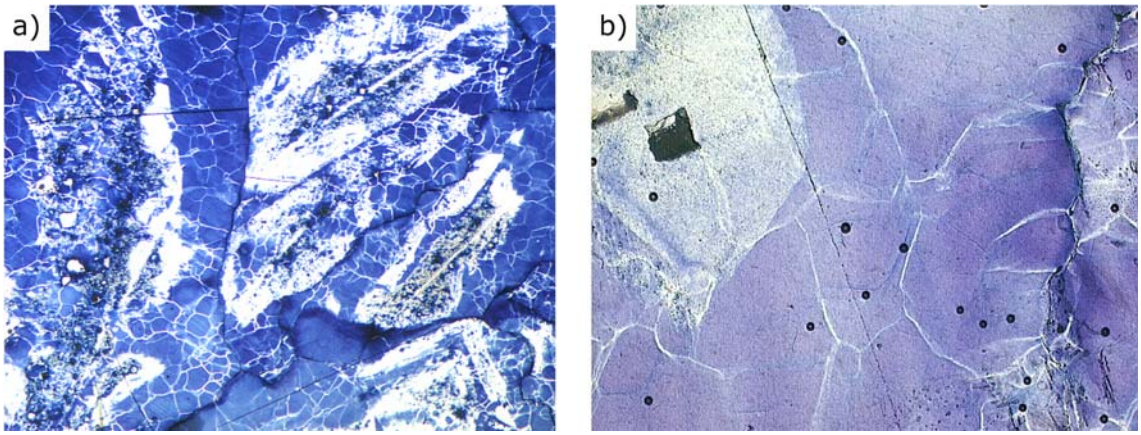

Fig. 15. Microstructures of sample from salt layer A (457.5 m, gamma-irradiated at 100 °C), photographed in plane polarized transmitted light. In both images the grain boundaries occur as dark curves, while the white, milky areas are remnants of chevron grains.
a) The clear, fluid-inclusion-free regions could be explained by a recrystallization mechanism of grain boundary migration. However, the presence of subgrains both in the chevrons and in the fluid-inclusion-free region implies that the structure is syndepositional and is a product of dissolution and precipitation processes. Image width is 16 mm.
b) Similar structure as shown in image "a". Milky, fluid-inclusion-rich (upper left corner) and clear, fluid-inclusion-free halite are separated by a sharp, curved line. The presence of subgrains in both the milky and clear parts is strong evidence that the structure was not developed by grain boundary migration. Note the serrated grain boundary at the right side. Image width is 1 mm.

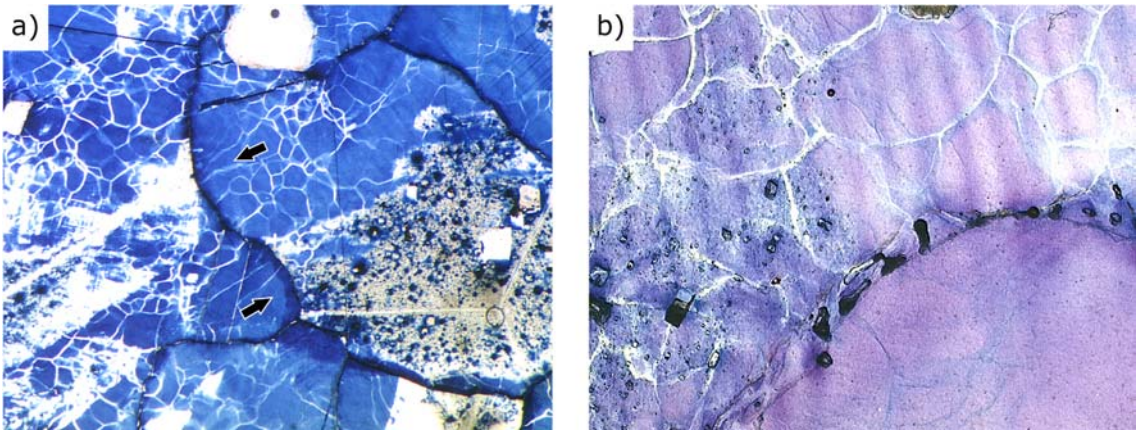

Fig. 16. Photomicrographs show the microstructures of a sample from salt layer A (457.5 m, gamma-irradiated at 100 °C), photographed in plane polarized transmitted light. In both images the grain boundaries occur as dark curves, while the white, milky patches are remnants of fluid inclusion-rich chevron grains.
a) Elongated subgrains indicative of grain boundary migration. Grain boundary migration (see arrows) erases the old, milky, fluid-inclusion-rich part of the old, deformed grains and produces strain-free regions. Since the strain-free grains are free of fluid inclusions, it seems very likely that the fluid inclusions in the deformed and consumed grain were transformed into the grain boundaries during grain boundary migration recrystallization. Image width is 8 mm.
b) Similar structure as shown in the "a" image. A grain with relatively little substructure replaces the primary, fluid-inclusion-rich, highly substructured grain. Here again, the migrating grain boundary seems collecting the fluid inclusions at the grain boundary. Fluid inclusions at the grain boundary occur as dark spots in the image. Image width is 1 mm.

An important observation is that the boundary between milky, fluid-inclusion–rich and clear, fluid-inclusion–free halite can be either inside a grain or at a grain boundary (Figs. 15 and 16). If it is inside a grain the clear, fluid-inclusion-free part is in some cases subgrain-rich, in some cases subgrain-free (Figs. 15 and 16). In many cases grain boundaries are in contact with a milky, fluid-inclusion-rich part of a grain.

5 Interpretation and discussion

5.1 Syndepositional (primary) structures

All samples contain structures interpreted as syndepositional in origin. The truncated chevron grains and the vertically elongated clear halite grains are features which compare well with those reported by Lowenstein and Hardie, 1985, who described the characteristic features of salt pan evaporites. Ephemeral salt pans are normally dry, shallow depressions, filled with layered halite. The halite layers evolve by repeated cycles of desiccation, flooding, evaporative concentration and re-desiccation. The flooding stage brings unsaturated floodwater into the dry salt pan, and converts it into a brackish lake. The unsaturated water partly dissolves the old salt crust, preferentially at grain boundaries, producing a karst-like surface. As the floodwater becomes more saturated with respect to NaCl due to the dissolved salt and continuous evaporation, crystallization starts at the brine surface, where halite hopper crystals and plates form, which sink to the bottom (Fig. 3 in Appendix). On the bottom of the brine pool, the sunken crystals and the old, eroded salt crystals start to grow in crystallographic continuity with seed crystals by precipitation from the concentrated floodwater. Growth competition between the overgrowing crystals produces vertically elongated chevron halite crystals (Nollet et al., 2005), with upward directed apices. In the

desiccation stage, as the saline lake dries out, void-filling clear halite crystallizes from the residual groundwater brine. Lowenstein and Hardie (1985) argue that the salt pan environment is best identified by the presence of dissolution features. Clear halite truncating chevron halite grains, and vertically elongated clear halite grains in the cores studied are interpreted as dissolution structures and are regarded as strong evidence for the salt pan environment.

Syndepositional structures documented in recent ephemeral salt pans have been extensively reported in ancient salt deposits (Dellwig, 1955; Wardlaw and Schwerdtner, 1966; Casas and Lowenstein, 1989; Benison and Goldstein, 2001; for overview see Warren, 1999). Our interpretation of the synsedimentary structures in the Röt salt layers is consistent with these previous works (Fig. 17).

The lowermost and uppermost samples (layer A 457.5 m (Fig. 9) and layer D 423.3 m) are rich in chevrons and primary, dissolution related-features: chevron halite layers that formed in the salt pan during concentration of the brine; and clear halite that crystallized in former voids during the desiccation phase. The relative abundance of clear halite in some samples may imply that the chevron layer underwent repeated episodes of dissolution and precipitation.

In the C layer (443.5 m) the elongated, truncated chevron grains, dissolution pipes (Fig. 7), and the presence of large (1.5 cm to 3 cm), fluid-inclusion-poor, blocky halite grains above the truncation surface marked by anhydrite partings are also features which fit well with the salt pan model. Thus the chevron halite layers are interpreted as forming by competitive growth of bottom-nucleated crystals in the saline lake phase, with the void-filling clear halite crystallized during the desiccation phase. The horizontal truncation surface is interpreted to be a result of dissolution caused by arrival of unsaturated flood water. The presence of chevrons in the bottom layers may be explained by the shallow water environment, since water shallow enough allows fluctuations in NaCl saturation level and thus fluctuations in growth rate. The rhythmic alternation in growth rate results the development of alternating fluid-inclusion-rich and fluid-inclusion-poor bands corresponding to high growth rate and low growth rate periods (Roedder, 1984; Handford, 1990). The blocky crystals are interpreted as forming in concentrated, relatively deep water (deep enough to prevent the development of fluid inclusion bands). The intercalated small hoppers in the blocky grains are probably sunken hopper crystals formed at the brine-air interface (Arthurton, 1973). The second sample studied from the C layer (430.9 m) that is made up entirely of large, fluid-inclusion-free, blocky crystals, has the same appearance as that found in the upper part of the C layer (443.5) m sample (Fig. 7). Those large blocky halite crystals are also interpreted to have formed in concentrated, relatively deep water in the evaporative concentration stage of the salt pan.

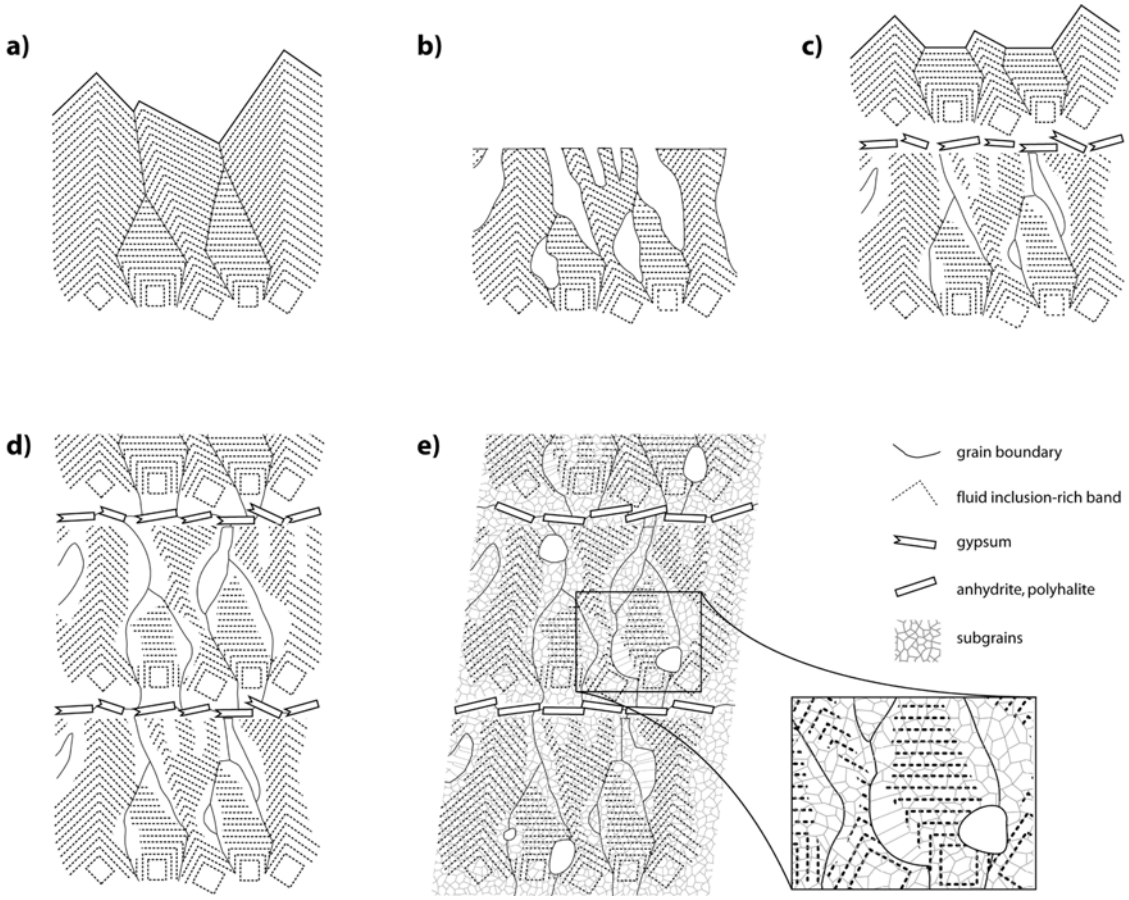

Fig. 17. Diagram illustrating the evolution of the Hengelo rock salt. (a) Overgrowth of seed crystals with different orientation in the evaporative concentration stage of the salt pan cycle. Favourably-oriented crystals override those which have unfavourable orientation. Growth layering (black parallel lines) is a sequence of alternating fluid-inclusion-rich and fluid-inclusion-poor bands. The growth of the crystals continues until the saline lake dries completely out (desiccation stage) (b) Formation of dissolution surface and cavity due to the arrival of undersaturated water during the flooding stage. (c) Evaporation concentrates the undersaturated water, and thin crust of gypsum crystals precipitates from the concentrated water. With further evaporation the system arrives back to the evaporative concentration stage and the gypsum layer is overgrown by a new halite layer. Dissolution voids are filled with clear halite. (d) Layered halite rock evolved by repeating salt pan cycles. The remaining pore spaces are completely filled with clear halite at shallow burial depth. (e) As the salt deforms, the deformation-induced grain boundary migration recrystallization starts to erase the primary structures. Due to this process, the identification of synsedimentary features becomes progressively more difficult as deformation and recrystallization continue (modified after Shearman, 1970).

Extreme truncation of chevrons by clear halite, a common feature in many ancient salt pan evaporites, is best illustrated by the example of the C core (443.5 m) (Fig. 7). In this core only a few percent (up to 10 %) of chevrons are preserved, with the rest made up of clear halite filling dissolution pipes. In earlier work on ancient bedded halite (i.e. Wardlaw and Schwerdtner, 1966; Wardlaw and Watson, 1966), it was argued that it was impossible to produce such mature chevron halite layers by synsedimentary dissolution-reprecipitation alone. The main argument against the dissolution-reprecipitation process was the assumption that the entire salt layer would collapse if it were pervasively truncated by dissolution pipes. These authors thus considered recrystallization as a likely additional effect for producing those features. However, others (Shearman, 1970; Lowenstein and Hardie, 1985; Casas and Lowenstein, 1989) pointed out that the structure can entirely be explained by a repeated dissolution-reprecipitation processes, and argued that recrystallization is not necessarily

required for producing that feature. In this study, the lack of evidence for extensive deformation-induced recrystallization processes (see below) in the truncated chevron layer supports the view that deformation-induced recrystallization was not involved in development of those structures.

5.2 Deformation-related structures

The majority of the grains in the samples studied contain subgrains (Figs. 7 and 9). The polygonal shape of the subgrains suggests deformation dominated by climb-controlled creep (Senseny et al., 1992), although some microstructural evidence may point to the contribution of cross-slip is also present (Fig. 10). The lack of evidence for flattened grains point to a total strain of <10 % (Jackson, 1985). Geological maps of the Twenthe-Rijn area (Geluk and Duin, 1997; Doornenbal et al., 2002a) show that the salt is displaced along NW-SE trending faults, and the most plausible assumption is to associate the deformation of the salt layers with these faults and thus to the Cretaceous inversion tectonic event (de Jager, 2003).
Subgrain-free regions, elongated subgrains at grain boundaries and bulged grain boundaries provide clear evidence for strain energy driven grain boundary migration (Drury and Urai, 1990; Bestmann et al., 2005). Observations on both etched and irradiated samples show that new, less substructured halite is replacing highly substructured grains (Figs. 9, 11, 12, 13, 14, 15). In many cases the migrating grain boundaries consume old, milky, fluid-inclusion-rich parts of a grain (Figs. 12 and 16). Since the area that was swept by grain boundary migration is fluid-inclusion-free, it seems very likely that this process transfers brine into the grain boundaries and provides conditions for pressure solution creep (Urai, 1983; Urai et al., 1986; Spiers et al., 1990).
Although grain boundary migration is common, the recrystallized volume is only a few volume percent (Fig. 9).
Sizes of entirely substructure-free grains vary between the size of a subgrain and a few millimeters (Figs. 9 and 11), suggesting that formation of new high-angle grain boundaries by progressive subgrain rotation is also possible in salt in nature (Drury and Urai, 1990). To date, subgrain rotation has only been documented in halite experimentally deformed dry and at high temperature (Guillopé and Poirier, 1979; Franssen, 1993). Although microstructural evidence reported here points to the presence of subgrain rotation recrystallization, an EBSD analysis of selected regions (e.g. Fig. 11) is necessary and in progress to address this question in more detail.

Water content in the Röt salt is high owing to the numerous primary fluid inclusions (e.g. Fig. 9) and, as shown above, evidence for grain boundary migration is present. It would be expected that as a grain boundary sweeps through a milky, fluid-inclusion-rich area and collects the fluid inclusions, this process amplifies (since fluid increases grain boundary mobility) and continues until the majority of the grains recrystallize and the driving force is eliminated. Considering that the deformation (and creation of driving force) was at least 65 Ma years ago, it is puzzling to see that so many of the deformed grains are not recrystallized, because halite recrystallizes readily at room temperature (Schenk and Urai, 2004). One hypothesis for this phenomenon could be the change in the burial depth, and thus a change in temperature. According to the burial history of Röt strata in vicinity of Hengelo (NITG, 1998), the salt strata were deformed at a maximum burial depth of 1.2 to 1.5 km (Jurassic and Cretaceous). Keeping in mind the recent depth of the beds (<500 m), however, it is unlikely

that this drop in temperature (about 30 °C) had a major effect on the rate of recrystallization. Another explanation could be a reduction in driving force (recovery, subgrain formation) or a reduction in grain boundary mobility due to a change in fluid structure at grain boundaries (Urai et al., 1986; Peach et al., 2001; Schenk and Urai, 2004).

5.3 Differential stress and strain rate calculation

In most materials which deform by dislocation creep processes, the steady state subgrain size is inversely proportional to the stress difference ($\sigma_1 - \sigma_3$) and independent of other variables. The relation is:

(1) $D = k\sigma^{-m}$

where D is the average subgrain size in μm, k and m are material constants and σ is the differential stress in MPa. Two recent datasets exist for experimentally deformed rock salt (Carter et al., 1993; Franssen, 1993) where the subgrain size and stress were measured. Plotting those data together, the parameters of the least squares fit line become k=215 and m=-1.15 (correlation coefficient = 0.90). In this paper we used these values for the stress calculation. For the subgrain diameter (D) calculation, subgrain boundaries from reflected-light photographs of etched thin sections and transmitted-light photographs of irradiated thin sections were digitized and then analyzed with the NIH Image software (http://rsb.info.nih.gov/nih-image/index.html). The software calculates the area of every subgrain, and the D value is obtained by calculating the diameter of a circle equivalent in area to that of the subgrain.

The calculated differential stress values (Table 1) are in good agreement with those reported for various bedded rock salts by Carter et al., 1993, and imply that the Hengelo salt underwent deformation at stresses of 0.5–1 MPa.

Table 1. Differential stress from subgrain size — $\sigma(MPa) = 107 D^{-0.87}(\mu m)$.

Sample	No. of analyzed subgrains	Mean subgrain diameter (μm)	1 S.D.	Calculated mean values for differential stress in MPa (95% confidence)
"D" layer (423.3 m)	301	289	143	0.60 – 0.97
"C" layer (430.9 m)	352	327	208	0.53 – 0.88
"C" layer (443.5 m)	343	391	223	0.45 – 0.77
"A" layer (453.5 m)	290	346	189	0.50 – 0.85

Theoretically, based on the distribution of differential stress magnitudes over the studied salt layers, it would be possible to characterize the type of deformation (simple shear vs. pure shear). This is because in case of simple shear one would expect the same differential stress values over the whole salt succession, while in case of pure shear the highest differential stress values would be expected at the top and at the bottom, the lowest values at the middle of the deforming salt succession.

Although the calculated mean differential stress values are slightly different in the four samples studied, the differences are not significant due to the overlapping range of predicted values (Figs. 18 and 19), preventing us from characterizing the type of the deformation (e.g. simple shear vs. pure shear).

During deformation of rock salt, creep processes are controlled by cross-slip (CS), climb (CL) and pressure solution (PS) (Spiers and Carter, 1996). Elaborate experiments on rock salt provided constitutive equations for dislocation creep processes (Carter et al., 1993) and for pressure solution (Spiers et al., 1990). Assuming that dislocation creep processes and pressure solution act in parallel, steady-state flow of natural rock salt can be approximated by the following equation:

(2) $\dot{\varepsilon} = \dot{\varepsilon}_{CS} + \dot{\varepsilon}_{CL} + \dot{\varepsilon}_{PS}$

where $\dot{\varepsilon}$ is the total strain rate in s^{-1}, $\dot{\varepsilon}_{CS}$ and $\dot{\varepsilon}_{CL}$ are strain rates from dislocation creep processes, and $\dot{\varepsilon}_{PS}$ is strain rate from pressure solution (by definition zero for dry salt). Microstructures observed in this study are consistent with climb-controlled and the fluid assisted diffusional-creep (c.f. Fig. 1 of Schenk and Urai, 2004). Thus it seems reasonable to use the corresponding constitutive equations for climb controlled creep (equation 3) and for pressure solution creep (equation 4) to calculate total strain rate.

(3) $\dot{\varepsilon}_{CL} = 8.1 \times 10^{-5} \exp\left(-51600 / RT\right)\left(\sigma_1 - \sigma_3\right)^{3.4}$ after Carter et al., 1993

(4) $\dot{\varepsilon}_{PS} = 4.7 \times 10^{-4} \exp\left(-24530 / RT\right)\left(\sigma_1 - \sigma_3\right) / TD^3$ after Spiers et al., 1990

where strain rate ($\dot{\varepsilon}$) is expressed in s^{-1}, the pre-exponential constant is in $MPa^{-n}s^{-1}$, apparent activation energy is in $Jmol^{-1}$, Boltzmann's gas constant (R) is in $Jmol^{-1}K^{-1}$, temperature (T) is in ^{o}K, differential stress ($\sigma_1 - \sigma_3$) is in MPa and grain size (D) is in mm.
For the calculations we assumed that the deformation occurred at a depth of ~1.5 km in the Cretaceous time. Since we are lacking of paleogeothermal data for the study area, we used that of present day (~30-35 ^{o}C/km; Haenel, 1980), thus we assumed that T=323 ^{o}K.
Calculated strain rate values (Table 2) show that in finer grained samples, solution precipitation creep contributes to total strain rate at least in the same order of magnitude as dislocation creep processes. In the relatively coarse-grained sample (C layer, 430.9 m) dislocation creep is the main deformation mechanism.

Table 2. Strain rate calculated from equation (3) and equation (4). Total strain rate ($\dot{\varepsilon}$) is the sum of the two values (equation 2).

Sample	No. of analyzed grains	Mean grain diameter (mm)	1 S.D.	$\dot{\varepsilon}_{CL}$ (s^{-1})	$\dot{\varepsilon}_{PS}$ (s^{-1})	$\dot{\varepsilon}$ (s^{-1})
"D" layer (423.3 m)	24	6.01	2.08	$6.31\times10^{-14} - 3.33\times10^{-13}$	$4.31\times10^{-13} - 7.03\times10^{-13}$	$4.94\times10^{-13} - 1.04\times10^{-12}$
"C" layer (430.9 m)	3	25.91	12.59	$4.20\times10^{-14} - 2.40\times10^{-13}$	$4.77\times10^{-15} - 7.96\times10^{-15}$	$4.68\times10^{-14} - 2.47\times10^{-13}$
"C" layer (443.5 m)	15	8.80	5.28	$2.34\times10^{-14} - 1.49\times10^{-13}$	$1.02\times10^{-13} - 1.76\times10^{-13}$	$1.26\times10^{-13} - 3.25\times10^{-13}$
"A" layer (453.5 m)	52	4.91	2.82	$3.51\times10^{-14} - 2.07\times10^{-13}$	$6.25\times10^{-13} - 1.12\times10^{-12}$	$6.97\times10^{-13} - 1.32\times10^{-12}$

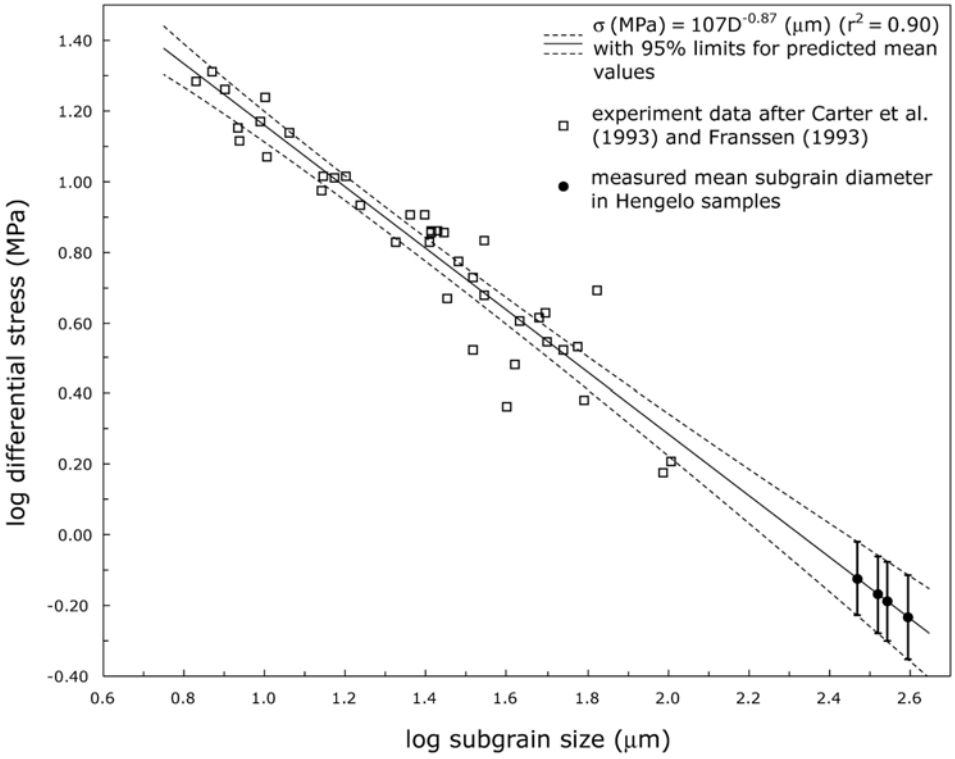

Fig. 18. Logarithmic subgrain size vs. logarithmic differential stress of experimental data from Carter et al. (1993) and Franssen (1993). The least squares fit line of the combined data set was used to calculate the differential stress for the Hengelo samples (Table 1).

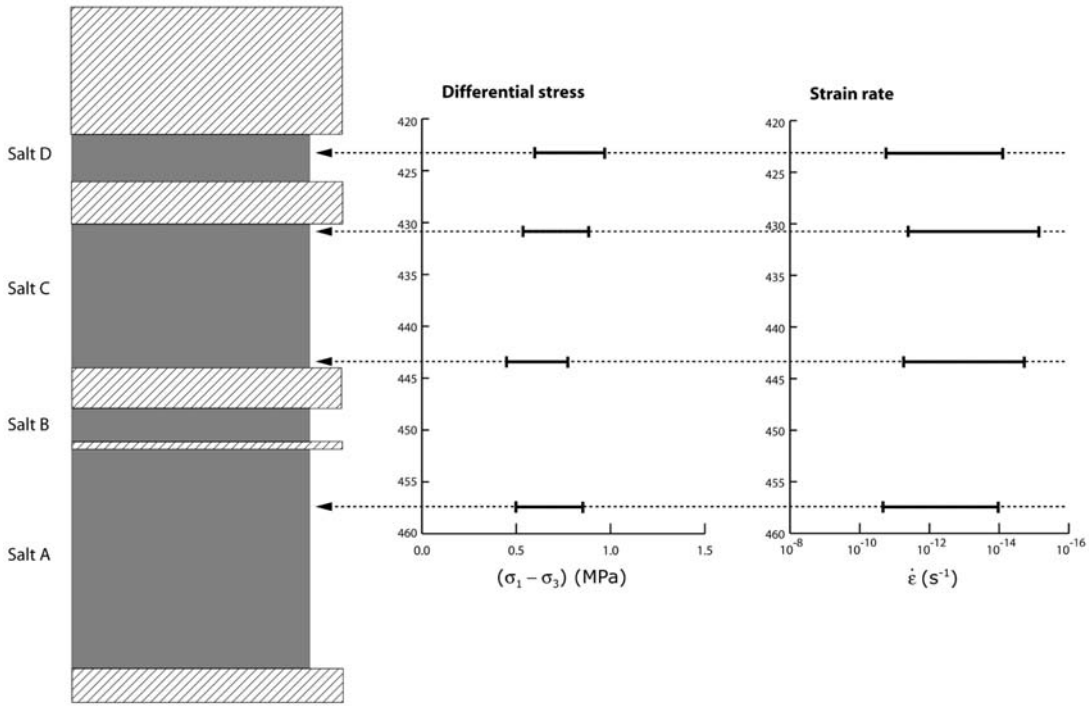

Fig. 19. Graph shows the calculated differential stress and the strain rate distribution over the inspected salt layers. For discussion see text.

Experiments on bedded and domal salts (Wawersik and Zeuch, 1986; Hunsche et al., 2003) showed that while the form of the constitutive laws governing creep rate are similar, actual creep rates in different types of salts vary over a factor of ±10. This variation in creep rate can be attributed to secondary phases, solid solution impurities, grain size and dislocation density (Pfeifle et al., 1995). In our calculations we took a factor of 10 to be a plausible range. The uncertainty in the creep rate is too large to allow detection of significant differences in strain rate across the layers (Fig 19.).

6 Conclusions

In this paper, with the aid of microstructural analysis, we differentiated between primary (synsedimentary) and secondary (deformation-related) microstructures present in the Röt salt. Most of the primary structures are still preserved and modifications by recrystallization have been subordinate. In our samples, recrystallization of salt is incipient, but it shows how associated processes erase primary structures, making identification of synsedimentary features progressively more difficult as deformation and recrystallization continues. Nevertheless, in the case of slightly deformed salts, there are already microstructures, e.g. grain boundary migration-type microstructures (c.f. Fig. 15 and 16), which, without a careful microstructural analysis, could be misinterpreted. One other important implication of this paper is the evidence for a process (grain boundary migration) that transports and concentrates primary fluid-inclusion brines into grain boundaries. This implies that the amount of brine at the grain boundaries increases as the grain boundaries sweep through a fluid-inclusion-rich area, thus giving rise to pressure solution creep, which accordingly can contribute to the total strain rate at least in the same order of magnitude as dislocation creep processes. Keeping in mind that many of the bedded halites are of salt pan origin and thus rich in fluid inclusions, it is likely that the pressure solution creep is significant in halite alongside dislocation processes, at least in the early phases of halokinesis.

Acknowledgements

The authors thank Wim Paar (Akzo Nobel company) for the salt core samples, Manfred Thomé at the Jülich Forschungszentrum for carrying out the gamma-irradiation and H. W. den Hartog (University of Groningen) for helpful discussion on gamma-irradiation. This work was performed as a part of the SPP 1135 project (nr. UR 64/5-1-2), and was financed by the DFG (Deutsche Forschungsgemeinschaft). The manuscript benefited from thorough reviews by Timothy Diggs and Chris Spiers.

References

Arthurton, R. S., 1973. Experimentally produced halite compared with Triassic layered halite-rock from Chesire, England. Sedimentology 20, 145-160.

Benison, K. C., Goldstein, R. H., 2001. Evaporites and siliciclastics of the Permian Nippewalla Group of Kansas, USA: a case for non-marine deposition in saline lakes and saline pans. Sedimentology 48, 165-188.

Bestmann, M., Piazolo, S., Spiers, C. J., Prior, D. J., 2005. Microstructural evolution during initial stages of static recovery and recrystallization: new insights from in-situ heating experiments combined with electron backscatter diffraction analysis. Journal of Structural Geology 27(3), 447-457.

Carter, N. L., Horseman, S. T., Russell, J. E., Handin, J., 1993. Rheology of rocksalt. Journal of Structural Geology 15(9-10), 1257-1271.

Casas, E., Lowenstein, T. K., 1989. Diagenesis of saline pan halite: comparison of petrographic features of modern, Quaternary and Permian halites. Journal of Sedimentary Petrology 59(5), 724-739.

de Jager, J., 2003. Inverted basins in the Netherlands, similarities and differences. Geologie en Mijnbouw 82(4), 355-366.

Dellwig, L. F., 1955. Origin of the salina salt of Michigan. Journal of Sedimentary Research 25(2), 83-110.

Doornenbal, H., Duin, E. J. T., de Haan, H., 2002a. Actualisering van de bestaande geologische kaarten van de concessie Adolf van Nassau en van de concessie Twenthe-Rijn, Buurse en Uitbreiding Twenthe-Rijn. TNO report: NITG 02-194-C, Nederlands Instituut voor Toegepaste Geowetenschappen TNO.

Doornenbal, H., Duin, E. J. T., de Haan, H., 2002b. Actualisering van de bestaande geologische kaarten van de concessieAdolf van Nassau en van de concessie Twenthe-Rijn, Buurse en Uitbreiding Twenthe-Rijn. NITG 02-194-C, TNO.

Drury, M. R., Urai, J. L., 1990. Deformation-related recrystallization processes. Tectonophysics 172, 235-253.

Franssen, R. C. M. W. 1993. Rheology of synthetic rocksalt with emphasis on the influence of deformation history and geometry on the flow behaviour, Rijksuniversiteit Utrecht.

Garcia Celma, A., Donker, H. (Editors), 1996. The Effect of Gamma Radiation in Salt, EUR-Report 16743EN.

Geluk, M. C., Duin, E. J. T., 1997. Kartering Twenthe-Rijn, Uitbreiding Twenthe-Rijn en Buurse Concessie. NITG 97-69-C, TNO.

Geluk, M. C., Röhling, H.-G., 1997. High-resolution sequence stratigraphy of the Lower Triassic "Buntsandstein" in the Netherlands and northwestern Germany. Geologie en Mijnbouw 76, 227-246.

Guillopé, M., Poirier, J. P., 1979. Dynamic recrystallization during creep of single crystalline halite: an experimental study. Journal of Geophysical Research 4, 5557-5567.

Haenel, R. 1980. Atlas of Subsurface Temperatures in the European Community. Commission European Community, Brussels,

Handford, R. C., 1990. Halite depositional facies in a solar salt pond: A key to interpreting physical energy and water depth in ancient deposits? Geology 18, 691-694.

Hardie, L. A., Lowenstein, T. K., Spencer, R. J. 1983. The problem of distinguishing between primary and secondary features in evaporites. In: Schreiber, B. C. & Harner, H. L. (Eds.), Sixth Symposium on Salt I. Salt Institute, Alexandria, Virginia, USA, 11-39.

Harsveldt, H. M. 1980. Salt resources in the Netherlands as surveyed by AKZO. In: Coogan, A. H. & Hauber, L. (Eds.), Fifth Symposium on Salt 1, Hamburg, Germany, 65-81.

Hunsche, U., Schulze, O., Walter, F., Plischke, I., 2003. Projekt Gorleben. Thermomechanisches Verhalten von Salzgestein. 9G2138110000, BGR, Hannover.

Jackson, M. P. A. 1985. Natural strain in diapiric and glacial rock salt, with emphasis on Oakwood Dome, East Texas, 143, 73

Joffé, A. 1928. The physics of crystals. McGraw-Hill, New York,

Kovalevych, V., Peryt, T. M., Beer, W., Geluk, M., Halas, S., 2002. Geochemistry of Early Triassic seawater as indicated by study of the Rot halite in the Netherlands, Germany, and Poland. Chemical Geology 182(2-4), 549-563.

Lowenstein, T. K., Hardie, L. A., 1985. Criteria for the recognition of salt-pan evaporites. Sedimentology 32, 627-644.

NITG. 1998. Geological Atlas of the Subsurface of The Netherlands, Explanation to map sheet X: Almelo-Winterswijk, Nederlands Instituut voor Toegepaste Geowetenschappen TNO, Haarlem, 143

Nollet, S., Urai, J. L., Bons, P. D., Hilgers, C., 2005. Numerical simulations of polycrystal growth in veins. Journal of Structural Geology 27(2), 217-230.

Peach, C., Spiers, C. J., Trimby, P. W., 2001. Effect of confining pressure on dilatation, recrystallization, and flow of rock salt at 150 °C. Journal of Geophysical Research 106(13315-13328).

Pfeifle, T. W., Vogt, T. J., Brekken, G. A., 1995. Correlation of chemical, mineralogic and physical characteristics of Gulf Coast dome salt to deformation and strength properties. Contract No. 1-92, RESPEC Inc., Rapid City.

Przibram, K., 1954. Irradiation colours in minerals. Endeavour 13(49), 37-41.

RGD. 1993. Geologische Kaart van Nederland 1:50 000, Blad Almelo Oost/Denekamp (28O/29), Rijks Geologische Dienst, Haarlem,

Roedder, E., 1984. The fluids in salt. American Mineralogist 69, 413-439.

Schenk, O., Urai, J. L., 2004. Microstructural evolution and grain boundary structure during static recrystallization in synthetic polycrystals of Sodium Chloride containing saturated brine. Contributions to Mineralogy and Petrology 146(6), 671-682.

Senseny, P. E., Hansen, F. D., Russell, J. E., Carter, N. L., Handin, J., 1992. Mechanical behaviour of rock salt: phenomenology and micromechanisms. Int. J. Rock Mech. Min. Sci & Geomech. Abstr. 29(4), 363-378.

Shearman, D. J., 1970. Recent halite rock, Baja California, Mexico. Transaction of Mining and Metallurgy 79B, 155-162.

Spiers, C. J., Carter, N. L. 1996. Microphysics of rocksalt flow in nature. Fourth Conference on the Mechanical behaviour of Salt, The Pennsylvania State University, June 17 and June 18, 1996.

Spiers, C. J., Schujtens, P. M. T. M., Brezowski, R. H., Peach, C., Liezenberg, J. L., Zwart, H. J. 1990. Experimental determination of constitutive parameters governing creep of rocksalt by pressure solution. In: Knipe, R. J. & Rutter, E. H. (Eds.), Deformation Mechanisms, Rheology and Tectonics 24. Geol. Soc. London Spec. Publ., 215-227.

Urai, J. L. 1983. Deformation of wet salt rocks, Universiteit Utrecht.

Urai, J. L., Spiers, C. J., Peach, C., Franssen, R. C. M. W., Liezenberg, J. L., 1987. Deformation mechanisms operating in naturally deformed halite rocks as deduced from microstructural investigations. Geologie en Mijnbouw 66, 165-176.

Urai, J. L., Spiers, C. J., Peach, C. J., Zwart, H. J., 1985. A laboratory investigation into the interaction of recrystallization and radiation damage effects in polycrystalline salt rocks, HPT Laboratorium, Insititut voor Aardwetenschappen, Utrecht.

Urai, J. L., Spiers, C. J., Zwart, H. J., Lister, G. S., 1986. Weakening of rocksalt by water during long term creep. Nature 324, 554-557.

van Lange, M. W. P. 1994. The development, geology and lithology of the Central-Northern part of the Hengelo rock salt solution mining area and its geotechnical characterisation, No. 126, 77

van Opbroek, G., den Hartog, H. W., 1985. Radiation damage of NaCl: dose rate effects. Journal of Physics. C: Solid State Phys. 18, 257-268.

Wardlaw, N. C., Schwerdtner, W. M., 1966. Halite-Anhydrite seasonal layers in the Middle Devonian Prairie Evaporite Formation, Saskachewan, Canada. Geological Society of America Bulletin 77, 331-342.

Wardlaw, N. C., Watson, D. W., 1966. Middle Devonian salt formations and their bromide content, Elk Point Area, Canada. Canadian Journal of Earth Sciences 3, 263-275.

Warren, J. 1999. Evaporites - Their evolution and economics. Blackwell Science Ltd, Oxford, 437

Wawersik, W. R., Zeuch, D. H., 1986. Modeling and mechanistic interpretation of creep of rock salt below 200 C. Tectonophysics 121, 125-152.

Appendix

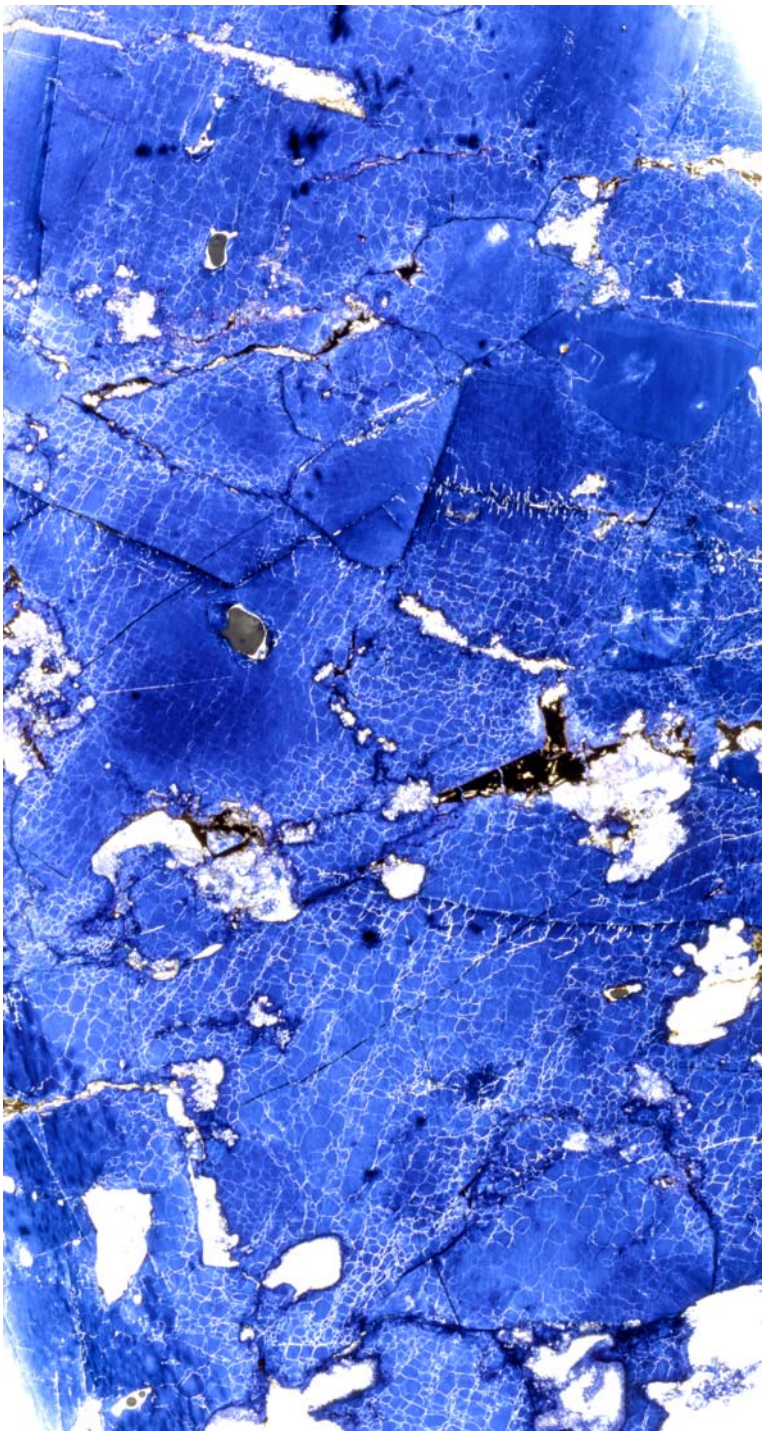

Fig. 1. Overview image of a thin section from salt layer C (430.9 m) photographed in transmitted light. The sample was gamma-irradiation decorated at 100 °C. Grain boundaries occur as dark curves and white polygons are subgrains. A few new, recrystallized, strain-free grains or grain regions are visible. The sample is coarse-grained. Note the absence of fluid-inclusion-outlined chevrons and hoppers. Image width is 3 cm.

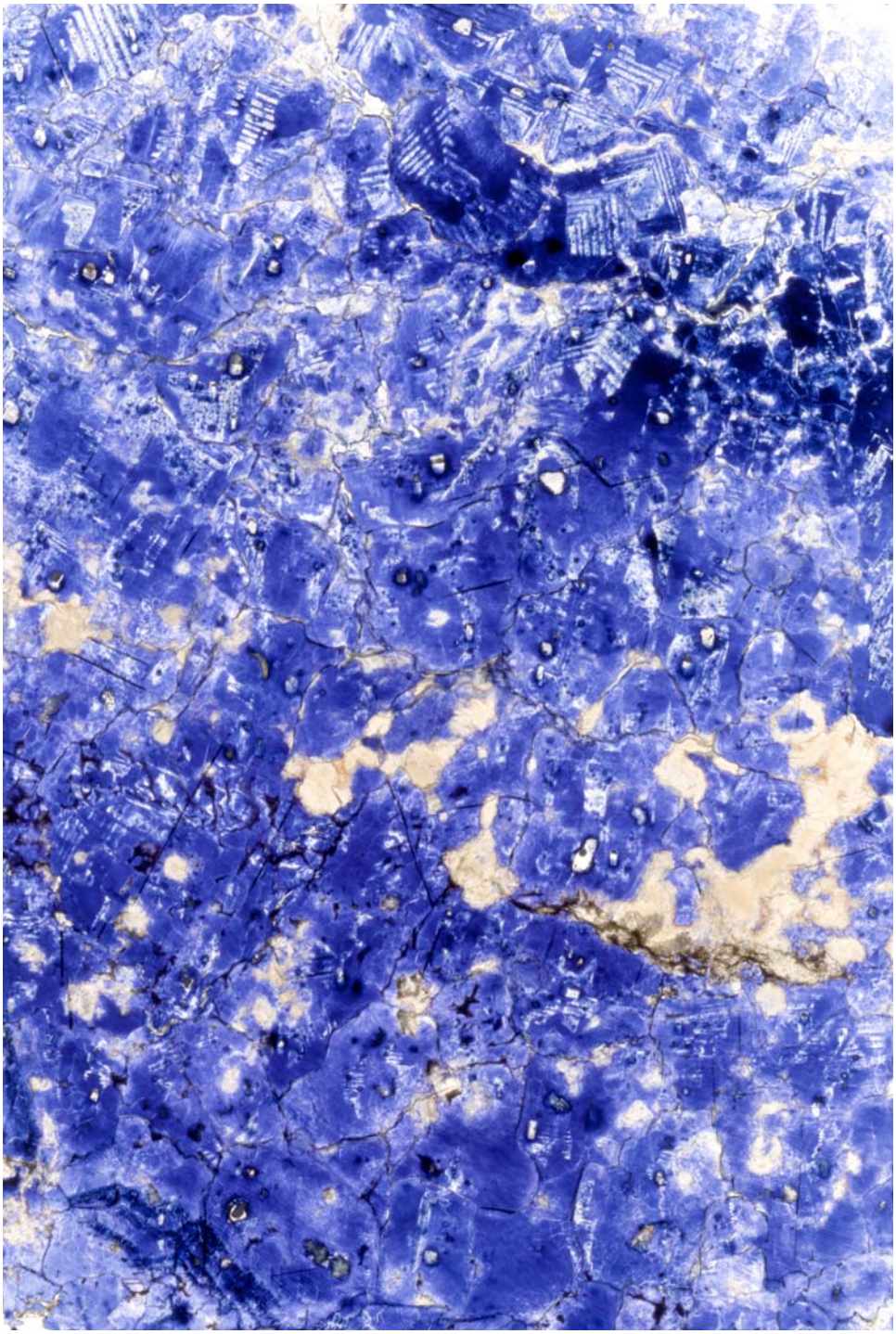

Fig. 2. Overview image of a thin section from salt layer D (423.3 m) photographed in transmitted light. The sample was gamma-irradiation decorated at 100 °C. Grain boundaries occur as dark curves; white patches are fluid-inclusion-outlined chevrons and hoppers; and white polygons are subgrains. The yellowish patches are polyhalite and anhydrite. A very few new, recrystallized, strain-free grains or grain regions are visible. Note the abundance of chevron grains at the upper part of the image. Image width is 4 cm.

Fig. 3. Overview image of a thin section from a recent salt deposit from the Dead Sea (photographed in transmitted light). The sample is from a few meters of depth. Grain boundaries occur as dark curves; gray patches are fluid-inclusion-outlined chevrons and hoppers. The black areas between the grains are primary pores, which were filled with resin during sample preparation. In the middle of the image, a fine-grained layer of halite is visible. This layer is very likely consisting of sunken halite rafts. The coarse-grained part of this sample is an analogue for the Hengelo samples deposited in shallow-water environment. Image width is 4 cm.

Chapter 3: Deformation mechanisms and fluid flow properties of rocksalt as evidenced by microstructures – a case study on Zechstein (Z1) rocksalt from Neuhof salt mine (Germany) *

Zsolt Schléder, János L. Urai, Sofie Nollet and Christoph Hilgers

Abstract

In this paper Zechstein (Z1) rocksalt core samples from the immediate vicinity of the Hessen potash bed from the Fulda basin are analyzed. The analyzed halite is folded into tight, isoclinal folds and is cut by an undeformed, 1 cm thick, coarse-grained halite vein. The microstructures were investigated in etched, gamma-irradiated thin sections from both the wall rock and from the vein.

The lack of synsedimentary dissolution structures and the widespread occurrence of plate-shaped and hopper grains in the wall-rock suggests that the sedimentary environment was perennial lake. Deformation microstructures are in good agreement with the solution-precipitation creep process. Strength variations in anhydrite-rich and poor layers are accounted for the strong folding in the halite beds. The vein is completely sealed and composed mainly of euhedral to subhedral halite grains, which often overgrow the wall-rock grains. Those microstructures, together with the presence of occasional fluid inclusion bands suggest that the crystals grew into a solution-filled open space.

Based on considerations on the maximum value of in-situ differential stress and dilatancy criteria plus on the amount of released fluids from the potash bed during metamorphism and the volume change, it is proposed that the crack was generated by hydrofracturing of the rocksalt due to the presence of the salt metamorphic fluid at near-lithostatic pressure.

Keywords: Halite, potash salt, deformation mechanism, hydrofracture

* Schléder, Z., Urai, J. L., Nollet, S., Hilgers, C., In Review. Deformation mechanisms and fluid flow properties of rocksalt as evidenced by microstructures – a case study on Zechstein (Z1) rocksalt from Neuhof salt mine (Germany). International Journal of Earth Sciences.

1 Fluid transport in rocksalt

Study of Casas and Lowenstein, 1989, Lowenstein and Spencer, 1990 on Quaternary halite deposition showed that the effective porosity and permeability decreases drastically in the shallow subsurface. After about 50 m of burial the halite is nearly completely cemented, and is without any visible porosity. At depth of 100 m, the halite is tight, entirely cemented and has no measurable permeability. The very low permeability of halite is demonstrated by laboratory measurements and its ability to seal large hydrocarbon columns and fluid pressure cells. This very low permeability is maintained during halokinesis, although there are some processes which can lead to the increase in permeability.

For example, Fokker, 1995 considered the long term evolution of salt permeability after abandonment of solution mining caverns. He showed that when fluid pressures in the cavern approach lithostatic due to creep convergence, diffuse dilatancy of the roof occurs and the permeability of the salt increases to allow the slow escape of the fluids. Similar high-pressure fluid pockets (porous salt) occur also in nature and these are presumably also slowly moving upwards by similar processes. This process might operate in other rock types, as suggested by the mobile hydrofracture model in Bons, 2001. The detailed nature of the relation between the effective stress, differential stress and permeability was studied in a series of experiments by Urai et al., 1986b, Peach et al., 2001 and Popp et al., 2001. The authors noted that the permeability of rocksalt increases by five orders of magnitude if deformed at low temperature and mean effective stress due to microcracking and dilatancy. Similar dilatancy was reported by Wallner, 1986 and Lux, 2005, who noted that diffuse dilatancy occurs with dilated grain boundaries when the fluid pressure slightly exceeds σ_3 (minimum principal stress), while hydro-fracturing occurs when the fluid pressure is significantly exceeds σ_3. Natural occurrence of diffuse dilatancy was reported by Schoenherr et al., 2005 in rocksalt samples from vicinity of oil fields of the Oman salt basin. They found oil entrapped along cleavage planes and at grain boundaries in halite. They suggested that in the presence of high fluid pressure the effective stress was decreased in the salt so that dilatancy was reached.
A different process leading to increased permeability of salt was reported by Lewis and Holness, 1996, who measured the equilibrium water-halite dihedral angles in grain boundary triple junctions. At temperatures <100 ^{o}C these were higher than 60^{o}, such that the small amounts of brine present in the salt are distributed in micrometer-size isolated fluid inclusions, dramatically reducing the permeability. At temperatures above 100 ^{o}C and pressures of 70 MPa this value decreases below 60^{o}, leading to a redistribution of the fluid into a thermodynamically stable network of connected, fluid filled channels at grain boundary triple junctions, dramatically increasing the permeability (comparable to that of sandstones). This process might well be operative in nature, although only in deeply buried rocksalts. Calculating with an ambient geothermal gradient and with the density of rocksalt the process is supposed to be operative at minimum depth of about 3-4 km.

The fluids in rocksalt may be externally derived, meaning that they can originate from below the salt succession or enter as meteoric waters from the sides into the salt body. Alternatively, the fluids may be generated inside the salt body, such as the gypsum to anhydrite conversion (if gypsum was primarily deposited) according to following reaction:
$CaSO_4 \cdot 2H_2O \rightarrow CaSO_4 + 2H_2O$, This reaction would result in a release of 40 % structural water that is saturated with $CaSO_4$ (Borchert and Muir, 1964). The conversion is dependent on many parameters (salinity, pore fluid pressure), and occurs between 70-105 °C, i.e. in depths of few meters to a few kilometer (Jowett et al., 1993; Warren, 2006). There are some indications that this fluid may be retained in the evaporitic sequence during the burial, and is expelled during halokinesis (Nollet et al., 2005a). Similarly, if a potash layer is intercalated, mineral transformation of the constitutive minerals (i.e carnallite to sylvite) may also lead to release of structural water (Borchert and Muir, 1964). The process can be written as: $KMgCl_3 \cdot 6H_2O + 4H_2O \rightarrow KCl + Mg^{2+} + 2Cl^- + 10H_2O$, showing that this process needs some extra water to become active.
In the shallow-water environment, where there is a fluctuation in growth rate of halite crystals, the halite often incorporates brine inclusions (Roedder, 1984; Lowenstein and Hardie, 1985; Handford, 1990). The overall amount of such inclusions may make up 5 % of the rocksalt (Roedder, 1984). During deformation induced recrystallization of the rocksalt the fluid inclusions are swept out by the migrating grain boundary, and convert to grain boundary fluid (Schléder and Urai, 2005). This fluid is then presumably able to migrate along the grain boundaries during recrystallization of the rocksalt (process unknown).
Concentration measurements of Br in rocksalt proved to be a very effective method in characterizing the primary/secondary origin of rocksalt (Kühn, 1957; Fischbeck and Bornemman, 1988; Siemann and Schramm, 2002). Similarly, elaborate works on the fluid chemistry gave important constraints on the possible sources of fluids in rocksalt (e.g. Herrmann, 1981; Herrmann and Knipping, 1989; Siemann and Ellendorff, 2001). Although the composition of fluids in rocksalt is well-known, the processes which allows the migration of these fluids in rocksalt is still poorly understood.
In this work we present a microstructural study on a highly deformed and recrystallized Zechstein (Z1) rocksalt from Neuhof salt mine (Germany). This folded rocksalt is cut by halite veins which are completely sealed by coarse-grained halite. Based on the microstructural features we discuss the possible deformation and recrystallization mechanisms, constraints on the provenance of fluid, fluid transport processes and probable mechanism leading to vein formation.

2 Regional setting and samples studied

The Hessen basin, which is a southern embayment of the Permian Zechstein basin (Fig. 1), is divided into two sub-basins; the Werra and Fulda basins (Skowronek et al., 1999; Becker, 2002). Both basins are filled with an approximately 300 m tick Z1 evaporitic sequence, lying unconformably on earlier deposited Permian sediments (Figs. 2 and 3). The Zechstein is composed predominantly of halite, but the sequence also includes two 1-2.5 m thick potash horizons (Hessen and Thüringen, Jahne et al., 1970). The sedimentary environment of the evaporitic sequence is predominantly shallow water (Becker, 2002). The Z1 evaporites are overlain with some 350 m thick, siliciclastic Buntsandstein sediments. Younger Mesozoic strata – lower Keuper – can only be found in the Fulda-graben which separates the Werra and Fulda basins (Fig. 3). It is assumed that sediments were deposited at least until the Dogger, and that the total thickness of Mesozoic sediments very likely exceeded 1100 m (Oesterle and Lippolt, 1975; Käding and Sessler, 1994). The sedimentation was ceased by the end of Jurassic and was followed by erosion until the Tertiary (Leammlen, 1970). The Miocene tectonic activity in the area is documented by the large accumulation of volcanic rocks on the surface (Vogelsberg, west of the Fulda basin) and by few 1-2 m thick basalt dykes which cut through the evaporite sequence (Knipping and Herrmann, 1985; Käding and Sessler, 1994).

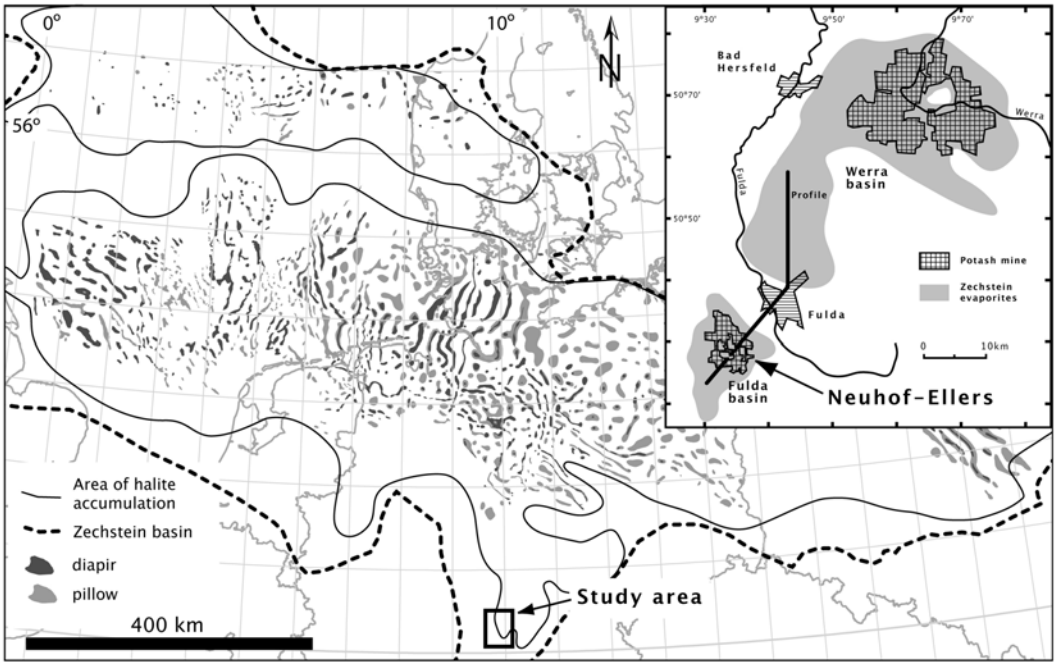

Fig. 1. The Permian Zechstein basin after Lohkämper et al., 2003 with the location of the Werra-Fulda basins is indicated (rectangle). Insert: detailed map of the Werra and Fulda basins (after Roth, 1957).

The Hessen potash layer in the Fulda basin is of economic importance (Beer, 1996). At present this potash horizon is at 500 m depth (Fig. 3). The potash deposit is only present in the central part of the basin because the 5 km wide region at the margins are completely leached due to contact with meteoric water. In that part the former potash layers now consist exclusively of a few centimeter large clear, euhedral halite crystals (Kühn, 1957; Leammlen, 1970). Where not leached, the layer consists mainly of kieserite, sylvite and halite (Hartsalz) with subordinate langbeinite, kainite, rarely carnallite and incorporates some thin clay layers (Kühn, 1957; Roth, 1955; Leammlen, 1970; Oesterle and Lippolt, 1975). At the upper part of the potash seam, a 40-50 cm thick halite layer is also incorporated. Above the seam, in the lowermost part of the Upper Werra rocksalt, a 0.3-2 m thick halite layer with subordinate sylvite and carnallite can be found (Fig. 2). Although the thick halite layers are horizontal and undeformed above this halite rich layer and below the potash level, the intercalated clay and halite layers in the Hessen potash seam – and especially the layer at the lowermost part of the Upper Werra rocksalt – are occasionally extensively folded (Roth, 1955; Kühn, 1957; Leammlen, 1970). The folds are tight, isoclinal with a near vertical axial plane (Fig. 4). The vergence of the folds is NE and the potash layer is often sheared off from the horizontal bottom and top halite layers (Hoppe, 1960). According to Leammlen, 1970, the deformation was triggered by differential loading when basin became buried in the Jurassic and Cretaceous. Some authors (see Hoppe, 1960) suggested that Tertiary deformation phases also played an important role in the deformation of the layers, and that the rocksalt succession deformed in a brittle manner.

In this paper we studied folded rocksalt samples from the central part of the Fulda basin from the Hessen potash layer. Samples were taken from a horizontal exploration borehole at the Neuhof-Ellers salt mine. The exploration borehole (diameter ~7 cm) was completed by the Kali und Salz GmbH with continuous coring of the complete borehole. From this core material we selected a 12 m long section, which contained intensely folded halite layers. The exact orientation of the borehole is unknown, though the material represents the highly deformed Lower Werra rocksalt which was folded into the potash layer (R. Stax, pers. comm.). A detailed inspection showed that this interval contains four, approximately 1 cm thick, coarse-grained halite filled veins, from which the longest was selected for this study (Fig. 5). The orientation of the veins – as we could judge from the core samples – do not seem to correlate with each other and to any particular direction of the fold structures (axial plane etc.).

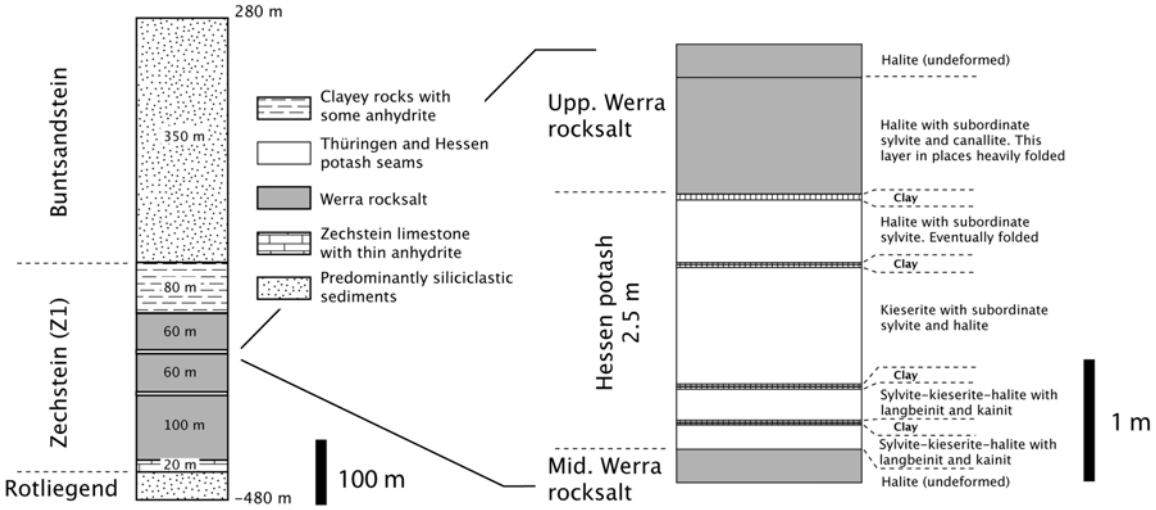

Fig. 2. Lithostratigraphic column of the Fulda basin and the Hessen potash layer after Leammlen, 1970 and Käding and Sessler, 1994.

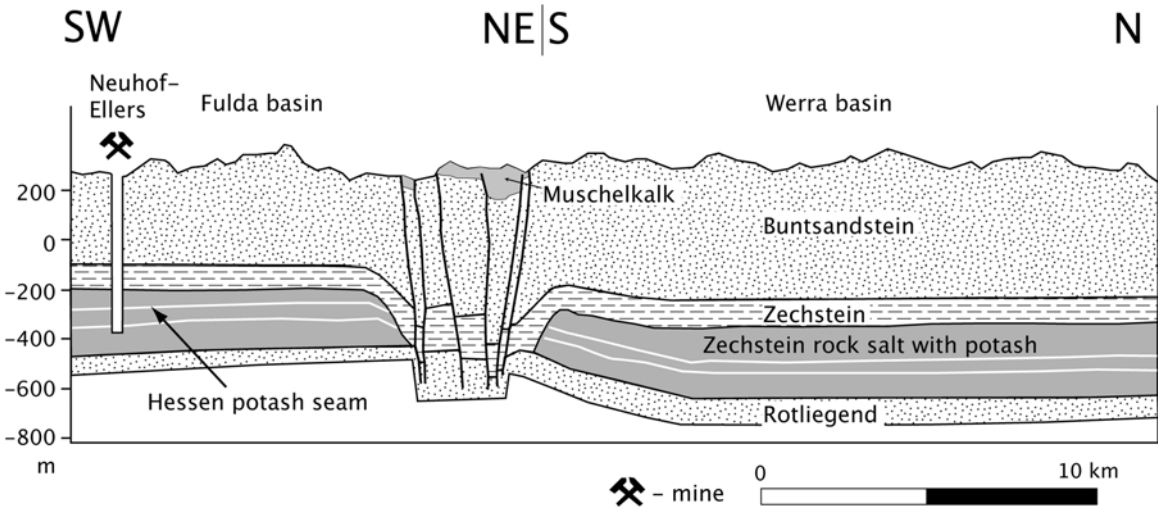

Fig. 3. Cross-section throughout the Fulda and Werra basins (after Beer, 1996). The samples studied were collected in the Hessen level of Neuhof mine. For the location of the profile see Fig. 1.

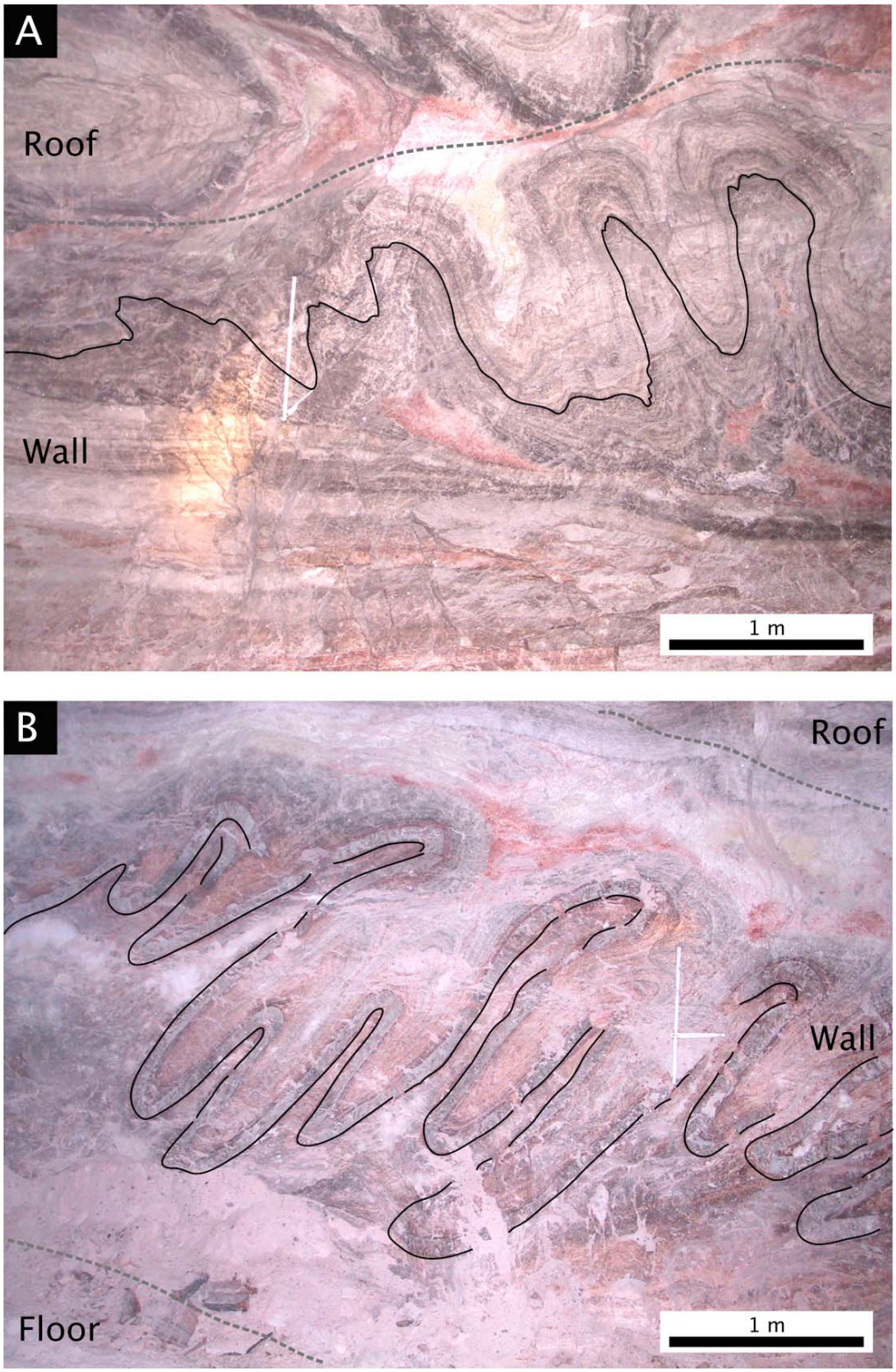

Fig. 4. The lower part of the Upper Werra Rocksalt is heavily folded in some parts of the mine. A: tight, isoclinal folds of halite and anhydrite with some reddish potash minerals. The vergence of the fault is NE. Note that the bottom layers are undeformed. B: Isoclinal folds of halite and clay layers (vergence: NNE).

3 Methods

Slabs were cut off from the sample, perpendicular to the vein. The slabs were then further prepared following the method described in Schléder and Urai, 2005. This involved gamma-irradiation of the samples at 100 °C, with a dose rate of 1-4 kGy/h to a total dose of 4 Mgy, followed by thin sections preparation from the slabs. The gamma-irradiation technique reveals otherwise invisible microstructures such as growth bands, subgrain boundaries somewhat in a similar way as the cathodoluminescence technique for carbonate and quartz (Murata and Smith, 1946; Przibram, 1954; Wilkins and Bird, 1980; Urai et al., 1987; Schléder and Urai, 2005). The sections were analyzed with transmitted and reflected light microscopy.

4 Observed microstructures and deduced mechanisms

4.1 Wall rock

The samples consist of alteration of 0.5 mm thin layers of anhydrite/polyhalite and 5 mm thick layer of halite (Fig. 5), cut by a 1 cm thick vein which is filled with 5 mm large, subhedral halite grains.

The pure halite (~99 %) layers consist of grains with sizes between 0.5 and 1 mm, often rich in primary fluid inclusions. The grains usually show core-mantle structures with a fluid-inclusion-rich core and a fluid-inclusion-free rim (Fig. 7B and D). In some cases the core is absent and halite grains are completely fluid-inclusion-free (Fig. 6D). Occasionally the two neighbor grains are truncated so that their fluid-inclusion-rich parts are in contact. We interpret such core-mantle and truncated structures as they evolved with non-conservative grain boundary migration. Synsedimentary dissolution-reprecipitation process were very likely not involved in producing those structures as none of the fluid-inlcusion-rich cores show karst-like, clear halite-filled dissolution structures.

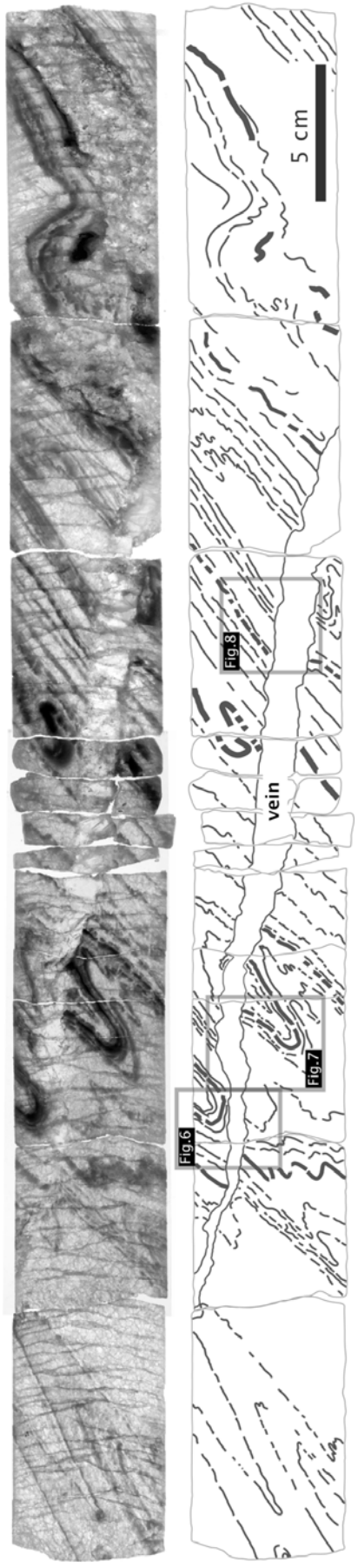

Fig. 5. Scanned image of the studied core interval together with the hand-drawing of traced anhydrite layers (black lines). The transparent layer which cut through the folded layers is a coarse grained halite filled vein. Note that there is a slight offset in the wall-rock across the vein. The locations of the studied thin sections are indicated with rectangles.

The lack of any dislocation related microstructures such as slip bands or subgrains and the presence of truncated grain cores suggest that the main deformation mechanism in this fine-grained rocksalt is solution-precipitation creep (Fig. 6 and 7). Such deformation mechanism was shown to be characteristic for fine-grained wet rocksalt (Urai et al., 1986b; Spiers and Schutjens, 1990). During this process the halite goes into solution in the highly stressed part and precipitates in the less stressed part (Urai et al., 1986a).
Due to the deformation the halite, grains become elongated compared to the intact grains and may have an aspect ratio up to 2. The elongation is subparallel to the axial plane of the fold (Fig. 7D), suggesting that the deformation was contemporaneous with the folding. An important observation is that the reprecipitated areas are fluid-inclusion-free, suggesting solution-precipitation creep during which the primary fluid inclusions were converted to grain boundary fluid. Approximately 35 % of the area of the material in the halite layers is fluid-inclusion-free. The surface energy driven grain boundary migration perhaps played a role in the recrystallization as most of the triple junctions are close to 120°.

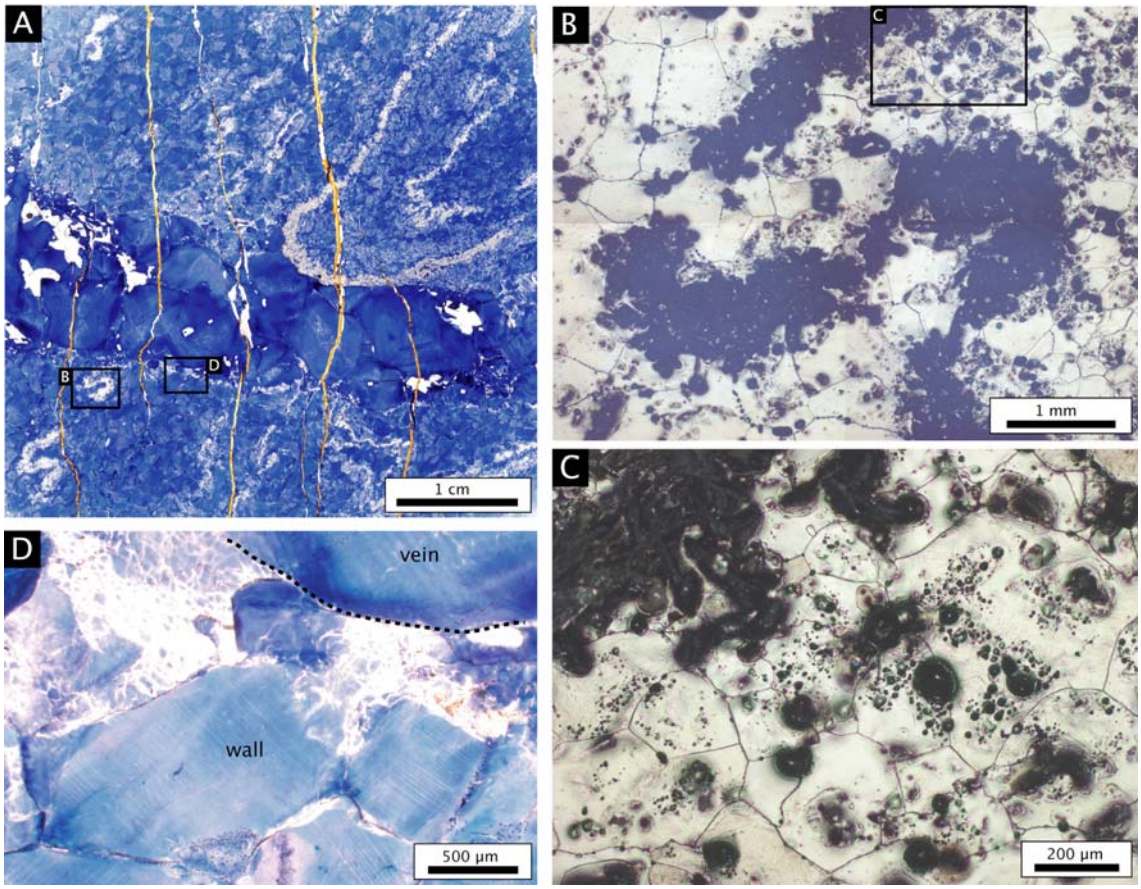

Fig. 6. A: overview gamma-irradiated thin section. For the location see Fig. 5. White anhydrite bands are isoclinally folded. The E-W trending coarse-grained part is the vein. B: detail of a part of a folded anhydrite layer in reflected light. For the location see image A. Note that the anhydrite layers are boudinaged, and that the halite grains are free of substructures. C: detail of image B. The black dots inside the halite grains are primary fluid inclusions opened up during sample preparation. Note again that the halite is without any substructure. D: detail of the vein-wall interface photographed in transmitted light (for location see image A). The grain boundaries occur as dark lines, the subgrains as white polygons. Note that at the presence of subgrains is limited to a narrow zone at the vein-wall interface.

The anhydrite layers are often boudinaged at the limbs of the fold and show minor folds at the internal part of the hinge zone (Fig. 6A and 7A). They often contain very small, equidimensional halite grains (0.5 mm on average) which contain numerous, small (< 50 μm), cubic, primary fluid inclusions. These small halite grains do not show any microstructural evidence of deformation or recrystallization, except where the layers are boudinaged or folded (Fig. 6B and C). In these parts, the grains show a core-mantle structure with a fluid-inclusion-rich core and a fluid-inclusion-free rim or, alternatively, the grains may be without any core and are completely fluid-inclusion-free. The fluid-inclusion-free area in the anhydrite rich layers makes up to 5 % of the salt.
This difference in extent of the deformation in the anhydrite rich and anhydrite poor layers can be explained by the higher mechanical strength of the anhydrite-rich layer causing strain concentration in the halite-rich layers (Bons, 1993). This difference in rheology might also be accounted for the strong folding of the rocksalt layers.

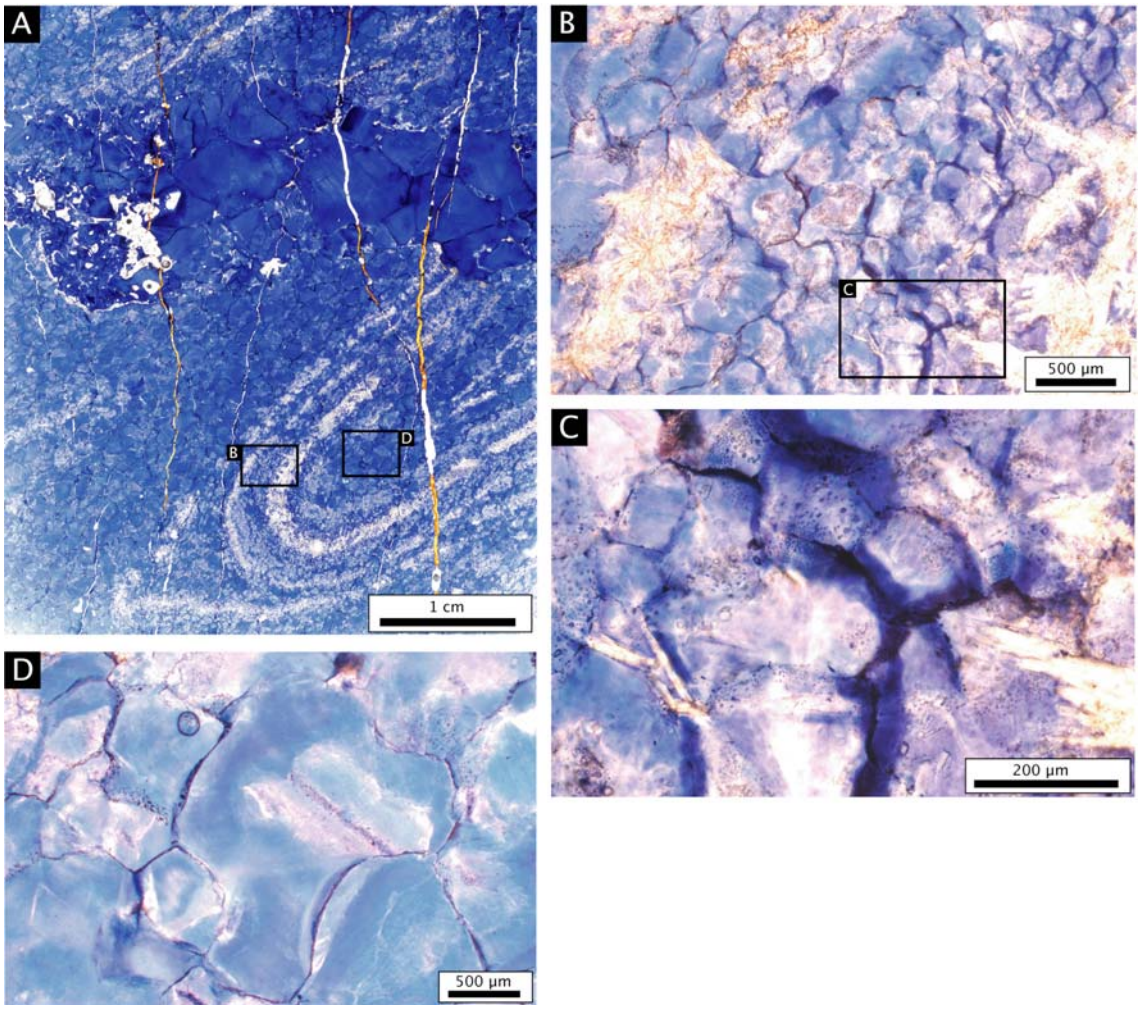

Fig. 7. A: gamma-irradiated thin section. The thin anhydrite layers (white) outline the tight isoclinal folds. Note that the E-W trending vein contains also subordinate amount of anhydrite (occur as white patches). The N-S oriented cracks were presumably introduced during the drilling and are now filled with resin. The locations of detail images of B and D are indicated with rectangles. B: detail transmitted light image shows a halite layer between two anhydrite bands. The off-white parts inside the halite grains are the fluid-inclusion-rich part. The fluid-inclusion-parts are interpreted as they formed during deformation during which the moving grain boundaries swept out the inclusions from the grains. Note that the fluid-inclusion-free parts are favorably oriented sub-parallel to the axial plane of the fold. C: detail of the image B shows a axial-plane-

parallel recrystallized band. D: Transmitted light detail image of the scanned thin section. Grain boundaries occur as dark lines. The grain in the middle contains an elongated fluid-inclusion-rich plate. Such a plate is interpreted as nucleated at the brine-air interface, after which it sank to the bottom. The plate is surrounded with fluid-inclusion-free rim, which is interpreted as recrystallized part.

The microstructures show that primary subaqueous depositional structures are well preserved. The layers are composed exclusively of halite cumulates – mm sized plates, cubes and hoppers (Figs, 7B and D) – very likely originally crystallized at the brine-air interface (Warren, 2006). The lack of a syndepositional dissolution surface implies that the halite was precipitated in a perennial halite-saturated brine (Lowenstein and Hardie, 1985). The thin anhydrite layers might have precipitated originally as gypsum when the brine body was diluted cyclically with halite-unsaturated water but was converted later to anhydrite during burial (Shearman, 1970). The timing of this mineral transformation is not entirely clear.
Halite grains close to the vein occasionally contain well-developed, equidimensional subgrains. The thickness of such subgrain-rich zone does not exceed a few millimeters. The presence of these subgrains very likely relates to the brittle process with which the vein opened up.

Based on the microstructures, it is inferred that the operating deformation mechanism during folding is solution-precipitation creep. The rheology of halite deforming by this process can be described by the following flow law of:

$$\dot{\varepsilon} = 4.7 \times 10^{-4} \exp\left(-24530 / RT\right)\left(\sigma_1 - \sigma_3\right) / TD^3$$ after Spiers et al., 1990

for which the strain rate (ε) is in s^{-1}, the pre-exponential constant is in $MPa^{-n}s^{-1}$, apparent activation energy is in $Jmol^{-1}$, Boltzmann's gas constant (R) is in $Jmol^{-1}K^{-1}$, temperature (T) is in *K*, differential stress (σ_1 - σ_3) is in *MPa* and grain size (D) is in *mm*. For the calculations, we lack the exact temperature value during the deformation, but based on considerations on the required temperature for metamorphosis of the potash minerals and formation of langbeinite, it has been suggested that the deepest burial exceeded 1 km (Oesterle and Lippolt, 1975), and that the geothermal gradient was extremely high (1 °C / 16 m Werner and Doebl, 1974). This suggests that the temperature was around 80 °C. In-situ paleo-differential stress values are not available for the samples, though this is relatively unimportant as the solution-precipitation creep process is largely independent of differential stress. The strain rate calculation implies that this fine-grained salt is very weak, i.e. deforms relatively fast ($\dot{\varepsilon}$ ~ $5x10^{-10}$ 1/s for T=353 K and D=0.5 mm) even at low differential stresses (σ_1-σ_3=0.1-0.3 MPa). Although we are unable to constrain the in-situ differential stress value at Neuhof, we assume that the differential stress was below 0.3 MPa, because such a fine-grained wet salt described here cannot support more differential stress (Urai et al., 1986b).

4.2 Vein

The vein is filled mainly with large halite crystals (5 mm) and in some samples with a few percent of anhydrite (Figs. 6-8). The halite grains are euhedral and the gamma-irradiated sections show growth banding with alteration of darker coloured and pale-coloured layers. The orientation of the growth bands is crystallographically controlled and parallel to {100} facets (Fig. 8B-D). In some crystals, fluid inclusions arranged parallel to the growth banding are observed, implying that the growth occurred in the presence of fluids. No subgrains were

observed in the halite grains, except some elongated ones, which are perpendicular to the grain boundaries (Fig. 8C). These subgrains are very similar to those observed by Nollet et al., 2005a and are interpreted as grown synkinematically with the growth of the crystal. Such edgewise propagation of subgrain boundaries behind migrating grain boundaries was also reported by Means and Ree, 1988 in experimentally deformed octachloropropane. Equidimensional subgrains or lobate grain boundaries were not observed in the vein, suggesting that the grains are undeformed, implying thus that the vein postdates the folding of the halite layers.

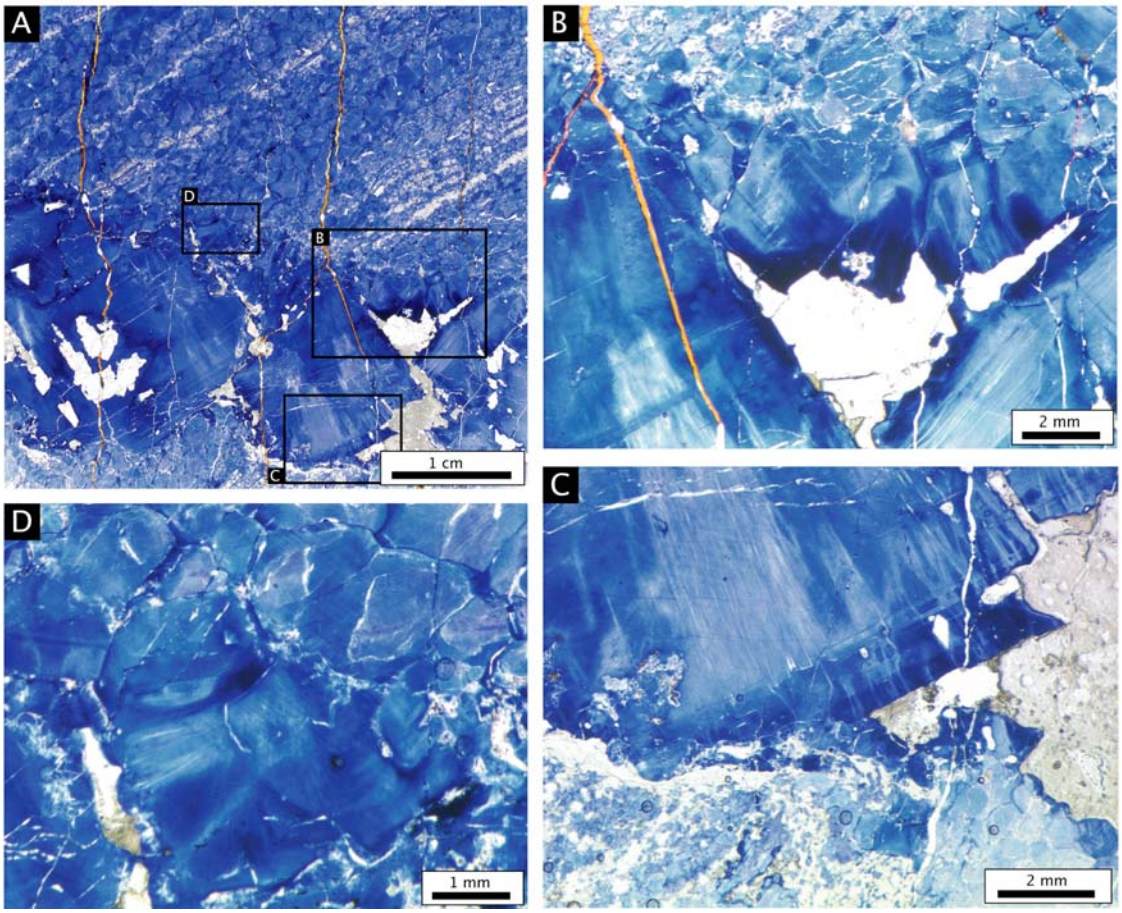

Fig. 8. A: gamma-irradiated thin section scanned with transmitted light. The E-W trending vein is filled with large euhedral grains. Anhydrite and potash mineral is also intercalated (occur as white patches). The places of detail images of B, C and D are indicated with rectangles. B: detail of the wall-vein interface. Note that the crystals are overgrowth of the wall rock grains. The N-S oriented cracks are due to drilling and sample preparation. The white material patch indicates the former place of the potash, which has been dissolved during sample preparation. C: detail of the contact of the coarse grained vein halite and the wall rock. The elongated white lines are grown-in subgrains. Note the growth bands which are parallel to the {100} crystal facets. At the right side, the white patch shows the former place of the intercalated potash. D: additional image illustrating the vein-wall interface. Note that the vein crystals overgrow the wall-rock grains.

Similar blocky veins to those described were widely observed for example in shale, sandstone and limestone (Fisher and Brantley, 1992, Bons and Jessel, 1997; Hilgers, 2000; Nollet, 2005). Numerical simulations of crystal growth in fractures have shown that such veins form when the opening velocity of the fractures is larger than the growth velocity of the crystals (Hilgers et al., 2001; Nollet et al., 2005b). This indicates that the formation of such veins require

relatively wide, open gaps, which stay open as long as they become sealed with crystals growing in the gap.
The crystals in the vein may either grow by epitaxial overgrowth of the wall-rock crystals, or after nucleation of new crystals in the oversaturated fluid in the gap (e.g. Bons and Jessel, 1997). In the case where the crystals overgrow the wall-rock crystals, growth competition takes place based on differences in the crystallographic orientation, resulting finally in a microstructure with a crystallographic preferred orientation (Nollet et al., 2005b). In the vein studied here, some vein-filling halite crystals are clearly the result of epitaxial overgrowth on wall-rock halite grains, although some do not have a connection to the wall-rock, and are completely enclosed with other crystals (Fig. 5A). This apparent feature may well be due to sectioning effect. The crystals, which are overgrowth of wall-rock grains, have a profound cornet-inward orientation (Fig. 5C), most probably reflecting growth competition (Thijssen, 1995; van Suchtelen, 1995).

5 Discussion

The presence of subgrains along the vein wall interface suggests that opening and subsequent vein growth was related to fracturing. The presence of primary fluid inclusions along the crystal facets and the absence of deformation in the vein microstructure implies growth in an unstrained environment. Different mechanisms may provide space for vein formation.
It is known from the literature that in ephemeral sedimentary environment the rocksalt often contains desiccation cracks, which are later filled with halite during synsedimentary processes. The presence of the studied vein can not be explained with such mechanism as the vein microstructure is undeformed and the vein is not folded.
Hoppe (1940) suggested that the rocksalt deformed in a brittle manner during the late Tertiary tectonic uplift of the area and implied that the veins might be associated to those deformations. However, it has been shown that even salt glaciers at the surface deform in a ductile way and do not show brittle deformation (Talbot and Aftabi, 2004), suggesting that Hoppe's statement should be treated with caution. A further objection against this theory is that a crack which opens up with dilation would be closed shortly after due to the ductile flow of the salt.
Yet an other alternative for the presence of veins in the vicinity of potash levels is that they are generated by hydrofracturing in a similar way as has been experimentally reproduced by Lux, 2005. According to this mechanism, to reach dilatancy the effective stress Hessen layer (~ 25 MPa) had to be reduced to arrive at the dilatancy field (Fig. 9). This mechanism would allow the crack to contain fluid at sufficient pressure which supports the lithostatic pressure and provides the time for the euhedral vein crystals to seal the fracture. Clearly, to be able to hydrofracture the salt large amount of overpressured fluid is needed. In what follows, we evaluate whether this mechanism is an alternative explanation for the vein generation in the rocksalt.
It is worth to note here that open cracks containing high pressured fluid or gas have been reported in several potash mines (Baumert, 1928 ;Weiss, 1980). Borchert and Muir, 1964 noted asymptotic decrease of flow rate of fluids with time from such cracks in potash mines and suggested that the cracks are not penetrative and are not in contact with meteoric waters.

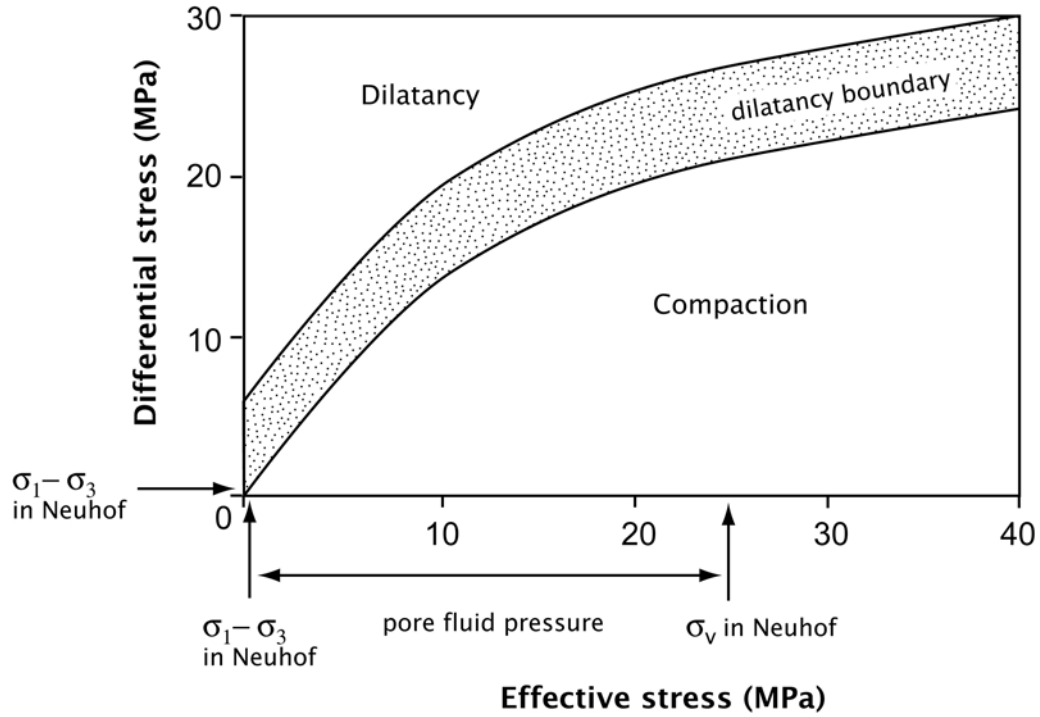

Fig. 9. Graph shows the non-dilatant field and the dilatant field for rocksalt (after Popp et al., 2001). We consider the hydrofracturing as one possible mechanism for the formation of the veins in the Hessen layer. To reach dilatancy, the effective stress at Neuhof (~ 25 MPa) had to be reduced to arrive at the dilatancy field. This might be attained by the presence of high-pressured fluids resulted from mineral transformations.

5.1 Fluid sources

The origin of potash minerals is an unsolved problem in many potash deposits worldwide (Warren, 2006). It is generally agreed that a paragenesis of sylvite, kieserite and halite is not a primary precipitate, since it would require sea temperature above 72 °C. This suggests that these are results of subsequent transformation of some pre-existing primary potash minerals (Kühn, 1957; Warren, 2006). Gottesmann, 1963 found microstructural evidence for the transition of primary carnallite to sylvite in the Stassfurt potash seam, and suggested that such metamorphism of carnallite is a common mechanism in the potash beds. Observations on recent potash precipitates also suggest that the carnallite is the main potash phase (Warren, 2006). On the contrary, based on mutual relationship between halite and sylvite, Lowenstein and Spencer, 1990 argued that sylvite rather than carnallite was the primary precipitate in the Rhine Graben (Germany), Salado formation (New Mexico, USA) and Prairie formation (Saskatchewan, Canada). Borchert and Muir (1964, p 172) suggested that the secondary sylvite might convert back to carnallite when in contact with $MgCl_2$ rich brines, making the differentiation between primary and secondary potash minerals very difficult. According to Baar, 1959 the carnallite conversion to sylvite accompany by volume decrease.

The origin of the potash layers in the Werra and Fulda basins is also not entirely clear (Käding and Sessler, 1994). Roth, 1955 suggested a metamorphic origin for the langbenite in the Hessen layer by metamorphosis of sylvite and kieserite in the presence of NaCl, containing solution according to: $2KCl + 3\ MgSO_4{\cdot}H2O \rightarrow K_2SO_4{\cdot}2MgSO_4 + MgCl_2 + 3\ H_2O$. Oesterle and Lippolt, 1975 investigated the age of the langbeinite crystals using K/Ar and

Rb/Sr radiometric methods and found that the langbeinite was formed at 150 Ma ago. They argued that the langbeinite formation coincides with the deepest burial (>1100 m) and main deformation of the salt layers, which results in the strong folding of the halite layer. They argued that the geothermal gradient was high, and that the temperature of 83 °C was reached at that depth (Werner and Doebl, 1974). In their model, Cenozoic tectonics and the Miocene volcanism do not have a significant effect on the salt succession. Kühn (1957) suggested that the kainit is also a metamorphic mineral and a result of the reaction of sylvite and kieserite ($KCl + MgSO_4 \cdot H2O + 2H_2O \rightarrow KCl \cdot MgSO_4 \cdot 3H_2O$). He noted that the kainit generation would accompany in volume increase of 28%.
As all the above cited studies suggest that the Hessen layer underwent significant metamorphism, it seems viable to assume that all the sylvite in the Hessen layer was once carnallite and following reaction occurred: $KMgCl_3 \cdot 6H_2O + 4H_2O \rightarrow KCl + Mg^{2+} + 2Cl^- + 10H_2O$. Thus if we consider that the layer contains of about 20 % of sylvite (Roth, 1955) and that this sylvite was originally carnallite, the conversion results in release of 1.4 m^3 of water per 1 m^3 of admixture of halite, kieserite and carnallite. It has to be noted here that presence of the water, which results in the breakdown of the carnallite, is not entirely clear. It may have been generated by the dehydration of clay, gypsum-anhydrite conversion in the rocksalt layers or intergranular water resulting from recrystallization of rocksalt.

Mineral transformation also occurred in the anhydrite layers. Since the $CaSO_4$ precipitates primarily gypsum rather as anhydrite (Warren, 2006 and references therein) it is supposed that the ~8 m thick anhydrite bed at the bottom and the top of the Z1 sequence was once a gypsum layer which later converted to anhydrite. During conversion, according to the equation of: $CaSO_4 \cdot 2H_2O \rightarrow CaSO_4 + 2H_2O$, it is calculated that 1 m^3 gypsum results in 0.62 m^3 af anhydrite and 0.48 m^3 of $CaSO_4$ rich water (Borchert and Muir, 1964, p 133). It is very likely that the water, released from this mineral conversion, did not play a significant role in the metamorphic processes in the Hessen layer, because there is some 150 m thick rocksalt between the anhydrite and potash layers, through which this amount of fluid had to migrate. The conversion of the thin gypsum layers (now anhydrite) observed in the samples also did not lead to the release of significant amount of fluids, as suggested by the thickness of those layers (~ 0.5 mm).

Another possible fluid source is the expulsion of primary fluid inclusions during recrystallization of rocksalt. According to measurements on the samples in reflected light, the area occupied by fluid inclusions in the fluid-inclusion-rich core is about 4 %. Assuming that the fluid-inclusions occurred evenly distributed over the halite grain before recrystallization, we take this value as representative water content for the undeformed state. Based on a combination of transmitted and reflected light images of gamma-irradiated sections, we measured that the recrystallized part of the grains is about 30 %. Thus, the calculated amount of water which is released during recrystallization is 0.012 m^3 per 1 m^3 of deformed halite. The amount of this fluid, similarly to that produced by the transformation of gypsum to anhydrite in the samples, is very small. Some water is also expelled from the clay layers during their compaction, though the amount of these fluids is also very small.

Considering all the possibilities for fluid sources, it seems viable that the mineral transformations might have provided water, which in turn led to hydrofracturing of rocksalt. The most plausible water supply is that from the potash bed during the conversion of potash

minerals. We suggest that this fluid as it becomes overpressured, perhaps due to the volume increase during the formation of some of the potash minerals, leads to the overpressure of the fluid, which in turn then is able to hydrofracture of the salt (Fig. 9).

5.2 Precipitation of halite in the vein

Detailed calculations of the required amount of fluids from which the halite precipitated as well as the consideration of all the processes leading to the complete sealing of the vein is beyond of the scope of this paper thus here we shall only briefly address those problems. Once the crack opens, there are different possibilities for supersaturation of the fluid and precipitating of halite from the solution, for example drop in temperature, in pressure or mixing of different solutions. Temperature or pressure drops requires very large amount of fluids to completely seal a vein so that it is very unlikely that they played an important role in precipitating halite (Adams, 1931; Herrmann and Knipping, 1989). Mixing of solutions with different chemical composition can precipitate the maximum amount of halite. Herrmann and Knipping, 1989 consider mixing of $MgCl_2$ and NaCl solutions, and calculate that 12,2 m^3 NaCl solution and 13 m^3 $MgCl_2$ solution is required for complete sealing of a 1 cm thick 10 m x 10 m tabular shaped fracture. After the complete sealing, the amount of the rest solution is 23.4 m^3. Based on Br concentration measurements of a halite filled vein, Fischbeck and Bornemman, 1988 suggest this process as most plausible explanation for the sealing of halite veins. It has to be noted here that while the $MgCl_2$-rich solution can be easily explained by metamorphic reactions in the potash layer, the source of the required amount of NaCl solution is far from clear.

6 Conclusion

In this paper we analyzed folded rocksalt sample with a coarse-grained halite filled vein from the vicinity of the Hessen potash layer (Fulda basin). The aim was to characterize the deformation mechanism in the rocksalt and to constrain the processes which led to the vein formation based on the microstructures. We conclude the following:

- The depositional environment for the rocksalt is very probably perennial lake. The salt crystals nucleated at the brine-air interface, and then sunk to the bottom of the lake. The anhydrite layers were presumably precipitated as gypsum and are due to cyclic arrival of arrival of halite unsaturated water.
- Due to the synsedimentary processes, the rocksalt sample is fine-grained, so that it deforms entirely with solution-precipitation processes. Strength variations in anhydrite-rich and poor layers are accounted for the strong folding in the halite beds.
- The Zechstein evaporite contain undeformed euhedral halite veins. The vein-wall interface shows a zone of subgrains, indicating strain localization possibly due to fracturing. The vein microstructure (subeuhedral grains) suggests that they grow freely into an open space.
- The potash mineral transformations results in large amount of fluids. Due to the volume increase after the metamorphism this fluid become overpressured.
- Evaluation of different processes suggests that hydrofracturing of rocksalt at almost lithostatic fluid pressures is the most likely process which led to the crack formation.

References

Adams, L. H., 1931. Equilibrium in binary systems under pressure. I. An experimental and thermodynamic investigation of the system NaCl-H2O at 25 °C. J. Am. Chem. Soc 53, 3769-3813.

Baar, C. A., 1959. Über gleichartige Gebirgsverformungen durc bergmännischen Abbau von Kaliflözen bzw. durch chemische Umbildung von Kaliflözen in geologischer Vergangenheit. Freiberger Forsch.-H., 137-159.

Baumert, B. 1928. Über Laugen- und Wasserzuflüsse im deutschen Kalibergbau, RWTH Aachen.

Becker, F., 2002. Zechsteinkalk und Unterer Werra-Anhydrit (Zechstein 1) in Hessen: Fazies, Sequenz-stratigraphie und Diagenese. Geologische Abhandlungen Hessen 109, 1-231.

Beer, W. W., 1996. Kalilagerstatten in Deutschland. Kali und Steinsalz 12(Heft 1), 18-30.

Bons, P. 1993. Experimental deformation of polyphase rock analogues. Unpublished PhD thesis, University of Utrecht.

Bons, P., 2001. The formation of large quartz veins by rapid ascent of fluids in mobile hydrofractures. Tectonophysics 336, 1-17.

Bons, P., Jessel, M. W., 1997. Experimental simulation of the formation of fibrous veins by localised dissolution-precipitation creep. Mineralogical Magazine 61, 53-63.

Borchert, H., Muir, R. O. 1964. Salt Deposits. The origin, metamorphism and deformation of evaporites. D. van Nostrand Company, Ltd., London, New York, Toronto, 338

Casas, E., Lowenstein, T. K., 1989. Diagenesis od saline pan halite: comparison of petrographic features of modern, Quaternary and Permian halites. Journal of Sedimentary Petrology 59(5), 724-739.

Fischbeck, R., Bornemman, O., 1988. Genetische Überlegungen aufgrund von Brom-Bestimmungen an halitischen Kluftfüllungen is Salzgesteinen des Salzstocks Gorleben, Niedersachsen. Fortschritte der Mineralogie 66(1), 35.

Fisher, D. M., Brantley, S. L., 1992. Models of quartz overgrowth and vein formation: deformation and episodic fluid flow in an ancient subduction zone. Journal of Geophysical Research 97, 20043-20061.

Fokker, P. A. 1995. The behaviour of salt and salt caverns, TU Delft.

Gottesmann, W., 1963. Eine häufig auftertende Struktur des Halits im Kaliflöz, Stassfurt. Geologie 12(5), 576-581.

Handford, R. C., 1990. Halite depositional facies in a solar salt pond: A key to interpreting physical energy and water depth in ancient deposits? Geology 18, 691-694.

Herrmann, A. G., 1981. Grundkenntnisse ueber die Entstehung mariner Salzlagerstätten. Der Aufschluss - Zeitschrift fuer Freunde der Mineralogie und Geologie Jh. 32(Feb. 1981), 1-72.

Herrmann, A. G., Knipping, B., 1989. Stoffbestand von Salzstöcken und Langzeitsicherheit für Endlager radioaktiver Abfälle. PTB informiert: Fachbeiträge zur Sicherstellung und zur Endlagerung radioaktiver Abfälle 1(89), 2-50.

Hilgers, C. 2000. Vein growth in fractures - experimental, numerical and real rock studies. Unpublished PhD thesis, RWTH Aachen.

Hilgers, C., Koehn, D., Bons, P., Urai, J. L., 2001. Development of crystal morphology during unitaxial growth in a progressively widening vein: II. Numerical simulations of the evolution of antitaxial fibrous veins. Journal of Structural Geology 23, 873-885.

Hoppe, W., 1960. Die Kali- und Stensalzlagerstätten des Zechsteins in der Deutschen Demokratischen Republik. Teil 1: Das Werra-Gebiet. Freiberger Forsch.-H. C 97(I), 166.

Jahne, H., Oettel, S., Voitel, R., 1970. Die feinstratigrapische Gliederung des Salinars im Zechstein 1 des Werra-Kaligebietes. Ber. deutsch. Ges. geol. Wiss. A. Geol. Paläont. 15(4), 505-515.

Jowett, E. C., Cathles, L. M., Davis, B. W., 1993. Predicting depths of gypsum dehydration in evaporitic sedimentary basins. The American Association of Petroleum Geologists Bulletin 77(3), 402-413.

Knipping, B., Herrmann, A. G., 1985. Mineralreaktionen und Stofftransporte an einem Kontakt Basalt-Carnallitit in Kalisalzhorizont Thüringen der Werra-Series des Zechsteins. Kali un Steinsalz 9, 111-124.

Käding, K. C., Sessler, W., 1994. Befahrung Kalibergwerkes Neuhof-Ellers der Kali und Steinsaz AG bei Fulda (Exkursion G am 8. April 1994). Jber. Mitt. oberrhein. geol. Ver. 76, 191-197.

Kühn, R., 1957. Führung durch das Kalibergwerk Neuhof-Ellers, obere Sohle, nebst einigen Beiträgen zur Petrographie des Werra-Fulda-Kalireviers. Fortschritte der Mineralogie 35, 60-120.

Leammlen, M. 1970. Geologische Karte von Hessen 1:25000 mit Erläuterungen. Blatt Nr. 5523 Neuhof, Wiesbaden, Germany,

Lewis, S., Holness, M., 1996. Equuilibrium halite-H2O dihedral angles: High rock-salt permeability in the shallow crust? Geology 24(5), 431-434.

Lohkämper, T. H. K., Jordan, G., Costamagna, R., Stöckhert, B., Schmahl, W. W., 2003. Phase shift interference microscope study of dissolution-precipitation processes of nonhydrostatically stressed halite crystals in solution. Contributions to Mineralogy and Petrology 146(3), 263-274.

Lowenstein, T. K., Hardie, L. A., 1985. Criteria for the recognition of salt-pan evaporites. Sedimentology 32, 627-644.

Lowenstein, T. K., Spencer, R. J., 1990. Syndepositional origin of potash evaporites: petrographic and fluid inlcusion evidence. Amercan Journal of Science 290, 1-42.

Lux, K.-H., 2005. Long-term behaviour of sealed liquid-filled salt cavities - A new approach for physical modelling and numerical simulation - Basics from theory and lab investigations. Erdöl Erdgas Kohle 121, 414-422.

Means, W. D., Ree, J. H., 1988. Seven types of subgrain boundaries in octachloropropane. Journal of Structural Geology 10, 765-770.

Murata, K. J., Smith, R. L., 1946. Manganese and lead coactivators of red fluorescence in halite. American Mineralogist 31, 527-538.

Nollet, S. 2005. Fracture sealing processes in sedimentary basins – a multi-scale approach. Unpublished PhD thesis, RWTH Aachen.

Nollet, S., Hilgers, C., Urai, J., 2005a. Sealing of fluid pathways in overpressure cells - a case study from the Buntsandstein in the Lower Saxony Basin (NW Germany). International Journal of Earth Sciences 94(5-6), 1039-1056.

Nollet, S., Urai, J. L., Bons, P. D., Hilgers, C., 2005b. Numerical simulations of polycrystal growth in veins. Journal of Structural Geology 27(2), 217-230.

Oesterle, F. P., Lippolt, H. J., 1975. Isotopische datierung der Langbeinitbildung in der Kalisalzlagerstätte des Fuldabeckens. Kali und Steinsalz 6, 391-398.

Peach, C. J., Spiers, C. J., Trimby, P. W., 2001. Effect of confining pressure on dilatation, recrystallization, and flow of rock salt at 150°C. Journal of Geophysical Research 106(B7), 13,315-13,328.

Popp, T., Kern, H., Schulze, O., 2001. Evolution if dilatancy and permeability in rock salt during hydrostatic compaction and triaxial deformation. Journal of Geophysical Research 106(B3), 4061-4078.

Przibram, K., 1954. Irradiation colours in minerals. Endeavour 13(49), 37-41.

Roedder, E., 1984. The fluids in salt. American Mineralogist 69, 413-439.

Roth, H., 1955. Ausbildung und Lagerungsformen des Kaliflöz "Hessen" im Fuldagebiet. Z. deutsch. geol. Ges. 105(4), 674-684.

Roth, H., 1957. Befahrung des Kalisalzbergwerkes "Wintershall" der Gewerkscahft Wintershall in Heringen/Werra. Fortschr. Miner. 35(1), 82-88.

Schléder, Z., Urai, J. L., 2005. Microstructural evolution of deformation-modified primary halite from the Middle Triassic Röt Formation at Hengelo, The Netherlands. International Journal of Earth Sciences 94, 941-955.

Schoenherr, J., Urai, J. L., Littke, R., Kukla, P., Newall, M., Al-Abry, N., Larroque, J.-M. 2005. Hydrocarbon-bearing Halite in the Ara Group (South Oman Salt Basin). General Assembly, European Geosciences Union, Vienna, 24-29 April 2005, 692.

Shearman, D. J., 1970. Recent halite rock, Baja California, Mexico. Transaction of Mining and Metallurgy 79B, 155-162.

Siemann, M. G., Ellendorff, B., 2001. The composition of gases in fluid inclusions of late Permian (Zechstein) marine evaporites in Northern Germany. Chemical Geology 173(1-3), 31-44.

Siemann, M. G., Schramm, M., 2002. Henry's and non-Henry's law behavior of Br in simple marine systems. Geochimica et Cosmochimica Acta 66(8), 1387-1399.

Skowronek, F., Fritsche, J.-G., Aragon, U., Rambow, D., 1999. Die Versenkung und Ausbreitung von Salzabwasser im Untergrund des Werra-Kaligebiets. Geologische Abhandlungen Hessen 105, 1-83.

Spiers, C. J., Schutjens, P. 1990. Densification of crystalline aggregates by fluid phase diffusional creep. In: Barber, D. J. & Meredith, P. D. (Eds.), Deformation processes in minerals, ceramics and rocks. Unwin Hyman, 334-353.

Talbot, C. J., Aftabi, P., 2004. Geology and models of salt exreusion at Qum Kuh, central Iran. Journal of the Geological Society 161, 321-334.

Thijssen, J. M., 1995. Simulation of polycrystalline growth in 2+1 dimensions. Physical Review Letters 51, 1985-1988.

Urai, J. L., Means, W. D., Lister, G. S. 1986a. Dynamic recrystallization of minerals. In: Hobbs, B. E. & Heard, H. C. (Eds.), Mineral and rock deformation: laboratory studies. AGU Geophysical Monograph 36. American Geophysical Union, 161-199.

Urai, J. L., Spiers, C. J., Peach, C., Franssen, R. C. M. W., Liezenberg, J. L., 1987. Deformation mechanisms operating in naturally deformed halite rocks as deduced from microstructural investigations. Geologie en Mijnbouw 66, 165-176.

Urai, J. L., Spiers, C. J., Zwart, H. J., Lister, G. S., 1986b. Weakening of rock salt by water during long-term creep. Nature (London) 324(6097), 554-557.

van Suchtelen, J. 1995. The geometry of crystal growth. In: Sunagawa, I. (Ed.), Morphology of crystals. Kluwer, Dordrecht, 419.

Wallner, M. 1986. Frac-pressure risk in rock salt. SMRI Autumn Meeting, Amsterdam, The Netherlands, 21-24 September, 1986, 1-14.

Warren, J. 2006. Evaporites: sediments, resources and hydrocarbons. Springer, 1036

Weiss, M. H., 1980. Möglichkeiten der entstehung sowie art, umfang und Tektonische stellung von Rissen und Klüften in Slazgebirge. GSF Bericht T-200.

Werner, D., Doebl, F., 1974. Eine geothermische Karte des Rheingrabenuntergrundes. No. 8.

Wilkins, R. W. T., Bird, J. R., 1980. The use of proton irradiation to reveal growth and deformation features in fluorite. American Mineralogist 65, 374-380.

Appendix

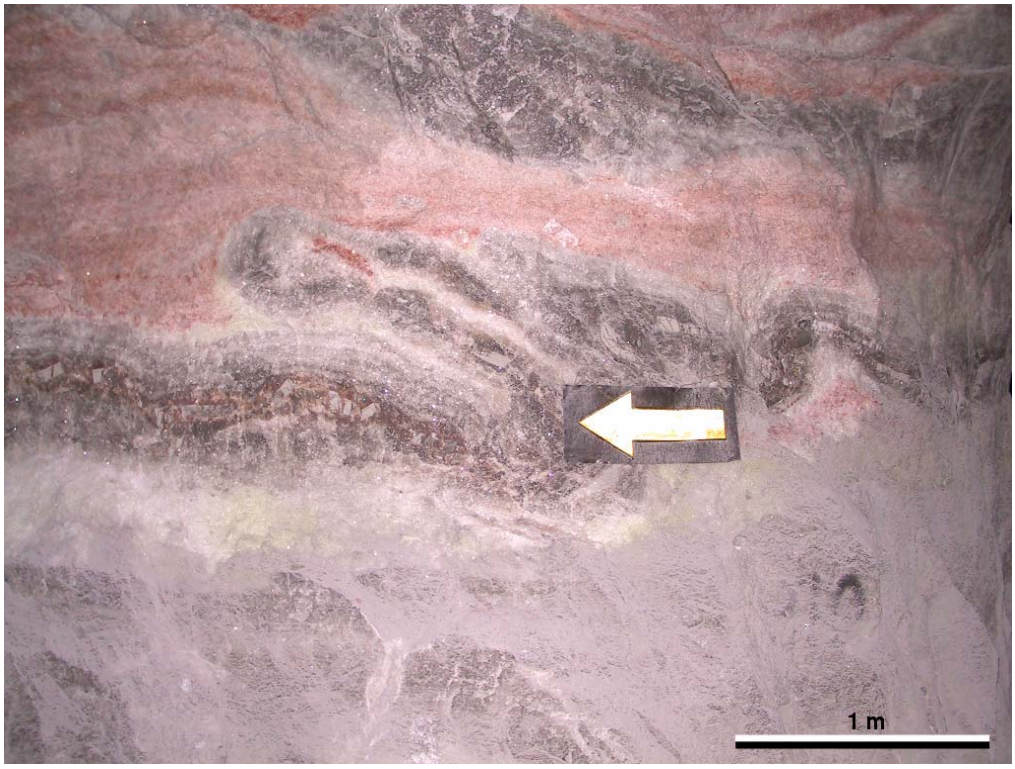

Fig. 1. Folded halite and clay layer in the Hessen potash layer.

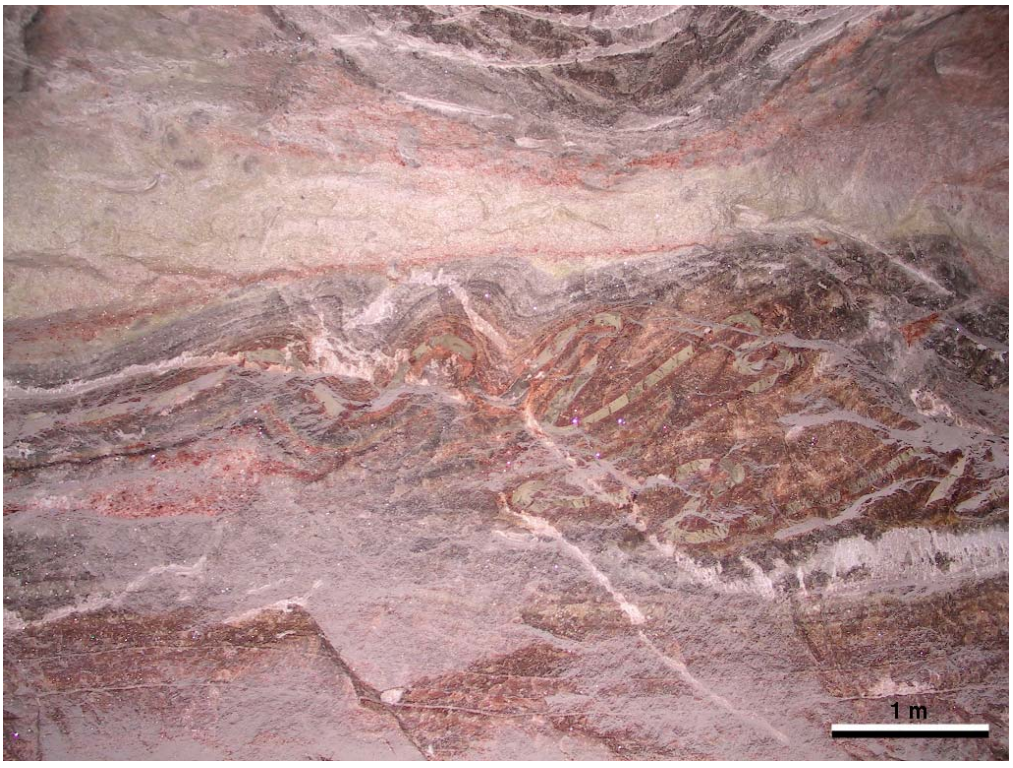

Fig. 2. Intensely folded clay layers in the Neuhof-Ellers potash mine. Note that at the bottom the halite layers are free of deformation.

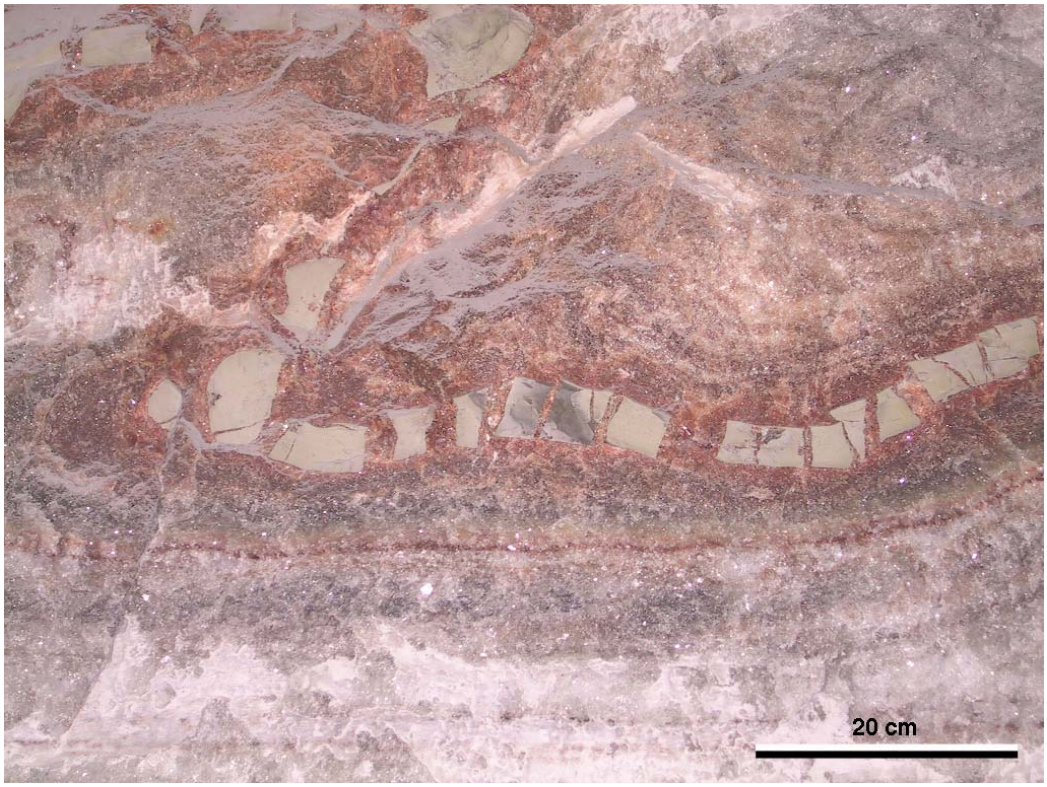

Fig. 3. Boudinaged and folded clay layer in the Hessen potash seam. The gray halite layers at the bottom are undeformed and belong to the Middle Werra rocksalt.

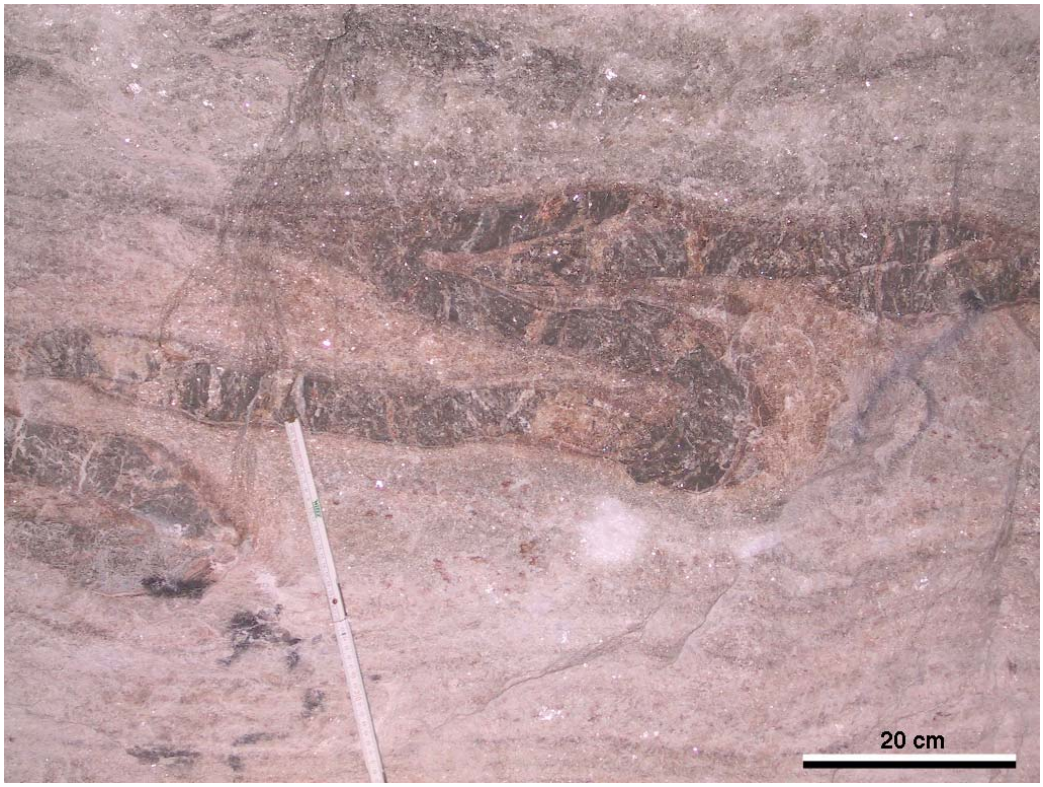

Fig. 4. Folded clay layers from the Hessen potash seam. Note that the clay layer is extremely rich in thin, halite filled veins.

Fig. 5. Isoclinally folded clay layers in the Hessen potash layer. The clay layer is cut through by several, halite filled veins.

Fig. 6. Imbricated boudains of clay layer in the Hessen potash seam. The gap between the boudains is filled with fibrous red-coloured halite.

Chapter 4: Dynamic and static recrystallization-related microstructures in halite samples from the Kłodawa salt wall (central Poland) as revealed by gamma-irradiation *

Zsolt Schléder, Stanisław Burliga and János L. Urai

Abstract

Microstructures of 33 rocksalt specimens from gallery walls from the highly strained part of the Kłodawa Salt Structure (Poland) were analyzed in gamma-irradiated and etched thin sections in reflected and transmitted light. Two types of microstructures could be distinguished i) dynamic recrystallization related ones caused by natural deformation and ii) static recrystallization related ones with uncertain origin, perhaps caused by subsequent mine-wall convergence.

Natural deformation-related microstructural features are the abundant subgrains and strain-free regions at grain boundaries together with elongated subgrains which imply dislocation climb controlled creep accompanied with fluid-assisted grain boundary migration as the deformation mechanism. Using subgrain size piezometry, differential stresses between 0.9 to 3.1 MPa were calculated.

All the samples contain a few percent (< 5 %) of euhedral statically recrystallized phase. In three samples the euhedral, statically recrystallized grains may comprise up to 85 % of the material. The microstructure suggests that the static recrystallization post-date the natural deformation-related features. The static recrystallization is thought to be due to mine-wall convergence. The pervasive crack system in the samples may also be explained by the stress concentration and subsequent minor mine-wall convergence. Detailed observations of the mutual relationship between the micro-cracks and the euhedral, statically recrystallized phase imply that as the new grains have grown, and their grain boundaries have swept through the material, some of the pre-existing cracks have not been consumed by the migrating boundary. This indicates that the material left behind by a migrating grain boundary is not entirely crack-free but inherits some microstructures from the consumed, old grains.

The presence of mining-induced static recrystallization warrants careful microstructure analysis before rocksalt samples being analyzed from mine galleries.

Keywords: Naturally deformed rocksalt, salt mine, dynamic recrystallization, mine-wall convergence, static recrystallization

* Schléder, Z., Burliga, S., Urai, J. L., In Press. Dynamic and static recrystallization-related microstructures in halite samples from the Kłodawa salt wall (central Poland) as revealed by gamma-irradiation. Neues Jahrbuch für Mineralogie und Petrologie.

1 Introduction

To date, studies of microscope-scale, deformation-related features in naturally deformed rocksalt have provided important insights into deformation and recrystallization mechanisms of halite. Urai et al. (1987) reported deformation mechanism of dislocation climb controlled creep accompanied with recrystallization mechanism of fluid-assisted grain boundary migration (FAGBM) from Zechstein salt (Asse salt mine). Miralles et al. (2000) systematically sampled and studied surface outcrops of Eocene rocksalt of the southern Pyrenees and proposed that synkinematic, fluid-assisted mechanisms (solution-precipitation creep and FAGBM) played the main role during the deformation of the salt diapir. Schléder & Urai (2005) focused on slightly deformed bedded Röt salt from the Netherlands, and concluded that dislocation creep mechanisms combined with solution-precipitation creep was the main deformation mechanism.

In this paper we present results of a study on highly strained rocksalt from a mine gallery of the Kłodawa Salt Structure. The study initially aimed to compare deformation mechanisms that operate in nature in different salt layers in a wide range of settings. Altogether 33 samples were analyzed. First inspection of the samples indicated that all the samples show comparable microstructures except three samples, which showed extensive static recrystallization. In this paper we focus on the statically recrystallized samples. The importance of getting insights into the cause of static recrystallization is stressed by the fact that such mine galleries are considered as suitable locations for storing radioactive or dangerous waste. The widespread usage of caverns as hydrocarbon or gas storage also implies the necessity of thorough knowledge of the micro-scale processes that operate in the walls of openings in salt bodies.

The study was dominantly based on inspection of gamma irradiated rock salt samples. This technique has proved to be one of the most effective methods in analyzing the internal structure of halite (Wilkins et al. 1981; Urai et al. 1987) and some other minerals (Wilkins & Bird 1980b; Wilkins & Bird 1980a). It reveals variations in defect and impurity content within crystals allowing different generations of halite and different deformation mechanisms to be distinguished (Przibram 1956; Urai et al. 1985; Van Opbroek & Den Hartog 1985; Garcia Celma & Donker 1996). Experimental work has shown that during irradiation a new, strain-free, euhedral halite phase also grows at the expense of old, deformed ones during irradiation, which partly alters the original structure (Garcia Celma & Donker 1996). Thus, special attention was also paid to those irradiation-induced structures when completing this work.

2 Geological setting

Kłodawa Salt Structure is one of the most prominent salt ridges occurring in the Danish-Polish Trough, extending over a distance of about 60 km and rising from a depth of about 6 km (Fig. 1). It contains Zechstein salt series, which became intensely folded, faulted and boudinaged during the complex structural evolution between the Triassic and Palaeogene. Geological observations carried out in the mine in the Kłodawa Salt Structure show that the eastern portion of the structure consists of relatively weakly disturbed Zechstein sequences, while its inner and western portions consist of strongly folded and distorted sequences (Figs. 2 and 3).

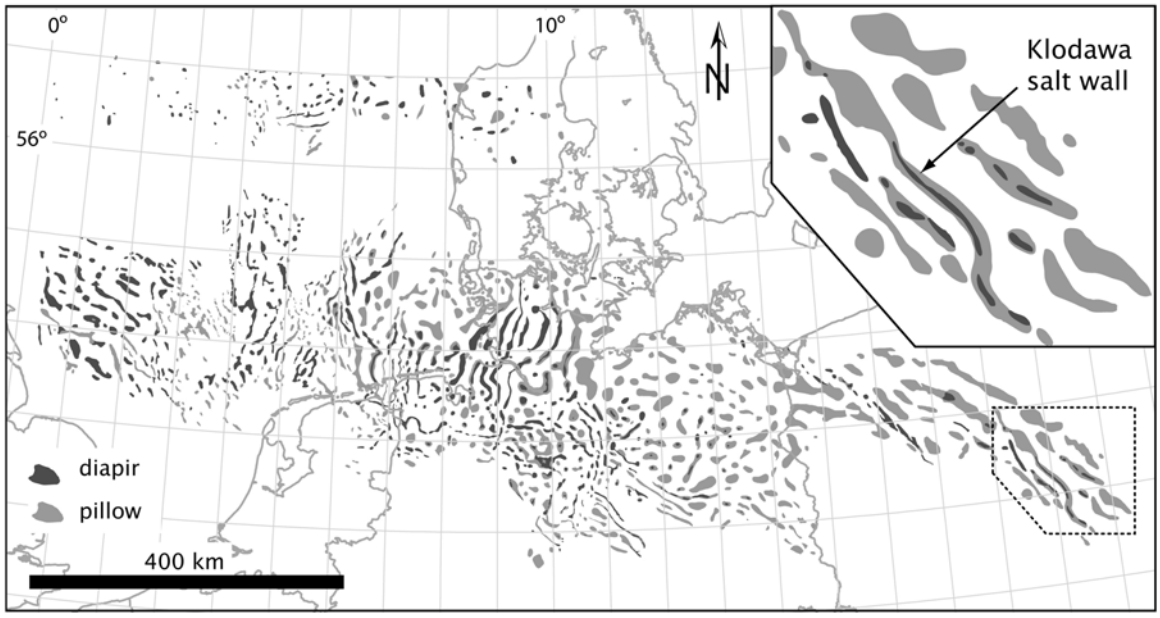

Fig. 1. Map showing the Zechstein basin (after Lockhorst 1998). Insert: location of the Klodawa Salt Structure (modified after Dadlez 2003).

The intensity of strain is related to lithological variation of the Zechstein series: the most severe tectonic deformation is observed within rocksalt and potash complexes and the weakest within more competent rocks – anhydrites, dolomites, clays and clayey salts (Burliga 1996).

A microstructural study was performed in order to inspect the stress and deformation features within rocksalt samples. For this analysis, the most strongly deformed portion of the Kłodawa Salt Structure was selected for sampling, i.e. its western side (Fig. 2).

33 spatially oriented samples were taken along a profile, which cut perpendicularly numerous fold structures of different scale, built of the Na4 Youngest and Na3 Younger Halite rocksalts (Fig. 4). These rocksalts are folded together with clayey salts and anhydrites into sheath folds at various scales. The fold limbs and axial planes are very steep-to-vertical and strike concordantly with the salt structure extension (Fig. 5). Fold hinge zones are very narrow and commonly modified by minor shear folding. The axial planes of all generation sheath folds are mutually parallel. Because of gallery dimensions, the exact tectonic position of only a few samples could be assessed (see Fig. 4). Most of the samples were taken along a profile with the aim of sampling different halite units (Fig. 4). During sampling we have focused on the pure halite layers as these horizons are thought to have experienced the most severe tectonic deformation.

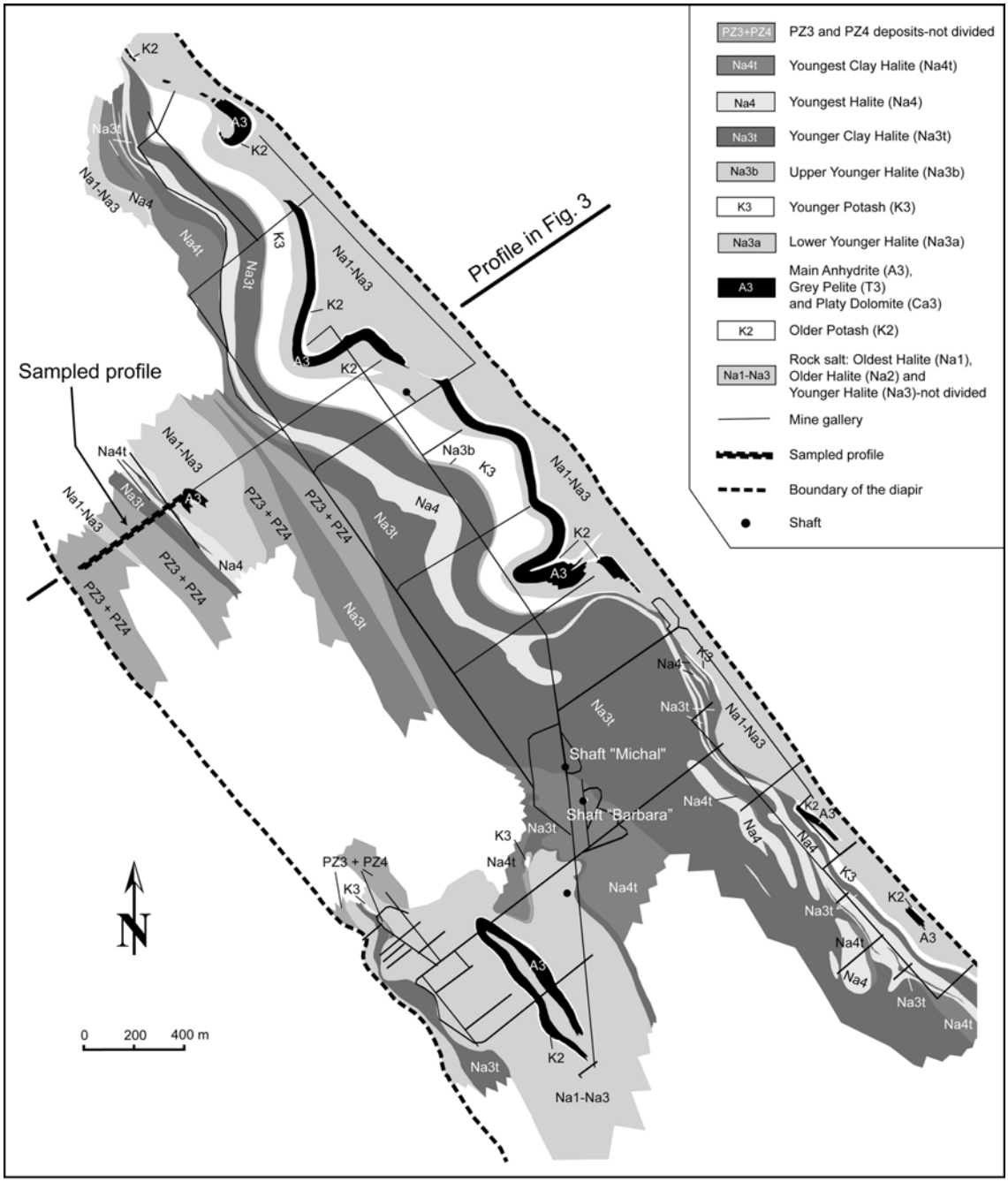

Fig. 2. Simplified geological map of the sampled mine level (-600 m). The position of the cross-section (Fig. 3) and the sampled profile is also indicated (modified after Burliga et al. 2005).

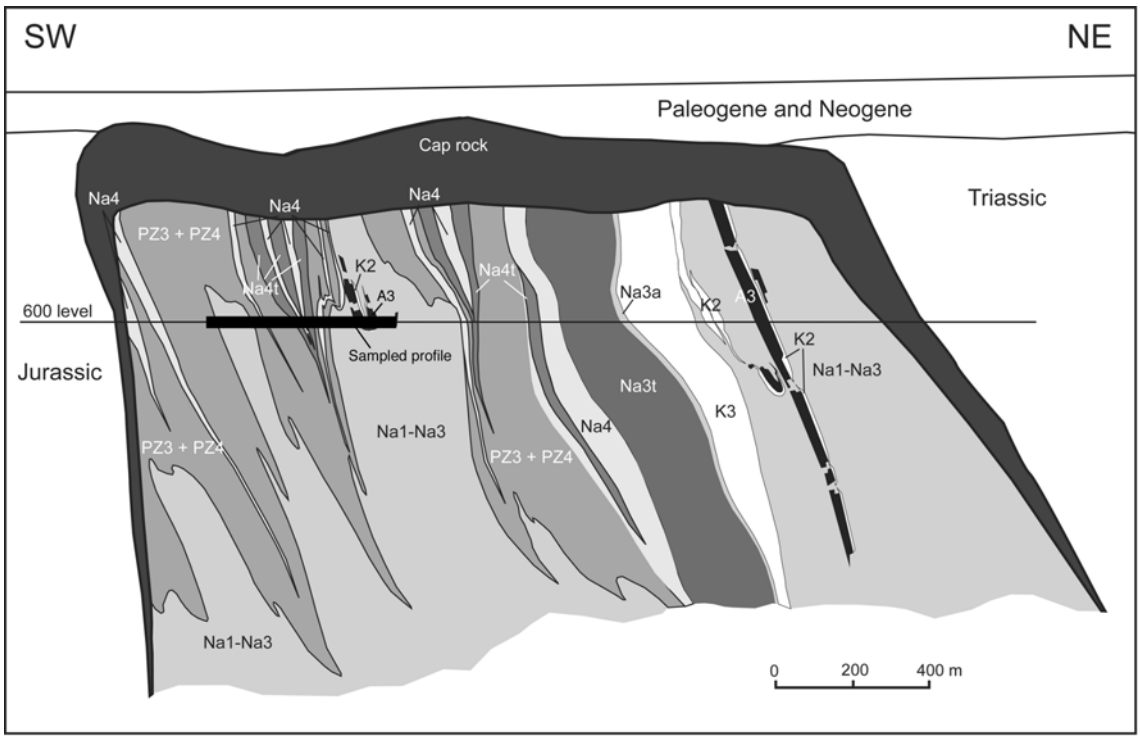

Fig. 3. Cross-section throughout the central part of the Klodawa Salt Structure. The sampled profile at the level -600 m is indicated with a black rectangle (modified after Burliga et al. 2005). The legend is the same as in Fig. 2. No vertical exaggeration.

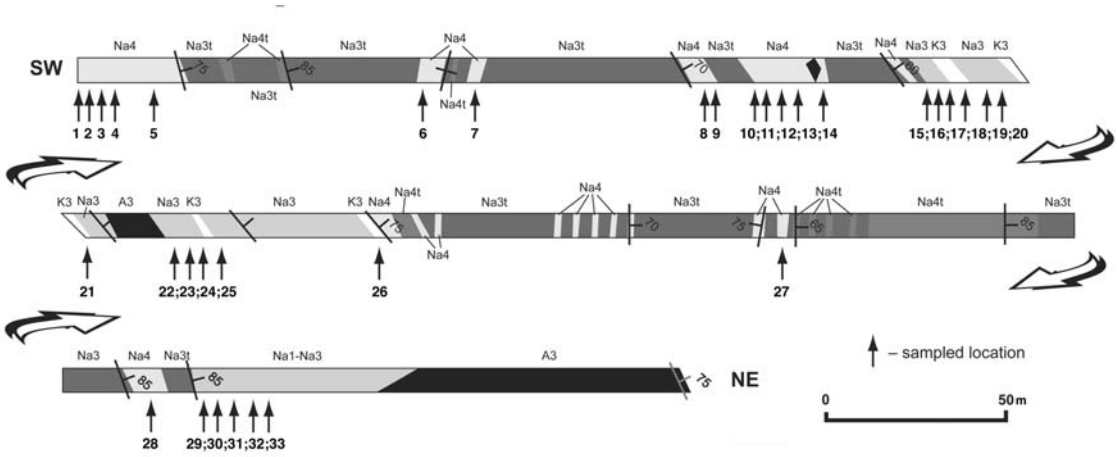

Fig. 4. Detailed stratigraphy of the sampled gallery. The arrows indicate the sampled localities. Note that the PZ3 and PZ4 units shown on the Fig. 2 have been further divided into individual units. For legend see Fig. 2.

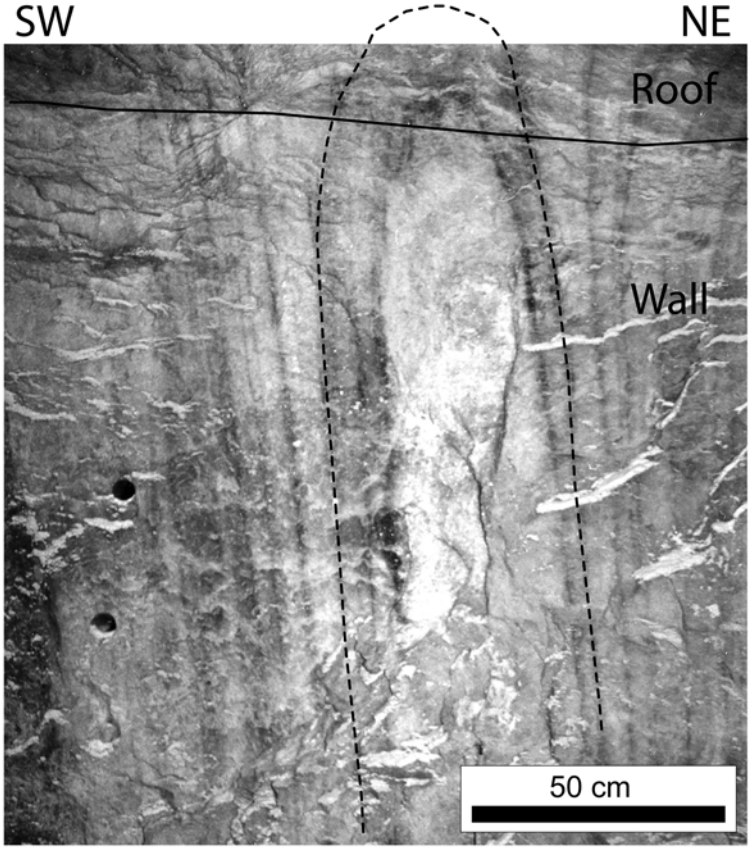

Fig. 5. Photo shows a near-vertical sheath fold. In the sampled gallery such structures are the most common.

3 Methods

From the oriented samples, 5 x 5 x 1 cm slabs were cut perpendicular to the bedding with a high-speed diamond saw using a small amount of water as cutting fluid to prevent micro-cracking. The slabs were gamma-irradiated in the research reactor of the Forschungszentrum Jülich with dose rates varying between 1 kGy/h to 3 kGy/h to a total dose of 3 MGy at a constant temperature of 100 °C. To check the effect of gamma-irradiation on microstructures, a few control samples were irradiated in the same conditions but to a total dose of 50 kGy (3 days of irradiation). After the gamma-irradiation, thin sections were prepared from the slabs, which were inspected with transmitted and reflected light petrographical microscope. The thin section preparation involved dry grinding of the slabs using grinding paper, which was followed by mounting to a glass plate using Körapox. The mounted slabs were cut with a diamond saw using small amount of water and the thin sections were grinded down to a thickness of about 20 μm and then etched using slightly undersaturated NaCl solution following the method of Urai et al. (1987). During every sample preparation step particular attention was paid to avoid introduction of any artificial microstructures, especially cracks. After the comparison of cracks in halite grains in the as-collected samples with those seen in thin section, we convinced ourselves that no additional cracks were introduced during sample preparation.

4 Petrography

Most of the analyzed samples consist of pure halite with a few percent of anhydrite and/or polyhalite as main impurity phases. Two of the samples (nr. 3 and 15) also contained admixture of few percent of potash salts. The internal structure of rocksalts depicts a variation in grain structure, their mutual relations and individual characteristics. Despite various locations of the samples within rocksalt units, generally they show very similar set of microstructures therefore they are characterized together. The exceptions are samples 8, 13 and 31 which contain abundant euhedral phase (see below).

The average grain size, measured by equal circular diameter method (ECD), varies between 3 to 25 mm (Table 1). The aspect ratio is around one, but locally may attain up to two and in such cases the rocksalt possesses a distinct fabric due to shape-preferred orientation. In transmitted light most of the gamma-irradiated rocksalt samples appears dark blue. In all the samples a few percent (<5 %) of euhedral, pale blue phase is present, however in three samples the euhedral, pale blue coloured crystals with banding might account for up to 85 % of grain constituents (samples 8, 13 and 31). The contact between these euhedral and dark blue grains is colourless and occasionally it forms rims around the euhedral, pale blue grains. In some cases the colourless phase contains tiny (<10 μm) fluid and gas inclusions aligned into bands parallel to the grain boundary.
The grain boundaries are typically irregular although the euhedral grains have straight boundaries. They are invariably ornamented with fluid inclusions and secondary phases. It is worth noting that, in contrast to euhedral grains, fluid inclusions were rarely observed inside halite grains (Fig. 6a, b and c). In some grains Na-precipitate decorated slip lines were observed (Fig. 6c).

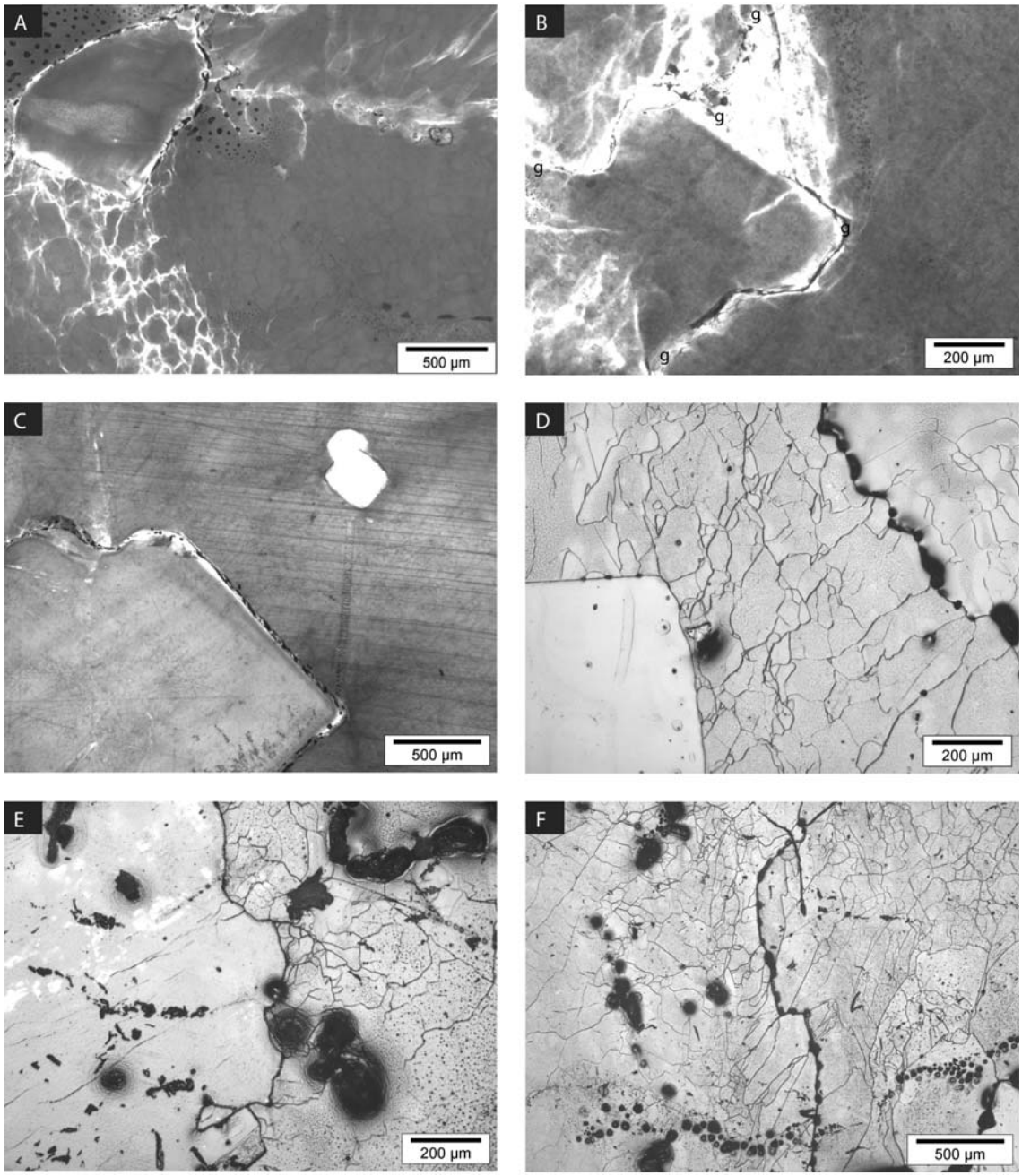

Fig. 6. Micrographs illustrate characteristic microstructures in the Klodawa salt. A) Two grains, one is without any substructure and one is locally rich in subgrains. The subgrains show up as white polygons. We interpret this micrograph as the substructure-free grain grows at the expense of the deformed neighbour. Transmitted light image of a gamma-irradiated thin section. B) Three grains separated by grain boundaries (g). All the grains are locally rich in subgrains. We interpret this image as the bottom left grain grows into the subgrain rich grain part of the other two grains. Transmitted light image of a gamma-irradiated thin section. C) Two grains separated by grain boundary (show up as dark line). The upper grain contains numerous Na colloid decorated slip lines (E-W trending lines). This image is interpreted as the undeformed grain grows at the expense of the deformed one. The white grain in the deformed grain is polyhalite. Transmitted light image of a gamma-irradiated thin section. D) Two grains (bottom left and top right) consume the subgrain-rich grain in the middle. The black spots at the grain boundaries are fluid inclusions opened up during sample preparation. Note that the grain at top-right itself also contains subgrains. Reflected light image of etched thin section. E) Two grains separated by a grain boundary (N-S trending, wavy black line). The grain at the right hand side contains numerous equiaxial subgrains, the grain at the left contains elongated subgrains. We interpret that the left grain replaces the highly substructured on the right, and the grain boundary migration results in elongated "grown-in"subgrains. Reflected light image of etched thin section. F) Image shows two

grains separated by a N-S trending grain boundary. Both grains are rich in subgrains and contain elongated subgrains at the grain boundary region. Such elongated subgrains can be interpreted as the grains completely consumed a former deformed old grain which was between the two grains, or, alternatively the microstructure evolved with crack-seal mechanism (see text for explanation). Reflected light image of etched thin section.

In most of the samples pervasive, grain-scale crack system is present with their orientation controlled presumably by crystallographic directions of the individual grains. The micro-crack system is marked by fluid inclusions and pale blue-to-colourless halos (Fig. 7a). The individual cracks may penetrate both the dark blue and pale blue phases as well as they can terminate at the boundary between the dark blue and pale blue grains (Fig. 7b, d). Less commonly the facets of pale blue grains are shifted across the micro-cracks or the growth bands have asymmetric thickness across the micro-cracks (Fig. 7b, d). Less frequently, along the cracks arrays of fine, <0.5 mm size, pale blue grains occur (Fig 7a). Similar arrays were occasionally also observed along grain boundaries.

In reflected light most of the grains reveal well-developed equiaxial subgrains, however at grain boundaries they are occasionally elongated (Fig. 6d, e and f). Subgrain size ranges from 50 to 220 μm (Fig. 6d, e and f). The euhedral phases are commonly free of any substructure, although they occasionally contain elongated subgrains (Fig. 7).

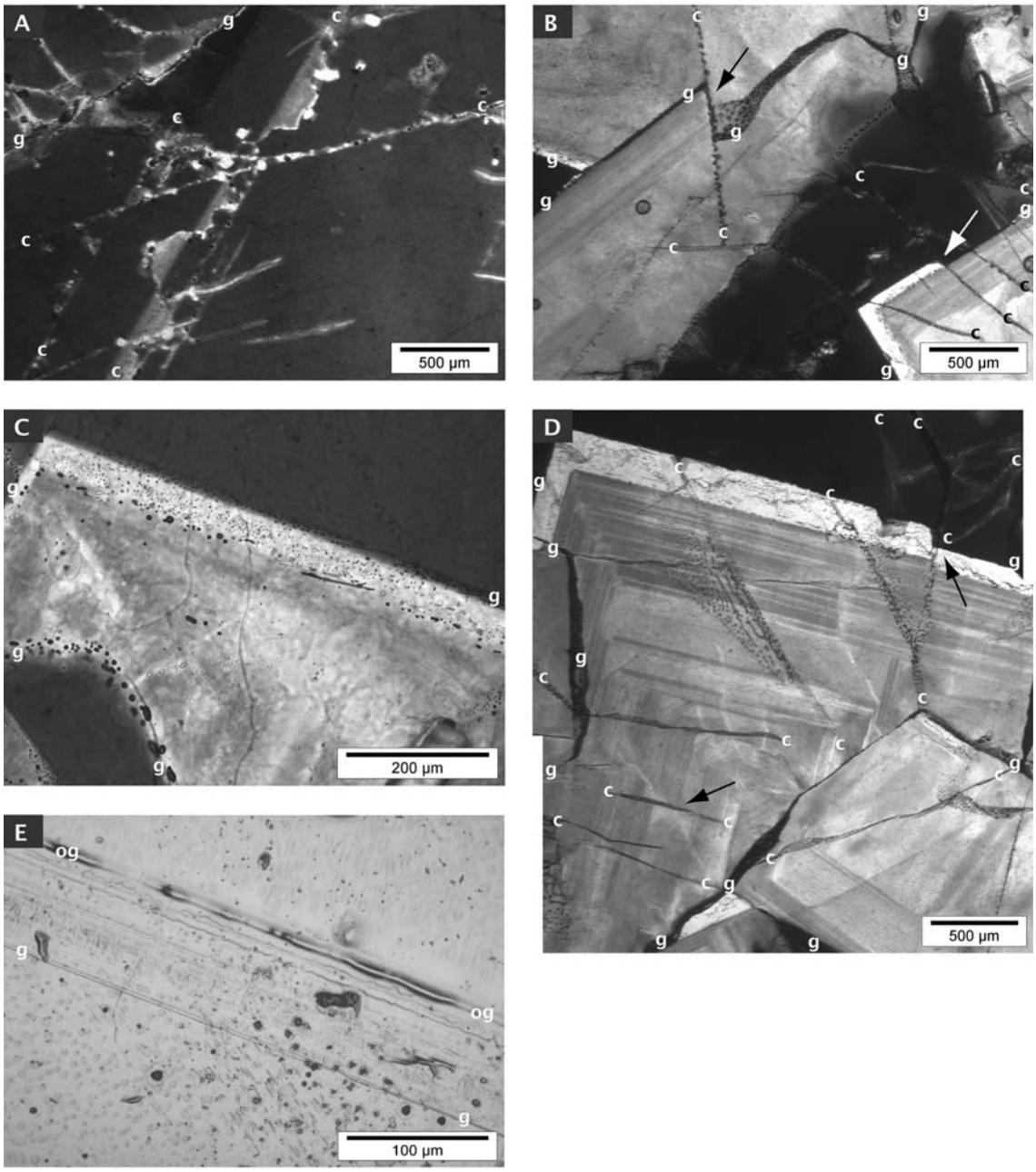

Fig. 7. A micrograph illustrating relationships between cracks, pale blue and colourless phase. A) Cracks (c-c) cut through a grain and also penetrate into the neighbour grain. The grain boundary (g-g) between the two grains shows up as a dark line. In the NE-SW oriented crack a number of pale bluepale blue phases (show up as pale-gray) are observed. This relationship suggests that the cracks are older than the pale blue phase. B) Five grains separated by grain boundaries (g-g). Numerous cracks are also seen (c-c). The facets of the euhedral grain at the bottom right are shifted by one of the cracks. At the middle of the image (see black arrow) the grain boundary, which separates two pale blue grains, is also shifted across the crack. This interaction of facets, grain boundaries with the cracks implies that at least some of the cracks are older than the recrystallization. C) pale blue (pale-gray) euhedral grain rimmed by the colourless phase contains numerous tiny inclusions, which in the image show up as dark spots. These inclusions are thought to consist of H_2 presumably produced by back-reaction of the colloidal sodium while the grain boundary migrated and the grain consumed its highly deformed neighbour. D) Four grains separated by grain boundaries (g-g). Similarly as in the image B, the cracks (c-c) shifting growth bands, as well as the grain boundary across the cracks can be observed (see arrows). The white rim is thought to be grown during gamma-irradiation. E) Image of etched thin section shows the colourless phase in reflected light. The og-og line marks the boundary between the pale blue and the colourless phase, the g-g marks the grain boundary between the colourless and the dark blue phase. The fine parallel lines between the og-og and g-g contain numerous tiny gas

inclusions, which opened up during etching. The gas inclusions are the product of back-reaction during gamma-irradiation.

5 Discussion

The observed microstructures suggest that in the samples studied there are two classes of structures. One is due to natural deformation and associated dynamic recrystallization. Most of the samples show such microstructures. Another, less common set observed in three samples (nr. 8, 13 and 31) is interpreted as produced by static recrystallization (Fig. 8). Thus, in the following chapters these microstructures are referred as dynamic recrystallization and static recrystallization related and they are discussed separately.

5.1 Dynamic recrystallization-related microstructures

In this set of microstructures the ubiquitous subgrains indicate dislocation creep as a dominant deformation mechanism (Fig. 6). Although we did not find direct microstructural evidence for solution-precipitation creep, it may well be that this grain-size sensitive deformation mechanism also contributed to the total strain rate, especially in the fine-grained samples (c.f. Spiers & Carter 1998). The elongated subgrains at grain boundaries are interpreted to have formed by grain boundary migration recrystallization mechanism (see Fig. 8a). This interpretation is consistent with earlier work on halite (Schléder & Urai 2005) and some other material (Means & Ree 1988). The elongated subgrains occurring at both sides of a grain boundary (e.g. Fig. 6f) can be explained in two different ways. One is that the two grains simultaneously and completely replaced a highly deformed third one resulting in elongated subgrains on both sides. The other explanation is that by crack-seal mechanism (Ramsay 1980), that is the two neighbour grains move away from each other with the gap opening between them is subsequently sealed with precipitates from the grain boundary fluid. In this case the microstructure points to grain boundary sliding as a supplementary deformation mechanism.

Subgrain size additionally was used for calculating paleo-stresses that prevailed during deformation. In 15 samples the equaxial subgrains were analyzed following the method described by Schléder & Urai (2005). Applying the equation of $_{1}- _{3} = 107\ D^{-0.87}$ (op. cit.), where the differential stress is expressed in MPa and the subgrain size in μm, the obtained differential stress values range on average between 0.9 and 3.1 MPa (Table 1).

Sample nr.	Grain diameter [mm]	Average subgrain diameter [μm]	Nr. of analyzed subgrains	1 st. dev.	Calculated differential stress [MPa]	Area % of euhedral phase
1	–	–	–	–	–	< 5
2	–	–	–	–	–	< 5
3	5	113	188	73	1.73	< 5
4	–	–	–	–	–	< 5
5	–	–	–	–	–	< 5
6	–	–	–	–	–	< 5
7	–	–	–	–	–	< 5
8	3	216	66	138	0.98	70
9	–	–	–	–	–	< 5
10	4.5	93	116	55	2.04	< 5
11	3.5	180	67	108	1.15	< 5
12	3.5	56	185	34	3.17	< 5
13	4	71	74	42	2.60	85
14	–	–	–	–	–	< 5
15	–	–	–	–	–	< 5
16	5	106	55	84	1.82	< 5
17	6	111	94	67	1.76	< 5
18	–	–	–	–	–	< 5
19	8	178	110	121	1.16	< 5
20	6.5	141	239	99	1.42	< 5
21	–	–	–	–	–	< 5
22	25	168	169	119	1.22	< 5
23	–	–	–	–	–	< 5
24	–	–	–	–	–	< 5
25	–	–	–	–	–	< 5
26	–	–	–	–	–	< 5
27	–	–	–	–	–	< 5
28	–	–	–	–	–	< 5
29	–	–	–	–	–	< 5
30	3	157	100	105	1.29	< 5
31	3	84	67	67	2.24	80
32	5	160	108	116	1.27	< 5
33	10	194	91	140	1.08	< 5

Table 1. Table showing the measured grain, subgrain diameters and the calculated differential stress values for 15 samples. Note the high area percentage of the euhedral phase in samples 8, 13 and 31.

This range of differential stress values is in a good agreement with earlier studies on naturally deformed salts (Carter et al. 1993). While some of the highest differential stress values were calculated for two of the highly recrystallized samples (nr. 13 and 31) surprisingly the other statically recrystallized sample (nr. 8) shows the lowest differential stress value.

Elongation of subgrains at grain boundary regions together with the strongly localized occurrence of fluid inclusions at the grain boundaries imply that fluid-assisted grain boundary migration was the main recrystallization mechanism. The lack of any primary structures, such as primary (synsedimentary) fluid inclusions in grains, suggests that these were swept during grain boundary migration and the salt had completely recrystallized during its deformation. All the above listed features are consistent with so far published data on naturally and experimentally deformed rocksalt (Carter et al. 1982; Carter & Hansen 1983;

Urai et al. 1987; Senseny et al. 1992; Carter et al. 1993; Spiers and Carter 1998; Peach et al. 2001; Schenk & Urai 2004; Ter Heege et al. 2005).

5.2 Static recrystallization-related microstructures

Euhedral overgrowth structures similar to those presented in this paper have been widely reported for gamma-irradiated rocksalt (Przibram 1956; Garcia Celma & Donker 1996). So far, such structures have been interpreted as a result of gamma-irradiation, which induces defects within the crystal lattice. As the defect density increases in two neighbour grains, either the old grain boundary begins to migrate or a new grain nucleates at the grain boundary and it grows at the expense of the two old, deformed grains. Both processes result in a new, strain free, pale blue to colourless phase. Such a phase was also observed invariably in all irradiated specimens from the Klodawa Salt Structure. However, a contrasting content of pale blue faceted crystals within three specimens implies that the irradiation-induced recrystallization cannot exclusively be accounted for the origin of the pale blue and colourless phases. One must also exclude the irradiation dose as the possible cause for the observed extensive static recrystallization of the three samples as one control sample which was irradiated only for three days still depicts the same microstructures. Therefore the growth of euhedral phase is not related to the gamma-irradiation alone. Fluid and gas inclusions in the colourless phase may be the product of back-reaction of sodium colloids during grain boundary migration (Fig. 7c), thus indicating that this phase was grown during irradiation (Fig. 7c and e) (Garcia Celma 1993). In this process, as the grain boundary migrates and the grain boundary brine interacts with the colloidal Na, H_2 gas is released according to the equation of: $2Na+2H_2O \quad 2NaOH+H_2$. This is additionally supported by detailed observations of mutual relations between pale blue and colourless phases, which show that where both the colourless phase and the pale blue phase are present, the colourless one occurs invariably as rims around the pale blue phase, and never as inclusions inside the pale blue phase (Fig. 7b, c and d). The new, pale blue phase commonly nucleates at the old grain boundary region as evidenced by concentric growth bands. The nucleation of new strain-free grains is common in many materials, although the physics behind the nucleation process is poorly understood (Urai et al. 1986; Prior et al. 2004). The driving force for the static recrystallization arises from the internal strain energy, which induces nucleation and subsequent grain boundary migration (Humphreys & Hatherly 1996). The increase of strain energy, which led to nucleation of new grains in the euhedral-grain-rich samples, is difficult to identify. Comparing to other naturally deformed salts (Urai et al. 1987; Schléder & Urai 2005), the microstructures and subgrain sizes are much alike, suggesting that natural process have not played a role in producing these new, recrystallized phases. A possible mechanism could be the mine wall convergence (see Fig. 8b-e), which may have increased the internal strain energy, which subsequently led to nucleation of new grains. It remains, however, temporarily unsolved why this phenomenon occurs only locally.

The parallel dark blue bands seen in the pale blue, euhedral phase are best interpreted as growth bands and are much alike as seen in fluorescence studies on artificial, doped halite crystals by Murata & Smith (1946). The difference in colour intensity between the bands is interpreted to be due to differences in impurity content (Murata & Smith 1946). The fact that the growth bands have asymmetric thickness across the micro-cracks and that the facets of the euhedral phase are shifted across the micro-cracks (Fig. 7b and c) implies that the cracks are older than the new pale blue, euhedral phase. Additionally, small, <0.5 mm sized pale

blue coloured crystallites were also observed inside the cracks, which supports this assumption (Fig. 7a). If the cracks were younger than the euhedral phase then the euhedral crystals should be dark blue in transmitted light as a late cracking event would have introduced new dislocations and the gamma-irradiation is sensitive to the dislocation density. Taken those findings together, this implies that as the new phase grows at the expense of the old deformed ones, some of the pre-existing micro-cracks are not erased from the material. Recently, some other authors arrived at somewhat similar conclusions by inspecting partly recrystallized, experimentally deformed rocksalts. Bestmann et al. (2005) noted that when grain boundary migration occurs between two substructured grains then the swept area inherited some microstructures from the consumed grain. In the same experiment the newly nucleated grains that swept faster over substructured old grains did not take over the microstructures of the consumed grains.

It is important to speculate on the origin of the pervasive crack system. From microstructural studies, it seems that the micro-cracks are rather uncommon features in naturally deformed rocksalts (Urai et al. 1987; Miralles et al. 2000; Schléder & Urai 2005), however recently Schoenherr et al. (2005) reported hydrocarbon impregnated micro-cracks from the vicinity of highly over pressured reservoirs and suggested that they aroused due to presence of fluids at lithostatic pressure. Although we cannot entirely rule out this mechanism provoking the pervasive crack system seen in the specimens studied, the fact that they occur only in 3 samples may suggest that this process did not play a role in generating the micro-cracks. Another possible candidate mechanism for the micro-cracking is that due to stress concentration around mine galleries. This process occurs in underground openings and is also a well-known phenomenon in some salt mines (slab-like slaking). The convergence process may well be responsible for the increase in strain energy, which in turn also controls the abundance of the new, euhedral statically recrystallized phase.

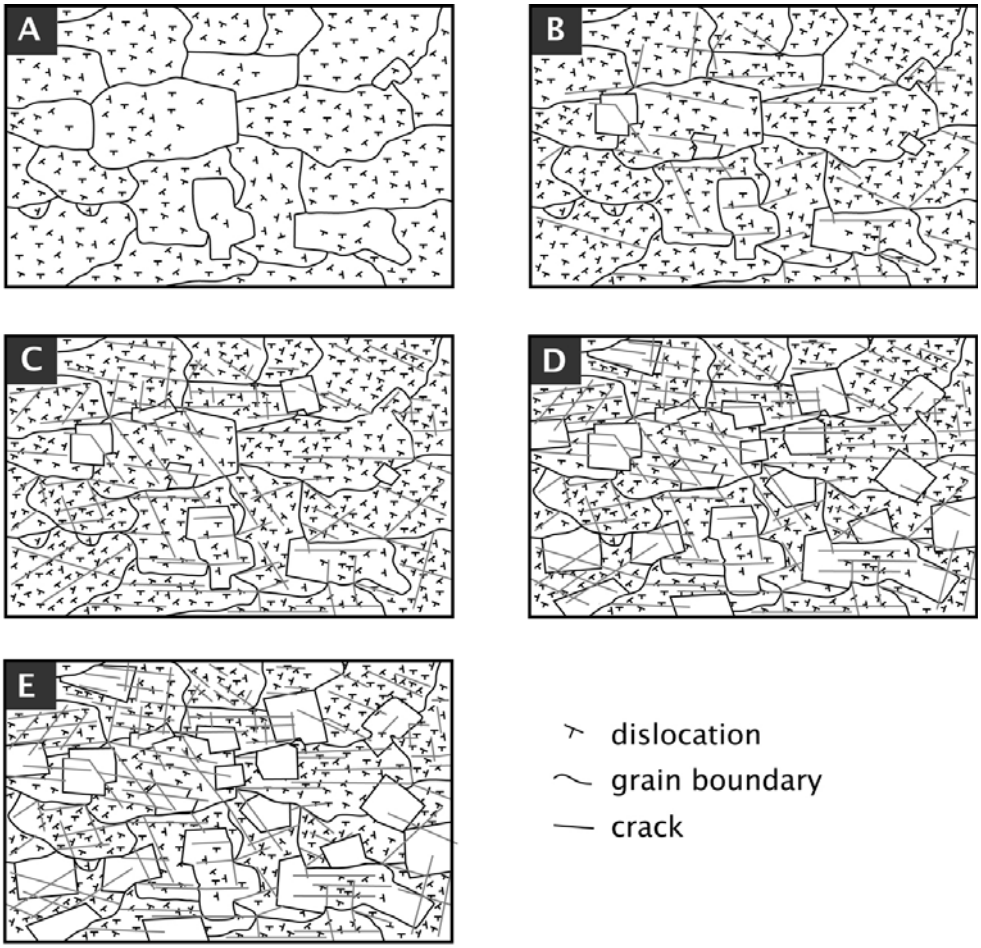

Fig. 8. Cartoon illustrates a likely evolution of microstructures in the Kłodawa samples. A: Salt deforming under natural conditions (low strain rate, high confining pressure). The dislocation density in the individual grains is dependent on the relative orientation of stress field and grain's slip system. Grains with high dislocation density are replaced by their neighbour grains. The main deformation mechanism is a combination of dislocation creep and solution-precipitation creep and perhaps grain boundary sliding. The main recrystallization mechanism is fluid-assisted grain boundary migration. Note that the dislocations in the grains are arranged into subgrain walls. For the sake of simplicity, the subgrain boundaries and second phases have not been shown on the drawing. B: As the stress concentration around the mine gallery causes further deformation and as the mine walls converge, the dislocation density increases and cracks parallel to (100) develop. Contrary to the microstructures depicted in A, these new dislocations are not arranged into subgrain walls. Due to the increase in dislocation density some of the old grain boundaries start to migrate, and a few new grains nucleate at grain boundaries. These newly nucleated grains grow at the expense of the old, highly deformed ones. Note that the microstructure is not altered significantly compared to the image A. Most of the samples studied in this paper depict microstructures B. C: As the mine wall convergence continues, the new phase progressively replaces the old grains and some new cracks are also introduced. As the new phase grows at the expense of the old ones, the old cracks are not erased by the migrating grain boundaries. D: In a very few extreme cases the new phase extensively replaces the old grains. This might be due to further mine-wall convergence and subsequent increase in dislocation density and/or due to presence of air humidity. E: During gamma-irradiation, minor amount of additional recrystallization occurs with the new phases further replacing the old ones. Note that neither the gamma irradiation nor the sample preparation did alter the microstructures significantly. The image width for all the cartoons is about 3 cm.

Peach et al. (2001) systematically investigated the relation between the recrystallization and the confining pressure and noted that when the confining pressure is too low to prevent dilatancy (i.e. micro-cracks occur in the sample), and the intracrystalline brine escapes, the recrystallization is inhibited, and the rocksalt shows continuous work hardening. In this study, recrystallized, euhedral grains and micro-fractures co-exist, suggesting that some other

mechanism was operative, which provided brine/air humidity to the grain boundaries, thus gave arise to recrystallization. It is perhaps the air humidity, which is conducted via capillary processes into the salt through the pervasive crack system. This assumption, however, leaves the question unanswered why the static recrystallization occurs only locally even though the humidity level is assumed to be the same for the whole gallery.

6 Conclusion

The inspection of rocksalt samples from the highly strained portion of the Kłodawa Salt Structure revealed that the rocksalt had recorded similar deformation processes and similar stress conditions throughout the analyzed area. As evidenced from microstructures the main deformation mechanism was dislocation creep accompanied with fluid assisted grain boundary migration recrystallization. These features are in agreement with published data obtained from other salt bodies. However localized occurrence of some phenomena indicates that there are also additional factors, which control the microstructural development of halite and rocksalt.

The pervasive micro-cracks seen in the specimens are interpreted to originate from the stress concentration around the mine gallery, i.e. they are not inherited due to natural deformation (Fig. 8). Similarly the presence of the new euhedral grains in some specimens implies that static recrystallization is also locally an important process and it evolves in a response to mine-wall convergence or other not deciphered mining works. Detailed observations on the mutual relationship between the cracks and the statically recrystallized phase indicate that the micro-cracks are not eliminated from the material by recrystallization process, e.g. by migrating grain boundaries. According to our observations on irradiated samples the pale blue, euhedral phase partly, if not entirely, records pre-irradiation recrystallization of halite within the rocksalt. This implies that the analysis of any gamma-irradiated naturally deformed rock salt sample should be more cautious, as not all pale phases and euhedral grains develop due to gamma-irradiation. Further important consequence is that samples taken from salt mine galleries for microtectonic or crystal fabric studies may contain significant artefacts due to static recrystallization after mining. For example CPO measurements in halite by neutron diffraction (Kern & Richter 1985; Skrotzki 1994; Scheffzük 1998) may be misinterpreted if these new grains are not recognized. Static recrystallization of halite in walls of waste repositories is a previously unrecognized recovery process, which removes damage from the deformed halite.

Acknowledgments

The authors thank the staff of the Kłodawa Salt Mine for hospitality and assistance during sample collection. Manfred Thomé at Forschungszentrum Jülich is thanked for carrying out and supervising the gamma-irradiation. Detailed reviews of Sandra Piazolo and Andrzej Zelazniewicz helped to improve the manuscript. ZS and JLU kindly acknowledge the financial support of the DFG (UR 64/1 & 2). This work is part of the DFG SPP 1135 project. SB was financed by the Polish Committee for Scientific Research, project No 6 P04D 026 20.

References

Bestmann, M., Piazolo, S., Spiers, C.J., Prior, D.J. (2005) microstructural evolution during initial stages of static recovery and recrystallization: new insights from in-situ heating experiments combined with electron backscatter diffraction analysis. journal of structural geology 27(3): 447-457

Burliga, S. (1996) kinematics within the klodawa salt diapir, central poland. in: alsop gi, blundell dj, davidson i (eds) salt tectonics. geological society of london special publication, vol 100, pp 11-21

Burliga, S., Janiów, S., Sadowski, A. (2005) Mining perspectives in the Kłodawa Salt Mine considering modern knowledge on tectonics of the Kłodawa Salt Structure. Technika Poszukiwa Geologicznych Geosynoptyka i Geotermia 4: 17-25

Carter, N.L., Hansen, F.D. (1983) Creep of rocksalt. Tectonophysics 92: 275-333

Carter, N.L., Hansen, F.D., Senseney, P.E. (1982) Stress magnitudes in natural rock salt. Journal of Gephysical Research 87: 9289-9300

Carter, N.L., Horseman, S.T., Russell, J.E., Handin, J. (1993) Rheology of rocksalt. Journal of Structural Geology 15(9-10): 1257-1271

Dadlez, R. (2003) Mesozoic thickness pattern in the Mid-Polish Trough. Geological Quarterly 47(3): 223-240

Garcia Celma, A. (1993) Radiation Damage in Natural and Synthetic halite. Report ECN-C--93-087, ECN Energy Innovation

Garcia Celma, A., Donker, H. (Editors) (1996) The Effect of Gamma Radiation in Salt. EUR-Report Nr. 16743EN.

Humphreys, F.J., Hatherly, M. (1996) Recrystallization and related annealing phenomena, vol. Pergamon, pp 497

Kern, H., Richter, A. (1985) Microstructures and textures in evaporites. In: Wenk HR (ed) Preferred orientation in deformed metals and rocks. An introduction to modern texture analysis. Academic Press, pp 317-333

Lockhorst, A. (Editor) (1998) NW European Gas Atlas-Composition and Isotope ratios of Natural Gases, GIS application on CD by the British Geological Survey, Bundesanstalt fur Geowissenschaften und Rohstoffe, Danmarks og Gronlands Geologiske Undersogelse, Nederlands Instituut voor Toegepaste Geowetenschappen, Panstwowy Instytut Geologiczny, European Union.

Means, W.D., Ree, J.H. (1988) Seven types of subgrain boundaries in octachloropropane. Journal of Structural Geology 10: 765-770

Miralles, L., Sans, M., Pueyo, J.J., Santanach, P. (2000) Recrystallization salt fabric in a shear zone (Cardona Diapir, southern Pyrenees, Spain). In: Vendeville BC, Yossi M, Vigneresse J-L (eds) Salt, shale and igneous diapirs in and around Europe. Geological Society of London Special Publications, vol 174, pp 149-167

Murata, K.J., Smith, R.L. (1946) Manganese and lead coactivators of red fluorescence in halite. American Mineralogist 31: 527-538

Peach, C., Spiers, C.J., Trimby, P.W. (2001) Effect of confining pressure on dilatation, recrystallization, and flow of rock salt at 150 °C. Journal of Geophysical Research 106(13315-13328)

Prior DJ, Bestmann M, Halfpenny A, Mariani E, Piazolo S, Tullis J, Wheeler J (2004) Recrystallization and grain growth in rocks and minerals. Materials Science Forum 467-470: 545-550

Przibram, K. (1956) Irradiation colours and luminescence, vol. Pergamon Press, Oxford, pp 332

Ramsay, J. (1980) The crack-seal mechanism of rock deformation. Nature 284: 135-139

Scheffzük, C.M. (1998) Neutronographische texturanalysen und Mikrostrukturuntersuchungen natürlicher und triaxialer verformter halite. Unpublished PhD thesis at RWTH Aachen University

Schenk, O., Urai, J.L. (2004) Microstructural evolution and grain boundary structure during static recrystallization in synthetic polycrystals of Sodium Chloride containing saturated brine. Contributions to Mineralogy and Petrology 146(6): 671-682

Schléder, Z., Urai, J.L. (2005) Microstructural evolution of deformation-modified primary halite from the Middle Triassic Röt Formation at Hengelo, The Netherlands. International Journal of Earth Sciences 94: 941-955

Schoenherr, J., Urai, J.L., Littke, R., Kukla, P., Newall, m., Al-Abry, N., Larroque, J.-M. (2005) Hydrocarbon-bearing Halite in the Ara Group (South Oman Salt Basin). Abstract at General Assembly, European Geosciences Union, Vienna, 24-29 April 2005, p. 692

Senseny, P.E., Hansen, F.D., Russell, J.E., Carter, N.L., Handin, J. (1992) Mechanical behaviour of rock salt: phenomenology and micromechanisms. Int. J. Rock Mech. Min. Sci & Geomech. Abstr. 29(4): 363-378

Skrotzki, W. (1994) Mechanisms of texture develompent in rocks. In: Bunge HJ, Siegesmund S, Skrotzki W, Weber K (eds) Texture of Geological Materials. DGM Informationsgesellschaft, Oberursel, pp 167-186

Spiers, C.J., Carter, N.L. (1998) Microphysics of rocksalt flow in nature. Fourth Conference on the Mechanical behaviour of Salt, The Pennsylvania State University, June 17 and June 18, 1996, Trans Tech Publication Series on Rock and Soil Mechanics, vol 22, pp. 115-128

Ter Heege, J.H., De Bresser, J.H.P., Spiers, C.J. (2005) Rheological behaviour of synthetic rocksalt: the interplay between water, dynamic recrystallization and deformation mechanisms. Journal of Structural Geology 27(6): 948-963

Urai, J.L., Means, W.D., Lister, G.S. (1986) Dynamic recrystallization of minerals. In: Hobbs BE, Heard HC (eds) Mineral and rock deformation: laboratory studies. American Geophysical Union, vol 36, pp 161-199

Urai, J.L., Spiers, C.J., Peach, C., Franssen, R.C.M.W., Liezenberg, J.L. (1987) Deformation mechanisms operating in naturally deformed halite rocks as deduced from microstructural investigations. Geologie en Mijnbouw 66: 165-176

Urai, J.L., Spiers, C.J., Peach, C.J., Zwart, H.J. (1985) A laboratory investigation into the interaction of recrystallization and radiation damage effects in polycrystalline salt rocks - report over the period March - October 1985. HPT Laboratorium, Instituut voor Aardwetenschappen, University of Utrecht, p 66

Van Opbroek, G., Den Hartog, H.W. (1985) Radiation damage of NaCl: dose rate effects. Journal of Physics. C: Solid State Phys. 18: 257-268

Wilkins, R.W.T., Bird, J.R. (1980a) Characterization of healed fracture surfaces in fluorite by etching and proton irradiation. Lithos 13: 11-18

Wilkins, R.W.T., Bird, J.R. (1980b) The use of proton irradiation to reveal growth and deformation features in fluorite. American Mineralogist 65: 374-380

Wilkins, R.W.T., Bird, J.R., Ewald, A.H. (1981) Observations on deformation microstructures and fluid inclusions in proton-irradiated halite. N. Jb. Miner. Abh. 141(3): 240-257

Chapter 5: Deformation and recrystallization mechanisms in mylonitic shear zones in naturally deformed extrusive Eocene-Oligocene rocksalt from Eyvanekey plateau and Garmsar hills (central Iran) *

Zsolt Schléder and János L. Urai

Abstract

Microstructural processes in mylonitic shear zones from extrusions of Eocene-Oligocene rocksalts from Garmsar hills and Eyvanekey plateau (central Iran) are described and analyzed. The halite samples were studied by transmitted light microscopy of gamma-irradiated thin sections, subgrain size palaeopiezometry of polished and chemically etched samples and texture measurements by electron backscatter diffraction (EBSD).

The studied shear zones are thin (<5 cm), subhorizontal and bedding parallel. The protomylonite comprises 2-6 mm sized grains, occasionally rich in primary fluid inclusions indicative of their primary non-recrystallized state. Abundant, well-developed subgrains suggest that the protomylonite was deformed mainly by dislocation processes. Elongated subgrains at grain edges point to recrystallization by fluid-assisted grain boundary migration. Recrystallized, strain-free grains are common. The material in the mylonitic zones is fine-grained (~0.6 mm) with strong shape preferred orientation. Microstructures such as oriented fibrous overgrowths and growth banding (observed in gamma-irradiated sections) suggest that the principal deformation mechanism was solution-precipitation creep (non-conservative grain boundary migration and grain boundary sliding accommodated by solution-precipitation). Crystal fabrics measured by EBSD show a weak crystallographic preferred orientation that is consistent with solution-precipitation accommodated grain boundary sliding.

Using published flow laws the strain rate in the fine-grained mylonites is about 10^{-10} 1/s, which is in a good agreement with earlier in situ measurements on glacier salt flow rate.

Keywords: Rocksalt, salt glacier, halite mylonite, shear zone, deformation mechanism, solution-precipitation creep

* Schléder, Z., Urai, J. L. 2007. Deformation and recrystallization mechanisms in mylonitic shear zones in naturally deformed extrusive Eocene-Oligocene rocksalt from Eyvanekey plateau and Garmsar hills (central Iran). Journal of Structural Geology 29 (2), 241-255.

1 Introduction

Over the past 50 years our understanding of the salt-sediment system has increased tremendously. Aspects of the dynamics of salt tectonics and sealing of fluids are quantified, but many questions are unresolved to date (Jackson, 1995). Salt is also useful as analogue material for understanding the microstructural processes and textural development in silicate rocks (Drury and Urai, 1990).

An interesting, yet poorly understood phenomenon is the extraordinary mobility of glacier salt that flows downhill at geologically high strain rates at very low shear stress in the Zagros Mountains and in central Iran (Talbot, 1979; Talbot and Rogers, 1980; Talbot, 1981; Talbot and Jarvis, 1984; Talbot, 1998; Talbot et al., 2000; Talbot and Aftabi, 2004). Recognition of equivalents of these salt glaciers was documented by studies of the Gulf of Mexico salt province (Fletcher et al., 1995), where the extruded salt flows on the sea floor under a thin, unconsolidated layer of sediment. Besides the recent examples, salt glaciers were shown to have been present in many salt bearing sedimentary basins during their geologic evolution (Volozh et al., 2003; Mohr et al., 2005).

If glacier salt had the well known rheology of domal salt (Wawersik and Zeuch, 1986; Carter et al., 1993; Ter Heege et al., 2005b) the salt glaciers would be far too strong to flow under their own weight. Solution-precipitation creep was inferred to account for the unusual weakening of glacier salt (Wenkert, 1979). The model explains fairly well the observed shear stress and strain rate (<0.25 MPa, $1.1x10^{-11}$ to $1.9x10^{-9}$ 1/s (Jackson, 1985)) in salt glaciers as creep due to diffusion of ions through an interstitial salt-brine solution. This weak behavior was also observed in experimentally deformed fine-grained wet salt (with water content about 0.05 wt%) by Urai et al. (1986), and extensive work by others (Spiers et al., 1990, Lohkämper et al., 2003) has clarified many details of this process.

The average grain size in domal salt is around 5-30 mm (Warren, 2006). Solution-precipitation creep is dominant over dislocation creep in fine-grained wet salt. From Kuh-e-Namak (Dashti, Iran) salt glacier, Talbot (1981) reported processes of progressive subgrain rotation and tensional failure on cleavage planes which resulted in grain size reduction. He also proposed that fluid-assisted grain boundary migration is important both in domes and glaciers. By studying one sample of naturally deformed glacier salt from Iran, Urai et al., 1986) noted that the halite grains do not contain any substructure but do show the same microstructural features as seen in the fine grained, synthetic wet halite deformed under wet conditions.

The aim of this study is to extend our understanding of deformation and recrystallization mechanisms in halite (Urai et al., 1986; Wawersik and Zeuch, 1986; Urai et al., 1987; Spiers et al., 1990; Senseny et al., 1992; Carter et al., 1993; Peach et al., 2001; Watanabe and Peach, 2002; Hunsche et al., 2003; Ter Heege et al., 2005a; Ter Heege et al., 2005b; Pennock et al., 2005) to processes in glacier salt. The samples analyzed in this study are from the Garmsar hills and Eyvanekey Plateau (central Iran), where the Eocene-Oligocene salt was squeezed out under the thin cover of Alborz mountains.

2 Salt extrusions in central Iran

2.1 Lithostratigraphy in the Great Kavir and in its sub-basins

In central Iran Tertiary salt reaches the surface in many places. The most voluminous salt outcrops can be found in the Great Kavir basin and in its peripheral sub-basins (Qom, Garmsar and Damghan basins) (Fig. 1). The Tertiary, which lies unconformably on folded Mesozoic strata, starts with marine, Eocene sediments, associated with volcanic rocks (Jackson et al., 1990).

The first evaporites (~500 m thick) were deposited during the middle Eocene in the southern part of the Great Kavir basin. Due to regression towards the end of Eocene, deposition of gypsiferous rocksalt started in the northern part of the basin (Qom and Garmsar). The deposition of these evaporites lasted until the latest Eocene - early Oligocene (Fig. 2A) leading to the accumulation of a few hundred meter thick evaporite sequence (Jackson et al., 1990).

During late Eocene tectonic movements, the sub-basins became separated from the Great Kavir basin. After these tectonic movements a new sedimentary cycle started, the base of which is marked by a distinct unconformity. This new cycle started with red continental clastics and Oligocene evaporites (Lower Red Formation, LRF), which are overlain by an upper Oligocene - lower Miocene marine unit, the Qom formation, in turn overlain by the Miocene Upper Red Formation (URF) (Jackson et al., 1990; Talbot and Aftabi, 2004). The LRF reaches its maximum thickness of ~1000 m south of the Qom basin and consists mainly of red sediments intercalated with volcanics. Evaporites of the LRF are ~300 m thick in the Qom basin, further east the beds changes to nonevaporitic clastic facies (Jackson et al., 1990). The Qom formation is a 1000 m thick sequence of platform-type limestone, marl shale, sandstone and gyprock (Gansser, 1960a; Gretener, 1982; Jackson et al., 1990).

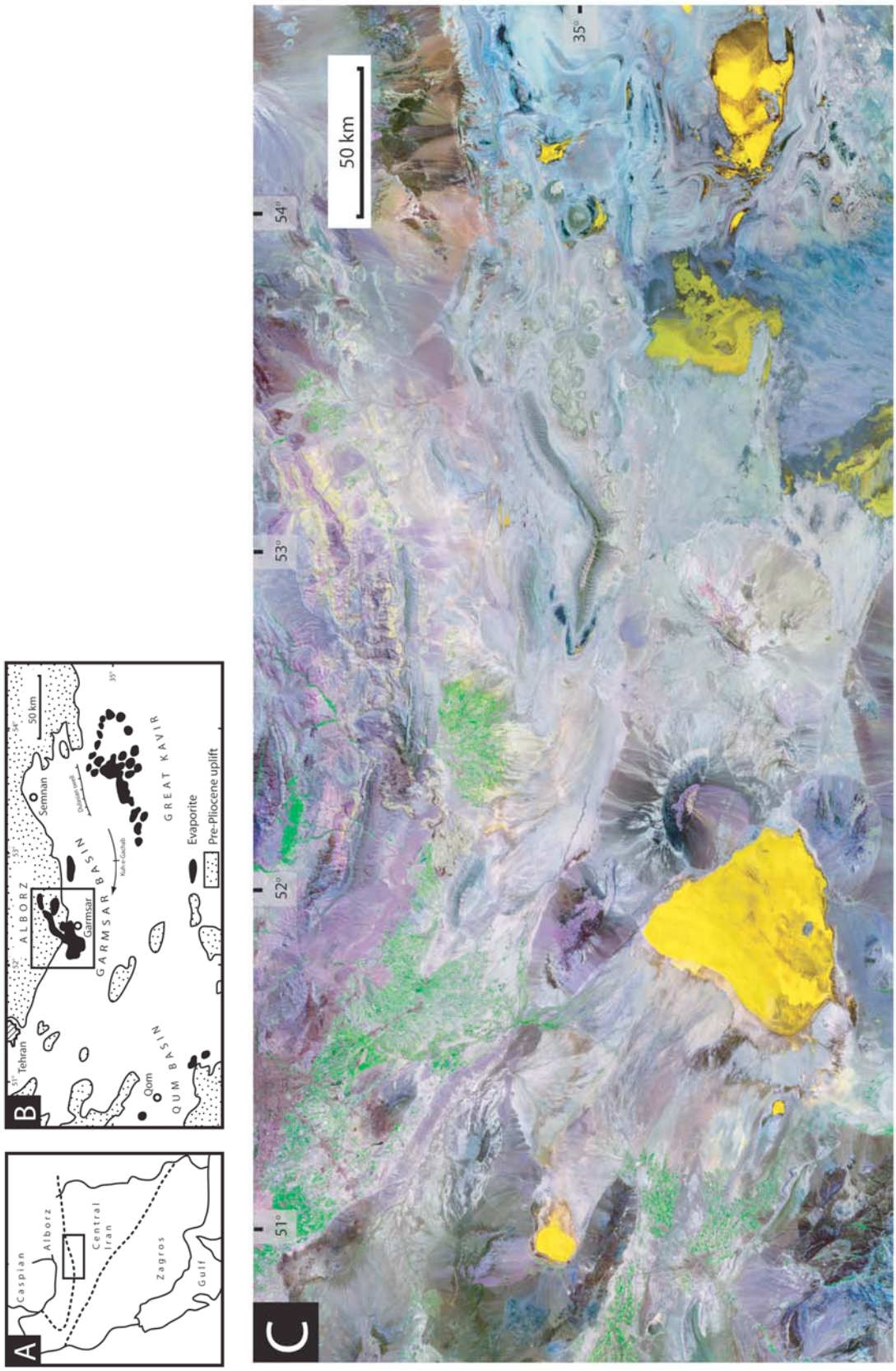
A
Caspian
Alborz
Central Iran
Zagros
Gulf
B
Tehran
ALBORZ
Semnan
Garmsar
GARMSAR BASIN
GREAT KAVIR
QUM BASIN
Qom
50 km
Evaporite
Pre-Pliocene uplift
C
50 km
51°
52°
53°
54°
35°

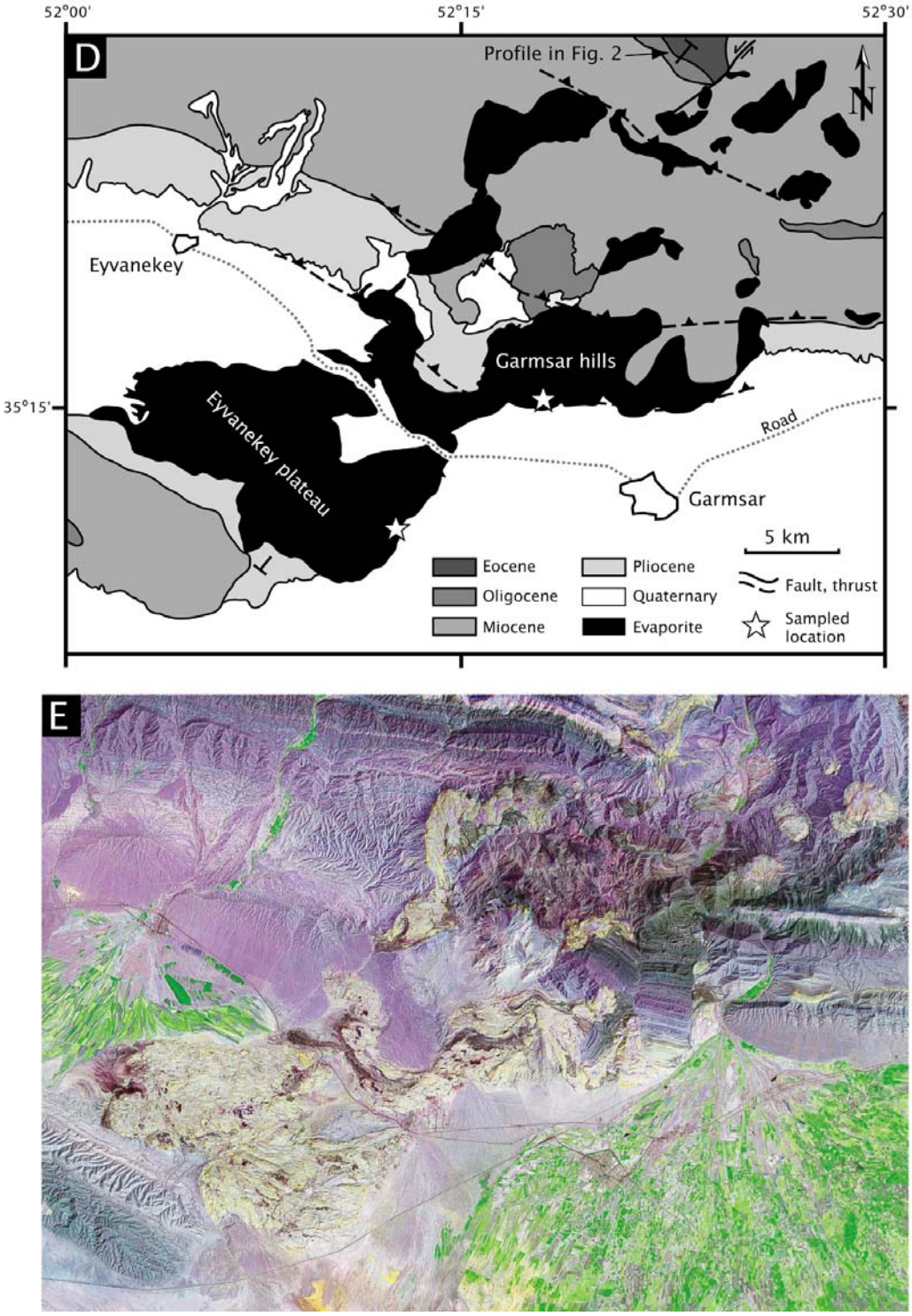

Fig. 1. Simplified regional setting of Garmsar hills, Eyvanekey plateau and surroundings. A: location in the map of Iran. B: evaporites on the surface in the Garmsar basin and adjoining Qum and Great Kavir basins (after Jackson et al., 1990; Talbot and Aftabi, 2004). C: GeoCover landsat image corresponding to cartoon B. D: Simplified geological setting of Garmsar hills and Eyvanekey plateau after geological map of Amini and Rashid, 2005).E: GeoCover landsat image corresponding to area of map D (source: https://zulu.ssc.nasa.gov/mrsid/).

The Miocene URF reaches the maximum thickness of ~5000 m in the Qom and the Garmsar basins. The URF can be divided into a lower evaporitic and an upper sandy part in the Qom basin, while in the Garmsar basin it can be subdivided into three members (Jackson et al., 1990). The lowermost member (~700 m) consists of a rhythmic saline facies with thin (<10 m) impure rocksalt beds. The middle member (~3000 m) is gypsiferous mudrock, the uppermost member is composed of cyclic saline mudrock gyprock alterations (Fig. 2A). However, a fully reliable stratigraphic subdivision of the URF in the Great Kavir is hampered by the lack of paleontologic and subsurface data and the dominance of monotonous mudrocks (Jackson et al., 1990).

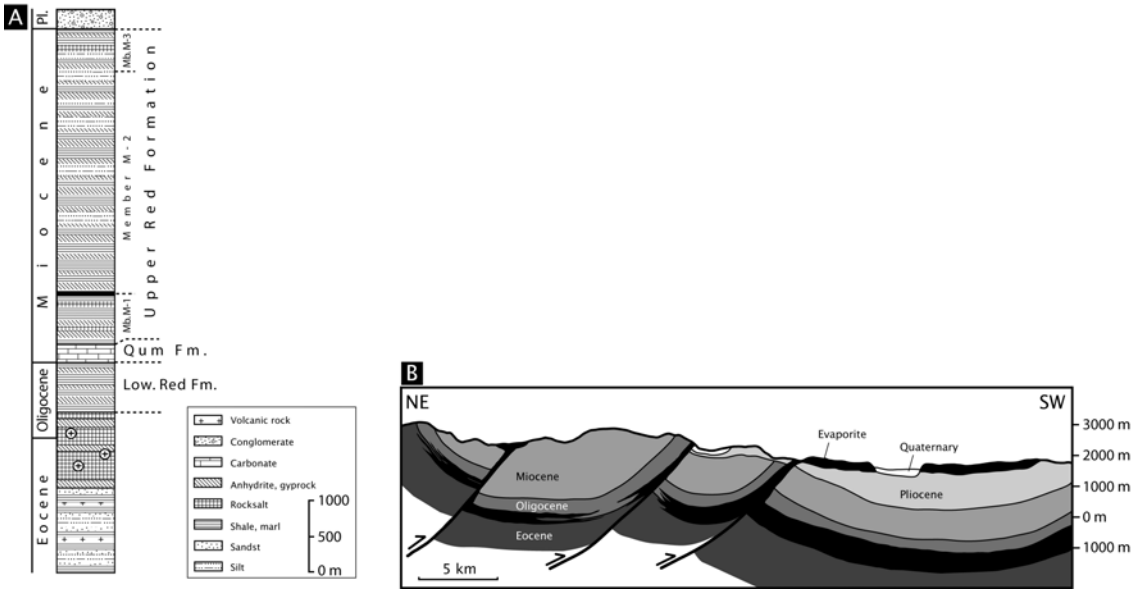

Fig. 2. A: Lithostratigraphical column of the Garmsar basin after Jackson et al. (1990). The Eocene-Oligocene rocksalt is the main source for the extrusions of Garmsar hills and Eyvanekey plateau. B: cross-section through the Garmsar hills and Eyvanekey plateau (modified after Amini and Rashid, 2005). For the position of the profile see Fig. 1D. Vertical exaggeration is about twofold.

Several authors (Gansser, 1960b; Jackson et al., 1990; Talbot and Aftabi, 2004) proposed that all the salt structures in central Iran involve the same two salt sequences: a relatively pure, upper Eocene - lower Oligocene salt (base of lower Oligocene Lower Red Formation) and a variegated, impure lower Miocene salt sequence (lower Miocene Upper Red Formation).

2.2 Geological setting of Eyvanekey plateau and Garmsar hills

The Garmsar basin (Figs. 1 and 2) is a peripheral embayment of the Tertiary Great Kavir basin, separated by the Kuh-e-Gachab and Dulasian swell. The Tertiary depocenter in the Garmsar Basin is situated roughly between the cities of Eyvanekey and Garmsar. As the stratigraphy is strongly distorted by salt tectonics, their exact thickness is not resolved, but proposed to exceed 8000 m in this foredeep (Jackson et al., 1990).

The Tertiary salt was extruded under the thin cover of Alborz mountains and reached the surface north of Garmsar and was further squeezed to south producing a 20 x 10 x 0.2 km Eyvanekey plateau salt sheet (Figs. 1 and 2B) (Talbot, pers. comm.; Talbot, in prep.). The Eyvanekey plateau and the Garmsar hills consist predominantly of large diapiric masses of

salt and gyprock with inclusions of mafic volcanic rocks with subordinate marl, calcareous marl, shale and sandstone (Amini and Rashid, 2005). Owing to the lack of fossils, the exact age of the evaporitic mass cannot be determined although based on lithologic similarities to Qom Kuh and the Great Kavir diapirs (Talbot and Aftabi, 2004), it is very likely that both the hills and the plateau are made up of evaporites both of upper Eocene and Oligocene age. It is also unknown whether the salt sheet is still moving today (Talbot, pers. comm.).

The present surface of the evaporite extrusion in the plateau and hills is covered predominantly with light green to pale brown gypsite with subordinate marl and calcareous marl (Amini and Rashid, 2005). Rocksalt outcrops are rare, but halite is accessible in the numerous open-pit and underground salt mines that were opened in the last 10 years (Talbot, in prep.).

Although in both locations the salt is strongly deformed by sets of recumbent folds, the bedding is generally subhorizontal. Commonly the salt mass contains thin layers of halite with strong shape preferred orientation: halite mylonites.

2.3 Samples

In this study we report detailed microstructural analysis of mylonitic halite samples from two, currently abandoned, open-pit salt quarries (Fig. 1D). One sample was collected at the southern edge of the Garmsar hills (co-ordinate: 35°16'N; 52°17'E, sample referred to as "GH" hereinafter). This sample comprises a few, <1 cm thin mylonitic zones and protomylonites (Fig 4A). In the whole outcrop, the mylonitic zones are commonly less than 5 cm thick, and develop parallel to the bedding at the bottom of the individual beds (Fig. 3). In outcrop, the salt is horizontally bedded, with beds of about 20 cm thick, which often show gradual colour change of grayish white to white and slight grain size change from finer at the bottom and coarse grains at the top (Fig. 3). We interpret this variation in individual beds to reflect the variations in sedimentary conditions. Abundant primary features (see below) in the non-recrystallized grains imply that the salt is not completely recrystallized.

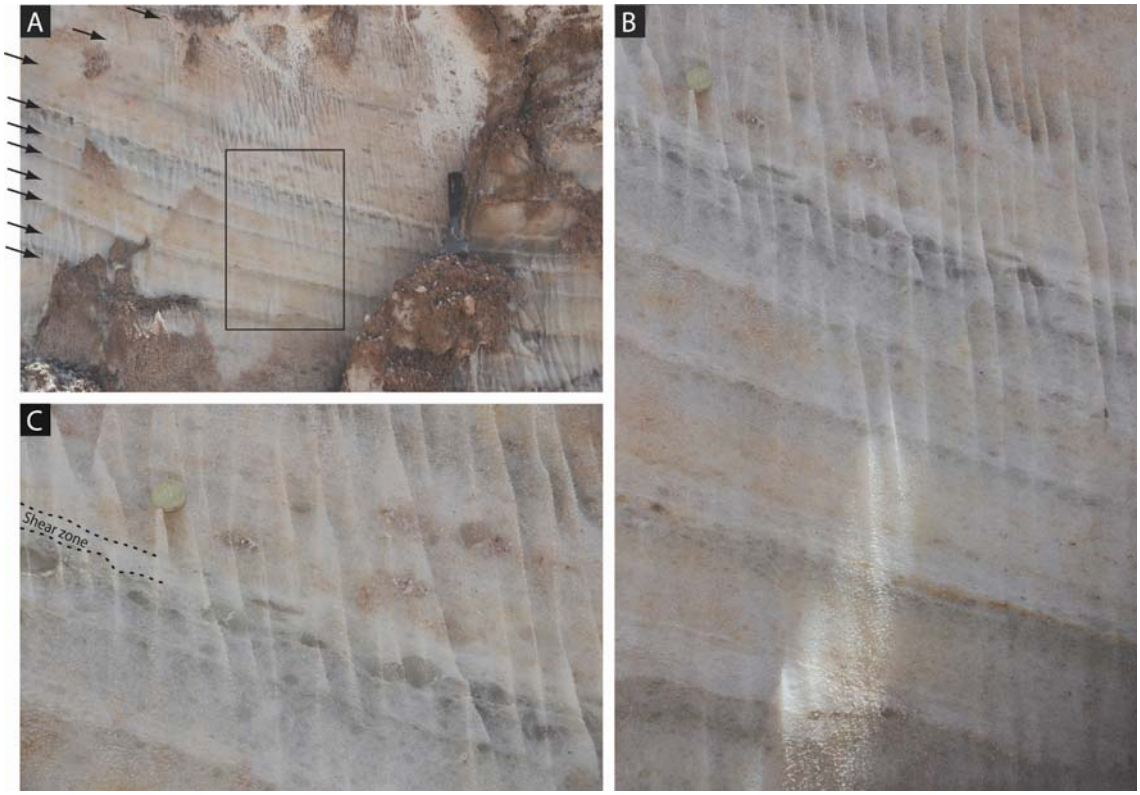

Fig. 3. A: bedding parallel mylonitic zones in a salt wall (looking E) exposed near the abandoned salt mines in the Garmsar hills. The strata dip 10° to SW. The mylonitic zones are relatively thin (<3 cm, see arrows) and are characterized by strong shape preferred orientation and small grain size. The position of the B image is indicated with the rectangle. Hammer for scale. B: detail of the image A. Note that the shear zones occur often above coarse-grained, dark gray coloured layers. The vertical fluting is a karstic feature due to rainwater. Coin (d = 2cm) for scale. C: detail of image B. Note the flattened porphyroclast in the shear zone and the abundance of large grains at the bottom of the shear zone.

We note that the similar-looking beds in the outcrop may represent only one or two beds, which were isoclinally folded – although the hinges of these were not found in our outcrops. Such bedding parallel shear zones were also observed by Talbot in the Kuh-e-Namak salt glacier (Talbot, 1981), suggesting that they are fairly common in extrusive salts.

The other sample was collected at the eastern edge of the Eyvanekey plateau (co-ordinate: 35°12'N; 52°12'E, sample referred to as "EP" hereinafter). This sample is about 5 cm thick and consists of mylonitic salt with strong shape preferred orientation (Fig 4B).

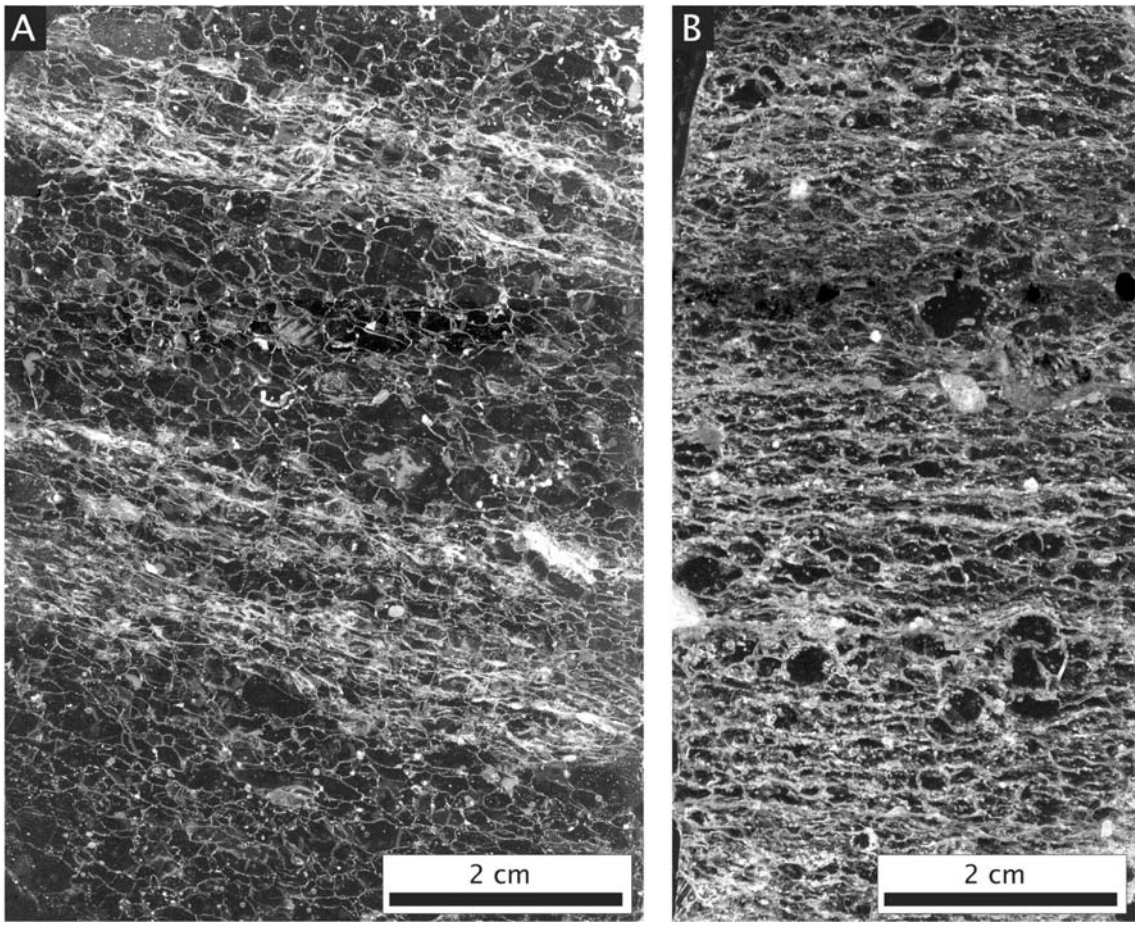

Fig. 4. Dark-field image of scanned thin sections of the samples studied. The grain boundaries and secondary phases show up as light lines and patches, the halite grains occur as dark areas. The Garmsar hill sample (A) contains a few shear zones, the Eyvanekey plateau sample (B) is entirely made up of mylonitic material.

3 Methods of study

Samples were cut parallel to the lineation and perpendicular to the foliation using a diamond saw with a small amount of water to prevent microcracking (Schléder and Urai, 2005). After this, the samples were decorated by gamma-irradiation in the Research Reactor of Forschungszentrum Jülich using a technique similar to Urai et al., 1985). The irradiation was done in a purpose-built heated container at a constant temperature of 100 °C. The dose rate was between 4 kGy/h and 6 kGy/h and the total dose was about 4 MGy. The colour intensity developed in the samples during gamma-irradiation reflects the heterogeneous distribution of solid solution impurities and crystal defects in halite grains (Murata and Smith, 1946; Przibram, 1954; van Opbroek and den Hartog, 1985; Urai et al., 1985; Garcia Celma and Donker, 1996).

Thin sections were prepared following the procedure of Spiers et al. (1986), Urai et al. (1987) and Schléder and Urai (2005). Thus, the samples were mechanically ground and polished dry on grinding paper, etched in 5% undersaturated NaCl solution for 10 s, subsequently rinsed for 3 s with a strong jet of n-hexane and finally dried in a jet of warm air. This sample preparation removed surface scratches and revealed dislocation substructure. The thin sections were studied with reflected and transmitted, plane polarized light microscopy.

To attempt to reveal variation in trace element content in selected grains, conventional microprobe analyses (Type: JEOL JXA-8900R) were carried out at the RWTH Aachen.
On the EP sample, crystallographic orientation data was acquired from EBSD patterns using a JEOL 6100 (at the RWTH Aachen), typically operating with acceleration voltage of 20 kV and beam current of 8 nA. The EBSD patterns were indexed with the CHANNEL 5 software (HKL Technologies) using the file for halite consisting of 46 lattice planes.
Multiple beam maps (12 horizontal x 4 vertical) were used to map the specimen. For an individual map, data points were collected on an orthogonal grid of 106 x 73 at a fixed step size of 40 μm by moving the sample and keeping the beam stationary. After the mapping, the individual maps were stitched together using the CHANNEL 5 software. Misorientation between two stitched maps is <3°, and is due to the gradual orientation error in each individual map. Misorientation data between individual grains were calculated separately for each map and these data were used for the misorientation distribution histogram. The quality of the EBSD data is very good – the fraction of patterns that could no be indexed was below 10 % – with the exception of the immediate vicinity of the margins of individual maps, where typically 1-2 pixels could not be indexed. The maps were further processed in order to remove erroneous data and to provide more complete reconstruction of the microstructure (Prior et al., 2002; Bestmann and Prior, 2003). The accuracy of individual measurement is better than 1°. The misorientation angle between two grains was calculated by selecting the minimum misorientation angle from all possible symmetric variants (Wheeler et al., 2001).

4 Results

4.1 Observations on microstructure and texture measurement

Both samples studied in this paper are almost pure halite (~98%) with polyhalite, anhydrite and limestone fragments as main impurity phase. The GH sample contains a few thin mylonitic zones and protomylonite, the EP sample is made entirely up of mylonitic material (Fig. 4). In thin section the mylonites from both locations show comparable microstructures; the descriptions presented here apply to both samples. The transition from coarser grained protomylonite to the fine-grained mylonite is rather sharp, but the interface is quite wavy (Fig 4A).

4.1.1 Protomylonite

The protomylonite consists of slightly elongated, 2 to 6 mm large grains. The aspect ratio of the grains is about 1.5-2 with the long axis parallel to the mylonitic zones and bedding (Figs. 4A and 5). This shape preferred orientation (SPO) forms a weak foliation that is clear in outcrop. Commonly, the foliation is oriented at a few degrees to the bedding.
Inspection of unirradiated thick sections (~1 mm) under plane polarized transmitted light reveals that some grains contain regions with numerous fluid inclusions (Fig. 5A). The fluid inclusions are smaller than 50 μm and show negative crystal shape. Commonly the inclusions are arranged into thin, approximately 500 μm wide, parallel bands. The cloudy, fluid-inclusion-rich part of a grain is commonly truncated by the upper and lower neighbour grains, while fluid-inclusion-free, clear halite rims the cloudy part to the directions of the SPO (Figs. 5A and C). Gamma-irradiated sections show white polygonal subgrain boundaries in many grains (Figs. 5C). Subgrains in the grain interiors are equiaxial and have an average

size of about 120 μm. In contrast, subgrains close to grain boundaries have an elongated shape, with the elongation parallel to the direction of SPO (Fig. 5C and D). The length of such elongated subgrains can rarely reach 3 mm. In places, two neighbour grains contain such elongated subgrains. In that case, on both sides of the grain boundary which separates those two grains, the elongated subgrains terminate at the grain boundary. Inside the subgrain-poor region and very rarely between the white coloured polygons, a second-order, dark blue coloured, less developed polygonal structure is visible (Fig 5C). Besides the substructured grains described so far, not uncommonly small, 2-3 mm large grains without any substructure were also noticed (Fig 5D).

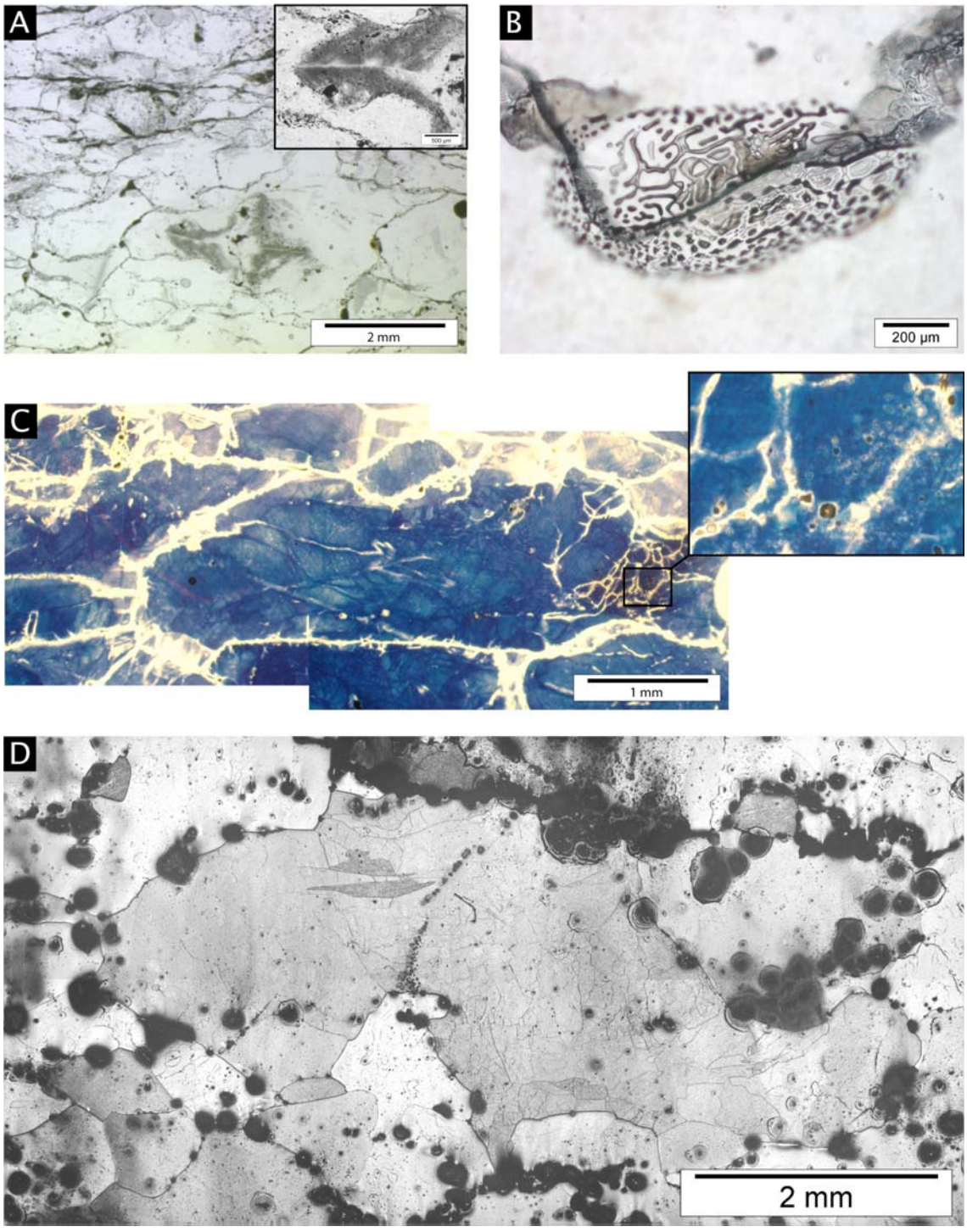

Fig. 5. Micrographs illustrate the characteristic microstructures observed in the protomylonite (sample GH). A: plane-polarized, transmitted light image in which the grain boundaries show up as dark lines, the secondary phases as dark patches. The image shows slight shape-preferred orientation and secondary phases inside of grains and at the grain boundaries. Insert: detail of a fluid inclusion-rich grain. B: Grain boundary structure, which shows interconnected, channel-like and separated, island-like fluid inclusions. Some of them opened during sample preparation and are filled with air, thus show up as brown coloured. C: Highly elongated grain with well-developed subgrains and fluid inclusions (see detail image) on the right and elongated subgrains on the left. Plane-polarized, transmitted light image of gamma-irradiated thin section. Our interpretation is that the once presumably equiaxed grain deformed with dislocation processes, as evidenced by the subgrains, after which recrystallization of fluid-assisted GBM took place, which resulted in an elongated shape. D: plane-polarized reflected light image shows a large, elongated grain with well-

developed subgrains inside the grain and elongated subgrains at the grain edges. The grain boundaries show up as dark lines. The black spots at the grain boundaries and inside of the substructured grain are fluid inclusions, which opened during sample preparation. The elongated subgrain boundaries at the grain edges point to recrystallization mechanism of fluid-assisted GBM.

Typically, the grain boundaries have an irregular, lobate morphology with occasional euhedral grain boundary segments. The grain boundaries are invariably filled with connected, lobately shaped fluid and gas inclusions (Fig. 5B). Based on our microstructural observations, connected porosity in our samples is very low.

The etched surface was also studied in plane polarized reflected light with the aim to verify that all the dislocation structures were decorated by gamma-irradiation (e.g. Fig. 5B). Comparing the transmitted light images and the corresponding reflected light images, shows that all the subgrains occurring as white polygons were also visible on the etched surface. In contrast, the second-order polygonal, dark-blue structure within subgrain poor regions were not visible on the surface.

Secondary phases were found frequently in the protomylonite. Commonly, these are 1-2 mm sized anhydrite crystals or occasional 1-3 mm large limestone fragments. The secondary phases are located commonly at the grain boundaries and more rarely inside the grains, mostly in thin curved bands.

4.1.2 Mylonite

The mylonitic material has a strong shape preferred orientation and foliation (Fig. 4B). In plane polarized light of unirradiated samples, the foliation is characterized by numerous impurity phases, such as anhydrite, polyhalite and some limestone fragments arranged into bands. The bands are thin (~1 mm), bedding parallel and have a more or less uniform spacing of about 5 mm. The halite grain size is about 0.6 mm on average, with a few large grains. Some of these large grains contain fluid inclusions identical to those in the protomylonite.

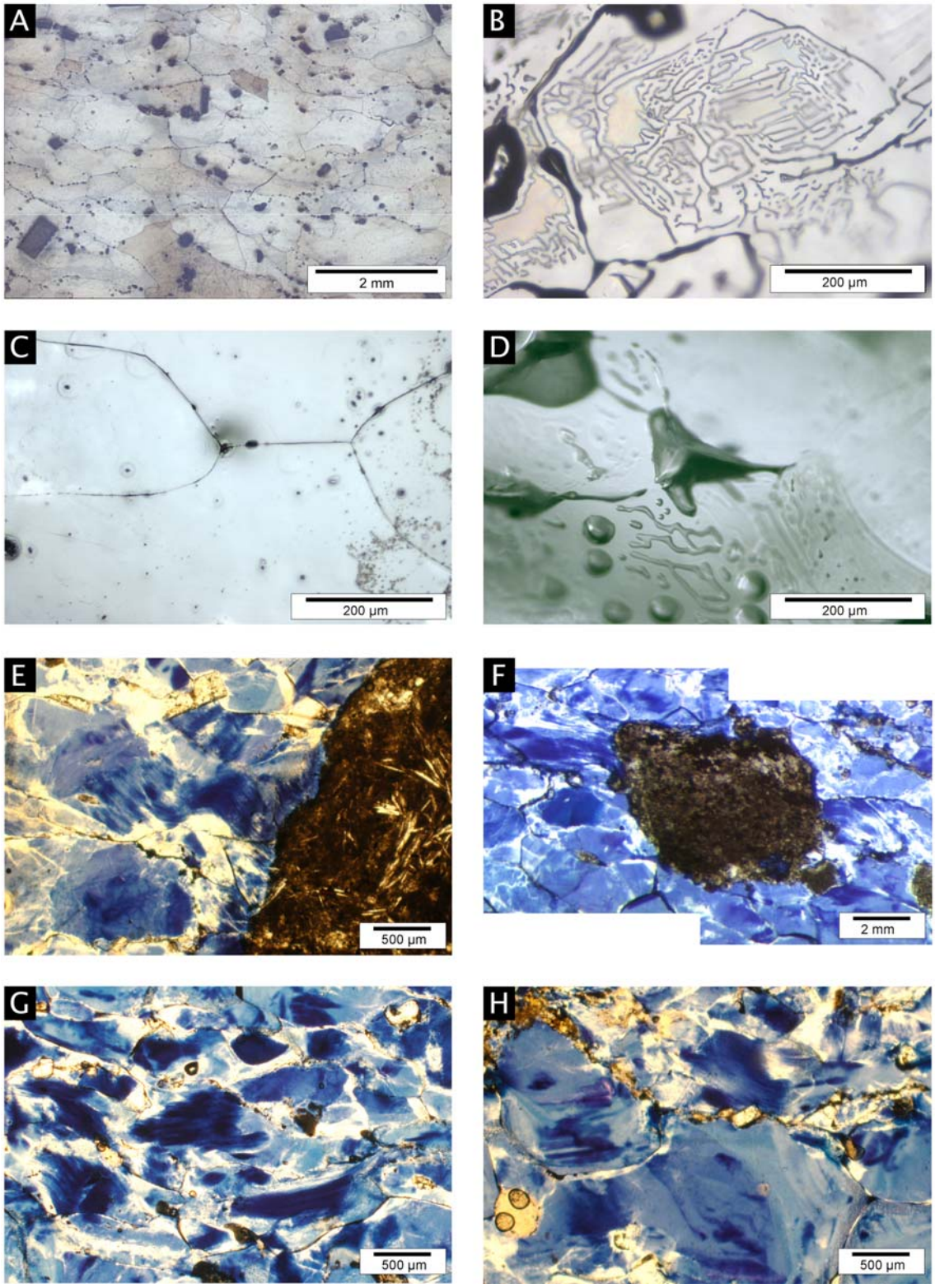

Fig. 6. Micrographs illustrate the characteristic microstructures observed in the mylonite. A: plane-polarized reflected light image shows straight to gently curved grain boundaries. Black spots at the grain boundaries and in the grains are either secondary phases or fluid inclusions which opened up during sample preparation. Note that the grains are substructure-free. B: interconnected fluid inclusions at the grain boundaries. Note also the subcontinuous fluid-filled tubes at the triple junctions. Plane-polarized, transmitted light image. C: Plane-polarized, reflected light image shows four grains separated by grain boundaries. Note the lack of substructures. D: the same area in transmitted light (focused deeper than image C) shows relatively large gas

(vapour?) inclusions at the grain boundaries and triple junctions. E-F: fibrous structure around a limestone fragment. Plane-polarized transmitted light image of gamma-irradiated section. These microstructures are interpreted as strain fringes (Passchier and Trouw, 2005). The black curves are grain boundaries the white particles at the grain boundaries are secondary phases (mainly anhydrite). G: Fibrous microstructure in the pure halite part. The grain boundaries show up as black curves. Note the widespread presence of the fibrous structures. H: dark coloured bands which are parallel to the grain boundaries. These dark bands might be regarded as evidence for non-conservative grain boundary migration.I: similar structure to G. The grain boundaries were slightly opened up during sample preparation. J. Core-mantle structure with fibrous structure inside the grain completely enclosed by non-fibrous halite.

Inspection of etched surfaces in reflected light shows that the vast majority of the small grains lack substructure (Figs. 6A and C), while the sporadic large ones contain well developed subgrains. In transmitted light, irregularly shaped, relatively large inclusions which appear dark grey or black can be observed, mostly on the triple junctions, less frequently on grain boundaries and very rarely inside a single grain (Figs. 6C and D). These inclusions tend to enlarge during dissolution of the sample, indicating a gas at slightly higher-than-atmospheric pressure. The grain boundary structure is similar to that in the protomylonite and contains amoeboid, inter-connected brine inclusions (Fig. 6B).

The inspection of gamma-irradiated mylonite in transmitted light reveals more microstructures not seen in the unirradiated sample (Fig. 6E-J). Large grains contain a set of fine, parallel bands. The orientation of these sets is crystallographically controlled and is parallel to (100) as shown by the orientation the cube fluid inclusions in the grains. In the fine grains, a core and mantle structure is commonly observed with dark blue core and pale blue rim. Also in the fine grained part, in some cases, dark bands are present which are oriented parallel with the grain boundaries (Fig. 6H). Intragranular, highly elongated fibre-like microstructures (~100-200 μm long fibres) around limestone fragments are common (Figs. 6E and F). Invariably, the fibers are parallel to the foliation. Such fibers are not exclusively present around limestone and anhydrite fragments, but also at halite-halite contacts, and in places completely enclosed inside single halite grains (Fig. 6J). In these cases they form a core-mantle structure with the fibrous microstructures inside the grain (core) rimmed by non-fibrous material (mantle). This mantle commonly shows banding parallel to the grain boundaries (Figs. 6H and J). Inspection of such fibrous structures in reflected light on etched surfaces reveals that these fibres are not individual grains, but that they are sometimes separated by subgrain boundaries or, more commonly, that no boundary at all is visible between two fibres in reflected light.

4.1.3 Crystallographic orientations in the mylonite

Full crystallographic orientation of ~500 grains was measured in sample EP using EBSD. In Fig. 7A-B, crystallographic orientation of individual grains (colour coded according to the crystallographic orientation) together with the corresponding gamma-irradiated thin section is shown. The relatively large grains, seen in the Fig. 7B are remnants of deformed porphyroclasts and occasionally contain primary fluid inclusions. The EBSD measurements confirm the microscope observation, that these grains are typically lack substructure. Figure 7C shows the corresponding pole orientations for the whole dataset. The fabric is close to random, with a very weak CPO. The few local maxima correspond to the large porphyroclasts. The grain size for the whole dataset was calculated based on the EBSD measurement. The grain size distribution is close to lognormal (Fig. 7D) with the arithmetic mean value around 0.6 mm. Minimum misorientation angle distribution for the complete

dataset – depicted on Figure 7E – shows that low angle misorientations are absent with the most common misorientation at 45º. The presence of that peak may be an artefact and may also relate to the presence of some relative large, 1-4 mm sized porphyroclast relicts embedded in the fine-grained material.

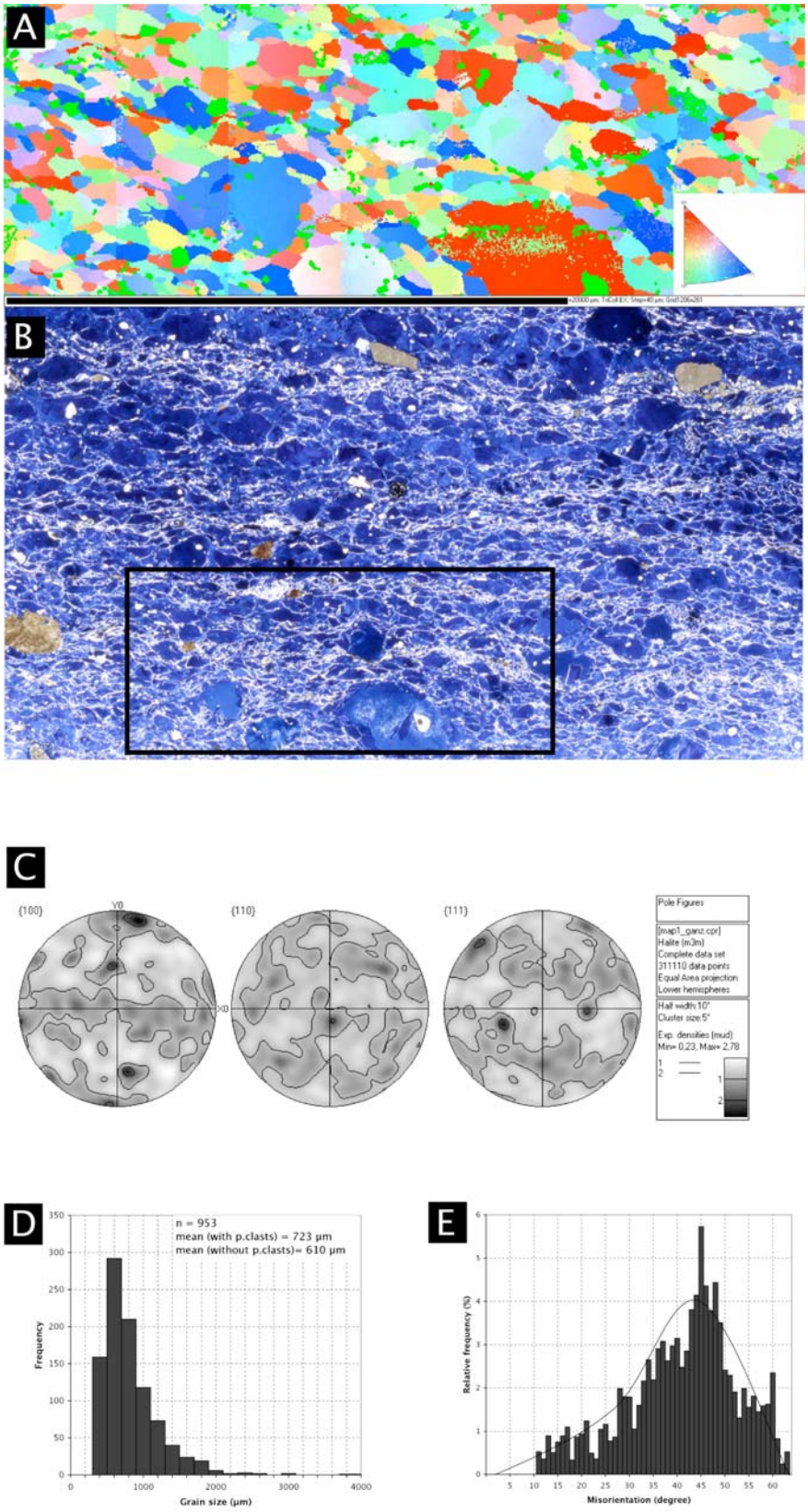

Fig. 7. A: part of the automated EBSD map of the EP sample. The map has been coloured according to orientation (green pixels = zero solution), with grain boundaries (>10° misorientation) coloured in black. The area was mapped in 48 maps, with a step size of 40 µm. B: microstructures of the thin section, showing the measured area in A. C: equal area, lower hemisphere projections of orientation data. The sample shows a

very weak crystallographic preferred orientation. The few local maxima correspond to the orientation data from the large porphyroclasts. D: grain size statistics based on the EBSD measurement. The mean grain size is about 0.6 mm. E: minimum misorientation angle distribution for all orientation data. The histogram represents neighbour pair misorientation. Solid black line indicates the theoretical misorientation distribution for randomly oriented grains.

5 Discussion

In most existing reports on deformation experiments on non-porous natural and synthetic rocksalts the steady-state creep behavior is controlled by dislocation mechanisms and solution-precipitation. In steady state creep, the grain size organizes itself into the boundary of grain size sensitive and grain size insensitive processes (de Bresser et al., 2001; Ter Heege et al., 2005a).

Experimental conditions range in temperature between 20-250 °C, strain rate 10^{-4} - 10^{-9} 1/s and confining pressure is up to 70 MPa. Before the onset of recrystallization, in coarse-grained salt the main deformation mechanism is dislocation creep, with the rate controlling mechanism of cross-slip of screw dislocations at high stresses of ~15 MPa and with rate controlling mechanism of dislocation climb at low stresses (5-15 MPa) (Carter and Hansen, 1983; Wawersik and Zeuch, 1986; Horseman and Handin, 1990; Horseman et al., 1992; Carter et al., 1993). Both mechanisms have their own characteristic microstructure: cross slip produces wavy slip bands, while climb produces equiaxial subgrains. In addition at sufficiently fine grain sizes (~500 μm) in wet salt solution-precipitation creep can control the rheology (Urai et al., 1986; Peach et al., 2001; Ter Heege et al., 2005b). Dislocation processes and solution-precipitation process act in parallel (e.g. Spiers and Carter, 1998). In the regime where dislocation creep controls the rheology, the trace amount of brine also plays an important role, as it drastically increases the grain boundary mobility and induces dynamic recrystallization by fluid-assisted grain-boundary migration (e.g. Watanabe and Peach, 2002).

5.1 Inferred deformation and recrystallization mechanisms based on the observed microstructures

5.1.1 Protomylonite

Before attempting to interpret the deformation-related microstructures and to evaluate the possible microstructural evolution of the samples, we first have to be able to unambiguously identify the primary, synsedimentary microstructures. There is a considerable amount of evidence in the literature that cubic fluid inclusions, arranged into bands parallel to (100), are entrapped when rocksalt is deposited in shallow water environment (see Warren, 2006 and references therein). As the halite deforms, grain boundary migration recrystallization removes those inclusions as the migrating boundary sweeps through them (Roedder, 1984; Schléder and Urai, 2005). One might use the presence of fluid inclusions as a criterion to distinguish between recrystallized and unrecrystallized parts. It has to be noted, however, that even in a shallow water environment not all the primary grains are necessarily rich in fluid inclusions (Shearman, 1970; Lowenstein and Hardie, 1985) or, additionally, the primary fluid inclusions may vary in a single grain, e.g. commonly there is a difference in the abundance of inclusions in salt that crystallized near the cube edge compared with that from the centers of the cube faces (Roedder, 1984). Thus, this microstructure gives only a lower bound of the amount of primary grains or, alternatively, upper bound of the amount of

recrystallization. In this paper we interpret the fluid inclusion-rich part of a grain as primary (e.g. Figs. 5A and C), and the origin of the fluid-inclusion-free regions as uncertain, unless other microstructures such as elongated subgrains point to recrystallization (e.g. Figs. 5C and F).

Well developed, equidimensional subgrains in the fluid-inclusion-rich part of the grains (Fig. 5C) point to dislocation processes, and were presumably produced during recovery by climb/glide of dislocations (e.g. Carter et al., 1993; Ter Heege et al., 2005b). The fact that the equidimensional subgrains laterally pass into elongated subgrains (Figs. 5C and D), suggests that the subgrain formation was followed by extensive grain boundary migration recrystallization. The elongated subgrains are interpreted to have evolved by edgewise propagation of subgrains behind migrating grain boundaries (Means, 1983, Means and Ree, 1988; Ree, 1991). The evidences for extensive GBM, in turn, may imply that grain dissection during GBM is also important mechanism in grain size reduction. In the subgrain-poor regions the presence of dark blue, subgrain-like polygonal microstructure (Fig. 5C) which was not etched is interpreted as low-energy subgrain walls, with insufficient amount of dislocations to become subgrains (Humphreys and Hatherly, 1996). If this suggestion is correct, this would indicate that concurrent subgrain formed behind the moving grain boundary during dynamic recrystallization.

In some cases the elongated subgrains occur at both sides of a grain boundary. Such a microstructure can be explained in two different ways. One explanation is that between the two recent grains there existed one highly deformed grain, which was simultaneously and completely replaced by its two neighbours, resulting in elongated subgrains on both sides. Alternatively this microstructure can be explained with a process somewhat similar to the crack-seal mechanism (Ramsay, 1980), that is the two neighbour grains move away from each other, perhaps with grain boundary sliding/solution precipitation creep or both, and a gap opens between them which is subsequently sealed with precipitates from the grain boundary fluid. In the latter case, the microstructure points to deformation by grain boundary sliding/solution-precipitation creep as an additional deformation mechanism beside the dislocation processes. It is hard to find unambiguous microstructural evidence for those mechanisms (Passchier and Trouw, 2005).

Equidimensional subgrains do not exclusively occur in the fluid-inclusion-rich part of the grains, but also in the fluid-inclusion-poor part. It can be that this part of a grain is also primary, e.g. it was never swept by a migrating boundary, or, alternatively, it can be that it represents an already recrystallized but subsequently deformed portion of a grain (Schléder and Urai, 2005).

New, substructure free, euhedral grains (Fig. 5D) can be explained by the process of nucleation, in which new grains nucleate at the grain boundary region and grow at the expense of the old, deformed ones. It is unclear whether these grains were nucleated during the upward transport, or are results of late, post-extrusion recrystallization after contact with rainwater. Regardless of their origin these grains are always smaller than the large elongated ones so that the original grain size of the host rock was coarser than that in our samples.

As possible processes for grain size reduction, based on studies of salt glacier in southern Iran, Talbot (1981) proposed processes of subgrain rotation and intergranular cracking of the porphyroclasts, which lead to grain size reduction. We did not find evidence for this in our samples, we note however, that Talbot (1981) studied Hormuz salt from a different setting with a possibly different deformation history (strain rate, differential stress) before and after

extrusion. It is also unclear whether the Garmsar prototype microstructures of the protomylonite represent steady state microstructure.

5.1.2 Mylonite

The lack of strong CPO (Fig. 7) and dislocation substructure suggests that the mylonite did not deform by dislocation processes. The large grains in the mylonites with well-developed subgrains, fluid inclusion bands and with sets of perpendicular dark bands seen in the gamma-irradiated sections indicate that these grains are almost certainly remnants of porphyroclasts. This assumption is in good agreement with experimental deformation on wet, fine grained halite by Urai et al., (1986) who showed that solution-transfer processes dominate over crystal plastic deformation mechanism in fine grained halite aggregates deformed at low differential stress.

Fibrous microstructures (Figs. 6E-J) around second-phase fragments and between halite grains point to deformation by grain boundary sliding (GBS). The fibrous structures then fill the voids between grains formed by grain boundary sliding. As the gap between two grains opens up they are continouosly sealed by precipitates from the grain boundary fluid (c.f. Fig. 1 of Schenk and Urai, 2004). Following this approach, fibrous structures around limestone particles are interpreted as strain fringes around rotating rigid blocks (Figs. 6E and F). Fibrous microstructures, similar to those reported here, were also observed in some other rocks, and are also consistent with grain boundary sliding and solution precipitation creep (Rutter et al., 1985; Cox and Etheridge, 1989).

The core-mantle structures with the fibrous microstructures inside a single grain, surrounded by non-fibrous material are interpreted as overgrowth structures (Figs. 6G-J) formed by non-conservative grain boundary migration. The growth bands may reflect changes in chemistry of the grain boundary fluid (Murata and Smith, 1946). Alternatively, the growth bands could record stages of grain boundary energy driven grain growth. We have attempted to measure the chemical variation inside such a banded grain using electron microprobe analysis, but results show that the impurity content is below the detection limit (0.02 %). The occurrence of dark blue fibrous microstructure may also be due to local enrichment in some chemical elements along the fibre though the exact mechanisms which is responsible for the development of such microstructure is not clear.

The presence of voids (Figs. 6C-D), seen now as vapour inclusions, could either be explained by the process of GBS or, alternatively, they may represent dissolution caused by rainwater. As the rainwater dissolves halite from the shear zone, the zone becomes enriched in residual secondary phases. It has been experimentally demonstrated by Hickman and Evans, 1991, that such a mixed-phase aggregate is particularly susceptible to pressure solution. The authors reported that a small percentage of secondary minerals – especially clays – dramatically enhances the rate of pressure solution. In the samples analyzed in this paper we did not find clays at the grain boundaries, neither in the wall rock nor in the shear zones, which would suggest that this enhanced pressure solution did not take place, though it may play a role in other extrusive rocksalts as they reportedly contain traces of clay minerals (Talbot and Aftabi, 2004).

5.2 Rheology of the extrusive salts as predicted by the flow laws

The deformation and recrystallization microstructures developed in the protomylonite and mylonite show that the microstructural processes are significantly different between the two rock types. Based on the microstructures we inferred above that the protomylonite presumably deformed mainly by dislocation creep, while the main deformation mechanisms in the mylonitic shear zones are solution-precipitation creep and GBS accommodated by solution-precipitation. In what follows we attempt to quantify the effect of these differences on rheology.

5.2.1 Stress and strain rate calculation

Experimental deformation of various rocks showed that there is a strong correlation between the steady state subgrain size D and flow stress σ (e.g. Twiss, 1977, Carter et al., 1993). This relationship for halite can be written by (Schléder and Urai, 2005):

$$D\ (\mu m) = 215\ \sigma^{-1.15}\ (MPa) \qquad (1)$$

The relationship can be used for estimating the paleostress in halite. For this calculation we measured the sizes of the equiaxial subgrains by the method of equal circular diameter (ECD), which involves the tracing of subgrain boundaries from digital photos of etched thin sections taken in reflected light, and calculating of the enclosed subgrain area using ImageJ software. The calculated differential stress for the protomylonite is 1.4 to 2 MPa (95 % confidential limits, Table 1), which is in good agreement with the literature data for other rocksalts (Carter et al., 1993). Such high differential stress clearly does not exist in the glacier and we interpret these microstructures to have formed during the upward transport of the salt mass in the extrusion canal. In the glacier itself, the deformation is driven by the downslope component of gravity. The common salt glacier thickness does not exceed 200 m, and with a slope of 5° the shear stress is about 0.4 MPa (Wenkert, 1979; Jackson, 1985).

Table 1. Statistics of grain and subgrain size and calculated differential stress, strain rate values.

Sample	Mean grain size (mm)	1 SD	Mean subgrain size (μm)	1 SD	Differential stress (MPa)	Assumed deformation temperature (°C)	Strain rate (1/s)
Protomylonite (GH)	4	2	114	71	1.4–2	40	$7.2\text{x}10^{-12}$ to $1.1\text{x}10^{-11}$ [c]
Mylonite (GH and EP)	0.6 [a]	0.35	–	–	~0.4 [b]	20	$1.2\text{x}10^{-10}$ [d]

a. The mean grain size in the mylonite was quantified based on EBSD measurements
b. Shear stress calculated for 200 m thick salt sequence and 5° slope.
c. For the protomylonite the total strain rate is a sum of those from Eqs. 2 and 3. For the mylonite the strain rate is calculated using Eq. 3.

It has been proposed that natural rocksalt deforms with a combination of dislocation climb and solution-precipitation creep processes which act in parallel (Spiers and Carter, 1998). The microstructures seen in the protomylonite are in agreement with this assumption, enabling us to calculate the strain rate using the Equation 2 for dislocation climb and

Equation 3 for solution-precipitation creep. For solution-precipitation creep there are numerous flow law parameters in the literature (Lohkämper et al., 2003). To calculate the strain rate we used the flow law parameters quoted by Spiers et al. (1990). In that work they calibrated the flow law on the basis of experiments on porous and dense polycrystalline aggregates of synthetic rocksalt.

$$\dot{\varepsilon}_{CL} = 8.1 \times 10^{-5} \exp\left(-51600 / RT\right)\left(\sigma_1 - \sigma_3\right)^{3.4} \quad \text{after Carter et al. (1993)} \tag{2}$$

$$\dot{\varepsilon}_{PS} = 4.7 \times 10^{-4} \exp\left(-24530 / RT\right)\left(\sigma_1 - \sigma_3\right) / TD^3 \quad \text{after Spiers et al. (1990)} \tag{3}$$

Where strain rate (ε) is expressed in s^{-1}, the pre-exponential constant is in $MPa^{-n}s^{-1}$, apparent activation energy is in $Jmol^{-1}$, Boltzmann's gas constant (R) is in $Jmol^{-1}K^{-1}$, temperature (T) is in ^oK, differential stress (σ_1 - σ_3) is in *MPa* and grain size (D) is in *mm*. For the calculation we assumed that the salt extrudes from a depth of 1.5 km (Fig. 2), thus we used 40 °C as deformation temperature for the protomylonite. This value is admittedly only a crude estimate, since we don't exactly know at which stage the protomylonite was deformed and what was the real geothermal gradient in the area.

The mylonite microstructures depict deformation mechanisms of solution-precipitation creep and GBS accompanied with solution-precipitation. We postulate that the rate limiting process is the solution-precipitation process, enabling us to describe its rheology by Eq. 3. For the mylonite we assumed that the shear zones developed and the deformation took place on the surface and that the deformation occurred mostly in the rainy, relatively cold seasons (Talbot and Rogers, 1980), thus we used 20 °C. The strain rate calculations for the protomylonite indicate that dislocation creep and solution-precipitation creep contribute approximately equally to the total strain rate (Fig. 8). It has to be noted here, that if we calculate only with the grain size of the large, elongated grains, dislocation creep dominates over the solution-precipitation creep.

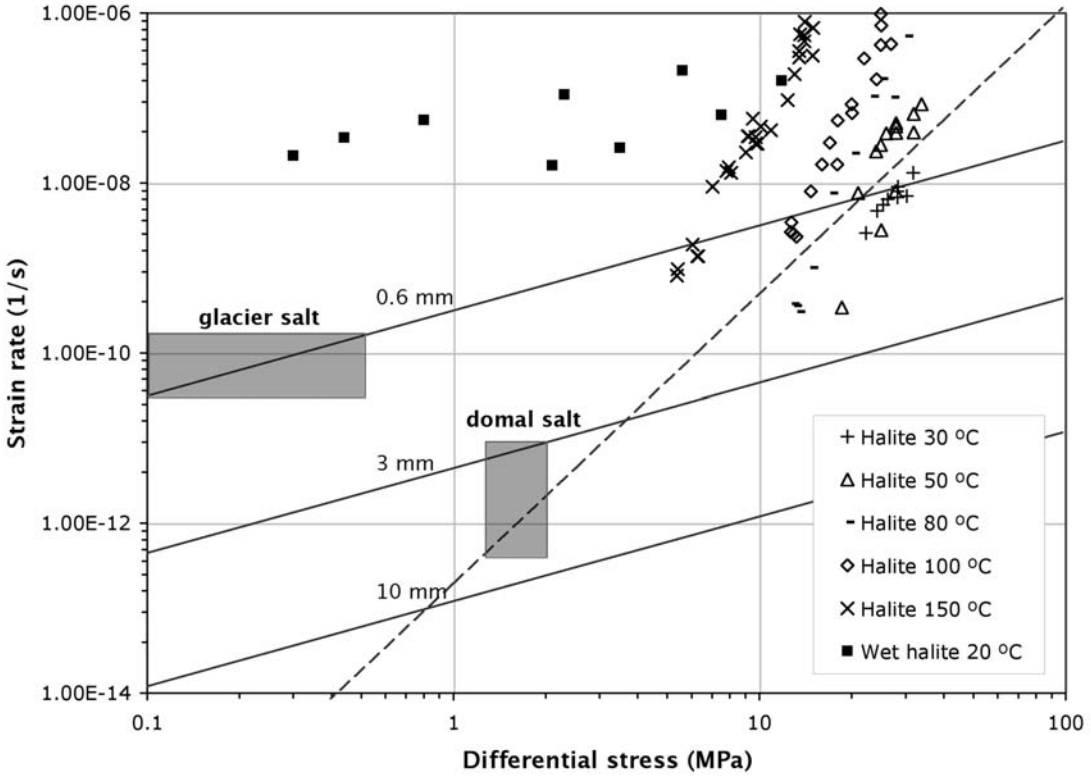

Fig. 8. The diagram shows the calculated differential stress values plotted against the calculated strain rate values for both the protomylonite and mylonite. The differential stress for the protomylonite was calculated using subgrain piezometry (1.4-2 MPa), while the shear stress arising from the downslope component of gravity was taken for the mylonite (<0.4 MPa). For the protomylonite, strain rate was calculated assuming deformation mechanisms of dislocation creep and solution-precipitation creep and that these processes act in parallel (Spiers and Carter, 1998). Thus, the flow law from Carter et al. (1993) is plotted for 40 ºC (dashed line) and the flow law for solution-precipitation creep (Spiers et al., 1990) for grain sizes of 3 mm and 10 mm for 40 ºC is also shown (solid lines). The strain rate for the mylonite was calculated assuming that the rate controlling mechanism is the solution-precipitation creep. Thus the flow law of Spiers et al., 1990 was taken and calculated for a grain size of 0.6 mm and a temperature of 20 ºC. The relevant field for both domal salt and the glacier salt is indicated with a gray rectangle. Besides these, experimental data from numerous sources (Hansen and Mellegard, 1980; Hansen and Carter, 1984; Handin et al., 1986; Spiers et al., 1986; Senseny, 1988; Horseman and Handin, 1990; Horseman et al., 1992; Hunsche et al., 2003) are also shown for comparison. The grain size in the wet halite test is ~0.1 mm, for the others it is significantly coarser: > 5 mm. Note that the experiment on fine grained wet halite shows a comparable rheology to that calculated for the glacier salt.

The strain rate calculated for the mylonite is about one or two orders of magnitude higher at much lower shear stress than in the protomylonite. It shows that this material is much weaker than the coarse grained counterparts. If the rheology is comparable to that observed in experiments of Spiers et al. (1986) and Urai et al. (1986) (Fig. 8), the calculated strain rate also agrees well with field measurements (Talbot and Rogers, 1980; Talbot et al., 2000), and corresponds to glacier flow of ~1 m in 2 years.

5.2.2 Initiation of the shear zone

As we discussed above, the protomylonite suggests dislocation creep at differential stress of 1.4 to 2 MPa. This deformation mechanism is characteristic for the upward transport of the

salt through the cold diapir stem. In the glacier the strain concentrates in multiple, narrow shear zones in which the salt deforms by mechanisms of GBS and solution-precipitation creep (Fig. 8). It follows that there has to be a zone where the two deformation mechanisms switch, i.e. where the deformation changes from a dislocation process controlled one to a GBS + solution-precipitation controlled one. Unfortunately, the limited outcrop did not allow us to locate where the salt is extruded. It is possible that the shear zones were already developed before the salt mass reached the surface, or that the strain was accumulated in shear zones when it was squeezed out and moved to its recent position.

Although the protomylonite in the Garmsar hills sample is considerably recrystallized, it is probable that the salt still retained some of its primary grain size variation when it reached the surface. This assumption is supported also by the fact that in the protomylonite primary microstructures such as fluid-inclusion-rich crystals still exist. If the salt retained some slight primary variations in its grain size, that in turn could influence the emplacement of the shear zone in the glacier. As the simplest solution, we suggest this process to be responsible for the emplacement of the bedding-parallel shear zones and that the spacing of the shear zones corresponds to the initial layering produced by primary (synsedimentary) processes (Shearman, 1970; Lowenstein and Hardie, 1985; Warren, 2006). Nevertheless, as the glacier advances downhill, and the whole glacier becomes strongly folded by sets of recumbent folds, resulting probably in that the individual shear zones also become folded.

Mylonitic shear zones illustrated here have never been described in deep salt mines and if they exist they may be quite uncommon indeed, although coarse-grained shear zones do exist during salt diapirism (Kupfer, 1974). Therefore we prefer the interpretation that such shear zones do not play an important role in deep subsurface halokinetic movement. In the salt extusion perhaps it is the low confining pressure which allows the development of mylonitic shear zones.

5.3 Brine in grain boundaries

Several in-situ field measurements showed that the downhill flow of the salt glacier is episodic. Talbot and Rogers (1980) reported accelerated flow after heavy rain, and noted that in dry seasons, the movement involves only daily thermal extension and contraction due to variations in air temperature. There is considerable evidence that these daily variations create an extensive and penetrative crack system (Talbot and Aftabi, 2004), which in turn is able to conduct the rainwater into the salt glacier. The process after which this conducted rainwater wets the whole shear zone is not entirely clear.

The mass transfer, necessary for the solution-precipitation process, could take place in either static fluid network or in migrating fluid. The episodic glacier flow may imply that the mass transport occurred in migrating undersaturated fluids. This assumption seems to be confirmed by the presence of numerous air inclusions at grain boundaries and triple junctions, which could be interpreted as the result of dissolution by the trespassing rainwater.

6 Summary and conclusions

Two mylonitic and protomylonitic samples from naturally deformed extrusive Eocene-Oligocene rocksalt from the Eyvanekey Plateau and Garmsar hills were studied with the aim to characterize the deformation and recrystallization mechanisms.

1. Conclusions presented in this study may be applicable to other areas where salt glaciers are or were present, since it is very likely, that the deformation involves similar mechanisms in any types of extrusive salts. Mechanics of actively deformed halite at the surface are those of the shear zones described in this paper. Thus the recent, shallow buried salt glaciers at the Gulf of Mexico may also deform by similar processes and be very weak and many of the ancient now deeply buried bedding parallel salt flanks (i.e. christmas-tree structures) were developed by similar processes in weak salt.
2. In the protomylonite dislocation climb controlled creep and solution-precipitation creep were the main deformation mechanisms during the upward transport of the rocksalt. The differential stress was between 1.4-2 MPa, as deduced from subgrain size piezometry.
3. As the rocksalt reaches the surface, numerous bedding-parallel shear zones develop, in which the deformation mechanism is solution-precipitation creep (non-conservative grain boundary migration and grain boundary sliding accommodated by solution-precipitation). The microstructural evidences for this are the fibrous structures, growth bands and the lack of crystallographic preferred orientation.
4. The grain size reduction, which is necessary for the grain size sensitive mechanism to become active occurs by nucleation of new grains and/or dissection by grain boundary migration.
5. The formation of the shear zones is perhaps controlled by synsedimentary variation in some mechanical properties, most probably grain size. Thus the synsedimentary process results in rhythmic variation in grain size, which grain size variation is maintained until the salt reaches the surface. In the salt extrusion, this variation might be the main controlling factor in the emplacement of the shear zone.
   The GBS and solution-precipitation allows the salt glacier to flow downhill under its own weight with a geologically high strain rate of about 10^{-10} 1/s.

Acknowledgements

The authors thank C. J. Talbot for providing sample EP, Dirk Kirch (IMM RWTH Aachen) for the orientation measurements and Manfred Thomé (Forschungszentrum Jülich) for carrying out the gamma irradiation. C. J. Talbot and Abbas Bahroudi are thanked for the introduction into the geology of Garmsar hills and Eyvanekey plateau. We thank the stuff at the Geodynamic Department of Geological Survey of Iran (GSI) in Tehran for the hospitality during the 2005 field season. For helpful discussions O. Schenk, J. Schoenherr, Chris Hilgers at the Dept. of Geologie-Endogene Dynamik (RWTH Aachen) are acknowledged. The manuscript was improved by thorough reviews of M. P. A. Jackson and W. Schmahl. This work was performed as part project of SPP 1135 (project UR 64/5-1-2) financed by the Deutsche Forschungsgemeinschaft.

References

Amini, B., Rashid, H. 2005. Garmsar Geological map 1:100000 in scale. Geological Survey of Iran, Tehran, Iran.

Bestmann, M., Prior, D. J., 2003. Intragranular dynamic recrystallization in naturally deformed calcite marble: diffusion accommodated grain boundary sliding as a result of subgrain rotation recrystallization. Journal of Structural Geology 25, 1597-1613.

Carter, N. L., Handin, J., Russell, J. E., Horseman, S. T., 1993. Rheology of rocksalt. Journal of Structural Geology 15(9/10), 1257-1271.

Carter, N. L., Hansen, F. D., 1983. Creep of rocksalt. Tectonophysics 92, 275-333.

Cox, S. F., Etheridge, M. A., 1989. Coupled grain-scale dilatancy and mass transfer during deformation at high fluid pressures: examples from Mount Lyell, Tasmania. Journal of Structural Geology 11(1-2), 147-162.

de Bresser, J. H. P., Ter Heege, J. H., Spiers, C. J., 2001. Grain size reduction by dynamic recrystallization: can it result im major rheological weakening? International Journal of Earth Sciences 90, 28-45.

Drury, M. R., Urai, J. L., 1990. Deformation-related recrystallization processes. Tectonophysics 172, 235-253.

Fletcher, R. C., Hudec, M. R., Watson, I. A. 1995. Salt glacier and composite sediment-salt glacier models for the emplacement and early burial of allochtonous salt sheets. In: Jackson, M. P. A., Roberts, D. G. & Snelson, S. (Eds.), Salt tectonics: a global perspective. AAPG Memoir, 65, 77-108.

Gansser, A., 1960a. Die Geologische erforschung der Qom gegend, Iran. Bulletin der Vereinigung Schweitzerisches Petroleum Geologen und Ingenieur 23, 1-16.

Gansser, A., 1960b. Über Schlammvulkane und Salzdome. Naurforschende Gesellschaft in Zürich Vierteljahrschrift 105, 1-46.

Garcia Celma, A., Donker, H. (Editors), 1996. The Effect of Gamma Radiation in Salt, EUR-Report 16743EN.

Gretener, P. E., 1982. Another look at the Alborz Nr. 5 in central Iran. Bulletin der Vereinigung Schweitzerisches Petroleum Geologen und Ingenieur 48, 1-8.

Handin, J., Russell, J. E., Carter, N. L. 1986. Experimental deformation of rocksalt. In: Hobbs, B. E. & Heard, H. C. (Eds.), Mineral and rock deformation: laboratory studies. AGU Geophysical Monograph 36. American Geophysical Union, 161-199.

Hansen, F. D., Carter, N. L. 1984. Creep of Avery Island rocksalt. Proceedings of the first Conference on mechanical Behavior of Salt, Clausthal-Zellerfeld, Germany, Trans. Tech. Publications, 53-69.

Hansen, F. D., Mellegard, K. D., 1980. Quasi-static strength and deformational characeristic of domal salt from Avery Island, Lousiana. ONWI-116, Report prepared by RE/SPEC Inc. for Office of Nuclear Waste Isolation.

Hickman, S. H., Evans, B., 1991. Experimental pressure solution in halite; the effect of grain/interphase boundary structure. Journal of the Geological Society 148, 549-560.

Horseman, S. T., Handin, J. 1990. Triaxial compression tests on rocksalt at temperatures from 50 °C to 200 °C and strain rates from 10−4 to 10−9 1/s. In: Duba, A. G., Durham, W. B., Handin, J. W. & Wang, H. F. (Eds.), The brittle-ductile transition in rocks 56. American Geophysical Union, Washington, DC, United States, 103-110.

Horseman, S. T., Russell, J. E. H., J., Carter, N. L. 1992. Slow experimental deformation of Avery Island salt. Proceedings of the Seventh Internation Symposium on salt, Kyoto, Japan, April 6-9 1992, Elsevier, Amsterdam, 1, 67-74.

Humphreys, F. J., Hatherly, M. 1996. Recrystallization and related annealing phenomena. Pergamon.

Hunsche, U., Schulze, O., Walter, F., Plischke, I., 2003. Projekt Gorleben. Thermomechanisches Verhalten von Salzgestein. 9G2138110000, BGR, Hannover.

Jackson, M. P. A., 1985. Natural strain in diapiric and glacial rock salt, with emphasis on Oakwood dome, East Texas, Bureau of Economic Geology, The University of Texas at Austin, Texas.

Jackson, M. P. A. 1995. Retrospective salt tectonics. In: Jackson, M. P. A., Roberts, D. G. & Snelson, S. (Eds.), Salt tectonics: a global perspective. AAPG Memoir 65, 77-108.

Jackson, M. P. A., Cornelius, R. R., Craig, C. H., Gansser, A., Stocklin, J., Talbot, C. J. 1990. Salt diapirs of the Great Kavir, central Iran. Geological Society of America, Boulder, 177.

Kupfer, D. H. 1974. Boundary shear zones in salt stocks. Fourth symposium on salt, Cleveland, Ohio, USA, 1, 215-225.

Lohkämper, T. H. K., Jordan, G., Costamagna, R., Stöckhert, B., Schmahl, W. W., 2003. Phase shift interference microscope study of dissolution-precipitation processes of nonhydrostatically stressed halite crystals in solution. Contributions to Mineralogy and Petrology 146(3), 263-274.

Lowenstein, T. K., Hardie, L. A., 1985. Criteria for the recognition of salt-pan evaporites. Sedimentology 32, 627-644.

Mohr, M., Kukla, P. A., Urai, J. L., Bresser, G., 2005. Multiphase salt tectonic evolution in NW Germany: seismic interpretation and retrodefromation. International Journal of Earth Sciences 94(5-6), 917-941.

Murata, K. J., Smith, R. L., 1946. Manganese and lead coactivators of red fluorescence in halite. American Mineralogist 31, 527-538.

Passchier, C. W., Trouw, R. A. J. 2005. Microtectonics. Springer.

Peach, C., Spiers, C. J., Trimby, P. W., 2001. Effect of confining pressure on dilatation, recrystallization, and flow of rock salt at 150 °C. Journal of Geophysical Research 106(13315-13328).

Pennock, G. M., Drury, M. R., Spiers, C. J., 2005. The development of subgrain misorientations with strain in dry synthetic NaCl measured using EBSD. Journal of Structural Geology 27, 2159-2170.

Prior, D. J., Wheeler, J., Peruzzo, L., Spiess, R., Storey, C., 2002. Some garnet microstructures: an illustration of the potential of orintation maps and misorientation analysis in microstructural studies. 2002 24, 999-1011.

Przibram, K., 1954. Irradiation colours in minerals. Endeavour 13(49), 37-41.

Roedder, E., 1984. The fluids in salt. American Mineralogist 69, 413-439.

Rutter, E. H., Peach, C., White, S. H., Johnston, D., 1985. Experimental 'syntectonic' hydration of basalt. Journal of Structural Geology 7(2), 251-266.

Schenk, O., Urai, J. L., 2004. Microstructural evolution and grain boundary structure during static recrystallization in synthetic polycrystals of Sodium Chloride containing saturated brine. Contributions to Mineralogy and Petrology 146(6), 671-682.

Schléder, Z., Urai, J. L., 2005. Microstructural evolution of deformation-modified primary halite from the Middle Triassic Röt Formation at Hengelo, The Netherlads. International Journal of Earth Sciences 94(5-6), 941-955.

Senseny, P. E. 1988. Creep properties of four salt rocks. Proceedings of the Second Conference on mechanical Behavior of Salt, Clausthal-Zellerfeld, Germany, Trans. Tech. Publications, 431-444.

Senseny, P. E., Hansen, F. D., Russell, J. E., Carter, N. L., Handin, J., 1992. Mechanical behaviour of rock salt: phenomenology and micromechanisms. Int. J. Rock Mech. Min. Sci & Geomech. Abstr. 29(4), 363-378.

Shearman, D. J., 1970. Recent halite rock, Baja California, Mexico. Transaction of Mining and Metallurgy 79B, 155-162.

Spiers, C. J., Carter, N. L. 1998. Microphysics of rocksalt flow in nature. Fourth Conference on the Mechanical behaviour of Salt, The Pennsylvania State University, June 17 and June 18, 1996, Trans Tech Publication Series on Rock and Soil Mechanics, 22, 115-128.

Spiers, C. J., Schutjens, P. M. T. M., Brezowski, R. H., Peach, C., Liezenberg, J. L., Zwart, H. J. 1990. Experimental determination of constitutive parameters governing creep of rocksalt by pressure solution. In: Knipe, R. J. & Rutter, E. H. (Eds.), Deformation Mechanisms, Rheology and Tectonics 24. Geological Society Special Publications, 215-227.

Spiers, C. J., Urai, J. L., Lister, G. S., Boland, J. N., Zwart, H. J., 1986. The influence of fluid-rock interaction on the rheology of salt rock, Department of Structural and Applied Geology, Institute of Earth Sciences, University of Utrecht, The Netherlands.

Talbot, C. J., 1979. Fold trains in a glacier of salt in southern Iran. Journal of Structural Geology 1(1), 5-18.

Talbot, C. J. 1981. Sliding and other deformation mechanisms in glacier of salt, S Iran, Trust and Nappe Tectonics. The Geological Society of London, 173-183.

Talbot, C. J. 1998. Extrusions of Hormuz salt in Iran. In: Blundell, D. J. & Scott, A. C. (Eds.), Lyell; the past is the key to the present. Geological Society Special Publications 143, 315-334.

Talbot, C. J., in prep. The Eyvanekey plateau, a 20 x 10 km sheet of allochtonous salt near Garmsar.

Talbot, C. J., Aftabi, P., 2004. Geology and models of salt exreusion at Qom Kuh, central Iran. Journal of the Geological Society 161, 321-334.

Talbot, C. J., Jarvis, R. J., 1984. Age, budget and dynamics of an active salt extrusion in Iran. Journal of Structural Geology 6(5), 521-533.

Talbot, C. J., Medvedev, S., Alavi, M., Shahrivar, H., Heidari, E. 2000. Salt extrusion at Kuh-e-Jahani, Iran, from June 1994 to November 1997. In: Vendeville, B. C., Mart, Y. & Vigneresse, J.-L. (Eds.), Salt, shale and igneous diapirs in and around Europe. Geological Society Special Publication 174, 93-110.

Talbot, C. J., Rogers, E. A., 1980. Seasonal movements in a salt glacier in Iran. Science 208, 395-397.

Ter Heege, J. H., De Bresser, J. H. P., Spiers, C. J., 2005a. Dynamic recrystallization of wet synthetic polycrystalline halite: dependence of grain size distribution on flow stress, temperature and strain. Tectonophysics 396, 35-57.

Ter Heege, J. H., De Bresser, J. H. P., Spiers, C. J., 2005b. Rheological behaviour of synthetic rocksalt: the interplay between water, dynamic recrystallization and deformation mechanisms. Journal of Structural Geology 27(6), 948-963.

Twiss, R. J., 1977. Theory and applicability of a recrystallized grain size paleopiezometer. Pageoph 115, 227-244.

Urai, J. L., Spiers, C. J., Peach, C., Franssen, R. C. M. W., Liezenberg, J. L., 1987. Deformation mechanisms operating in naturally deformed halite rocks as deduced from microstructural investigations. Geologie en Mijnbouw 66, 165-176.

Urai, J. L., Spiers, C. J., Peach, C. J., Zwart, H. J., 1985. A laboratory investigation into the interaction of recrystallization and radiation damage effects in polycrystalline salt rocks, HPT Laboratorium, Insititut voor Aardwetenschappen, University of Utrecht, The Netherlands.

Urai, J. L., Spiers, C. J., Zwart, H. J., Lister, G. S., 1986. Weakening of rocksalt by water during long term creep. Nature 324, 554-557.

van Opbroek, G., den Hartog, H. W., 1985. Radiation damage of NaCl: dose rate effects. Journal of Physics. C: Solid State Phys. 18, 257-268.

Volozh, Y., Talbot, C. J., Ismail-Zadeh, A., 2003. Salt structures and hydrocarbons in the Pricaspian basin. AAPG Bulletin 87(2), 313-334.

Warren, J. 2006. Evaporites: sediments, resources and hydrocarbons. Springer.

Watanabe, T., Peach, C., 2002. Electrical impedance measurement of plastically deforming halite rocks at 125 ºC and 50 MPa. Journal of Geophysical Research 107(B1), ECV 2-1 -2-12.

Wawersik, W. R., Zeuch, D. H., 1986. Modeling and mechanistic interpretation of creep of rock salt below 200 C. Tectonophysics 121, 125-152.

Wenkert, D. D., 1979. The flow of salt glaciers. Geophysical Research Letters 6(6), 523-525.

Wheeler, J., Prior, D. J., Jiang, Z., Spiess, R., Trimby, P. W., 2001. The petrological significance of misorientation between grains. Contributions to Mineralogy and Petrology 141, 109-124.

Appendix

Fig. 1. Shear zones at the Garmsar hills. Note that the shear zone is located at the top/bottom of the coarse-grained zones. Coin for scale.

Fig. 2. Isoclinally folded halite layers at Garmsar hills. The view is perpendicular to the axial plane of the fold. Coin for scale.

Fig. 3. Refolded fold in halite at Garmsar hills. Hammer for scale. The view is perpendicular to the aqxial plane of the fold. The brownish material is possibly remnants of dissolved potassic salt.

Fig. 4. Variation in grain size in rocksalt at Eyvanekey plateau. The bedding trends from the top right to the bottom left. The variation in grain size is thought to be primary and is due to synsedimentary processes. Pencil for scale.

Fig. 5. Elongated large grains in fine-grained matrix in the Eyvanekey plateau. These large grains might be relicts of primary, coarse-grained salt. Pencil for scale.

Fig. 6. Large, euhedral grains at the Eyvanekey plateau. The grains are strain-free, suggesting that they were produced by static recrystallization of the salt, perhaps due to contact with rainwater. Note that the salt is almost completely recrystallized and consists of strain-free grains. The white material at the grain boundaries is secondary salt and is due to efflorescence. Hammer for scale.

Chapter 6: Recrystallization mechanisms in highly deformed glacier salt from Qum Kuh, central Iran: First look

Zsolt Schléder and János L. Urai

Abstract

A common microstructure in many extrusive halite samples is the presence of relatively large (up to 4 cm), subgrain-rich porphyroclasts, surrounded by numerous small, (< 1 mm) strain-free subhedral grains. In order to get some insight into the process of formation of these new grains, orientation measurements using EBSD were carried out on a selected sample from the Qum Kuh salt extrusion. It can be shown that some new grains formed by subgrain rotation, while in the majority of cases the abrupt change in orientation suggest that the new grains were generated by nucleation, or subgrain rotation and some other process which further increased the misorientation between the old and the new grains.

Keywords: Rocksalt, salt glacier, EBSD, deformation mechanism

1 Motivation

Full understanding of dynamic recrystallization during rock salt deformation is the key for quantifying deformation conditions of rock salt in nature and predicting its rheology. Naturally deformed halite shows evidence for a wide range of deformation and recrystallization mechanisms (Urai et al., 1987). Grain size reduction during deformation may occur by grain boundary bulging, subgrain rotation or nucleation processes (Urai et al., 1986), perhaps in combination with microcracking under some conditions. However, as the majority of (domal) halite samples studied to date show large-strain steady state microstructures, the nature of nucleation process of recrystallization in salt is not clear, although the onset of grain boundary migration has been described in some slightly deformed rock salt (Schléder and Urai, 2005).

In this contribution we analyzed the crystallographic orientation of porphyroclasts and the surrounding small grains in a sample from a salt extrusion with the aim to constrain the process which led to their formation.

2 Local geology and the sample

Several diapirs of the Lower Oligocene Lower Red Fm and Lower Miocene Upper Red Fm salt sequence reach the surface in central Iran (Fig. 1) (Jackson et al., 1990). Those include the Qum Kuh near the city of Qum, some 150 km SSW of Tehran (Gansser, 1960; Jackson et al., 1990; Talbot and Aftabi, 2004).

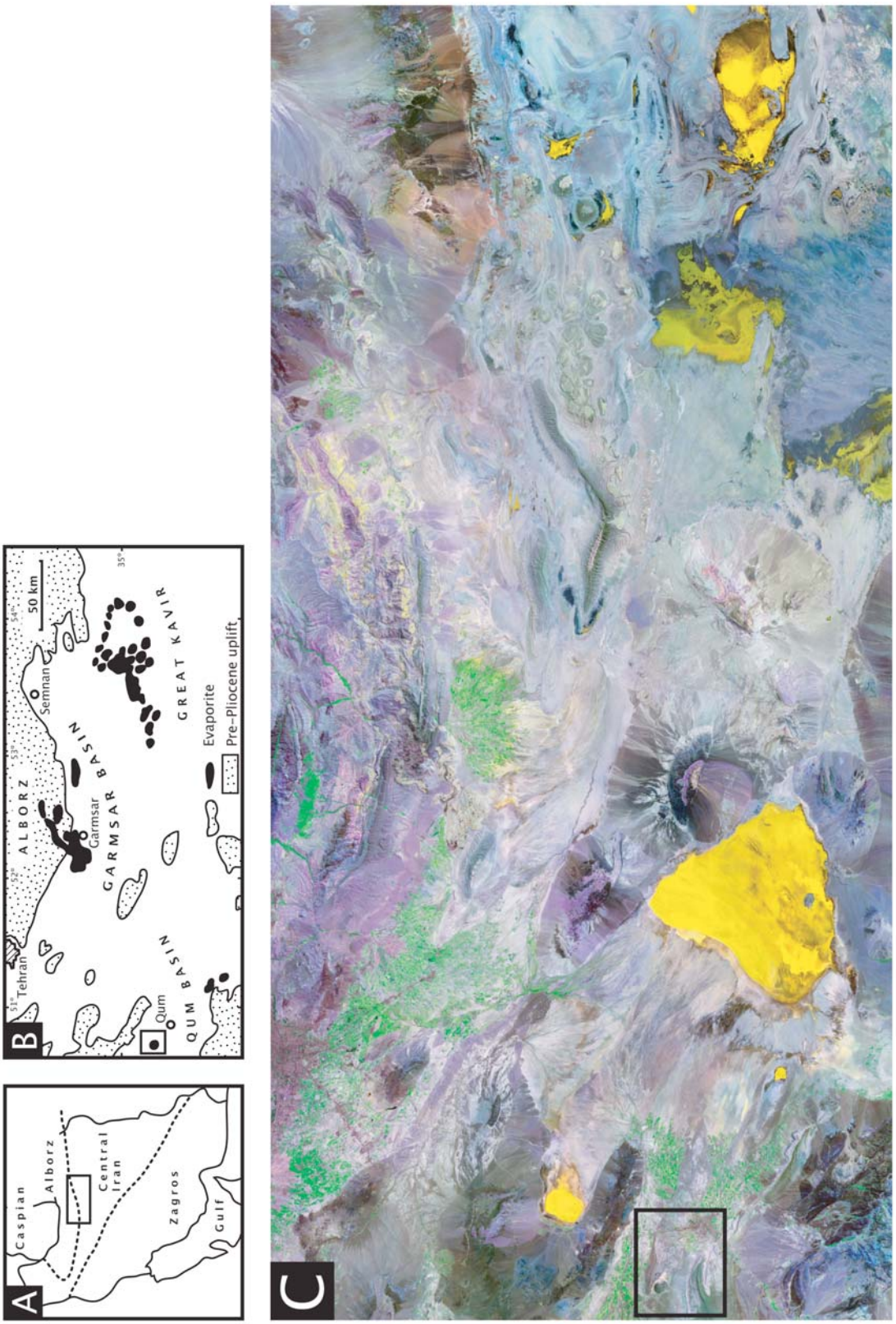
A
Caspian
Alborz
Central Iran
Zagros
Gulf
B
Tehran
Qum
Semnan
Garmsar
ALBORZ
GARMSAR BASIN
QUM BASIN
GREAT KAVIR
50 km
Evaporite
Pre–Pliocene uplift
C

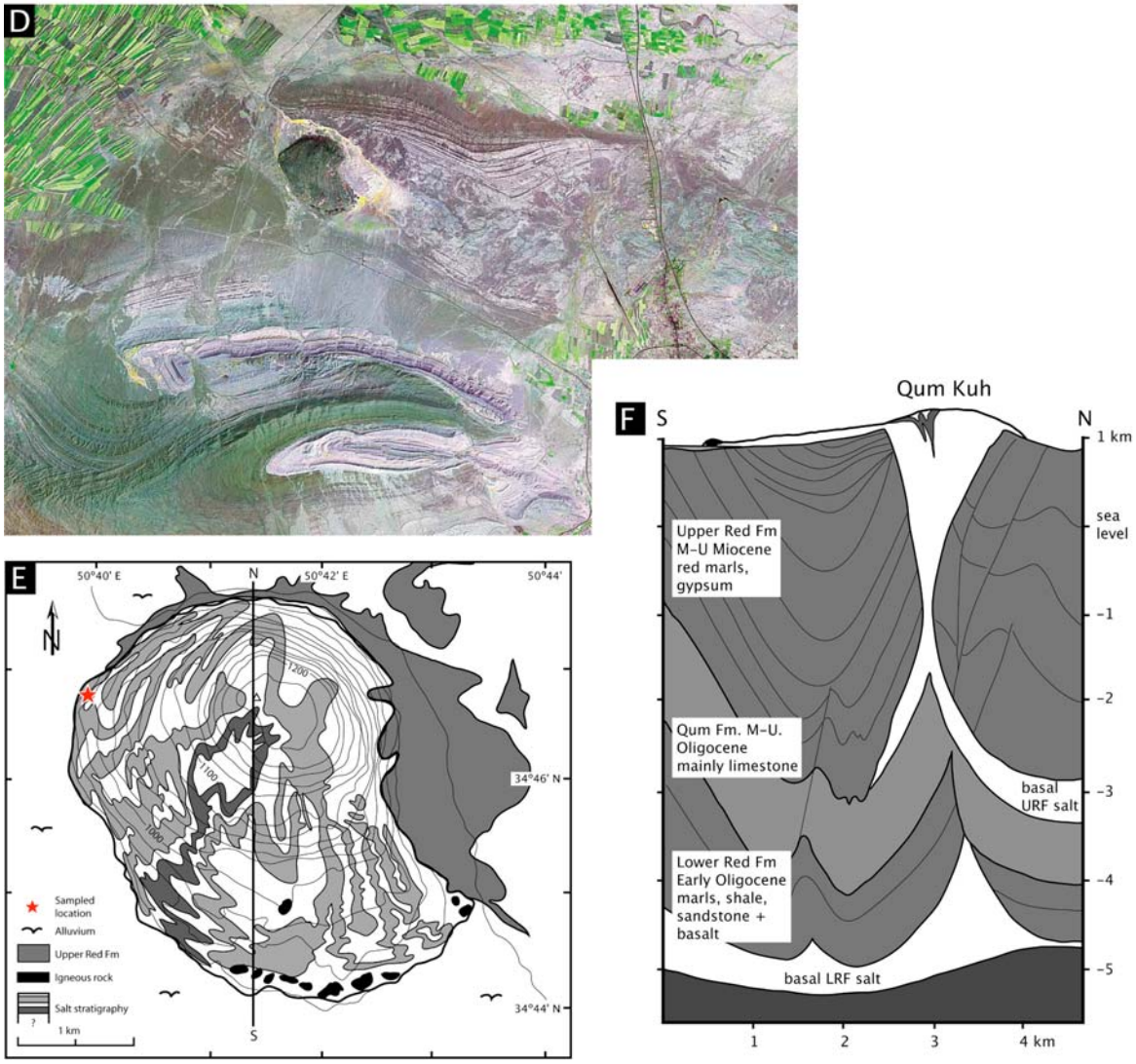

Fig. 1. Simplified regional setting of Qum Kuh. A: location in the map of Iran B: surfaced evaporites in the Garmsar basin and adjoining Qum and Great Kavir basins (after Jackson et al., 1990). The location of the study area is indicated with a rectangle. C: landsat image (GeoCover circa 2000, https://zulu.ssc.nasa.gov/mrsid) shows the same area as image D: detail of the landsat image showing the Qum Kuh (occur as black) and adjoining area. The white patch east of the hill is the salt withdrawal basin, filled with secondary salt. E: Geological map of the Qum Kuh, with some of the folded salt layers and the sampled locality is indicated (after Talbot and Aftabi, 2004). F: Cross-section throughout the salt structure of Qum Kuh (redrawn after Talbot and Aftabi, 2004). For the position of the profile see image F. No vertical exaggeration.

The salt emerged from a depth of 5.5-3 km along a releasing bend in a major dextral transpressive fault crossing the Qum basin (Jackson et al., 1990; Talbot and Aftabi, 2004). The salt surfaces at a rate of 82 mm a^{-1} through a 2.5x1 km vent. Analogue modelling suggests extrusion during at least 42 000 years (Talbot and Aftabi, 2004). The salt hill is 3 km wide and rises 315 m above the surrounding plateau. From the vent, an ~ 0.75 km long salt glacier flows to the west of the summit and ~ 2 km to the south (Fig. 1, Gansser, 1960; Talbot and Aftabi, 2004).

In the glacier the halite layers are commonly parallel to the base of the salt. The layers are folded in different generations of similar recumbent folds (Talbot and Aftabi, 2004).

In a field campaign some 20 samples were collected from different locations in the salt glacier. The salt layers contain large (up to 4 cm) porphyroclasts, surrounded by smaller grains. For this study, a fine-grained sample was selected which was suitable for orientation measurements. This sample was collected at the distal end of the western glacier (coordinates: UTM-39 N, E 470175, N 3846875; WGS-84). At this location recumbent folds are present, with salt which shows slight shape preferred orientation and foliation (Fig. 2, for more images see Appendix).

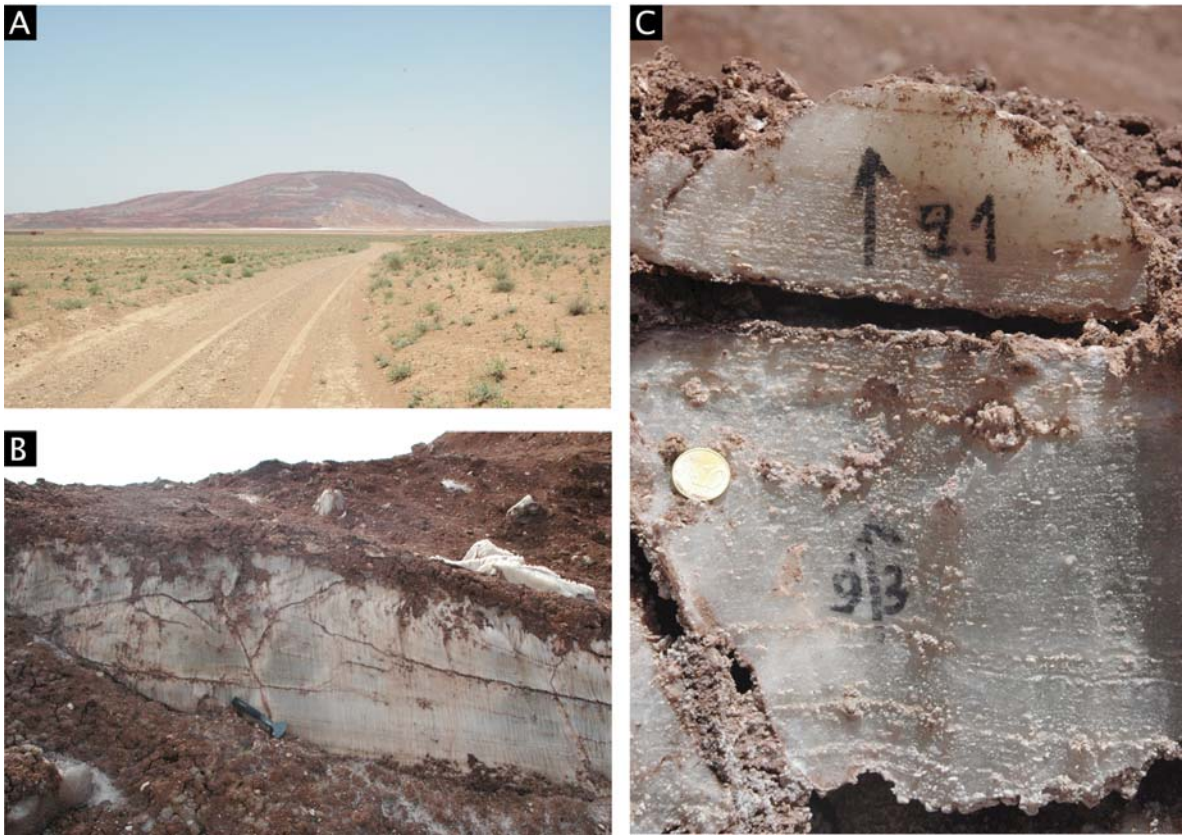

Fig. 2. A: Qum Kuh looking from SE. In the foreland of the salt hill the salt withdrawal basin is seen. B. folded salt layer in the western salt glacier (image orientation is E-W). Hammer for scale. C: studied samples. The salt shows slight shape preferred orientation. A weak foliation is present and is characterized by the favoured alignment of numerous secondary phases (mainly anhydrite). Coin (d = 2cm) for scale.

3 Sample preparation and methods

From the sample a slab was cut parallel to the lineation and perpendicular to the foliation. After that the sample was gamma-irradiated in the Research Reactor of Jülich at 100 °C with dose rate of 3-4 kGy/h to a total dose of 5.7 MGy. Etched thin sections were prepared following the technique described by Schléder and Urai, 2005. The microstructure was inspected in transmitted and reflected light. The electron backscatter diffraction (EBSD) measurements were carried out at the University of Bochum with a LEO1530 Gemini FESEM equipped with a Nordlys EBSD detector, with acceleration voltage of 20 kV and beam current of 8 nA using step size of 20 μm. The EBSD patterns were indexed with the HKL Channel 5 software. The quality of the EBSD data is very good with more than 90 % indexed pixels. The

maps were further processed in order to remove erroneous data and to provide more complete reconstruction of the microstructure (Prior et al., 2002; Bestmann and Prior, 2003).

4 Results and interpretation

The sample consists mainly of halite with subordinate anhydrite. The grain size distribution is bimodal, with numerous, approximately 2 mm-size porphyroclasts, surrounded by small, < 1 mm subhedral grains (Fig. 3). The porphyroclasts have an aspect ratio of 1.5-2 and invariably contain 50-100 μm equidimensional subgrains, with sometimes a subgrain-rich core and a subgrain-free mantle visible (Fig. 3C and F). The thickness of the subgrain-rich rim varies from 500 to 20 μm. In the latter case only a few well-developed subgrains are present in the vicinity of the grain boundary (Fig. 3F). The intensity of etching of the porphyroclasts is inhomogeneous (Figs. 4-6). The average size of the subgrains is around 70 μm. Applying subgrain size piezometry using the equation of:

$$D\ (\mu m) = 215\ \sigma^{-1.15}\ (MPa) \qquad (1)$$

(Schléder and Urai, 2005), the calculated differential stress is 2.6 MPa. This high stress very likely reflects the deformation conditions in the cold diapir stem during the final stages of extrusion. The small grains are strain-free and commonly show banding parallel to the grain boundary in the gamma-irradiated section (Figs. 3G and H). The banding is interpreted as growth bands (Murata and Smith, 1946) and may reflect changes in grain-boundary fluid chemistry during grain boundary migration. The grain boundary between the porphyroclasts-new grains invariably contains arrays of fluid inclusions (Fig. 3A), while the grain boundaries between the small grains are apparently fluid-inclusion-free (Fig. 3B). Based on the mutual relation between the porphyroclasts and the new grains (e.g. Fig. 3H) it is assumed that that the new grains grow at the expense of the old grains by strain induced grain boundary migration (Humphreys and Hatherly, 1996).

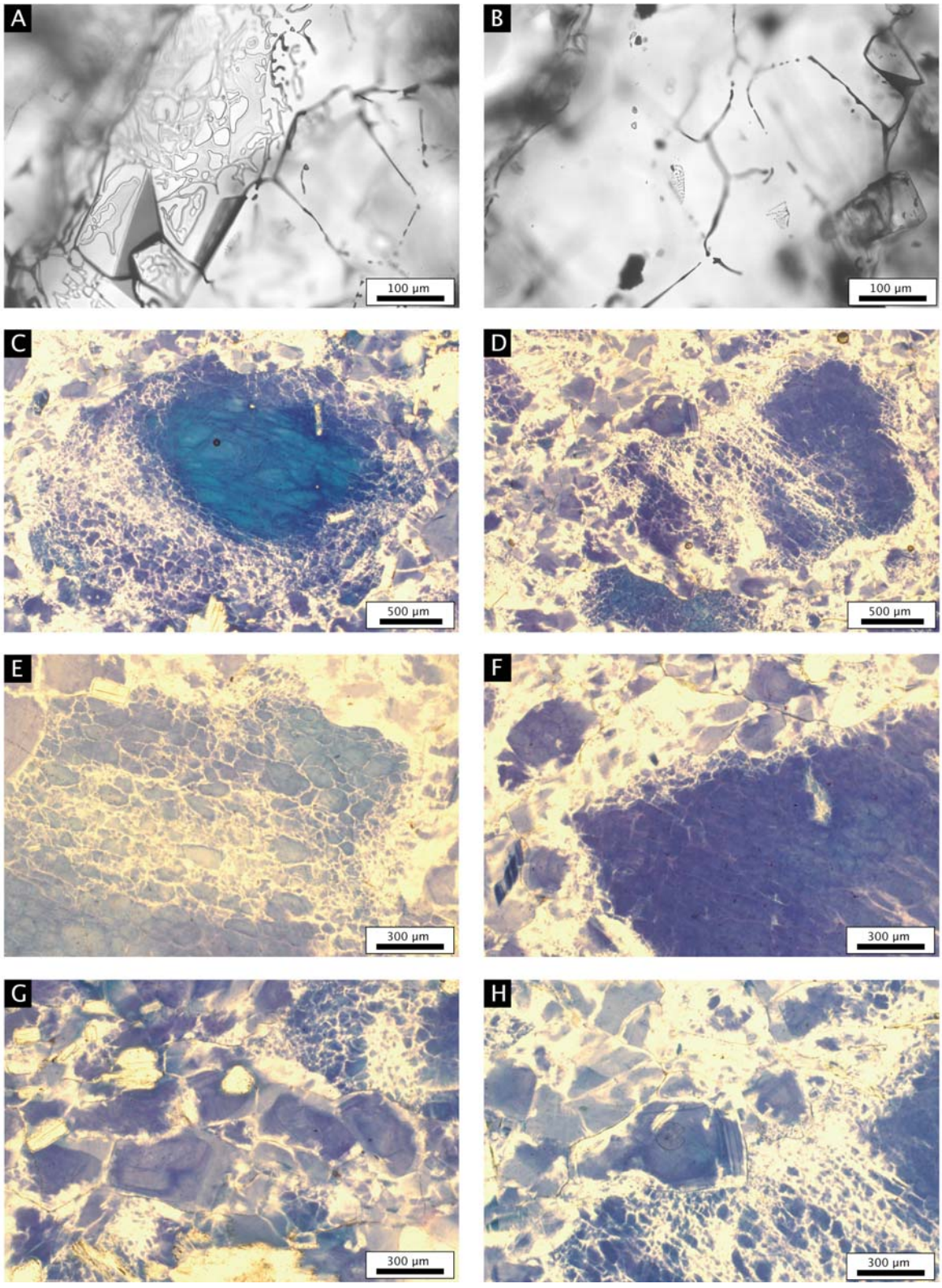

Fig. 3. Transmitted light micrographs of the studied sample. The shear direction is parallel to the long edge of the images (shear sense unknown). A: arrays of fluid inclusions at the grain boundary (upper left). This structure is characteristic for the grain boundaries between porphyroclast and strain-free grains. B fluid-inclusion tubes at the triple junctions. Such structure is typical for grain boundaries between strain-free grains. Micrographs C-H show gamma-irradiated samples. In the images the grain boundaries show up us thin dark lines (occasionally rimmed with a white halo), the subgrain boundaries as white lines. C: micrograph of a porhyroclast. The interior of the grain is substructure-poor, while the rim is rich in subgrains.

D: image shows a porhyroclast surrounded by several small grains. Note the inhomogeneous distribution of the subgrains in the porphyroclast. E: Subgrain structure in a porphyroclast. Note that some of the larger subgrains are surrounded by smaller subgrains. The micrograph is comparable to Fig. 4B. F: a porphyroclast with substructures. Note the relative abundance of subgrains at the immediate vicinity of the grain boundary. G & H: New, strain-free subhedral grains among the porphyroclasts. Most of the small grains show alterations of dark and pale blue coloured bands which are parallel to the grain boundaries. These bands are interpreted as growth banding.

The EBSD measurements show that inside the porphyroclasts the misorientations from 2 to 5° dominate with a few boundaries between 5-10° and very rarely with 10-15° misorientations (Figs. 4-6). We took 15° misorientation as lower limit for high-angle grain boundary (Bestmann et al., 2005). Comparing the etched thin section images and the EBSD patterns (e.g. Figs. 4B and C), it is apparent that some of the subgrain boundaries do not occur on the EBSD map, indicating that these boundaries have a lower misorientation than 2°.

In some cases the neighbor porphyroclasts have nearly the same crystallographic orientation (Figs. 5 and 6). It might be that these grains are two broken parts of an old pre-existing grain, or alternatively, it shows that the salt developed a strong crystallographic preferred orientation during dislocation processes. More measurements are needed to clarify whether grain cracking is a common process in salt in nature. In some cases, where the microscopic analysis indicates core-mantle structure, there is a progressive subgrain misorientation from the core of a grain towards the grain boundary, suggesting that some of the new grains have perhaps formed with subgrain rotation (Passchier and Trouw, 2005; Halfpenny et al., 2004). In the majority of the cases the misorientation between the porphyroclasts and the strain-free new grains is higher 30°, suggesting the subgrain rotation cannot be accounted for their formation. Perhaps another mechanism (nucleation) has controlled their formation, or was active after a new grain has formed by subgrain rotation (Prior et al., 2004; Halfpenny et al., 2004). Prior et al., 2004 suggested that after the new grains form they perhaps deform with solution-precipitation and grain boundary sliding processes which increases the misorientation of the old and the new grains. It has to be noted that no microstructures, which would support this assumption, have been observed (e.g fibrous-like microstructures in the small grains in gamma-irradiated thin sections).

Interestingly, where there is a difference in the intensity of etching inside a grain, the misorientation of that part is clearly indicated by the orientation measurements. Trimby et al., 2000 showed that the intensity of etching of substructures is orientation dependant and that the facets close to {111} are more deeply etched, while {100} are poorly etched. Since the difference in orientation difference between the subgrains is small (< 10°), it is unlikely that this effect is responsible for the abrupt change in etching intensity. More work is needed to resolve this problem.

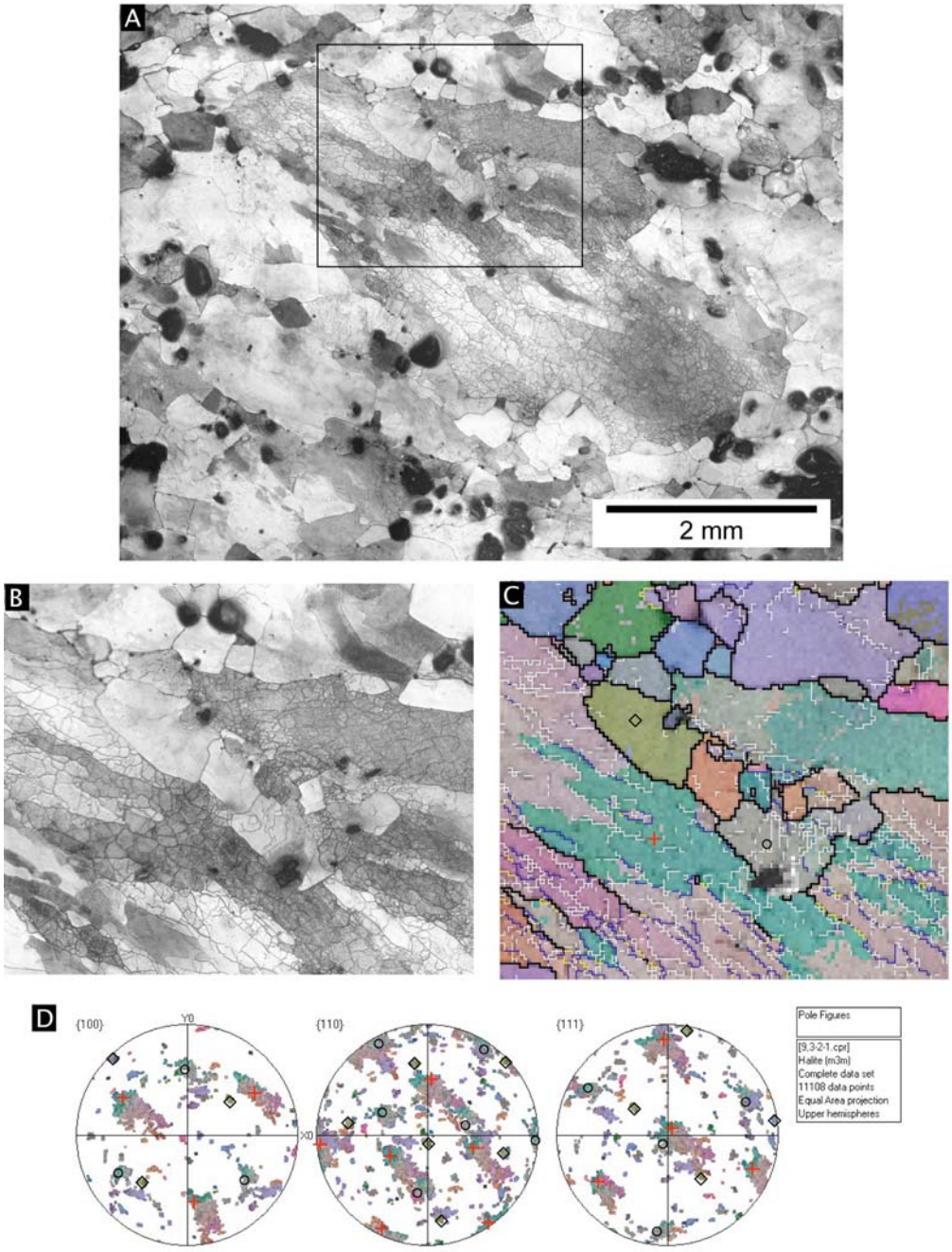

Fig. 4. A: reflected light micrograph of a subgrain rich grain surrounded by small, strain-free subhedral grains. The shear direction is parallel to the long edge of the image (shear sense unknown). Note that the new grains apparently also grow inside the substructured grain. Note also the NW-SE trending irregular bands indicated by the different intensity of etching. B: detail of image A showing subhedral grains inside the deformed grain. Note again how different parts of the deformed grain are differing in etching intensity. C: same area as B, mapped with a grid of 113 x 100. The map is colour-coded according to all Euler orientation. White boundary: 2-5° misorientation, blue: 5-10° misorientation, yellow: 10-15° misorientation and black: >15° misorientation. D: Equal area, upper hemisphere projection of all the data points. The orientation of the old grain is denoted with a red cross (see image C). As comparison, orientation of two neighbor grains is shown (see circle and diamond in image C). The grain denoted with circle has a rotational relationship around Z axis respect to the deformed grain.

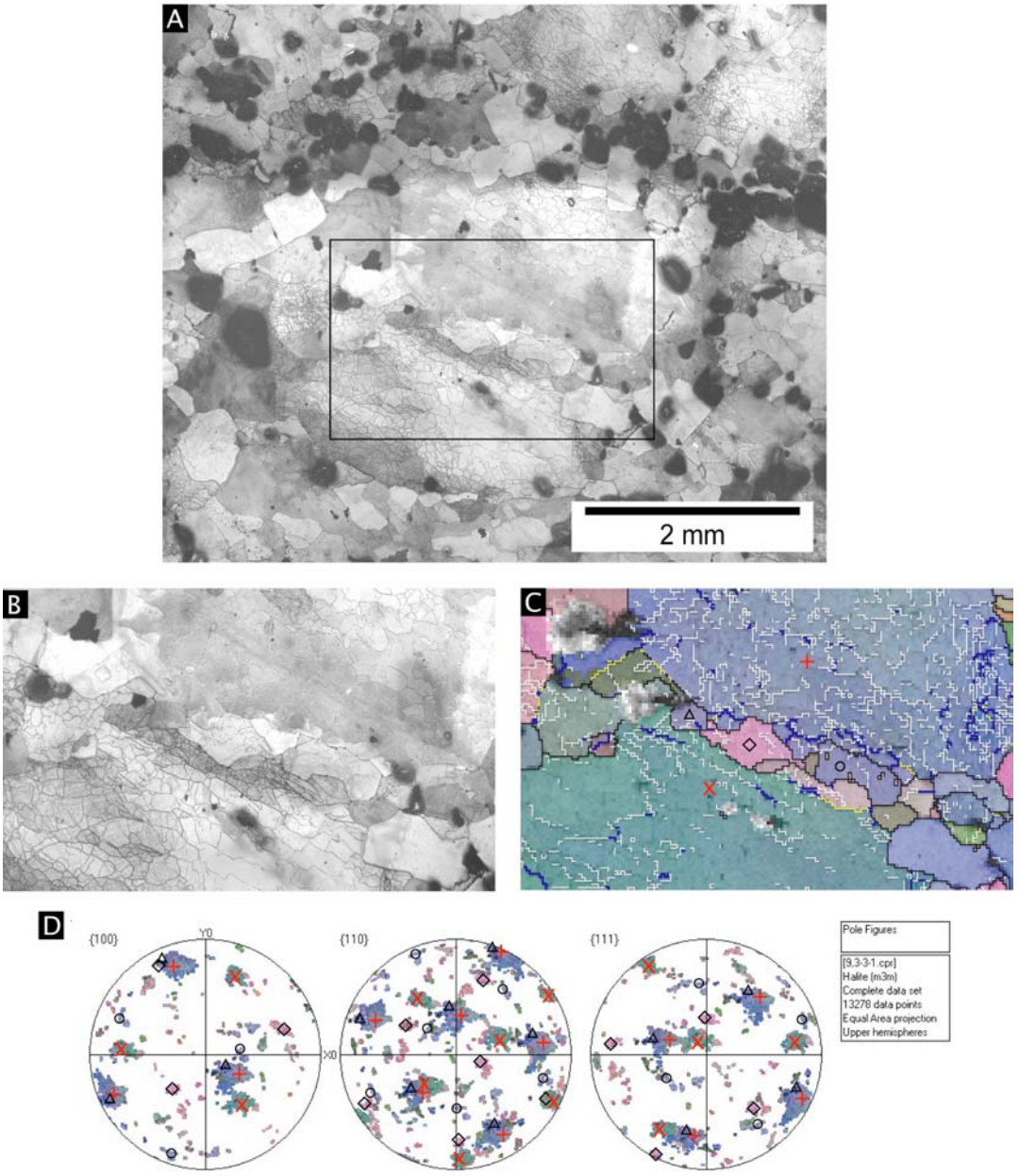

Fig. 5. A: micrograph, taken in reflected light, of two subgrain rich grains surrounded by small, strain-free subhedral grains. The shear direction is parallel to the long edge of the image (shear sense unknown). New grains are also present at the contact of the two deformed grains. B: detail of image A showing subhedral grains between the deformed grains. C: same area as B, mapped with a grid of 150 x 92. The map is colour-coded according to all Euler orientation. White boundary: 2-5º misorientation, blue: 5-10º misorientation, yellow: 10-15º misorientation and black: >15º misorientation. Note that sone of the subgrains at the immediate vicinity of the grain boundary have higher misorientation than the others. D: Equal area, upper hemisphere projection of all the data points. The orientation of the old grains are denoted with a red + and a red x (see image C). As comparison, orientation of three strain-free grains is also shown (see circle, diamond and triangle in image C). The orientation of the two deformed grains is close to each other, suggesting, perhaps, that they are broken parts of a pre-existing larger grain.

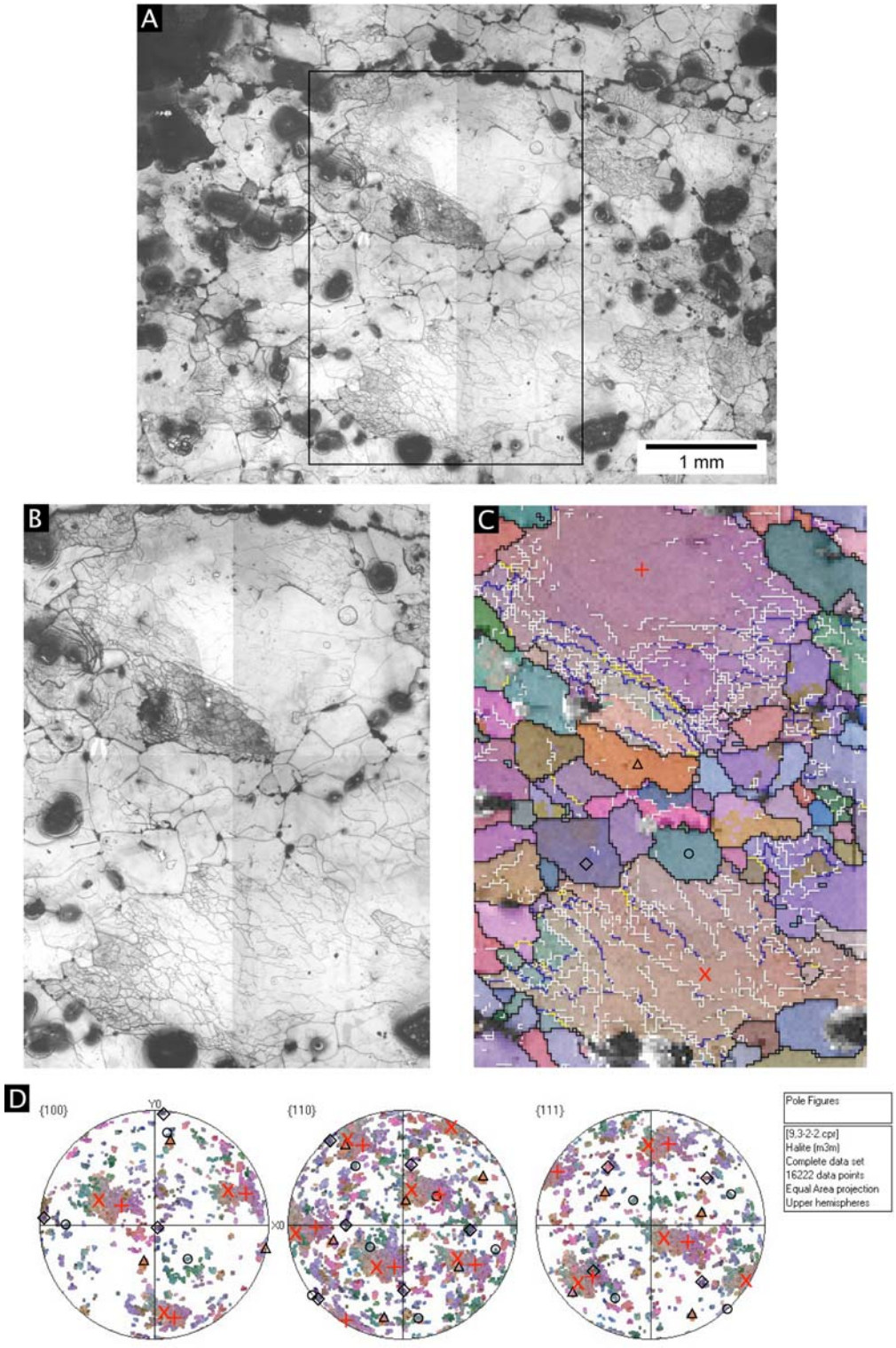

Fig. 6. A: Reflected light micrograph of two subgrain rich grains surrounded by small, strain-free subhedral grains. The shear direction is parallel to the long edge of the image (shear sense unknown). New grains are also present at the contact of the two deformed grains. B: detail of image A showing subhedral grains between the deformed grains. C: same area as B, mapped with a grid of 109 x 155. The map is colour-coded according to all Euler orientation. White boundary: 2-5° misorientation, blue: 5-10° misorientation, yellow: 10-15° misorientation and black: >15° misorientation. Note that the upper grain has a subgrain-poor core and a subgrain-rich rim, with some of the subgrains at the immediate vicinity of the grain boundary have higher misorientation than the others. D: Equal area, upper hemisphere projection of all the data points. The

orientation of the old grains are denoted with a red + and a red x (see image C). As comparison, orientation of three strain-free grains is also shown (see circle, diamond and triangle in image C). The orientation of the two deformed grains is close to each other, suggesting, perhaps, that they are broken parts of a preexisting larger grain.

5 Conclusion

In this contribution first result of crystallographic orientation measurements (using EBSD) of samples from Qum Kuh salt glacier are presented. In the sample, deformed porphyroclasts are present which are surrounded with small, strain-free grains. The measurements suggest that some of the new grains have formed by subgrain rotation. This is supported also by the subgrain-rich core and poor mantle structure. This suggests that – though this process is relatively unimportant in deep diapir salt – the subgrain rotation could also be of some importance in surface reaching salt structures. Most of the new, strain-free grains have a >30° misorientation respect to the porphyroclasts, indicating they could not have formed with subgrain rotation alone. It may be that other process was controlled the recrystallization (nucleation?) or that was active after subgrain rotation.

Acknowledgement

Thanks to Rolf Neuser (University of Bochum) for carrying out the EBSD measurements, to Jan Ter Heege (University of Bochum) for discussions on halite microstructures. C. J. Talbot and Abbas Bahroudi are acknowledged for the introduction into the geology of Qum Kuh. People at the Geodynamic Department of Geological Survey of Iran (GSI) in Tehran are thanked for the hospitality during the 2005 field season. This work was performed as part of SPP 1135 project (UR 64/5-1-2), financed by the Deutsche Forschungsgemeinschaft.

References

Bestmann, M., Piazolo, S., Spiers, C. J., Prior, D. J., 2005. Microstructural evolution during initial stages of static recovery and recrystallization: new insights from in-situ heating experiments combined with electron backscatter diffraction analysis. Journal of Structural Geology 27(3), 447-457.

Bestmann, M., Prior, D. J., 2003. Intragranular dynamic recrystallization in naturally deformed calcite marble: diffusion accommodated grain boundary sliding as a result of subgrain rotation recrystallization. Journal of Structural Geology 25, 1597-1613.

Gansser, A., 1960. Die Geologische erforschung der Qum gegend, Iran. Bulletin der Vereinigung Schweitzerisches Petroleum Geologen und Ingenieur 23, 1-16.

Halfpenny, A., Prior, D. J., Wheeler, J., 2004. Using electron backscattered diffraction (EBSD) to measure misorientation between 'parent' and 'daughter' grains. Implications for recrystallisation and nucleation. Materials Science Forum 467-470, 573-578.

Humphreys, F. J., Hatherly, M. 1996. Recrystallization and related annealing phenomena. Pergamon, p 497

Jackson, M. P. A., Cornelius, R. R., Craig, C. H., Gansser, A., Stocklin, J., Talbot, C. J. 1990. Salt diapirs of the Great Kavir, central Iran. Geological Society of America, Boulder, 177, 139

Murata, K. J., Smith, R. L., 1946. Manganese and lead coactivators of red fluorescence in halite. American Mineralogist 31, 527-538.

Passchier, C. W., Trouw, R. A. J. 2005. Microtectonics. Springer, 366

Prior, D. J., Bestmann, M., Halfpenny, A., Mariani, E., Piazolo, S., Tullis, J., Wheeler, J., 2004. Recrystallization and grain growth in rocks and minerals. Materials Science Forum 467-470, 545-550.

Prior, D. J., Wheeler, J., Peruzzo, L., Spiess, R., Storey, C., 2002. Some garnet microstructures: an illustration of the potential of orintation maps and misorientation analysis in microstructural studies. 2002 24, 999-1011.

Schléder, Z., Urai, J. L., 2005. Microstructural evolution of deformation-modified primary halite from the Middle Triassic Röt Formation at Hengelo, The Netherlands. International Journal of Earth Sciences 94, 941-955.

Talbot, C. J., Aftabi, P., 2004. Geology and models of salt exreusion at Qum Kuh, central Iran. Journal of the Geological Society 161, 321-334.

Trimby, P. W., Drury, M. R., Spiers, C. J., 2000. Misorientations across etched boundaries in deformed rocksalt: a study using electron backscatter diffraction. Journal of Structural Geology 22, 81-89.

Urai, J. L., Means, W. D., Lister, G. S. 1986. Dynamic recrystallization of minerals. In: Hobbs, B. E. & Heard, H. C. (Eds.), Mineral and rock deformation: laboratory studies. AGU Geophysical Monograph 36. American Geophysical Union, 161-199.

Urai, J. L., Spiers, C. J., Peach, C., Franssen, R. C. M. W., Liezenberg, J. L., 1987. Deformation mechanisms operating in naturally deformed halite rocks as deduced from microstructural investigations. Geologie en Mijnbouw 66, 165-176.

Appendix

Fig. 1. Large porphyroclasts in the western salt glacier close to the distal end. Hammer for scale.

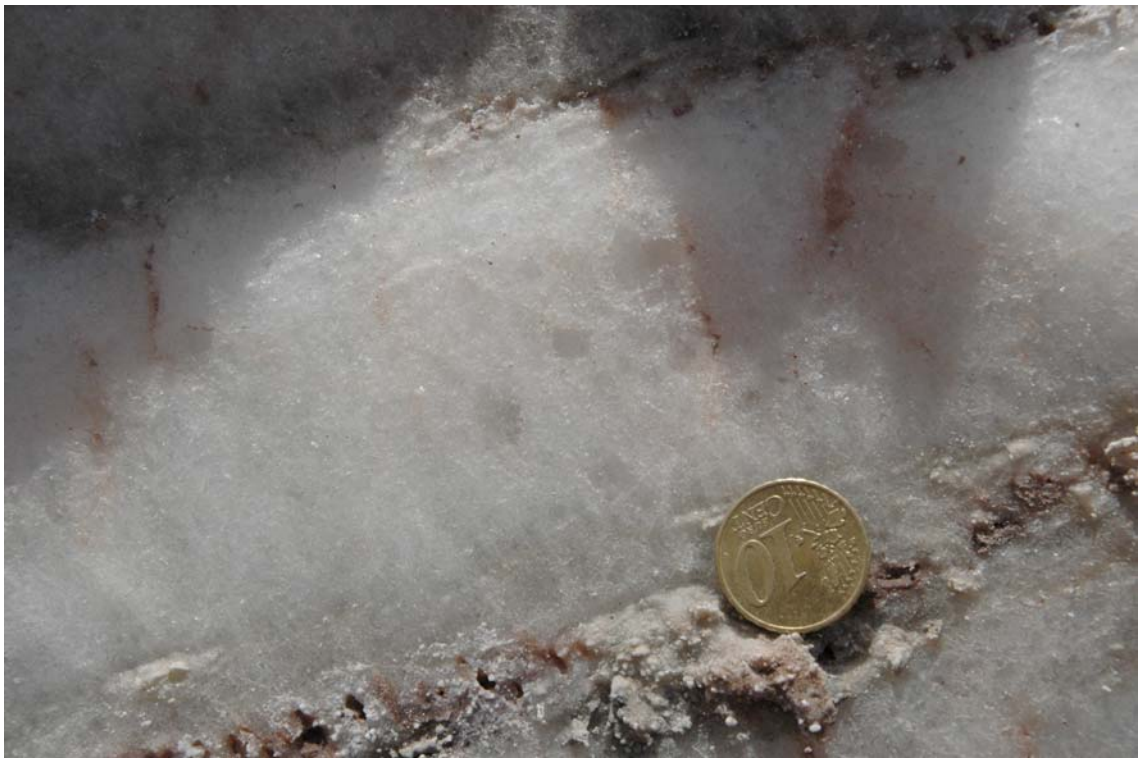

Fig. 2. Euhedral grains in fine-grained matrix. These grains are perhaps due to static recrystallization after the salt layer contacted with rainwater. Coin for scale.

Fig. 3. Coarse-grained salt at the bottom of the image and thin layer of fine-grained salt at the top. The fine-grained layer is interpreted as a shear zone. Coin for scale.

Fig. 4. Eastern part of the salt hill looking from the summit. Note the widespread presence of karstic features and the abundance of clay. Secondary-salt filled withdrawal basin at the distance.

Chapter 7: Evolution of rocksalt microstructure and rheology in different tectonic settings

Zsolt Schléder and János L. Urai

Abstract

In this paper we summarize microstructural studies carried out on naturally deformed salt samples from a wide range of settings starting from the primary undeformed to the highly deformed extrusive salt and attempt to define a consistent set of rheologies.
Large variation in rheology is common in layered salt from the onset of tectonic deformation. In halite dominated sequence, the rheology is controlled by grain size which in turn is a function of the deposition environment. Depending on the primary grain size the solution-precipitation mechanisms contribute to the total strain. Early deformation of salt is accompanied by expulsion of water from a variety of sources and water-assisted deformation and recrystallization mechanisms are fully active.
In salt diapirs small and large scale folding is common, caused by the large contrasts in mechanical properties of the salt layers deforming by dislocation creep and solution-precipitation creep. In the diapir stem when the salt is being extruded to the surface, differential stresses are the highest. Grain size reduction as a function of increasing strain is common though the exact process is unknown. In surface-reaching salt structures bedding-parallel mylonitic shear zones develop in the very fine grained salt with deformation mechanisms of solution-precipitation creep and grain boundary sliding. This salt is very weak and flows downhill under very low shear stresses.

1 Introduction

The picture that emerges from the previous chapters is a complex, diverse microstructural evolution and rheology in halite as a function of depositional architecture and tectonic history. In the last decades, extensive experimental work on the deformation of rock salt at a range of temperature, grain size, water content, strain rate and porosity has provided a solid framework to extrapolate these results to natural conditions. In the same period, there has been rapid growth in the understanding of salt tectonics, based on the large amount of 3D seismic data, on numerical modeling and on (partly) scaled analogue modeling. In these models, salt is invariably treated as a rather homogeneous continuum, with properties either assumed to be newtonian viscous or described by a power-law creep equation. What has been largely lacking is a comparison of the experimental results with naturally deformed salt, to test the assumptions on material models made in modelling salt tectonics.
By studying naturally deformed halite from a wide range of settings, this paper aims to provide a detailed basis for quantifying deformation mechanisms and rheology in halite in the salt tectonic cycle.

1.1 Rheology and deformation mechanisms in halite

In laboratory tests at temperatures relevant for salt tectonics the usual deformation mechanisms are a combination of dislocation creep and water-assisted dynamic recrystallization and solution-precipitation creep and grain boundary sliding (Ter Heege et al., 2005). Rheology is described by a temperature-activated power law creep equation (Carter et al., 1993). In this field, experimental data shows a large (factor of up to 1000) variation in creep strength for different types of natural salt rocks (e.g. Hunsche et al., 2003). Differences in chemistry, water content, second phases, deformation history may all play a role in these variations. For example, it has been experimentally demonstrated that samples containing impurities in solid solution have a substantially different rheology than pure halite (Heard and Ryerson, 1986).
In sufficiently fine grained wet halite, solution-precipitation creep can become the dominant deformation mechanism (Rutter, 1976; Gratier and Guiguet, 1986; Spiers et al., 1990; Hickman and Evans, 1991; Wheeler, 1992; Schutjens and Spiers, 1999; Renard et al., 2001; Dysthe et al., 2002; Gratier et al., 2003; Ford and Wheeler, 2004; Schenk and Urai, 2004).
A combination of flow laws for the different mechanisms leads to a multi-mechanism deformation map for rocksalt (Spiers and Carter, 1998) and suggests that under natural conditions flow will occur either by climb-controlled creep or solution-precipitation creep or by both, depending on the grain size of the salt.

1.2 Numerical and analogue models of salt tectonics

The numerical modelling techniques allow incorporation of realistic rheologies, complex geometries and boundary conditions and are especially useful for sensitivity testing. In addition to simplified analytical models which however serve well to elucidate some critical problems (Lehner, 2000; Fletcher et al., 1995; Triantafyllidis and Leroy, 1997), most work in modelling salt tectonics is based on numerical techniques (Last, 1988; van Keken et al., 1993; Podladchikov et al., 1993; Daudré and Cloetingh, 1994; Ismail-Zadeh et al., 2001; Kraus and Podladchikov, 2001; Schultz-Ela and Walsh, 2002; Gemmer et al., 2004).
Almost all work to date has been in 2D, concentrating on forward modelling of systems at different scales, and incorporating different levels of complexity. For example, some models try to incorporate realistic two-component rheology of the salt, while others use simple, temperature independent rheology. Overburden rheology is in some cases modelled as frictional-plastic with attempts to consider localized deformation, while other models assume linear viscous overburden. Although most models produce results which are in some aspects comparable with the natural prototypes, it is at present not completely clear how the combination of simplifications affect the results' relevance to natural prototypes.

Sandbox models have been extensively used in the past three decades for investigation of a large number of tectonic settings at different scales (ie, Koyi and Mancktelow, 2001). For salt tectonics applications, high viscosity silicone paste has found wide applications because it does not mix with sand and the scaling ratio in time allows for practical experiments within a day (Costa and Vendeville, 2002; Weijermars, 1986). The combination various boundary conditions, frictional plastic sand with user-defined sedimentation(rate) and Newtonian viscous putty produced a library of natural-looking (to a first order) model results. On the other hand, it is known that the model materials used for salt in the sandbox are not properly scaled and many relevant material parameters are only beginning to be understood (Adam et al., 2005).

To date none of the modelling studies to date has included a salt body with internal rheology contrasts of a factor of 1000 in models of salt diapirs, nor has the dramatic softening in extruded salt been included in geomechanical models.

2 Rocksalt microstructures from different tectonic settings

The microstructure of natural rocksalt is a function of depositional, diagenetic and deformation processes. Variations in the importance of these results a wide range of microstructures, ranging from the typical primary structures to the strongly deformed and completely recrystallized mylonites.

The first set of microstructures are a function of the depositional environment, synsedimentary processes and diagenetic processes at shallow depth, therefore it is of great importance that we understand the processes and the resulting microstructures before attempting to interpret microstructures of deformed and recrystallized salts.

Although there is a controversy in the literature, it is generally agreed that in the undisturbed ancient rocksalt deposits the primary microstructures that reflect the depositional conditions are preserved (Warren, 2006) (stage 1 in Fig. 1). Modern ephemeral and desiccated salinas produce salt-pan sequence and is a good analogue for microstructural evolution of many ancient, shallow-water deposit. Contrary to this, the lack of good analogue for deep-water evaporites makes the recognition and interpretation of ancient deep-water evaporite depositions difficult (Kendall and Harwood, 1996).

A characteristic microstructure for ephemeral salt-pan environment is composite halite grains locally rich in fluid inclusions but also containing irregular patches of clear halite free of fluid inclusions (Shearman, 1970; Lowenstein and Hardie, 1985). Not uncommonly, the transition from fluid-inclusion-rich material to clear halite is defined by a sharp curved surface within single halite grains.

A great number of studies were made on recent, shallow-water deposits and on slightly deformed ancient deposits and showed that many of the ancient salt structures were deposited in a perennial saline-lake or ephemeral salt-pan environment and show characteristic microstructure of fluid-inclusion-outlined, box- and plate-shaped or elongated chevron grains (Figs. 2a, b and d, Dellwig, 1955; Gottesmann, 1963; Wardlaw and Schwerdtner, 1966; Lowenstein and Hardie, 1985; Brodylo and Spencer, 1987; Hovorka, 1987; Lowenstein, 1987; Casas and Lowenstein, 1989; Handford, 1990; Schreiber and El Tabakh, 2000; Benison and Goldstein, 2001).

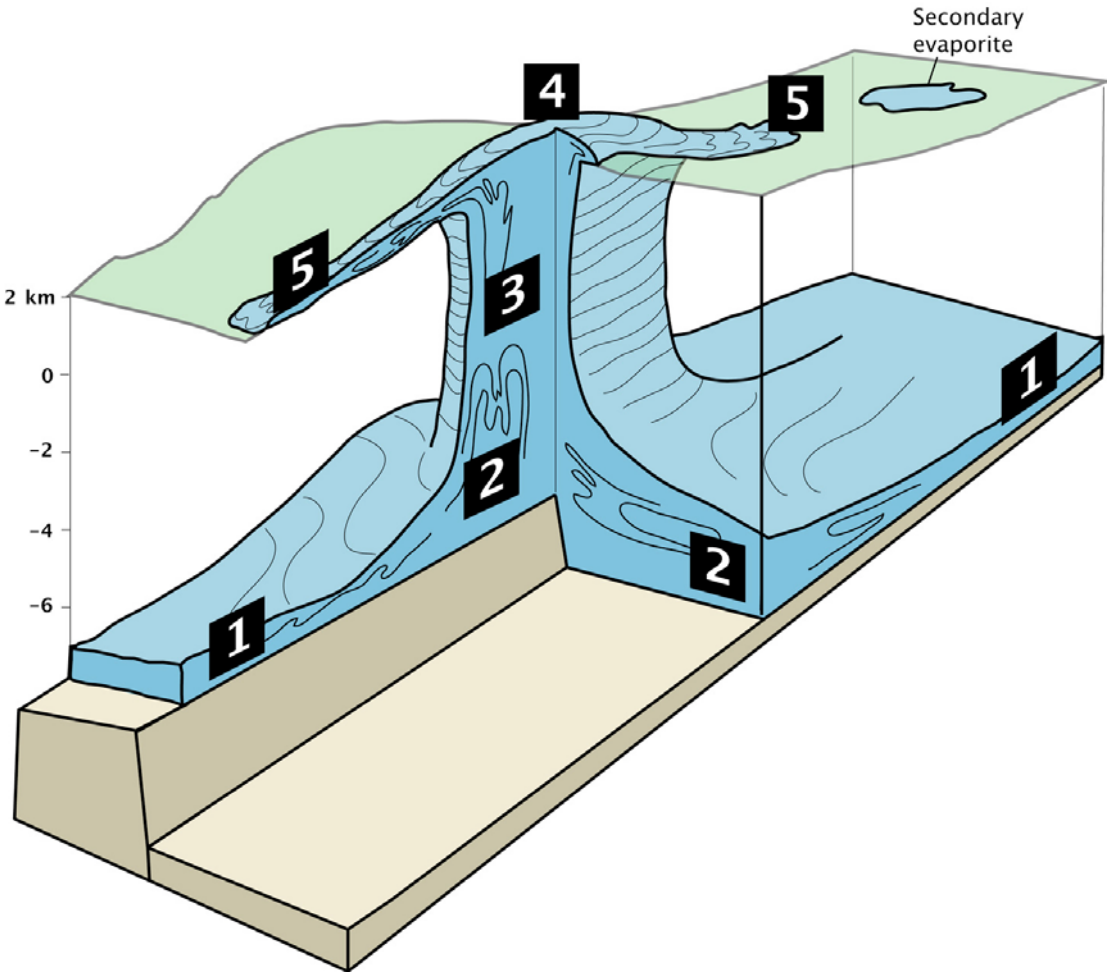

Fig. 1 Cartoon illustrates the structure of a diapir and a salt extrusion (after Talbot & Jarvis, 1984). The numbers denote the stages of evolution of microstructures as the salt rises from its source layer (1, 2), passes through the diapir stem (3, 4) and flows on the surface (5).

Samples analysed from slightly deformed horizontal bedded Röt salt (Triassic) from Hengelo, The Netherlands shows typical microstructures similar to that described by Lowenstein and Hardie (1985) and Shearman (1970). The samples show strong shape preferred orientation as most of the grains are elongated normal to bedding and truncated by subhorizontal irregular dissolution surfaces (Schléder and Urai, 2005). Depending on the water depth and wave energy, there are several models in the literature which predict halite crystal morphology in layered shallow-water evaporite (Arthurton, 1973). According to these, we interpret the elongated grains as have grown in mutual growth competition with coigns uppermost. Though we did not perform orientation measurements on the samples, we envisage that the sample has a moderate to strong CPO as a consequence of the growth competition theory. Broadly speaking, due to the depositional and crystal growth processes in the salt-pan, any shallow-water salt would possess a moderate to strong crystallographic and shape preferred orientation. The presence of subgrains in virtually all of the grains in the Hengelo samples suggest that the samples deformed by crystal plastic processes. The contribution of the solution precipitation could be only assessed by calculating the strain rates for dislocation creep and for solution-precipitation creep as it is generally very hard to find unambiguous microstructural evidence for solution-precipitation creep. In some of the finer grained samples calculations suggests that solution-precipatation creep is the main deformation mechnism.

The fact that the grain size plays the main role in the rheolgy of the halite and that the grain size in the primary salt is a function of sedimentary environment (Kendall and Harwood, 1996) suggests that sedimentary processes will be the main controlling factor on rheology, at least in the early phases of halokinesis. Generally, in shallow water environment there is a cyclic variation in grain size, with thin layer (~5 mm) of fine-grained layer and thick layer (few cm to dm) of vertically elongated grains (Shearman, 1970; Lowenstein and Hardie, 1985) suggesting that there will be weaker and stronger layers in the same cycle.

Due to slight deformation in the Hengelo samples strain induced recrystallization occurred. It is evidenced by microstructures such as elongated subgrains at grain boundaries, which point to fluid-assisted grain boundary migration. The recrystallization process produces grains with microstructures of locally fluid-inclusion-rich parts with patches if clear halite free of inclusions. This patchy microstructure is very similar to that produced by early dissolution and reprecipitation processes in the salt-pan making the interpretation difficult. This problem of distinguishing between primary and secondary features in halite is important and requires careful microstructural analysis (Wardlaw and Schwerdtner, 1966; Hardie et al., 1983; Roedder, 1984).

Based on laboratory tests, a few processes have been proposed which lead to grain size reduction in rocksalt. One process is grain dissection, when moving grain boundaries intersect and eventually result in a smaller grain size (Ter Heege et al, 2005). Other possible process is nucleation, when a new grain nucleates at the grain boundaries and grows at the expense of the deformed grains subsequently.

In the Hengelo samples the grain boundary migration recrystallization is incipient suggesting that the grain size has not been reduced by grain dissection, however a few new, strain free grains have been observed at the grain boundaries. The origin of these grains is uncertain, they either be a result of nucleation or subgrain rotation, a process which has not been confirmed in laboratory experiments.

Owing to the numerous fluid inclusions the Hengelo salt has a high brine content of up to 5 % (Roedder, 1984). Such high water content is probably characteristic for any shallow-water salts. With the onset of grain boundary migration as the grain boundary sweeps through a fluid-inclusion-rich part of a grain, the primary inclusions are collected at the grain boundary (Fig. 2b, Schléder and Urai, 2005). It is not known how the excessive brine released by the moving boundary migrates in the otherwise zero prosity halite and what is the detailed structure of the fluid filled boundary (Schenk and Urai, 2005). The zonation seen in the recrystallized halite in gamma-irradiated samples perhaps reflects the effect of change in the migrating grain boundary fluid composition (Fig. 2h).

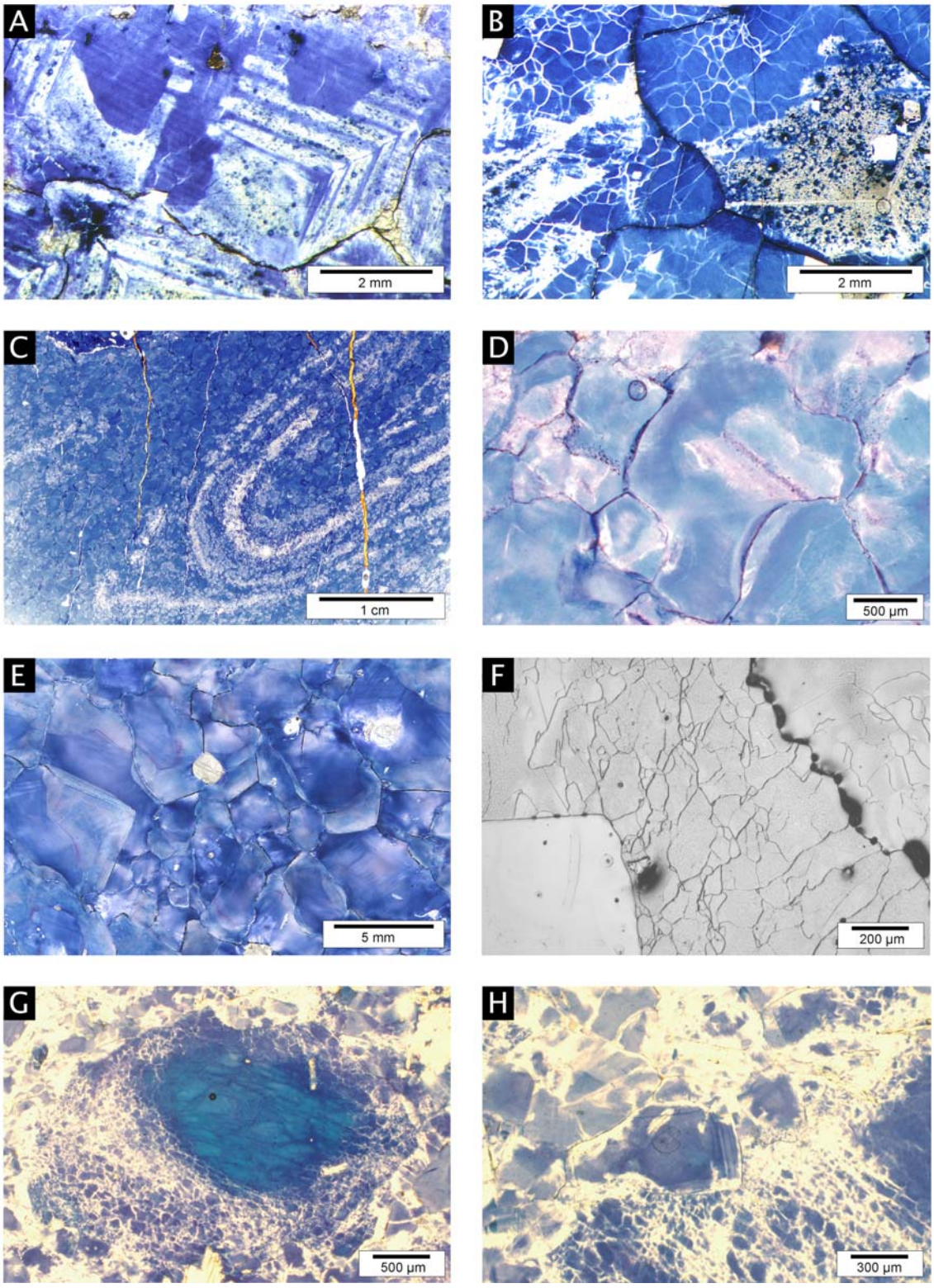
A
2 mm
B
2 mm
C
1 cm
D
500 µm
E
5 mm
F
200 µm
G
500 µm
H
300 µm

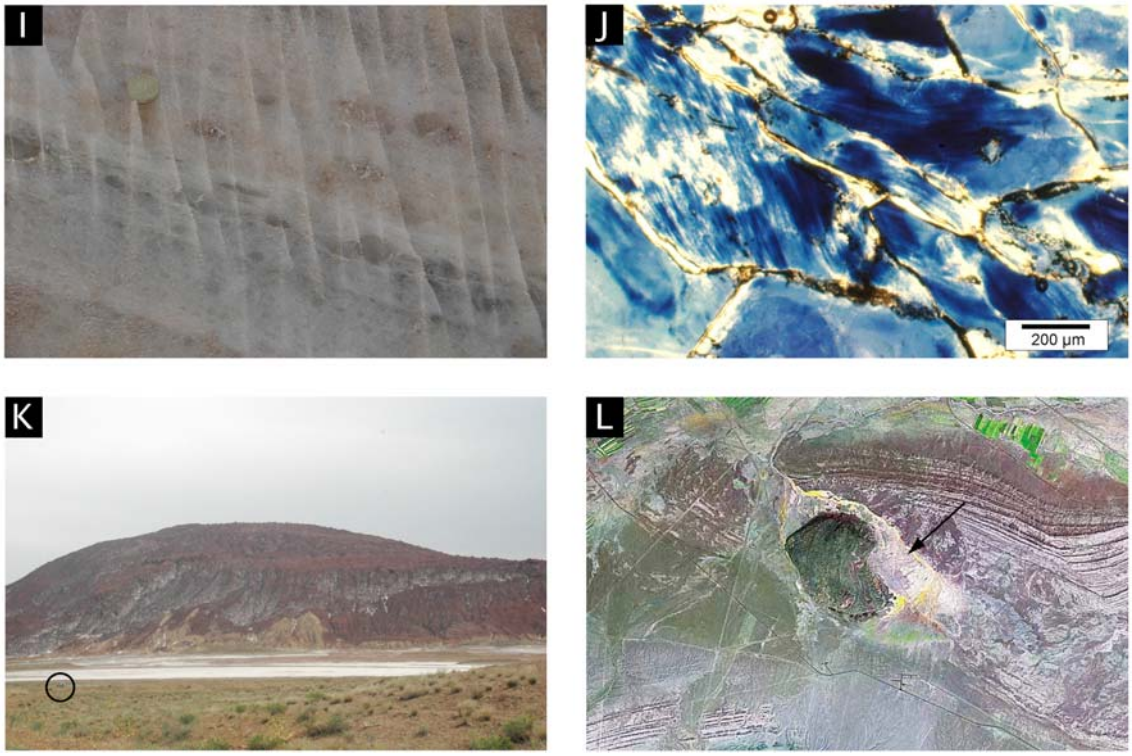

Fig. 2. Characteristic microstructures for the different stages of evolution of a salt structure. A: Primary fluid-inclusion-bands truncated by clear halite in slightly deformed Röt (Buntsandstein) salt layer from Hengelo, the Netherlands. This microstructure compares well with those produced by dissolution-reprecipitation processes in present-day salt pan halites (c.f. Shearman, 1970; Lowenstein and Hardie, 1985). Plane polarized, transmitted light image of gamma-irradiated sample. B: Elongated subgrains indicative of grain boundary migration. Grain boundary migration erases the old, milky, fluid-inclusion-rich part of the old, deformed grains and produces strain-free regions. Plane polarized transmitted light of gamma-irradiated section of Hengelo rocksalt. In both A and B images the grain boundaries occur as dark curves, while the white, milky patches are remnants of fluid inclusion-rich chevron grains. C: Scanned gamma-irradiated thin section of Zechstein (Z1) rocksalt from Neuhof, Germany. The thin anhydrite layers outline tight isoclinal folds. D: Detail of the image C. The grain boundaries occur as dark lines. The grain in the middle contains an elongated fluid-inclusion-rich plate. Such a plate is interpreted as nucleated at the brine-air interface, after which it sank to the bottom. The plate is surrounded with fluid-inclusion-free rim, which is interpreted as recrystallized part. E: Gamma-irradiated Zechstein (Z3) rocksalt from the Gorleben salt mine (Germany) shows commonly core-mantle structure with dark-blue coloured core and pale-blue rim. This microstructure is interpreted as reflect dynamic recrystallization. Note that the subgrains were not decorated by gamma-irradiation. F: Two grains (bottom left and top right) consume the subgrain-rich grain in the middle. The black spots at the grain boundaries are fluid inclusions opened up during sample preparation. Note that the grain at top-right itself also contains subgrains. Reflected light image of etched thin section of Zechstein (Z4) rocksalt from Klodawa salt mine, Poland. G: micrograph of a porhyroclast that is surrounded by many small, strain-free grains. The interior of the porphyroclast is substructure-poor, while the rim is rich in subgrains. The sizes of some of the new grains is comparable to that of subgrains. H: New, strain-free subhedral grains at the rim of a porphyroclasts. Most of the small grains show alterations of dark and pale blue coloured bands which are parallel to the grain boundaries. These bands are interpreted as growth banding. I: bedding parallel mylonitic zone in a salt wall of Oligocene-Miocene extrusive salt at Garmsar hills, Central Iran. The mylonitic zone is relatively thin (<3 cm) and are characterized by strong shape preferred orientation and small grain size. Note the flattened porphyroclast in the shear zone. Coin (d = 2cm) for scale. J: Fibrous microstructure in the pure halite part. The grain boundaries show up as black curves. The fibrous microstructures point to deformation mechanism of grain boundary sliding and solution-precipitation creep. K: Qum Kuh salt extrusion in Central Iran. The salt hill is made up of Oligocene-Miocene rocksalt. At the foreland of the salt hill is the salt withdrawal basin, filled with secondary salt. Jeep (encircled) for scale. Qum Kuh salt extrusion in landsat image (GeoCover circa 2000, https://zulu.ssc.nasa.gov/mrsid). The secondary salt filled depression is indicated with an arrow.

The strong influence of sedimentary environment on rheology is also apparent in salt samples from the Zechstein 1 (Neuhof-Ellers salt mine, Germany). This salt comprises of extremely fine-grained (<1 mm) fluid-inclusion-outlined plate and box shaped grains (Fig. 2d). The salt is interpreted to have formed in perennial salt lake environment. The halite layers are strongly deformed and are folded into steep-to-vertical isoclinal folds (Fig. 2c). Microstructural evidence for subgrains or for slip lines are absent suggesting that this salt deformed exclusively by solution-precipitation processes (Urai et al., 1987) what in turn implies that even at very low stresses this salt is extremely weak. Such weak layers are potentially common in layered salt from the onset of tectonic deformation (stage 2 in Fig. 1). A common microstructure in the Neuhof salt is the presence of patchy core-and-mantle structure with fluid inclusion-rich core and clear halite free of fluids. In this case these are best explained by deformation-induced grain boundary migration recrystallization process where the migrating grain boundaries erased primary fluid inclusion bands.
The salt core studied also contains a 1 cm thick coarse halite filled vein suggesting that brittle process can also occur in salt. Considerations on the dilation criteria and the possible maximum magnitude of the differential stresses in salt imply that fluids close to lithostatic pressure must have been involved in the brittle deformation of salt (Peach et al., 2001; Popp et al., 2001; Lux, 2005). The required fluid is thought to be associated with the metamorphism of potassic minerals in the vicinity of the rock salt studied.

As the salt rises, forms salt diapirs and salt walls and deforms further (stage 3 in Fig. 1) it is envisaged that in some highly deformed halite layers steady-state microstructure is produced after complete recrystallization of the salt (Hardie et al., 1983; Urai et al., 1987). It is less clear to what extent the halite is recrystallized and whether some of the primary grain size variations are maintained, however the abundance of primary structures in domal salts suggests that the recrystallization usually is far from complete at least in some parts of the salt body (ie, Gottesmann, 1963). It is assumed that at this stage is when the CPO inherited from the synsedimentary processes in shallow-water evaporites is gradually replaced by that produced by crystal plastic processes.
Microstructures studied in Zechstein samples from Germany and Poland (Asse, Gorleben and Klodawa salt diapirs Figs. 2e and f) imply that the main recrystallization mechanism is grain boundary migration (Urai et al., 1987) and show that in occasions primary fluid-inclusion-bands are still preserved. A very common deformation related microstructure is the presence of subgrains which indicates that crystal plastic mechanisms are active. Again, microstructural evidence for solution-precipitation creep was hard to find, however strain rate calculations suggest that it might become a dominant process in finer grained samples.
In salt diapirs and walls small and large scale folding is common, very likely caused by the differences in mechanical properties in the salt layers (Ramsay, 1967; Pfeifle et al., 1995). For example, systematic creep tests on Gorleben salt showed that there is a factor of 1000 variation in strength of the rock salt in one salt succession (Hunsche et al., 2003). This variation in rheology might be due to systematic variations in grain size, chemistry and in the amount of secondary phases.
The in-situ differential stresses for rocksalt can be calculated using subgrain size piezometry. The method is based on a laboratory-calibrated curve, which relates the subgrain size to the magnitude of differential stress. Using this method the calculated diferential stresses in domal salt is typically less than 2 MPa.

As the salt rises and passes through the diapir stem on the way to the surface (stage 4 in Fig. 1), the differential stresses are as high as 5 MPa. Samples from salt glaciers retain some microstructures characteristic for these conditions, which include subgrains, new very fine grains (~1 mm), and evidence for grain boundary migration (Figs. 2g and h). Grain size reduction as a function of increasing strain is widespread. The details of the microscale processes are not clear, but perhaps involve grain dissection during grain boundary migration, subgrain rotation and nucleation. Orientation measurements suggest that nucleation and probably subgrain rotation are common processes in grain size reduction. The commonly observed core-and-mantle structure with subgrain poor core and subgrain rich mantle is also consistent with this interpretation. In the literature, subgrain rotation recrystallization has not been confirmed in laboratory deformed samples.

At the surface, bedding-parallel mylonitic shear zones develop in the salt succession (Figs. 2i and j), where the deformation mechanism is solution-precipitation creep and grain boundary sliding (stage 5 in Fig. 1) as evidenced by fibrous microstructures and subgrain-free grains.

The controlling factor on the emplacement of the shear zones is not well known. It was suggested that if the grain size variation seen in the primary salt could be preserved until the salt reaches the surface then this cyclic variation in grain size could constrain the emplacement of the shear zones (Schléder and Urai, 2007). This speculation is supported by the fact that shear zones have been observed at the bedding boundaries. Once the shear zones develop, this salt is very weak (Fig. 3), and – if sufficiently wet – flows downhill at a rate of 10^{-10} 1/s (Jackson, 1985; Talbot and Rogers, 1980).

In the exposed salt glacier euhedral large grains can be observed, suggesting that static recrystallization due to the availability of (rain) fluid is a possible process. At the distal end of the salt glacier, the salt is dissolved by rainwater (Talbot, 1998). It is often observed in recent salt extrusions that this dissolved salt reprecipitates as secondary salt in the withdraval depression in the vicinity of the salt hill (Figs. 2.k and l, Jackson et al., 1990). This newly precipitated salt is the basis of the next stage of burial and deformation of this halite.

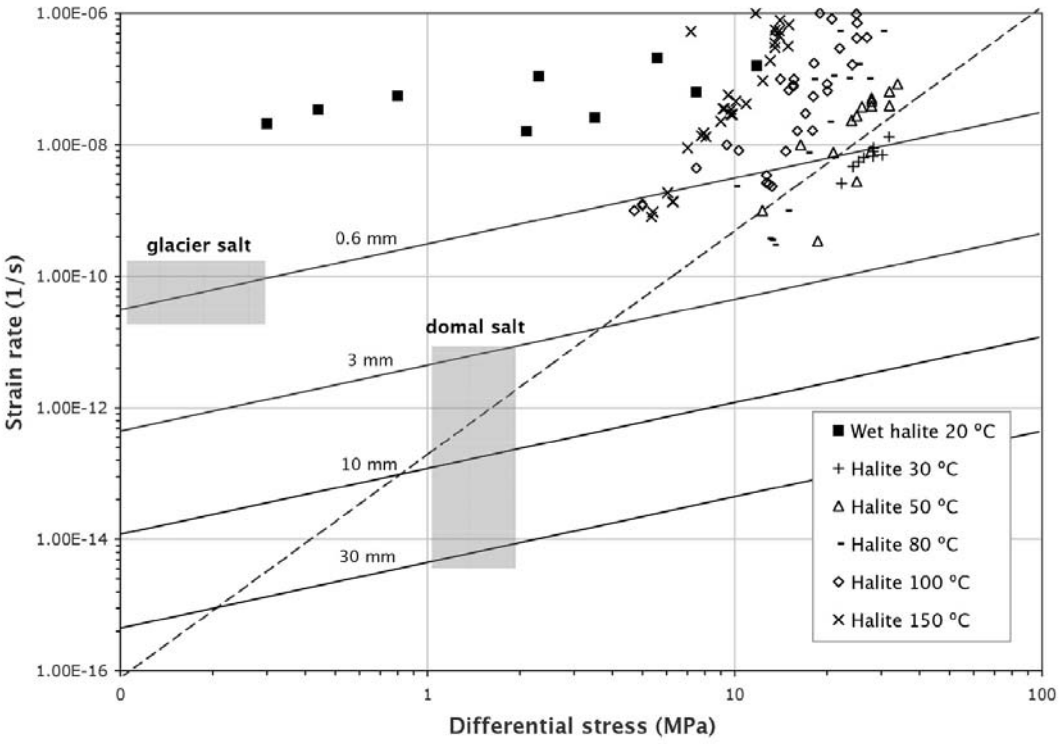

Fig. 3. Differential stress vs. strain rate diagram shows flow laws for dislocation creep (dashed line, after Carter et al., 1993a, T = 40 °C) and for solution-precipitation creep (for various grain sizes, after Spiers et al., 1990b, T = 40 °C). Depending on the grain size the main deformation mechanism may vary in the domal salt. The glacier salt and some of the primarily fine-grained salts deform exclusively by solution-precipitation creep. As comparison experimental data from numerous sources (Hansen and Mellegard, 1980; Hansen and Carter, 1984; Handin et al., 1986; Spiers et al., 1986; Senseny, 1988; Horseman and Handin, 1990; Horseman et al., 1992; Hunsche et al., 2003) are also shown.

3 Conclusion

Based on the studies carried out on naturally deformed samples it is evident that there is a surprising richness of microstructures and processes in natural salts. Further studies will certainly show more of the rich set of processes that occur in natural salt during deposition and deformation, but we believe that the main processes have been documented here. The studies from different tectonic settings outline the set of rheologies which should be used for refining models of salt tectonics (Fig. 3). If these rheologies are implemented, it is assumed that the models will produce more realistic-looking internal structures in the salt, and might also produce subtle but important differences in the external shape of evolving salt bodies. Based on studies presented in this work on natural salts from different settings, the main conclusions are:

- The rheology of undeformed halite is a function of grain size which in turn is dependent on synsedimentary and early diagenetic processes. This variation in grain size can be maintained during the salt tectonic cycle.
- Salts with salt-pan origin are expected to be with high brine content due to the numerous primary fluid inclusions. This fluid is swept out and collected at the grain boundaries by grain boundary migration and expelled from the halite succession.

- Dislocation processes and solution-precipitation creep accompanied with fluid-assisted grain boundary migration recrystallization is commonly observed in any salt tectonic setting. As the salt deforms and recrystallizes the primary grain size changes.
- Differential stresses are commonly below 2MPa but in the diapir stem it can be 5 MPa as calculated by subgrain size piezometry.
- In the salt glacier mylonitic shear zones develop. The deformation mechanism in the shear zones is grain boundary sliding accommodated by solution-precipitation creep. Static recrystallization in the salt glacier is possible.

References

Adam, J., Urai, J., Wieneke, B., Oncken, O., Pfeiffer, K., Kukowski, N., Lohrmann, J., Hoth, S., van der Zee, W., Schmatz, J., 2005. Shear localisation and strain distribution during tectonic faulting - new insights from granular flow experiments and high-resolution optical image correlation techniques. Journal of Structural Geology 27, 283-301.

Benison, K. C., Goldstein, R. H., 2001. Evaporites and siliciclastics of the Permian Nippewalla Group of Kansas, USA: a case for non-marine deposition in saline lakes and saline pans. Sedimentology 48, 165-188.

Brodylo, L. A., Spencer, R. J., 1987. Depositional environment of the Middle Devonian Telegraph Salts, Alberta, Canada. Bulletin of Canadian Petroleum Geology 35(2), 186-196.

Carter, N. L., Handin, J., Russell, J. E., Horseman, S. T., 1993a. Rheology of rocksalt. Journal of Structural Geology 15(9/10), 1257-1271.

Casas, E., Lowenstein, T. K., 1989. Diagenesis od saline pan halite: comparison of petrographic features of modern, Quaternary and Permian halites. Journal of Sedimentary Petrology 59(5), 724-739.

Daudré, B., Cloetingh, S., 1994. Numerical modelling of salt diapirism: influence of the tectonic regime. Tectonophysics 240(59-79).

Dellwig, L. F., 1955. Origin of the salina salt of Michigan. Journal of Sedimentary Research 25(2), 83-110.

den Brok, B., Morel, J., Zahid, M. 2002. In situ experimental study of roughness development at a stressed solid/fluid interface. In: de Meer, S., Drury, M. R., de Bresser, H. & Pennock, G. M. (Eds.), Geological Society Special Publications 200. Geological Society of London: London, United Kingdom, United Kingdom, 73-83.

Dysthe, D., Renard, F., Porcheron, F., B., R., 2002. Water in mineral interfaces - molecular simulations of structure and diffusion. Geophysical Research Letters 29, 13208-13211.

Fletcher, R. C., Hudec, M. R., Watson, I. A. 1995. Salt glacier and composite sediment-salt glacier models for the emplacement and early burial of allochtonous salt sheets. In: Jackson, M. P. A., Roberts, D. G. & Snelson, S. (Eds.), Salt tectonics: a global perspective. AAPG Memoir, 65, 77-108.

Ford, J. M., Ford, N. J., Wheeler, J., 2004. Simulation of grain boundary diffusion creep: analysis of some new numerical techniques. Proceedings of the Royal Society of London Series A 460, 2395-2413.

Ford, J. M., Wheeler, J., 2004. Modelling interface diffusion creep in two-phase materials. Acta Materialia 52, 2365-2376.

Gemmer, L., Ings, S. J., Medvedev, S., Beaumont, C., 2004. Salt tectonics driven by differential sediment loading: Stability analysis and finite element experiments. Basin Research 16, 199-218.

Gottesmann, W., 1963. Eine häufig auftertende Struktur des Halits im Kaliflöz, Stassfurt. Geologie 12(5), 576-581.

Gratier, J. P., Favreau, P., Renard, F., 2003. Modelling fluid transfer along Californian faults when integrating pressure solution crack-sealing and compaction processes. Journal of Geophysical Research 108(B2), 2104.

Gratier, J. P., Guiguet, R., 1986. Experimental pressure solution-deposition on quartz grains: the crucial effect of the nature of the fluid. Journal of Structural Geology 8(8), 845-855.

Handford, R. C., 1990. Halite depositional facies in a solar salt pond: A key to interpreting physical energy and water depth in ancient deposits? Geology 18, 691-694.

Handin, J., Russell, J. E., Carter, N. L. 1986. Experimental deformation of rocksalt. In: Hobbs, B. E. & Heard, H. C. (Eds.), Mineral and rock deformation: laboratory studies. AGU Geophysical Monograph 36. American Geophysical Union, 161-199.

Hansen, F. D., Carter, N. L. 1984. Creep of Avery Island rocksalt. Proceedings of the first Conference on mechanical Behavior of Salt, Clausthal-Zellerfeld, Germany, Trans. Tech. Publications, 53-69.

Hansen, F. D., Mellegard, K. D., 1980. Quasi-static strength and deformational characeristic of domal salt from Avery Island, Lousiana. ONWI-116, Report prepared by RE/SPEC Inc. for Office of Nuclear Waste Isolation.

Hardie, L. A., Lowenstein, T. K., Spencer, R. J. 1983. The problem of distinguishing between primary and secondary features in evaporites. In: Schreiber, B. C. & Harner, H. L. (Eds.), Sixth Symposium on Salt I. Salt Institute, Alexandria, Virginia, USA, 11-39.

Heard, H. C., Ryerson, F. J. 1986. Effect of cation impurities on steady-state flow of salt. In: Hobbs, B. E. & Heard, H. C. (Eds.), Mineral and rock deformation: laboratory studies. AGU Geophysical Monograph 36. American Geophysical Union, 99-115.

Hickman, S. H., Evans, B., 1991. Experimental pressure solution in halite; the effect of grain/interphase boundary structure. Journal of the Geological Society 148, 549-560.

Horseman, S. T., Handin, J. 1990. Triaxial compression tests on rocksalt at temperatures from 50 °C to 200 °C and strain rates from 10−4 to 10−9 1/s. In: Duba, A. G., Durham, W. B., Handin, J. W. & Wang, H. F. (Eds.), The brittle-ductile transition in rocks 56. American Geophysical Union, Washington, DC, United States, 103-110.

Horseman, S. T., Russell, J. E. H., J., Carter, N. L. 1992. Slow experimental deformation of Avery Island salt. Proceedings of the Seventh Internation Symposium on salt, Kyoto, Japan, April 6-9 1992, Elsevier, Amsterdam, 1, 67-74.

Hovorka, S., 1987. Depositional environment of marine-dominated bedded halite, Permian San Andres Formation, Texas. Sedimentology 34, 1029-1054.

Hunsche, U., Schulze, O., Walter, F., Plischke, I., 2003. Projekt Gorleben. Thermomechanisches Verhalten von Salzgestein. 9G2138110000, BGR, Hannover.

Ismail-Zadeh, A. T., Talbot, C. J., Volozh, Y. A., 2001. Dynamic restoration of profiles across diapiric salt structures: numerical approach and its applications. Tectonophysics 337(1-2), 23-38.

Jackson, M. P. A., 1985. Natural strain in diapiric and glacial rock salt, with emphasis on Oakwood dome, East Texas, Bureau of Economic Geology, The University of Texas at Austin, Texas.

Jackson, M. P. A., Cornelius, R. R., Craig, C. H., Gansser, A., Stocklin, J., Talbot, C. J. 1990. Salt diapirs of the Great Kavir, central Iran. Geological Society of America, Boulder, 177, 139

Jessell, M. W., Kostenko, O., Jamtveit, B., 2003. The preservation potential of microstructures during static grain growth. Journal of metamorphic Geology 21, 481-491.

Kendall, A. C., Harwood, G. M. 1996. Marine evaporites: arid shorelines and basins. In: Reading, H. G. (Ed.), Sedimentary Environments: Processes, Facies and Stratigraphy. Blackwell, 281-324.

Koyi, H. A., Mancktelow, N. S. (Editors), 2001. Tectonic Modeling: A Volume in the Honor of Hans Ramberg. Geological Society of America Memoir, 193, 286.

Kraus, B. J., Podladchikov, Y. Y., 2001. Forward and reverse modelling of the three-dimensional viscous Rayleigh-Taylor instability. Geophysical Research Letters 28(6), 1095-1098.

Last, N. C. 1988. Deformation of a sedimentary overburden on a slowly creeping substratum. In: Swoboda, G. S. (Ed.), Numerical Methods in Geomechanics, 577-585.

Lehner, F. K. 2000. Approximate theory of substratum creep and associated overburden deformation in salt basins and deltas. In: Lehner, F. K. & Urai, J. L. (Eds.), Aspects of Tectonic Faulting. Springer-Verlag, Berlin, 21–47.

Lowenstein, T. K., 1987. Evaporite depositional fabrics in the deeply buried Jurassic Buckner Formation, Alabama. Journal of Sedimentary Petrology 57(1), 108-116.

Lowenstein, T. K., Hardie, L. A., 1985. Criteria for the recognition of salt-pan evaporites. Sedimentology 32, 627-644.

Lux, K.-H., 2005. Long-term behaviour of sealed liquid-filled salt cavities - A new approach for physical modelling and numerical simulation - Basics from theory and lab investigations. Erdöl Erdgas Kohle 121, 414-422.

Peach, C., Spiers, C. J., Trimby, P. W., 2001. Effect of confining pressure on dilatation, recrystallization, and flow of rock salt at 150 °C. Journal of Geophysical Research 106(13315-13328).

Pfeifle, T. W., Vogt, T. J., Brekken, G. A., 1995. Correlation of chemical, mineralogic and physical characteristics of Gulf Coast dome salt to deformation and strength properties. Contract No. 1-92, RESPEC Inc., Rapid City.

Podladchikov, Y. Y., Talbot, C. J., Poliakov, A., 1993. Numerical models of complex diapirs. Tectonophysics 228, 189-198.

Popp, T., Kern, H., Schulze, O., 2001. Evolution if dilatancy and permeability in rock salt during hydrostatic compaction and triaxial deformation. Journal of Geophysical Research 106(B3), 4061-4078.

Ramsay, J. G. (Editor), 1967. Folding and Fracturing of Rocks. McGraw-Hill Book Company, 568.

Renard, F., Dysthe, D., Feder, J., Bjørlykke, K., Jamtveit, B., 2001. Enhanced pressure solution creep rates induced by clay particles: Experimental evidence in salt aggregates. Geophysical Research Letters 28, 1295-1298.

Renard, F., Ortoleva, P., 1997. Water films at grain-grain contacts: Debye-Huckel, osmotic model of stress, salinity, and mineralogy dependence. Geochimica et Cosmochimica Acta 61(10), 1963-1970.

Roedder, E., 1984. The fluids in salt. American Mineralogist 69, 413-439.

Rutter, E. H., 1976. The kinetics of rock deformation by pressure solution. Philosophical Transactions of the Royal Society of London A 283, 203-219.

Schenk, O., Urai, J., Piazolo, S., 2006. Structure of grain boundaries in wet, synthetic polycrystalline, statically recrystallizing halite – evidence from cryo-SEM observations. Geofluids 6(1), 93-104.

Schenk, O., Urai, J. L., 2004. Microstructural evolution and grain boundary structure during static recrystallization in synthetic polycrystals of Sodium Chloride containing saturated brine. Contributions to Mineralogy and Petrology 146(6), 671-682.

Schléder, Z., Urai, J. L., 2005. Microstructural evolution of deformation-modified primary halite from the Middle Triassic Röt Formation at Hengelo, The Netherlands. International Journal of Earth Sciences 94, 941-955.

Schreiber, B. C., El Tabakh, M., 2000. Deposition and early alteration of evaporites. Sedimentology 47(1), 215-238.

Schultz-Ela, D. D., Walsh, P., 2002. Modeling of grabens extending above evaporites in Canyonlands National Park, Utah. Journal of Structural Geology 24(2), 247-275.

Schutjens, P., Spiers, C. J., 1999. Intergranular pressure solution in NaCl: Grain-to-grain contact experiments under the optical microscope. Oil & Gas Science and Technology - Rev 54(6), 729-750.

Senseny, P. E. 1988. Creep properties of four salt rocks. Proceedings of the Second Conference on mechanical Behavior of Salt, Clausthal-Zellerfeld, Germany, Trans. Tech. Publications, 431-444.

Shearman, D. J., 1970. Recent halite rock, Baja California, Mexico. Transaction of Mining and Metallurgy 79B, 155-162.

Spiers, C. J., Carter, N. L. 1998. Microphysics of rocksalt flow in nature. Fourth Conference on the Mechanical behaviour of Salt, The Pennsylvania State University, June 17 and June 18, 1996, Trans Tech Publication Series on Rock and Soil Mechanics, 22, 115-128.

Spiers, C. J., Schutjens, P. 1990. Densification of crystalline aggregates by fluid phase diffusional creep. In: Barber, D. J. & Meredith, P. D. (Eds.), Deformation processes in minerals, ceramics and rocks. Unwin Hyman, 334-353.

Spiers, C. J., Schutjens, P. M., Brzesowsky, R. H., Peach, C. J., Liezenberg, J. L., Zwart, H. J. 1990a. Experimental determination of constitutive parameters governing creep of rocksalt by pressure solution. In: Knipe, R. J. & Rutter, E. H. (Eds.), Deformation mechanisms, rheology and tectonics. Geological Society of London Special Publications 54, 215-227.

Spiers, C. J., Schutjens, P. M. T. M., Brezowski, R. H., Peach, C., Liezenberg, J. L., Zwart, H. J. 1990b. Experimental determination of constitutive parameters governing creep of rocksalt by pressure solution. In: Knipe, R. J. & Rutter, E. H. (Eds.), Deformation Mechanisms, Rheology and Tectonics 24. Geol. Soc. London Spec. Publ., 215-227.

Spiers, C. J., Urai, J. L., Lister, G. S., Boland, J. N., Zwart, H. J., 1986. The influence of fluid-rock interaction on the rheology of salt rock, Department of Structural and Applied Geology, Institute of Earth Sciences, University of Utrecht, The Netherlands.

Talbot, C. J. 1998. Extrusions of Hormuz salt in Iran. In: Blundell, D. J. & Scott, A. C. (Eds.), Lyell; the past is the key to the present. Geological Society Special Publications 143, 315-334.

Talbot, C. J., Rogers, E. A., 1980. Seasonal movements in a salt glacier in Iran. Science 208, 395-397.

Ter Heege, J. H., De Bresser, J. H. P., Spiers, C. J., 2005. Rheological behaviour of synthetic rocksalt: the interplay between water, dynamic recrystallization and deformation mechanisms. Journal of Structural Geology 27(6), 948-963.

Triantafyllidis, N., Leroy, Y. M., 1997. Stability of a frictional, cohesive layer on a viscous substratum: Validity of asymptotic solution and influence of material properties. Journal of Geophysical Research 102, 20,551-20,570.

Urai, J. L., Spiers, C. J., Peach, C., Franssen, R. C. M. W., Liezenberg, J. L., 1987. Deformation mechanisms operating in naturally deformed halite rocks as deduced from microstructural investigations. Geologie en Mijnbouw 66, 165-176.

van Keken, P. E., Spiers, C. J., van den Berg, A. P., Muyzert, E. J., 1993. The effective viscosity of rocksalt: implementation of steady-state creep laws in numerical models of salt diapirism. Tectonophysics 225(4), 457-476.

Wardlaw, N. C., Schwerdtner, W. M., 1966. Halite-Anhydrite seasonal layers in the Middle Devonian Prairie Evaporite Formation, Saskachewan, Canada. Geological Society of America Bulletin 77, 331-342.

Warren, J. 2006. Evaporites: sediments, resources and hydrocarbons. Springer, 1036

Weijermars, R., 1986. Flow behavior and physical chemistry of Bouncing Putties and related polymers in view of tectonic laboratory applications. Tectonophysics 124, 325-358.

Wheeler, J., 1992. The importance of pressure solution and Coble creep in the deformation of polymineralic rocks. Journal of Geophysical Research 97, 579-4586.

Curriculum Vitae

Zsolt Schléder
Born on 1st of January, 1977 in Sárbogárd, Hungary
Hungarian nationality

Contact
e-mail: zsolt.schleder@googlemail.com

Education

2002-2006: PhD at RWTH Aachen University, Summa Cum Laude
1995-2001: Eötvös Loránd University, Budapest, Hungary. M.Sc. degree in Geology
1983-1994: Elementary and secondary school in Hungary

Industry

2006-recent: Structural geologist at Midland Valley Exploration Ltd.
2002-2006: Participation in industry sponsored projects at RWTH Aachen
2000–2002: Consultant in the Environmental Management office at DHV Hungary Ltd.

Research Projects

2002-2006: Deformation mechanisms and transport processes in naturally deformed halite samples. PhD Thesis. Supervisor: J. L. Urai.
1999-2001: Petrological and volcanological studies on a buried, late Miocene volcano at Little Hungarian Plain, NW Hungary. MSc Thesis at Eötvös L. University.
1997-2000: Participation in a petroarcheological (IGCP 442) research project supervised by the Hungarian National Museum and Eötvös L. University.

Research Interests

Deformation mechanisms, rheology of rocks
Prehistoric archeology
Volcanology

Awards

AGU Outstanding Student Award – 2005
Hetifeld-Preis at RWTH Aachen for outstanding PhD thesis – 2006

Languages spoken

English, German and Hungarian

Publications

Peer reviewed

Schléder, Z., Urai, J. L., Nollet, S., Hilgers, C., In Press. Deformation and recrystallization mechanisms and fluid flow properties of rocksalt as evidenced by microstructures – a case study on Zechstein (Z1) rocksalt from Neuhof salt mine (Germany). International Journal of Earth Sciences.

Schléder, Z., Burliga, S., Urai, J. L., In Press. Dynamic and static recrystallization-related microstructures in halite samples from the Kłodawa salt wall (central Poland) as revealed by gamma-irradiation. Neues Jahrbuch für Mineralogie und Petrologie.

Schléder, Z., Urai, J. L., 2007. Deformation and recrystallization mechanisms in mylonitic shear zones in naturally deformed extrusive Eocene-Oligocene rocksalt from Eyvanekey plateau and Garmsar hills (central Iran). Journal of Structural Geology 29(2), 241-255.

Schleder, Z., Urai, J. L., 2005. Microstructural evolution of deformation- modified primary Halite from Hengelo, the Netherlands. International Journal of Earth Sciences 94(5-6), 941-956.

Schléder, Z., Biró, K., Antoni, J. and Szakmány, G., 2003. Petroarchaeological studies on polished stone artefacts from Baranya county, Hungary II. Zengővárkony: notes on the production, use and circulation of polished stone tools. Annal. Museum Janus Pannonius, 47(2002): 130-145.

Biró, K., Szakmány, G. and Schléder, Z., 2001. Neolithic Phonolite mine and worshop complex in Hungary. Slovak Geol. Mag., 7(4): 345-350.

Biró, K., Dobosi, V. and Schléder, Z., 2000. Lithotheca II. - The Comparative Raw Material Collection of the Hungarian National Museum., Catalogue Vol. II.

Schléder, Z. and Biró, K., 1999. Petroarchaeological studies on polished stone artefacts from Baranya county. Annal. Museum Janus Pannonius, 43(1998): 75-101.

Unrefereed (last two years)

Hilgers, C., Pennock, G., Schleder, Z., Burliga, S., Urai, J. L. 2006. Microstructures of fibrous halite veins. TSK 11, Goettingen, Germany.

Hilgers, C., Schleder, Z., Urai, J. L. 2006. Microstructures in halite veins and their implication on the bulk permeability of rock. 7th Middle East Geosciences Conference and Exhibition, March 27 -29.

Urai, J., Schoenherr, J., Schleder, Z., 2006. Rheology of Ara salt based on creep tests (unpublished report prepared for Shell), Geologie-Endogene Dynamik, Aachen, Germany.

Schleder, Z., Schoenherr, J., Nollet, S., Urai, J. L., Hilgers, C., Kukla, P., Littke, R. 2006. Limits to the sealing capacity of Halite. General Assembly, European Geosciences Union, Vienna, Austria, 02-07 April 2006.

Schleder, Z., Urai, J. L. 2005. Deformation and Recrystallization Mechanisms in Mylonitic Zones in Naturally Deformed Extrusive Salts From Garmsar Hills and Qum Kuh (Central Iran). AGU Fall Meeting, San Francisco, CA, United States, 3-9.12.2005.

Schleder, Z., Urai, J. L. 2005. Deformation mechanisms and fluid flow properties of rocksalt. 4. Rundgespraech DFG-Schwerpunktprogramm, Geseke, Germany, 30.11-02.12.2005, 72-74.

Schleder, Z., Urai, J.L., Kirch, D., Talbot, C. and Hunsche, U., 2005. Deformation mechanisms in naturally deformaed extrusive salt from Iran. 15th Conference on Deformation mechanisms, Rheology and Tectonics, ETH Zürich, Zürich, Switzerland, 2-4.05.2005, p. 186.